Organo-functionalized inorganic nanofiltration membranes through engineering at the molecular level

Nikos Kyriakou

ORGANO-FUNCTIONALIZED INORGANIC NANOFILTRATION MEMBRANES THROUGH ENGINEERING AT THE MOLECULAR LEVEL

Nikos Kyriakou

ORGANO-FUNCTIONALIZED INORGANIC NANOFILTRATION MEMBRANES THROUGH ENGINEERING AT THE MOLECULAR LEVEL

DISSERTATION

to obtain
the degree of doctor at the Universiteit Twente,
on the authority of the rector magnificus,
prof. dr. ir. A. Veldkamp,
on account of the decision of the Doctorate Board
to be publicly defended
on Friday 14 October 2022 at 12.45 hours

by

Nikos Kyriakou

born on the 4th of December, 1987
in Lemesos, Cyprus

This dissertation has been approved by:

Supervisors
prof. dr. ir. A. Nijmeijer
prof. dr. A.J.A. Winnubst

Co-supervisor
dr. M.D. Pizzoccaro - Zilamy

Graduation Committee:

Chair / secretary: prof.dr. J.L. Herek

 Supervisors: prof.dr.ir. A. Nijmeijer
Universiteit Twente, TNW, Inorganic Membranes
prof.dr. A.J.A. Winnubst
University of Science and Technology of China/Universiteit Twente, TNW, Inorganic Membranes

Co-supervisor: dr. M.D. Pizzoccaro - Zilamy
Universiteit Twente, TNW, Inorganic Membranes

Committee Members: prof.dr.ir. J. Huskens
Universiteit Twente, TNW, Molecular Nanofabrication

prof.dr.ir. J.E. ten Elshof
Universiteit Twente, TNW, Inorganic Materials Science

prof. dr. V. Meynen
University of Antwerp

dr. A. Buekenhoudt
Flemish Institute for Technological research

prof.dr. E.J.R. Sudhölter
Universiteit Twente, TNW, Films in Fluids

Στους γονιεις μου, Ανδρέα και Φανή

Table of Contents

Summary

Organically functionalized inorganic hybrid membranes merge the good performance of polymers and the high chemical and mechanical stability of porous inorganic materials together towards high-performing membranes. The wide availability of polymers, as well as new chemical tools, such as "click" and reticular chemistry, allow for the synthesis of unique hybrid membranes that can be made to match a broad range of applications. This work focuses on new chemistries for the controlled formation of thin polymeric networks on a defined, porous inorganic support. The different chapters expand on the various syntheses and potential applications of these hybrid membranes for solvent filtration under harsh industrial conditions.

In **Chapter 1**, an introduction is given about industrial separations through using solvent tolerant nanofiltration membranes. Besides, this chapter is a survey on the state of the art of various methods for organically functionalizing/grafting inorganic materials.

Chapter 2 describes a grafting-to method in solution for the fabrication of four different polyethylene glycol (PEG)-functionalized inorganic membranes. The PEG molecules were functionalized via organophosphonic acid or organosilane functional groups on the inorganic surface. Each hybrid membrane featured similar polymers (PEG), with minor differences (end group or chain size), which allowed us to investigate the hydrolytic stability of the covalent bond between the functional group (organophosphonic acid and organosilane) and the inorganic surface under neutral (pH ≈ 7) conditions. This stability of the covalent bond was investigated on PEG-grafted γ-alumina flakes via liquid 1H NMR and on PEG-grafted membrane samples via water permeability tests. Both methods indicated that the organophosphonic acid grafted samples were stable in water up to 216h, whereas the organosilane-grafted samples showed rapid degradation in water. Finally, the work demonstrated a simple and green (water as solvent) method for the fabrication of hybrid organic-inorganic membranes.

Chapter 3 describes a simple solid-state grafting-to method to functionalize hydrophilic (PEG- and methoxy-PEG-phosphonic acids, PEGPA and MPEGPA) and hydrophobic (n-octadecyl, ODPA) organophosphonic acids on alumina supports. The solid-state grafting reaction was first studied on γ-alumina flakes (powder), and the interaction between organophosphonic acids and the surface was studied by FTIR, solid-state ^{27}Al NMR, and TGA. ODPA (hydrophobic) was found to form a

covalent bond with the inorganic surface under solid-state reaction conditions with high grafting densities of 3.2 P nm^{-2}. On the other hand, FTIR analysis of the PEGPA and MPEGPA grafted flakes did not directly confirm the formation of covalent grafting. Both samples showed lower grafting densities than the ODPA-grafted samples, regardless of the reaction temperature, but the PEGPA grafted samples showed significantly higher grafting densities than MPEGPA-grafted flakes, which was attributed to a side reaction occurring during grafting of PEGPA. The PEG-phosphonic acids were then grafted on flat-sheet alumina membranes to further study the effect of reaction temperature on the confinement (pore size reduction) of the polymer. It was found that increasing the reaction temperature facilitated higher grafting densities in the pores of the support (i.e., stronger confinement). Furthermore, it was confirmed that the reactive end-group (-OH) of PEGPA negatively affected the grafting reaction in the pores due to blocking reactive sites on the inorganic surface and consuming available organophosphonic acids. The effect of the reactive end-group of PEGPA was confirmed by analysing the membrane performance of the fabricated hybrid membranes, as they showed worse separation performance compared to MPEGPA-grafted membranes. Finally, this study shows that a simple and sustainable method (small amount of reactants) for the fabrication of these hybrid organic-inorganic membranes is possible.

Chapter 4 described a new grafting-from method that combines a "click" reaction with a vapour-liquid interfacial polymerization reaction to form an ultrathin polythioether layer on top of a porous alumina support. The method employed uses only a fraction of the amounts of reactants and solvents necessary to prepare hybrid organic-inorganic membranes with the conventional liquid-liquid interfacial polymerizations. The polythioether layer was formed on a pre-functionalized porous inorganic support via two consecutive thio-bromo click reactions. First, a reaction was performed in a solution of 1,3,5-tris(bromomethyl)benzene (3Br) under basic conditions at room temperature for up to 5 min. This impregnated membrane was subsequently treated with a vapour of 1,3-benzenedithiol. These two reactions resulted in the formation of a 50 nm-thin polythioether layer on top of the ceramic support. The physical and chemical properties of the polymeric layer were investigated by means of FTIR, TGA, NMR, FE-SEM, and spectroscopic ellipsometry. The chemical stability of the free-standing (prepared via liquid-liquid interfacial polymerization) polythioether layer was demonstrated in acid, base, hypochlorite, and several non-polar solvents. In addition, the layer was shown to be thermally stable up to a temperature of 150 °C. The potential as a nanofiltration membrane was demonstrated in different solvents, including ethanol and water, and

by showing a PEG molecular weight cut-off of 700 g mol^{-1} as well as a 93% retention of Rhodamine B (469 Da) in water.

Chapter 5 demonstrates a grafting-from synthesis for the controlled nanoconfinement, growth, and covalent attachment of a polyimide (PI) network inside the mesopores of γ-alumina layers. Different pre-functionalization steps for the γ-alumina layer were used in the synthesis of the same PI network (from melamine and pyromellitic dianhydride) under different reaction times (1 or 5 days). The pre-functionalization of the support was done either at the top surface or at the top and inner pore surface of the γ-alumina layer. Top surface pre-functionalization led to the PI growing only at the top and pore entrance of the γ-alumina layer. On the other hand, inner pore surface functionalization led to the PI growing over the whole surface of the γ-alumina layer. Still, with both pre-functionalization methods, the PI network was confined only to the γ-alumina layer. The properties of the PI hybrid membranes were studied via a series of analytical techniques, including FE-SEM, FTIR, AFM, water contact angle, and cyclohexane permporometry. The resulting PI hybrid inorganic membranes exhibited good and stable performance in various solvents of different polarities (water, DMF, and dioxane). These hybrid membranes were able to retain small organic dye molecules such as Rhodamine B (479 g mol^{-1}) from toxic solvents. Therefore, this type of membrane opens possibilities for a multitude of separation processes.

Chapter 6 focuses on methods for the synthesis of crosslinked crystalline polyimide (PI) materials. The aim of this work was to identify potential methods that are greener and more efficient than the in-situ method, as described in **Chapter 5**, without compromising the crystallinity of the final product. As described in the literature (solid-state and solvothermal), conventional synthetic methods were compared with a hybrid solid-state through pre-organization (SSP) method by studying the synthesis of a PI material through the monomer system of pyromellitic dianhydride/acid and melamine. The different synthetic methods were compared in regard to purity by FTIR and crystallinity by XRD. It was found that most methods, except for the solid-state, yielded PIs of good relative purity. However, the various methods used led to different crystallinity, which was attributed to the differences in the fabrication methods. The SSP method in NMP, water, and water/formic acid yielded a relatively crystalline and pure PI material. Furthermore, under SSP conditions, the formation of a PI material was facilitated below the melting point of both monomers for the first time. In addition, the SSP method was used to successfully fabricate PI layers on porous inorganic supports, demonstrating the potential of this method for membrane fabrication. Finally, this work demonstrates a simple alternative and green

synthesis method for the fabrication of crystalline PI powders and layers that can be applied in membrane technology but can also be expanded to other fields.

Chapter 7 evaluates the work, described in **Chapters 2** to **6**, and provides reflections on the key findings, remaining challenges, and potential new opportunities generated by this work. The chapter is divided into three sections; respectively, the hydrolytic stability of the covalent bonding between the organic group and inorganic support, the chemical synthesis methods, and the performance of the membranes are discussed. A detailed discussion is provided on the advantages and disadvantages of the grafting-to methods, as described in **Chapters 2** and **3**, while as well as disadvantages and potential suggestions for future research are given. The mechanism of the two grafting-to methods is discussed in detail and compared in regard to their grafting density and membrane performance. The two grafting-from methods described in **Chapters 4** and **5** are also critically evaluated in this chapter 7. Alternative methods and reactants are provided that can be used to potentially further optimize membrane stability and performance.

The performance of the different membranes is discussed in detail, particularly those of the PEG-phosphonic acids-grafted membranes, where many open questions remain about their retention performance. Finally, preliminary results are discussed on the retention performance and stability of PEG- (**Chapter 3**), polythioether- (**Chapter 4**), and polyimide-grafted (**Chapter 5**) membranes in water/dimethyl formamide and water/isopropanol mixtures with Rhodamine B dye. The results showed stable dye retention for these solvent mixtures, except for polyimide-grafted membranes. However, polyimide-grafted membranes with additional post-thermal treatment show stable performance in the different solvent mixtures without any degradation occurring. These preliminary results show that the hybrid organic-inorganic membranes can potentially be used for industrial nanofiltration applications.

Samenvatting

Het onderzoek, beschreven in dit proefschrift, richt zich op het functionaliseren of 'graften' van poreuze keramische membranen. Het gaat hier om zogenaamde organisch gefunctionaliseerde anorganische hybride membranen, welke de goede membraan prestaties van polymeren combineren met de hoge chemische en mechanische stabiliteit van anorganische materialen. De beschikbaarheid van een grote variatie aan polymeren en nieuwe chemische methodes, zoals "klik" en reticulaire chemie, maken de synthese mogelijk van unieke hybride membranen voor een breed scala aan toepassingen. In dit proefschrift ligt de focus op toepassingen van nieuwe chemische methoden voor de gecontroleerde vorming dunne polymere netwerken op een poreuze anorganische drager. De verschillende hoofdstukken gaan dieper in op de verschillende synthese methodes en de mogelijke toepassingen van deze hybride membranen voor filtratie van oplosmiddelen onder veeleisende, industriële omstandigheden.

In **Hoofdstuk 1** wordt een introductie gegeven over industriële scheidingen door gebruik te maken van oplosmiddel tolerante nanofiltratie membranen. Daarnaast geeft dit hoofdstuk een overzicht van de verschillende manieren om anorganische materialen organisch te functionaliseren/graften.

Hoofdstuk 2 beschrijft een chemische modificatie methode ('grafting') in oplossing voor de fabricage van vier verschillende polyethyleenglycol (PEG)-gefunctionaliseerde anorganische membranen. De PEG-moleculen worden chemisch gebonden aan het anorganische oppervlak, via organofosfonzuur of organosilaan functionele groepen. Elk hybride membraan heeft vergelijkbare polymeren (PEG), met alleen kleine verschillen in eindgroep of ketengrootte, waardoor het mogelijk is om de hydrolytische stabiliteit van de covalente binding tussen de functionele groep (organofosfonzuur en organosilaan) en het anorganische oppervlak te bestuderen onder neutraal (pH $\approx$ 7) omstandigheden. Deze stabiliteit van de covalente binding werd onderzocht met vloeistof ^{1}H NMR op PEG-gegrafte poreuze γ-alumina poeders en door middel van water permeatie testen op PEG-gegrafte membranen. Beide methodes gaven aan dat de met organofosfonzuur gegrafte preparaten tot 216 uur stabiel waren in water, terwijl de met organosilaan gegrafte preparaten een snelle degradatie in water vertoonden. Ten slotte demonstreerde het werk een eenvoudige en groene (water als oplosmiddel) methode voor de fabricage van hybride organisch-anorganische membranen.

Hoofdstuk 3 beschrijft een eenvoudige vaste-stof 'grafting-to' methode om poreuze aluminiumoxide dragers te functionaliseren met hydrofiele (Polyethylene glycol ω-fosfonzuur, PEGPA, en Poly[ethylene oxide], α-methoxy, ω-fosfonzuur, MPEGPA) of hydrofobe (n-octadecyl fosfonzuur: ODPA) organofosfonzuren. De graft reactie in de vaste-stof toestand werd eerst bestudeerd op γ-alumina poeders en de interactie tussen organofosfonzuren en het poeder oppervlak werden geanalyseerd met FTIR, vaste-stof ^{27}Al NMR en TGA. ODPA (hydrofoob) bleek een covalente binding te vormen met het anorganische oppervlak onder deze reactieomstandigheden, resulterend in een hoge (graft) dichtheid van ODPA op het alumina oppervlak. Aan de andere kant toonde de FTIR analyses van de met PEGPA en MPEGPA gegrafte poeders niet direct de vorming van covalente binding aan. Beide laatste materialen vertoonden lagere graft-dichtheden dan de met ODPA gegrafte poeders, ongeacht de reactietemperatuur, maar de met PEGPA gegrafte preparaten toonden significant hogere graft-dichtheden dan de met MPEGPA gegrafte poeders, wat een aanwijzing is dat er een nevenreactie heeft plaats gevonden tijdens het graften met PEGPA.

De PEG-fosfonzuren werden vervolgens gegraft op vlakke aluminiumoxide membranen om het effect van de reactietemperatuur op graft-dichtheid in de poriën van het keramisch membraan te bestuderen. Er werd gevonden dat een hogere reactietemperatuur een hogere graft-dichtheid in de poriën geeft, wat resulteert in kleinere poriën en daardoor een betere scheiding van het membraan van kleinere moleculen. Verder is bevestigd dat de reactieve eindgroep (-OH) van PEGPA, als gevolg van het blokkeren van reactieve plaatsen op het anorganische oppervlak en het consumeren van beschikbare organofosfonzuren, de graft reactie in de poriën negatief beïnvloedt. Dit effect van de reactieve eindgroep van PEGPA op de graft-dichtheid was ook duidelijk zichtbaar bij een studie naar de prestaties van de gefabriceerde hybride membranen aangezien deze slechtere scheiding vertoonden in vergelijking met MPEGPA-gegrafte membranen. Ten slotte toont deze studie aan dat het mogelijk is om dit type hybride organisch-anorganische membranen te fabriceren op een eenvoudige en duurzame manier (kleine hoeveelheid reactanten).

Hoofdstuk 4 beschrijft een nieuwe graft synthese methode die een "klik"-reactie combineert met een damp-vloeibare-fase grensvlak polymerisatie reactie om een ultradunne polythioether laag boven op een poreuze aluminiumoxide drager te vormen. Deze methode gebruikt slechts een fractie van de hoeveelheden reactanten en oplosmiddelen zoals die nodig zijn om hybride organisch-anorganische membranen te bereiden met conventionele vloeistof-vloeistof grensvlak polymerisaties. De polythioether laag werd gevormd op een vooraf gefunctionaliseerde poreuze anorganische drager via twee opeenvolgende thio-

broom-klikreacties. De eerste reactie werd uitgevoerd in een oplossing van 1,3,5-tris(broommethyl)benzeen (3Br) onder basische omstandigheden bij kamertemperatuur gedurende maximaal 5 minuten. Dit met 3Br geïmpregneerde membraan werd vervolgens behandeld in een chemische damp van 1,3-benzeendithiol. Deze twee reacties resulteren in de vorming van een 50 nm dunne polythioether laag aan de bovenkant van de keramische drager. De fysische en chemische eigenschappen van de polymeer laag werden geanalyseerd met FTIR, TGA, NMR, FE-SEM en spectroscopische ellipsometrie. De vrijstaande polythioether laag (bereid via vloeistof-vloeistof grensvlakpolymerisatie) toonde goede stabiliteit in zuur, base, hypochloriet en verschillende niet-polaire oplosmiddelen. Daarnaast werd aangetoond dat de laag thermisch stabiel was tot een temperatuur van 150 °C. Het potentieel als nanofiltratie membraan werd aangetoond in verschillende oplosmiddelen, waaronder ethanol en water, en door het aantonen van een PEG-moleculgewicht grenswaarde voor scheiding (Molecular Weight Cut Off: MWCO) van 700 g mol^{-1}, evenals een 93% retentie van Rhodamine B (molecuul gewicht: 469 Da); beiden in water.

Hoofdstuk 5 beschrijft een 'grafting-from' synthese voor de covalente binding en gecontroleerde groei van een polyimide (PI) netwerk aan het oppervlak en in de mesoporiën van γ-alumina lagen. Verschillende pre-functionalisatie stappen werden gebruikt bij de synthese van hetzelfde PI netwerk (bestaande uit melamine en pyromellietzuurdianhydride), welke laatste onder verschillende reactietijden werden uitgevoerd (1 of 5 dagen). Deze pre-functionalisatie werd alleen aan het bovenoppervlak uitgevoerd of aan het bovenoppervlak en in de poriën van de γ-alumina laag. Pre-functionalisatie van alleen het bovenoppervlak leidde ertoe dat de PI alleen groeide aan de bovenkant en de porie ingang van de γ-alumina laag. Aan de andere kant resulteerde functionalisering van het binnenste porieoppervlak in de vorming van PI over het hele oppervlak van de poriën van de γ-alumina laag. De eigenschappen van de PI-hybride membranen werden bestudeerd via een reeks analytische technieken, waaronder FE-SEM, FTIR, AFM, water contacthoek metingen en cyclohexaan permporometrie. De resulterende PI hybride anorganische membranen vertoonden goede en stabiele prestaties in verschillende oplosmiddelen van verschillende polariteit (water, DMF en dioxaan). Deze hybride membranen waren in staat om kleine organische kleurstofmoleculen zoals Rhodamine B (479 g mol^{-1}) uit giftige oplosmiddelen te verwijderen. Daarom opent dit type membraan mogelijkheden voor toepassing in een veelvoud aan scheidingsprocessen.

Hoofdstuk 6 richt zich op verschillende methoden voor de synthese van verknoopte ('cross-linked'), kristallijne polyimide (PI) materialen. Het doel van dit werk was om

mogelijke methoden te identificeren die groener en efficiënter zijn dan de in-situ methode die in Hoofdstuk 5 wordt beschreven, zonder de kristalliniteit van het eindproduct in gevaar te brengen. Conventionele synthetische methoden, zoals in de literatuur beschreven (vaste-stof en solvotherm), werden vergeleken met hybride vaste-stof reacties (SSP), uitgaande van een pre-organisatiemethode van het monomeersysteem van pyromelliet dianhydride / zuur en melamine. De verschillende synthetische methoden werden vergeleken met betrekking tot zuiverheid door middel van FTIR en kristalliniteit door XRD (Röntten diffractie) analyse. De meeste methoden, behalve de vaste-stof synthese, resulteerden in PI's met goede zuiverheid. De verschillende methoden leidden echter tot verschillende vormen van kristalliniteit, die werd toegeschreven aan de verschillen in de fabricagemethoden. De SSP-methode in NMP, water en water/mierenzuur resulteerde in een relatief kristallijn en zuiver PI materiaal. Verder werd onder SSP-omstandigheden voor het eers de vorming verkregen van een kristallijn PI materiaal beneden het smeltpunt van beide monomeren. Bovendien werd de SSP-methode gebruikt om met succes PI lagen aan te brengen op poreuze anorganische dragers wat het potentieel van deze methode voor membraanfabricage aantoont. Ten slotte toont dit werk de mogelijkheid aan voor een eenvoudig alternatief en een groene synthese methode voor de fabricage van PI poeders en lagen, die kunnen worden toegepast in membraantechnologie, welke ook tot andere toepassingsgebieden kan worden uitgebreid.

Hoofdstuk 7 evalueert het werk zoals beschreven in de **Hoofdstukken 2** tot en met **6** en geeft reflecties op de belangrijkste resultaten, resterende uitdagingen en potentiële nieuwe kansen die door dit werk worden gegenereerd. Het hoofdstuk is verdeeld in drie hoofdsecties waarin respectievelijk de hydrolytische stabiliteit van de covalente binding tussen de organische groep en de anorganische drager, de gebruikte chemische synthese methoden, en de prestaties van de membranen worden besproken. Er wordt gedetailleerde ingegaan op de voor- en nadelen van de twee 'grafting-to' methodes, zoals beschreven in de **Hoofdstukken 2** en **3**, terwijl mogelijke oplossingen door toekomstig onderzoek worden aangestipt. Het mechanisme van deze 'grafting-to' methode wordt in detail besproken en gerelateerd met grafting dichtheid en membraanprestaties. Daarnaast worden in dit **Hoofdstuk 7** ook de twee 'grafting-from' methodes, zoals beschreven in de **Hoofdstukken 4** en **5**, kritisch geëvalueerd. Alternatieve synthese methodes en reactanten worden voorgedragen om de stabiliteit en prestaties van deze type membranen mogelijk verder te optimaliseren.

De prestatie van de verschillende membranen wordt in detail besproken, in het bijzonder die van de PEG-fosfonzuren gegrafte membranen, waar veel open vragen zijn gebleven over hun retentie prestaties. Tot slotte worden de eerste voorlopige resultaten besproken van een vergelijking van de membraan prestaties en stabiliteit van PEG- (**Hoofdstuk 3**), polythioether- (**Hoofdstuk 4**) en polyimide- (**Hoofdstuk 5**) gegrafte membranen in water/dimethylformamide en water/isopropanol mengsels met Rhodamine B. De resultaten tonen een stabiele Rhodamine B retentie aan in deze mengsels van oplosmiddelen, met uitzondering van de met polyimide gegrafte membranen. Echter, polyimide gegrafte membranen, die een extra post-thermische behandeling hebben ondergaan, vertonen stabiele prestaties in de verschillende oplosmiddelmengsels. Deze eerste resultaten tonen aan dat de hybride organische-anorganische membranen potentieel kunnen worden gebruikt voor industriële nanofiltratie toepassingen.

Chapter 1

Introduction

1.1. Industrial separations

Separations are an intrinsic part of industrial processes as they are involved essentially wherever mixtures are present, including gas, solvent/solute, and reactants/products/by-products mixtures. An astonishing 10-15% of the world's total energy consumption is used for industrial separations.[1] This large amount of energy is partially due to the scale of separation processes but is mainly due to the use of high-energy demanding separation techniques, such as distillation, which the industry is heavily relying on.[1] On the other hand, pressure-driven membrane-based technologies can separate liquid mixtures (even at the molecular level) without phase transition and thus decrease the energy required for separations.[2] For example, according to Dong et al.,[3] the choice between a continuous distillation process (> 225 kJ mol^{-1}) or organic solvent reverse osmosis (OSRO; 1.7-3.5 kJ mol^{-1}) for separating an equimolar mixture of two organic components can result in an energy difference up to two orders of magnitude (Figure 1.1C). Thus, pressure-driven separation technologies can offer a viable solution for minimizing the energy required for industrial separations. Still, membrane processes have their limitations, such as the separation of high concentrated mixtures, and thus cannot completely replace thermally driven processes. On the other hand, for separations of heat-sensitive chemicals, such as pharmaceuticals, pressure-driven membrane technologies can be a promising solution in the future.[4]
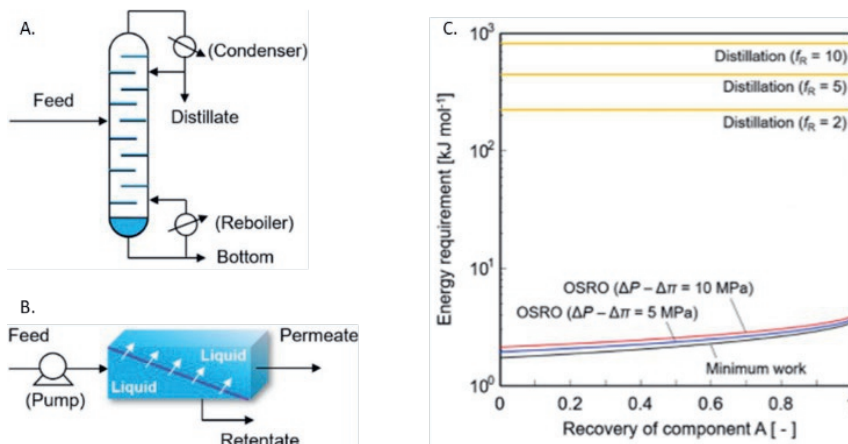
Figure 1.1: Schematic representation of organic solvent separation processes for continuous distillation (A) and OSRO (organic solvent reverse osmosis) (B). The energy requirements for the two methods for separation of an equimolar mixture of two components as a function of the recovery ratio of component A (C). The figure was adapted from [3].

Amongst different membrane technologies, nanofiltration (NF) is mainly used for the separation of liquid mixtures with solutes of molecular sizes between 0.5 and 2

12

nm (Figure 1.2). These mixtures include mixtures of solvents, homogeneous catalysts, antibiotics, peptides, and reaction intermediates. Therefore, NF technology can potentially lower the cost of industrial separations and mitigate waste production by purifying and reusing solvents.

NF membranes were first proclaimed in the early 1980s to distinguish from reverse osmosis (RO) membranes, which only allow for the permeation of water molecules.[5] Since the RO technology was already established, NF membranes were first used for wastewater treatment and water hardness reduction. However, the importance of NF technology became evident with its first use in nonaqueous mixtures. The potential use of membranes for the separation of organic mixtures down to molecular levels attracted the attention of the petrochemical industry, which resulted in the first application of the NF technology in nonaqueous mixtures, such as in the separation of hydrocarbons in petrochemical industry.[5] This led to the expansion of NF technology to organic solvents, which was dabbed as Organic Solvent Nanofiltration (OSN). The potential applications of chemically (or solvent) resistant NF membranes (CRNF or SRNF) extend through different industries, including the chemical, petrochemical, pharmaceutical, food, and textile industry. This new technology is regarded by specialists as a possible way for the intensification of industrial processes involving organic solvents.[6,7] Thus, SRNF technology can eliminate the need for energy-intensive separation technologies,[6,7] reduce environmental emissions and materials consumption,[6] and potentially allow a continuous process from raw materials to products.[8,9] For aqueous applications that can contain solvents or organic solutes and mixtures thereof, solvent tolerant NF (STNF) membranes are used. STNF membranes are stable in the presence of aqueous mixtures of solvents and solutes. The distinction between SRNF and STNF membranes will be highlighted in the next section.
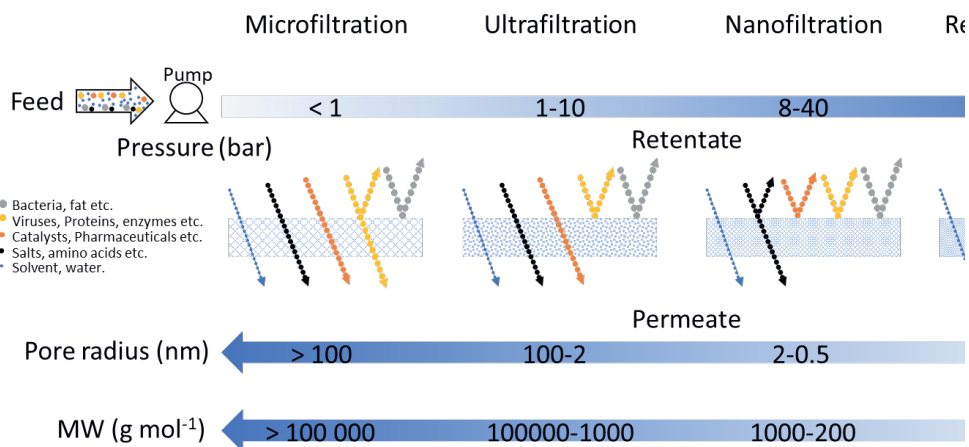
Figure 1.2: Membrane processes classification according to operating pressure, pore size (retained solute size), and retained solute molecular weight (MW). The figure was adapted from [5].

Even though NF technology has made enormous progress, there are major challenges that hinder their wider "spread" in industry. Firstly, the membrane (chemical, thermal and mechanical) stability requirements, which affect the long-term performance, differ from aqueous to nonaqueous applications of these membranes. Secondly, the lack of control over the microstructure of the selective layer during membrane fabrication, as well as their behaviour under operating conditions, has slowed down the development of NF technology. Thirdly, the unavailability of tools to understand and predict the performance of NF membranes restricts further developments toward industrial applications. Finally, the unavailability of multifunctional membranes weakens commercial interest in the technology. Only if NF technology answers the above questions it will force the industry to "retire" old energy- and resource-intensive methods and focus on developing and implementing membranes in industrial processes.

1.2. Solvent resistant and solvent tolerant nanofiltration membranes (SRNF and STNF)

NF membranes generally exhibit an asymmetric configuration and can be distinguished into different layers. At the side of the feed solution, a thin (nanometre scale) microporous (pore size 0.5-2 nm) selective layer resides on top of single or multi-layered support. The latter is typically the case with inorganic supports where they can consist of a combination of mesoporous and macroporous layers, for example, a system consisting of a thin layer of γ-alumina on thicker α-alumina

support. Typically, the macroporous layer is used to provide mechanical stability to the final membrane and is usually of millimetre thickness.

Besides pore size, the performance of a membrane is also related to intrinsic properties of the membrane material, such as hydrophilicity and physical/chemical interactions between the selective layer and the solvent/solutes. Good interaction between the solvent and the selective layer can increase the solvent flux leading to better membrane performances.[10,11] As such, a hydrophilic polymer, for example, polyethylene glycol (PEG), is preferred for separations in water or polar organic solvents, whereas polystyrene (PS) layers can be used for apolar solvents, such as toluene.

Polymeric separation layers that show high affinity towards the solvent tend to adsorb solvent molecules and swell. A small degree of swelling is expected with most polymers and can, in fact, enhance the performance of the membrane. This was shown on membranes with polyamide selective layers where the membranes (polymeric) were swollen in DMF. This allowed for the rearrangement of the macromolecular structure of the selective layer and led to the removal of any unreactive monomers or oligomers from the layer.[12] This membrane pre-treatment led to an increase in solvent flux as compared to non-pre-treated membranes.[12] This positive effect of solvent swelling on membrane performance was demonstrated with polyamide layers, supported on both polymeric[12] and inorganic[13] substrates. This means that it can also be of use for hybrid organic/inorganic membranes.

On the negative side, extensive and uncontrolled swelling leads to the degradation of some polymeric separation layers. Van der Bruggen et al.[14] and later Tempelman et al.[15] observed the destructive effects of swelling of polymeric membranes exposed to organic solutes (such as toluene) in water. According to Van der Bruggen et al.,[14] more swelling of the membrane material was observed when the interaction between organic solutes and membrane material was significantly stronger than the interaction between the solvent (water) and solutes. This effect was attributed to the surface properties of the membrane material (aromatic polyamide/polysulfone), which strongly attracted the most common organic aromatic solutes with a molecular weight below the cut-off of the membrane, allowing them to penetrate inside the selective layer.[14]

Tempelman et al.[15] observed similar trends with two different commercially available NF membranes (TriSep TS80 and DOW NF270, both polyamide supported on polysulfone). The membranes were tested in water saturated with toluene, an aromatic apolar and common solvent. However, Tempelman et al.[15] assumed that this degradation of the membrane was mostly related to the chemical stability of the support since others[16–19] have already established the stability of crosslinked

polyamide selective layers in different polar and apolar organic solvents. Therefore, Tempelman et al.[15] tested first the two membranes in pure water and then in water saturated with toluene. With the introduction of the mixture, the TS80 showed a significant increase in permeability as a function of time, whereas for NF270, a significant decrease was observed for the mixture as well as for pure water. The authors concluded that the two membranes performed differently in the aqueous mixture, with only TS80 showing degradation. This difference was attributed to the hydrophobic nature of TS80, which allowed a significant amount of toluene to adsorb in the membrane material. This adsorption led to dewetting of the top layer from the support and finally to the destruction of the membrane. Both studies[14,15] demonstrated that membranes operating in aqueous solutions containing even small amounts of organic solvents not only can foul the top layer but also lead to irreversible damage to the membrane material. Clearly, aqueous mixtures containing aromatic organic solutes are a special case in membrane technology. Since such mixtures can be found in both natural water sources (lakes, seawater, etc.) and chemical industry (such as produced water in the petrochemical industry), they need particular attention.

As a result, a solvent-resistant nanofiltration membrane (SRNF) can show good chemical stability against individual solvents but still degrade in the presence of aqueous mixtures of the same solvent. Solvent tolerant nanofiltration membranes (STNF) can operate in water-containing solvents, like toluene or DMF.[20] The importance of such distinction comes from the behaviour of organics in water. For example, according to Meyer et al.,[21] apolar organics exhibit low solubility in water and thus are forced to aggregate or cluster. This phenomenon is called the hydrophobic effect or interaction and is a/o the reason why oil forms droplets in water. However, in the presence of a polymer material, such as a selective membrane layer, the organic solutes will adsorb strongly to the organic phase leading to severe swelling and eventually degradation of the layer. Thus, the properties and materials required for the fabrication of SRNF or STNF membranes can differ significantly.

Some of the required properties for STNF membranes can be identified from the work of Van der Bruggen[14] and Tempelman et al.[15]. According to Van der Bruggen et al., more hydrophilic membranes show less adsorption to aromatic organic solutes, including organic solvents, and thus lower degree of swelling. Furthermore, it was pointed out that the crosslinking degree of the polymeric layers can decrease swelling and further stabilize the selective and supporting layers.[15,22,23] Finally, Tempelman et al.[15] suggest that the lack of strong adhesion between the selective layer and the support increases the possibility of dewetting or delaminating the selective layer from the support.

Not only solvent/solute affinity with the membrane material but also porosity, pore size, and pore morphology play a vital role in the membrane performance. Thin, microporous selective layers that exhibit high porosity with well-defined pore orientation (e.g., cylindrical pore shape) result in low tortuous layers and show minimal flow resistance to solvents while maintaining a small pore size. An example is given in the work of Jimenez-Solomon,[24] where one of the two monomers (e.g., 2,6-dihydroxyanthraquinone) employed in the production of the three different SRNF membranes showed some rigidity. The selective layer displayed some degree of structural organization which resulted in membranes with good solute rejections (200 Da), solvent permeabilities (0.5 – 8.5 L m^{-2} h^{-1} bar^{-1}), and stability in solvents like methanol and toluene. These results were forerunners to highly oriented membrane layers where the starting materials (e.g., monomers) have a high degree of organization. Such materials include metal-organic frameworks (MOF)[25] and covalent organic frameworks (COF).[26] However, in the case of STNF membranes, the polymeric layer should exhibit hydrophilic properties to minimize organic solute adsorption and thus reduce any possibility of excessive swelling and subsequent layer degradation. Hydrophilic layers are also necessary to promote high water flux through the selective layer.

Another important membrane property is the thickness of the selective layer, which has a direct effect on solvent permeability. Karan et al.[19] applied an 8 nm thick polyamide crosslinked layer on both polymeric and inorganic supports. These membranes rejected dyes of 246 Da with solvent permeabilities up to 50 L m^{-2} h^{-1} bar^{-1} even on the rigid alumina support (asymmetric with pore diameter varying from18 to 150 nm). The high solvent permeability was attributed to the ultrathin microporous layer that facilitated good separation and permeation performance. Such ultrathin layers could be fabricated via vapor phase polymerization[27], which can be replaced or used as complementary to liquid phase membrane preparation methods.

Finally, proper selection of the support is crucial for the stability and performance of the membrane. Superhydrophilic inorganic supports (water drops spread completely on the surface)[28] are suitable candidates due to their mechanical and chemical stability. In addition, inorganic materials, such as alumina, can be easily chemically functionalized with organic molecules, including polymers, to control the surface properties (pore size, hydrophilicity, etc.) of the final membrane.

Therefore, the research described in this thesis is focused on inorganic membrane supports that are organically-functionalized for use in molecular separations. The inorganic support provides the mechanical stability of the membrane, and the organic phase tunes the membrane properties. An intermediate inorganic layer with a smooth surface and a high concentration of reactive sites (e.g., hydroxyl groups) is used. As

such, the intermediate layer provides the basis for chemical functionalization of the support and the possibility of forming an ultrathin and smooth layer at the top or on the pore walls. Organo-functionalization of inorganic substrates with polymers or small organic molecules is achieved through physical or chemical interaction. Physical interactions include hydrogen bonds, dipole-dipole interactions, and others. Chemical functionalization, though, leads to the formation of a covalent bond between the organic and inorganic parts, which can lead to better chemical stability as compared to physical interactions. In this work, the main focus is on the chemical functionalization of inorganic supports.

1.3. Organically-functionalized inorganic membranes

Chemical functionalization of inorganic surfaces is studied extensively, and a plethora of reactive functional groups are identified. For example, Pujari et al.[29] and recently Merlet et al.[30] discussed several functional groups and the conditions under which these react with inorganic surfaces.

The kinetics of a grafting reaction depend on the reactants involved, as well as solvent, temperature, and catalyst.[31–34] This means that deriving a general description for the kinetics of grafting reactions is challenging. A simple description of the grafting density as a function of time for grafting an organic group on a dense inorganic surface is made by applying the models described in literature[34–36] and summarized in Figure 1.3. If we assume that the mechanism of a grafting reaction, whatever it is, does not change over time, we can expect that the grafting density will increase linearly over time (Figure 1.3 stage I). This can be a good assumption at the start of the grafting process. However, with increasing grafting density, diffusion of unreacted molecules towards the surface is hindered by the already grafted molecules, as indicated in Figure 1.3 stage II. This means that additional energy is needed for the unreacted molecules to approach the surface. Hence the energy barrier of the reaction is increasing, and the grafting rate is expected to slow down as a function of time. With more grafted molecules, the diffusion is further restricted, resulting in a non-linear relationship (Figure 1.3, stage II) between grafting density and reaction time. At a certain level of grafting density, the diffusion of new molecules towards vacant reactive sites on the inorganic surface is hindered significantly under the current reaction conditions, which limits further grafting (Figure 1.3, stage III). Thus, at the start of stage III, the grafting density is at a maximum under these reaction conditions.

A similar situation is expected for grafting porous substrates, which is more related to membrane fabrication. However, in this case, the reaction at the top surface of the support will be faster than on the surface of the pore surface due to the necessary diffusion of unreacted molecules in the (meso)pores. With increasing grafting density, the diffusion of unreacted molecules inside the pore will be significantly

18

limited.[35] The maximum grafting density is therefore also associated with the size of the grafting molecules used as well as the size of the pore. Besides, the grafting density in the pores could be potentially increased by adjusting the experimental conditions (e.g., temperature or solvent), which can influence the radius of gyration of the molecules in the solvent and their structural orientation, which potentially allows for more molecules to graft on the pore surface. Other ways to increase the grafting density inside the pores can include the use of polymers of smaller molecular weight (grafting-to) or the use of monomers to grow the polymer inside the pores (grafting-from), which would allow for more material to diffuse in the pores. Finally, grafting in the gas phase (CVD) might reduce diffusion limitation in the pore, resulting in a higher grafting density. A good understanding of the grafting reaction and the mechanism can be crucial for the formation of a grafted NF inorganic membrane with desirable membrane properties.
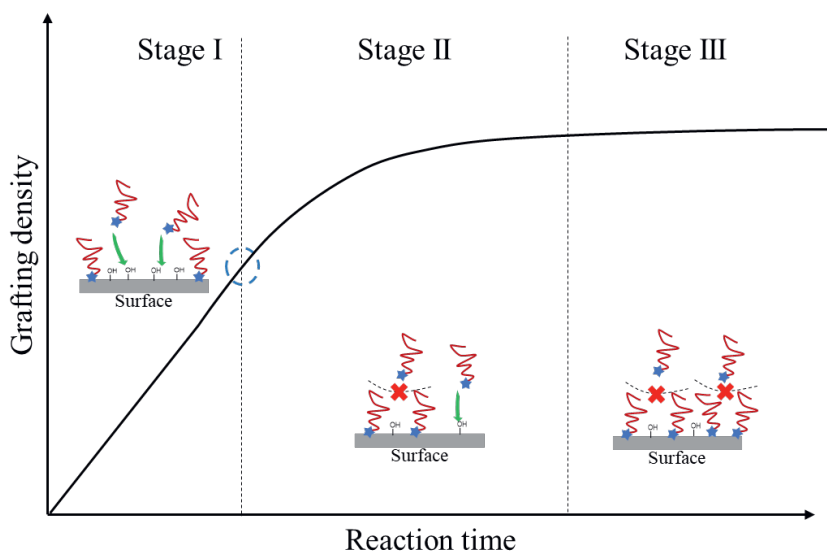
Figure 1.3: Schematic representation of the grafting density of a reaction between an organic group and a dense inorganic surface as a function of the reaction time. The three different stages of the grafting reaction are schematically presented in this diagram. This representation was inspired by references [24], [37,] and [38].

For the organo-functionalization of inorganic supports, two main approaches are used, grafting-to and grafting-from, as summarized in Figure 1.4. In the grafting-to approach, pre-made molecules are grafted on a pristine or pre-functionalized inorganic substrate. Grafting-to is a simple methodology that typically involves polymers already functionalized with a variety of linking groups. However, due to the relatively large size of the molecules that are typically used, the concentration of

the grafted species on the (pore wall) surface can be significantly lower than the theoretical amount for monolayer formation.[34] In the second method, the grafting-from approach, a small molecule consisting of a linking and a functional group (chain length of 5 to 10 atoms) is grafted on the support. In a subsequent step, an in-situ polymerization is promoted from the grafted species on the inorganic surface to form the polymer. Due to the relatively small size of the monomers used, less diffusion limitation is observed if compared with the grafting-to approach, and therefore grafting-from results in higher grafting densities.[34] However, grafting-from is a multistep method that requires precise control of the reaction conditions to form the desired molecular size of the grafted species. Furthermore, for in-situ polymerizations, often catalysts and other reagents (e.g., an initiator) are necessary for the formation of the polymer. Hence, for both approaches, there are compelling reasons in their favour for use in membrane fabrication.
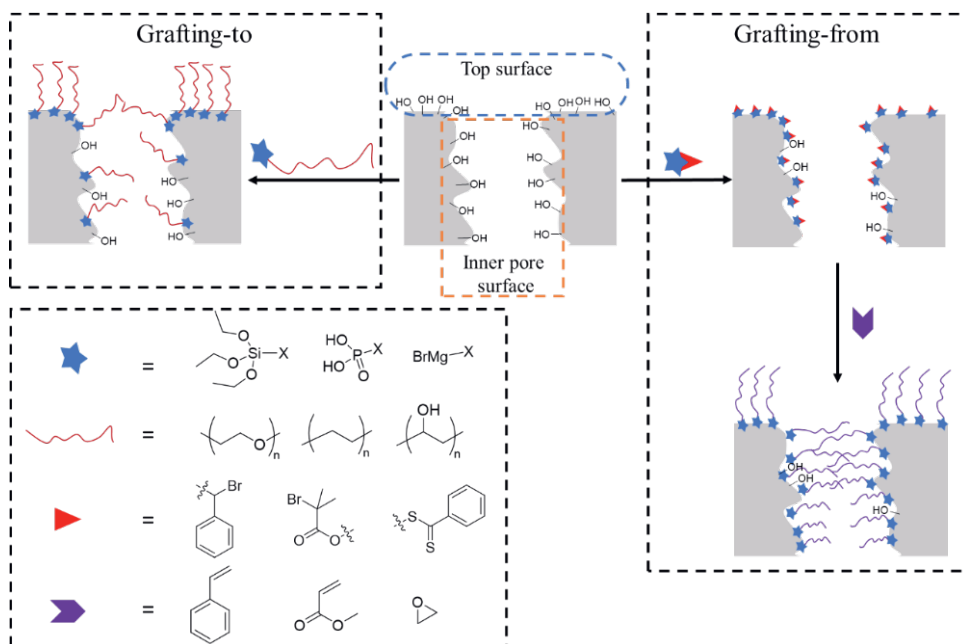
Figure 1.4: Schematic representation of grafting-to (A) and grafting-from (B) approaches, which are used in the chemical modification of inorganic substrates. (C) Examples of linking groups (★), polymers (〜), initiators/polymerization agents (▶), and monomers (➤) are used in membrane fabrication through the grafting of inorganic supports.

Another approach to describe the grafting of porous inorganic supports is to consider where the functionalized separation layer is located. One way is to graft inside the

20

inorganic pores, where the separation layer is not a defined polymeric layer but a combination of the inorganic matrix with small molecules, grafted evenly in the inorganic pores. Such membranes can be made by grafting brushes or small crosslinked polymeric chains inside an inorganic substrate, as demonstrated in Figure 1.5A. A second way is to graft the organic phase only at the top surface of the support leaving the pores pristine, as schematically given in Figure 1.5B. Such a selective layer is typically a crosslinked polymeric layer. To obtain such a configuration, a stepwise method is usually applied. Both functionalization methods will be respectively discussed in the next sections, 3.1 and 3.2, while in section 4, an evaluation of the preparation and performance of these membranes will be given, as well as the scope and objective of the research, as described in this thesis.
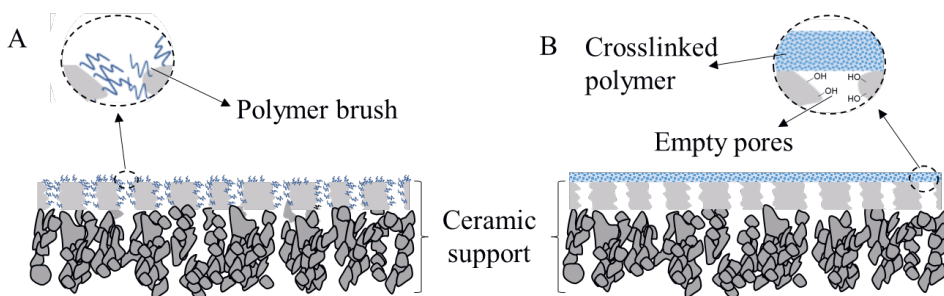
Figure 1.5: Schematic representation of two distinct organically functionalized inorganic membranes. (A) The organic layer, such as polymer brushes, functionalized inside the pores of the active inorganic layer and (B) on top of the inorganic support.

1.3.1. Polymers functionalized at the inner pore surface of the inorganic support

A system that is discussed well in many studies is grafting γ-alumina-coated α-alumina supports with PDMS.[39–43] PDMS is an apolar polymer, and by grafting it on the superhydrophilic alumina supports, apolar, hydrophobic membranes were formed. In these studies, the authors employed different polymer lengths (repeating units n = 10 and 39) to form brush-like layers in the pores of the γ-alumina layer. In all cases, a grafting-to approach was applied, where a small functional (linker) molecule was grafted via vapor phase in the pores of the support, followed by a reaction of the PDMS brushes with the linker molecule. The results showed that the brush-like[39,40,42] polymers showed better solute retention in toluene (65 % retention of a dye of 457 Da) in comparison to isopropanol (35 % retention).[39,40,42] Because of their apolar character, the PDMS brushes swell stronger in apolar toluene than in the polar isopropanol, leading to smaller pores and hence better retention of the dye

dissolved in toluene. This was also observed by Merlet et al.,[43] who studied in detail the transport behaviour of the confined grafted PDMS brushes in inorganic membranes using different solute/solvent mixtures. The authors correlated the stronger degree of swelling of the PDMS brushes in apolar solvents with better retention performance of the membranes and, in this way, demonstrated that the behaviour of the brush-like PDMS layer depends on the type of solvent used. According to Minko,[34] at high grafting densities, polymer brushes "push" one another and extend away from the surface, thereby minimizing the solvent dependence on swelling and consequently on membrane separation performance. Therefore, by increasing the grafting density in the pores, the solvent dependence on the separation performance is less, and the confined grafted PDMS membranes could potentially show a better separation performance, even in isopropanol.

Another way to minimize the reliance of polymer brushes swelling on separation performance is by crosslinking the polymer. Tanardi et al.[42] used a grafting-to approach were linear PDMS molecules were grafted and crosslinked in the confined pores of a γ-alumina layer through a stepwise method. The crosslinked PDMS layer showed a better separation performance in toluene (1.3 L m^{-2} h^{-1} bar^{-1}; 95 %) compared to isopropanol (0.4 L m^{-2} h^{-1} bar^{-1}; 80 %) with Sudan Black B used as solute (457 Da). Even though the crosslinked layer showed a better separation performance in an apolar solvent, the separation performance in both apolar and polar solvents was significantly improved compared to the brush-like PDMS layers discussed in the previous paragraph. Hence, crosslinking can minimize the dependency of the separation performance on the solvent of the polymer functionalized inorganic membranes.

Tanardi et al.[44] used the grafting-to method to form hydrophilic NF membranes by grafting polyethylene glycol (PEG) brushes on γ-alumina mesoporous layers (on α-alumina supports). The membrane performance was studied separately in a mixture of Sudan Black B (457 Da) in hexane (3.7 L m^{-2} h^{-1} bar^{-1}) or ethanol (0.8 L m^{-2} h^{-1} bar^{-1}). The membranes in hexane ("bad" solvent) showed a Sudan Black B retention of 54%, while in ethanol ("good" solvent), the retention reached 89%. Similarly to the PDMS grafted membranes, the retention mechanism was attributed to the varying degree of swelling of the grafts in the two solvents. For the characterization of the grafted species via FTIR and NMR and to determine its thermal stability, PEG grafted on γ-alumina powder was used as a model system. Even though the reactivity of the powder and the support should be similar, the powder differs significantly in shape, porosity, and surface area compared to the support and can lead to imprecise conclusions, which again hinders further understanding of the grafting reaction and separation mechanism.

Thus far, only organosilanes have been discussed here as coupling/linking agents in the fabrication of organically functionalized inorganic membranes. However, other coupling agents are available as well (e.g., Figure 1.4). The Buekenhoudt group at VITO used phosphonic acid, and Grignard reagents as coupling agents to graft small linear alkanes on microporous titania supports ($\varnothing_{pore} = 0.9 - 1$ nm).[45–48] The titania substrate was organically functionalized to either increase the membrane fouling resistance[49,50] by grafting small organic molecules, such as methyl or phenyl, or to enhance the NF performance in solvents,[51–53] by grafting linear alkanes (5 – 12 carbon atoms). For all cases, Grignard grafting was shown to be a good candidate for grafting titania supports toward the formation of stable NF hybrid membranes.

Merlet et al.[35] used the grafting-from approach to form polystyrene (PS) grafted inorganic membranes. In this work, the γ-alumina layer was first functionalized with a small initiator molecule, (3-trimethoxysilyl)propyl 2-bromo-2-methylpropionate, from which the in-situ polymerization was initiated to form PS grafted on the inorganic support and in the inorganic pores. The polymerization reaction (atom-transfer radical polymerization or ATRP) was optimized for both γ-alumina powders and flat-sheet alumina substrates. It was found that the kinetics of the reaction at the substrates' outer and inner (pore) surfaces were different with the polymerization at the outer surface of the substrate being significantly faster than the inner surface (i.e., pores). To adjust for this difference and to promote pore surface grafting, the initiator-grafted membranes were etched with oxygen plasma to deactivate only the initiator at the outer surface while the inner molecules were not affected. This forced the polymerization to occur only in the pore on the pore wall surface, yielding membranes with enhanced separation (90% retention of diphenyl anthracene or DPA: 330 Da) and a more than factor two increase in permeability (2 L m^{-2} h^{-1} bar^{-1}) performance compared to the unetched ones (86% DPA retention and permeability of 0.6 L m^{-2} h^{-1} bar^{-1}). This work showcased the importance of control over the grafting reaction and how it affects the performance of the membrane.

1.3.2. Polymer layer applied on top of an inorganic support

Organic layers, covalently bound at the top surface of inorganic supports, are also employed for NF applications. Such membranes usually fashion a thin and uniform selective layer on top of the support, which controls the separation efficiency of the membrane.

Amirilargani et al.[54] synthesized via a grafting-to method organically-modified alumina membranes with alternating co-polymers of maleic anhydride and various alkenes (from hexyl to octadecyl). The maleic anhydride was used to link the inorganic surface and the polymer. The researchers synthesized the co-polymers via a radical-initiated polymerization reaction and subsequently grafted them on γ-alumina in solution. The ring opening reaction between the maleic anhydride and the

inorganic surface took place at room temperature. FTIR analysis and water contact angle analyses were used to describe the modification of the inorganic support. However, the FTIR analysis provided limited information on the grafting reaction, and again γ-alumina flakes were used instead of the membrane. Furthermore, the ester bond (linker between inorganic and organic phase) was not explicitly shown by the FTIR analysis, and further discussion was not provided. This can mean that the polymer was either partly reacted or that polymers were physically adsorbed on the surface. Nevertheless, the significant increase in retention of Sudan black B (457 Da) in ethanol or toluene ($\sim$ 2 L m^{-2} h^{-1} bar^{-1}), as compared to the pristine support, established the successful formation of hybrid NF membranes.

In a recent publication, Amirilargani[55] employed an old-school type of material, melamine resin, to form a novel hybrid NF membrane on α-alumina supports via a grafting-from method. First, the α-alumina support was pre-functionalized with (3-aminopropyl)trimethoxysilane (APTES) to form a covalent bond between the organic and inorganic phases. Then, an in-situ polymerization between melamine and either terephthaldehyde (MT) or isophthaldehyde (MI) was performed in the presence of the pre-functionalized support to form a distinct separation layer. A direct confirmation of the formation of a distinct layer was done via FE-SEM, where the organic layer was shown to be deposited on top of the α-alumina support. The membranes were tested in toluene (MT: 7.8 L m^{-2} h^{-1} bar^{-1}; MI: 6 L m^{-2} h^{-1} bar^{-1}) and n-hexane (MT: 9.2 L m^{-2} h^{-1} bar^{-1}; MI: 6 L m^{-2} h^{-1} bar^{-1}) with various dyes, and both membranes showed near complete rejection of solutes of 457 Da. Interestingly, the two polymers (MT and MI) functionalized inorganic membranes showed different solvent permeabilities but similar dye retentions, which was attributed to the thicker layer formed with the MT (380 nm) as compared to the MY membrane (450 nm). It is suggested that the two different dialdehyde monomers result in layers with different microstructures due to their different geometries since both the thickness and the pore size (MT: 0.5 nm and MI: 0.4 nm) differ between the two membranes.

Amelio et al.[56] employed a layer-by-layer approach to grow a polyamide layer on top of a functionalized anodic alumina support. The membrane was first grafted with APTES, and subsequently, the membrane was immersed consecutively in different solutions containing each of the two monomers (trimesoyl chloride and m-phenyldiamine). The procedure was repeated for up to 6 cycles, and a comparison of the membrane microstructure (roughness, thickness, and hydrophilicity) and performance was made. The authors observed that by increasing the number of cycles, the permeability decreased from 14 to < 1 L m^{-2} h^{-1} bar^{-1} (6.5 cycles), and the sodium chloride (NaCl) rejection increased, reaching values up to 76% rejection (17.5% NaCl rejection after only 2 cycles). Unfortunately, the authors do not compare the rejection of the pristine support before modifying the surface. However, as the pristine support is an ultrafiltration membrane ($\text{\O}_{pore} = 20$ nm) is expected that

24

the support exhibits significantly lower retention of NaCl. The authors also showed that the roughness of the layer formed through their method was lower than the average layer produced *via* interfacial polymerization (IP). The aim of Amelio's work[56] was to reduce the roughness of the membrane surface in order to limit fouling, which was ultimately not directly proven.

Thus far, the polymer materials chosen for the separation layer were mainly amorphous polymers. However, in recent years the development of new chemical methods has resulted in the formation of crystalline porous polymers. These polymers are considered wonder materials in many fields. One of those fields is membrane technology, where these crystalline polymers are expected to show unprecedented performances due to their well-defined and porous structures and a high degree of crosslinking.

An example is the fabrication of an inorganic supported nanofiltration membrane by Fan et al.,[57,] who prepared a two-dimensional (2D) covalent organic framework (COF) on an inorganic support. A tubular, asymmetric, inorganic support was used consisting of a macroporous γ-alumina layer with 100 nm pore diameter (5 μm thickness),[58] supported on an α-alumina layer. An imine-linked COF layer was formed via a stepwise approach where the γ-alumina layer was first functionalized with APTES, then a layer of 1,3,5-triformyl-benzene (TFB) was attached to the outer surface of the support. Finally, the reaction between para-phenylenediamine (PDA) and TFB, catalysed by acetic acid in dioxane for 3 days, resulted in the final hybrid membrane. By combining SEM and EDS (Energy Dispersive X-ray Spectroscopy) analysis, the layer formation at the top of the inorganic support was confirmed (Figure 1.6a-c). The crystallinity of the polymeric layer was investigated by XRD analysis of the powder, separately formed during the fabrication of the membrane. By combining XRD results with molecular simulations, the authors demonstrated the formation of a well-defined 2D structure. In this regard, the authors expected that the separation layer exhibited similar structural characteristics as the powder, which would result in well-defined pore size and a layered structure. To prove this expectation, the authors tested the imine-linked COF inorganic membrane in a series of aqueous solutions of organic dyes ranging in molecular weight from 320 to 1000 Da. The membrane completely rejected solutes above 450 Da, which is correlated to a molecular size of approximately 1.2 nm. Besides, a pore size of 1.8 nm was calculated through molecular simulation for a crystalline 2D layered material which correlated well with the dye rejections, thus demonstrating that the layer formed on the inorganic support was structurally related to the simulated imine-linked COF material. Furthermore, the high water permeability ($40 - 80$ L m^{-2} h^{-1} bar^{-1}) of this COF membrane demonstrated the potential of porous 2D materials in membrane technology. However, the chemical stability of the polymer itself is doubtful since imines are known for their dynamic character under, particularly but not exclusively,

acidic conditions.[59] Overall, COF membranes have shown to be stable only in water and some organic solvents; however, thus far, no COF membrane has been tested under extreme pH or in the presence of other reactive chemicals, such as primary aliphatic amines. Thus, the COF membranes still need to prove themselves as potential candidates in SRNF/STNF.

Wang et al.[60] used a 3D imine-linked COF to graft on a γ-alumina tubular substrate (similar characteristics as in[57]) to form a nanofiltration membrane. According to the authors, a 2D COF, due to its planar geometry, cannot form a covalent linkage with the inorganic support and the COF, whereas a 3D COF is able to covalently link with the support. Furthermore, due to the high surface area of a 3D COF, it would allow for higher permeabilities than a 2D COF. However, as mentioned in the previous paragraph, a 2D COF can also be covalently grafted on an inorganic support via a similar preparation method.[57] Nevertheless, Wang et al.[60] prepared the 3D COF via a similar stepwise method as described by Fan et al.[57,] with the main difference being the monomers used (tetrakis-(4-anilyl)-methane and terephthalaldehyde). After synthesis of the 3D COF, analysis of the top surface by means of SEM showed the presence of aggregates on the support (Figure 1.6d) which, according to the authors, indicates good surface coverage. SEM-EDS analysis showed that the polymer was most probably not only on the top but also inside the inorganic support (Figure 1.6f). This is different from the imine COF, as described by Fan et al.[57], and can be related to the 3D structure of the polymer[60] that can grow in every possible direction, including in the pores of the support (100 nm). The 3D COF membrane was tested in aqueous solutions with different dyes, and the MWCO was approximately 410 Da. Interestingly, the MWCO of the 2D COF membrane described by Fan et al.[57] and this 3D COF membrane differ slightly, indicating similar pore sizes for both membranes. However, the 3D COF with a thicker selective layer (5.5 μm) exhibited significantly higher water permeability (150 L m^{-2} h^{-1} bar^{-1}) than the 2D COF (76 L m^{-2} h^{-1} bar^{-1}) with a thickness of 400 nm. of the 3D COF was, even though with even some crystals residing inside the inorganic matrix (Figure 1.6f) rendering the 3D COF layer significantly thicker than the 2D COF described by Fan et al.[57] The difference in thickness can be related to the different macrostructural nature of the two polymers. As shown in Figure 1.6d, the 3D COF forms particles inside the support, whereas the 2D COF (Figure 1.6a) forms a unified layer at the top of the support. On the other hand, the 3D COF, due to a more open structure, can lead to higher permeabilities compared to the 2D layer.
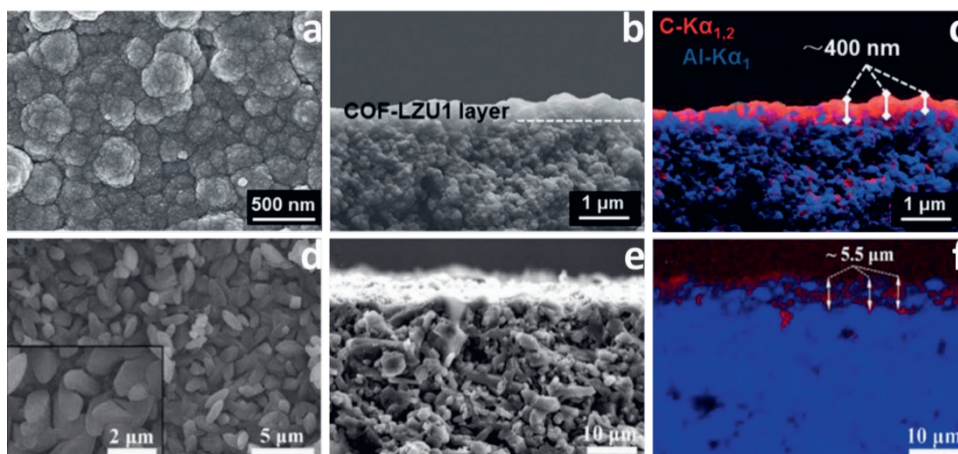
Figure 1.6: As reported in the literature, the SEM and EDS analysis of the two COF layers grafted on an alumina support. (a) Micrograph of the top surface of the 2D COF layer.[57] (b) Micrograph of the cross-section of the 2D COF layer grafted on an alumina support.[57] (c) EDS analysis of the cross-section of the 2D COF layer grafted on an alumina support.[57] (d) Micrograph of the top surface of the 3D COF layer.[60] (e) Micrograph of the cross-section of the 3D COF layer grafted on an alumina support.[60] (f) EDS analysis of the cross-section of the 3D COF layer grafted on an alumina support.[60]

1.4. Evaluation of state-of-the-art organo-functionalized inorganic membranes and scope of the thesis

The literature discussed in the previous sections shows that grafting inorganic membranes has significantly progressed membrane performance, particularly when highly ordered polymers are used. This progress is fuelled by innovative chemistries used nowadays to graft membranes, like controlled radical polymerizations. However, there are still some critical questions arising from this literature study. In this section, the work reported in the literature on grafted inorganic NF membranes, as described in sections 3.1 and 3.2, is evaluated, and several research questions are generated which relate to the aim of the work described in this thesis.

The grafting-to approach is the most commonly used functionalization method in the literature. This is because grafting-to is an easy, quick method, and with the grafting-to approach, commercially available polymers can also be used. However, with bulkier molecules (polymers), the grafting efficiency can be significantly low as larger molecules exert stronger steric hindrance to the free molecules in the bulk solution. On the other hand, with smaller molecules (e.g., monomers in case of grafting-from), the steric hindrance is significantly lower and the grafting efficiency high. To control the pore size and layer thickness, with grafting-to approaches, one

should control the precursor diffusion inside the pores of the inorganic layer at all times. Usually, grafting-to is done in the liquid phase under reflux conditions. However, better grafting efficiencies can be achieved by performing the reaction in the gas phase (chemical vapour deposition). In conclusion, it is crucial to understand the mechanism of the grafting reaction in order to be able to produce good and reliable NF hybrid membranes.

Concerning the materials used for the functionalization of inorganic membranes, organosilanes are the most widely applied family of linking groups. This is related to the commercial availability and the high reactivity of organosilanes with metal oxides (M-OH) in both solution and vapor phases, as well as their unique ability to homocondensate and form complete monolayers.[29,30] But organosilanes also have two major drawbacks. First, organosilanes react uncontrollably with water. This means that when during the grafting reaction, relatively large amounts of water are present on the inorganic surface (or even small amounts in the solvent), multilayers of organosilanes can form, resulting in defective organic layers.[29] The second drawback is the relatively low hydrolytic stability of the silanol bond with various inorganic surfaces, such as alumina and titania.[29,30] The instability seems to be catalytically activated under basic conditions.[61,62] However, not much has been done to study the stability of grafted organosilanes in pure water. Additionally, as organosilane stability is questioned, other linking groups that are more chemically stable should be considered.

Other emerging linking groups primarily used for the fabrication of organically-modified inorganic membranes are Grignard reagents[52] and phosphonates.[50] The former is a class of highly reactive organometallic (mainly magnesium) reagents that react with metal(loid) oxide surfaces (typically titania, silica, and potentially zirconia)[30] and form strong metal-carbon covalent bonds in a monodentate fashion. However, Grignard reagents react aggressively with water or oxygen, which means that the grafting reaction can only be conducted under highly scrutinized conditions (inert atmosphere and using anhydrous organic solvents).[30,63] On the other hand, phosphonates can react with the inorganic surface in water or other solvents, do not undergo homocondensation reactions preventing multilayer formation, and finally exhibit stable covalent bonds with alumina, zirconia, and titania.[29] Therefore phosphonates can be considered as potential alternatives to organosilanes. However, their reactivity with inorganic materials and their stability is not fully understood and needs further research on both the grafting chemistry and the performance of these membranes.

Thus far, most polymers used for grafting of inorganic membranes are typically, with some exceptions, hydrophobic or mostly consist of apolar backbones (e.g. aromatic rings). Polar polymers (e.g. polyvinyl alcohols) are unquestionably the best choice

for aqueous applications, as they "like" water and therefore show lower resistance to water flow than apolar polymers. For that reason, PEG can be interesting for aqueous applications.[44] Furthermore, ordered structures that have relatively large apolar backbones (aromatic rings) show remarkable performances, meaning that other properties, such as porosity and tortuosity, also have a significant effect on the performance of the final membrane. For example, imine-linked highly ordered polymers have successfully been applied for separations in aqueous environments.[57] Although the imine COFs are not highly hydrophilic, they showed exceptional performances for water applications. Their performance can be correlated to the high porosity of the polymers (60 – 80%) and their low tortuosity, as COFs exhibit a stacking behaviour that is almost perfectly aligned and forms straight channels.[57,60] Still, the imine COFs have not been tested yet in extreme pH's or in the presence of reactive chemicals, such as primary amines, where imine COFs are suspected of being chemically unstable.

In conclusion, the polymer properties and structure are critical for the final membrane properties and hence its performance. The location of the grafted layer can also be crucial in membrane performance. For example, Merlet et al.[35] increased the separation by confining the polymer in the pores, whereas Amirilargani et al.[54] achieved similar solvent permeabilities by only functionalizing the top surface of the support with an ultrathin layer. However, the best performances were reported for membranes where the organic layer was ordered, with low tortuosity, and with supports that exhibited large pore sizes.[57,60]

The scope of the work described in this thesis can be divided into the following three pathways:
1. Development of novel methods for the fabrication of organo-functionalized inorganic membranes.
2. In-depth characterization and understanding of the chemistry of the synthesized membranes
3. Application and performance of organo-functionalized inorganic membranes for STNF

These pathways are introduced in the following three sections, with reference to the chapters of the thesis, where they will be discussed in detail.

1.4.1. Development of novel methods for the fabrication of organo-functionalized inorganic membranes

Each chapter of this thesis describes an alternative method or chemistry to engineering at the nanoscale level, either the top or pore surface of an inorganic support towards the synthesis of NF membranes. These methods can be used as potential ways to fabricate chemically, thermally and mechanically stable NF

membranes. Furthermore, attention is paid to develop more green methods to replace the wasteful membrane preparation methods often used nowadays.

In **Chapter 2**, the influence of the linking group on the hydrolytic stability of the membrane is described. PEG-phosphonic acids and PEG-alkoxysilanes were grafted on γ-alumina supports, including flakes and flat-sheet membranes. Both materials were analysed by different techniques, including NMR and water permeability tests, to understand the long-term stability of the graft in water.

In **Chapter 3**, the main goal was to graft the pore surface of alumina supports with organophosphonic acids. A solid-state reaction was used with three different polymers, including two polar (PEG) and one apolar (octadecyl-). The chapter focuses on understanding the solid state reaction between organophosphonic acids and γ-alumina, as well as the influence of the polymeric chain on the grafting reaction. Finally, the potential of the method for membrane application is described.

In **Chapter 4**, the work is focused on the formation of a crosslinked thioether-based polymeric layer on top of an alumina support. A grafting-from approach is applied, employing a "click" reaction along with a vapor polymerization, occurring at the interface between liquid and gas. The use of a "click" reaction and vapor phase polymerization allowed for lower monomer use and hence less formation of waste. This preparation method is one of the few methods reported in membrane fabrication that uses vapor-liquid reactions and is the only one done on a porous support.

In **Chapter 5**, the goal is to form a well-ordered crystalline polyimide (PI) network via a grafting-from approach. Here, the influence of the initiator location on the inorganic surface will be described in detail. The membranes were tested in a series of solvents to study their stability in water and organic solvents with varying polarities. One aim was to find an efficient way to control the in-situ formation of the polymeric network on a porous inorganic support by controlling the location of the grafting reaction.

In **Chapter 6**, different reported synthetic methods for the formation of crystalline PI materials are studied in detail. Additionally, an alternative, easy, and potentially green PI synthesis is developed and compared with the reported methods. The study focuses on the yield of the different syntheses and the structure of the final PIs formed. Finally, as a case study, the method developed in this chapter was applied to an inorganic porous support to showcase the potential of the method to coat porous surfaces with PI materials.

1.4.2. In-depth characterization and understanding of the chemistry of the synthesized membranes

By understanding the chemical make-up of the grafted polymer on the inorganic support, its location, microstructure, crystallinity, etc., a better understanding of the membrane performance and the stability of the membrane under filtration conditions are obtained. FTIR, due to its simplistic and non-destructive method of analysis, was used throughout the different chapters. In some cases, NMR was also used to study the chemical structures of the polymeric layer. Cyclohexane permporometry, again a non-invasive method, was used to investigate the pore size of the inorganic hybrid membranes after various chemical treatments. Even though the method is limited to the molecular size of cyclohexane (0.9 nm), this analysis still provides insights into the pore diameter range of the synthesized membrane samples and is used extensively in this work. Other techniques, such as atomic force microscopy (AFM) and thermogravimetric analysis (TGA), are used as complementary techniques to understand better the materials produced through this work. All these methods together facilitated accurate descriptions of the membranes fabricated and could be used for potentially up-scaling the membrane fabrication, and/or improving the materials through adjusting the methods, and finally to develop materials for other research areas.

In **Chapter 2**, liquid ^{1}H NMR and water permeability were employed as in situ methods to understand the hydrolytic stability of the grafted samples. Electron microscopy (SEM) was used to visualize the effect of the chemical treatment, such as polymerization, on our inorganic supports. In **Chapters 4** and **5**, SEM was used to localize the polymer on the inorganic support. In **Chapter 4**, due to the ultrathin layers formed on the support, spectroscopic ellipsometry was used to corroborate the results obtained with SEM analysis to further support the formation of a homogeneous and ultrathin thioether-based layer.

Elemental analysis, such as energy-dispersive X-ray spectroscopy (EDS) or X-ray fluorescence (XRF), were used as complementary methods for qualitative elemental analysis. For instance, in **Chapter 4**, XRF was used to measure the relative amounts of bromide on the surface of the support after each reaction step. EDS was used in **Chapter 5** to understand the influence of the pre-functionalization step on the grafting-from method applied to synthesize the final membranes.

1.4.3. Application and performance of organo-functionalized inorganic membranes

Organo-functionalized inorganic membranes have the advantage of high chemical, thermal and mechanical stability over their polymeric counterparts. Thus, these

membranes can be used in applications where polymeric membranes fail, including aqueous mixtures of solvents that show destructive effects on polymeric membranes.[15] In this work, a series of different organically functionalized inorganic membranes were prepared that can be categorized into three main groups; PEG- (**Chapters 2** and **3**), polythioether (**Chapter 4**), and polyimide-grafted (**Chapter 5**) alumina membranes.

In **Chapter 2**, the performance of PEG grafted membranes in an aqueous environment for prolonged times is described. In **Chapter 3**, the PEG grafted membranes were thoroughly washed under high water pressures and subsequently tested in water. Furthermore, in **Chapter 7**, a preliminary investigation was done on the performance of the PEG grafted membranes in water/solvent mixtures.

The thioether-based membranes, described in **Chapter 4**, were tested continuously in water and organic solvents to study their chemical stability. Besides, the thermal stability of these membranes was also investigated. Furthermore, in **Chapter 7**, preliminary results are given on the performance of the thioether-membranes in water/solvent mixtures to further understand their stability in real applications.

Similarly, the PI nanoconfined membranes, described in **Chapter 5**, were tested in a series of solvents to study their performance as NF membranes. Furthermore, in **Chapter 7**, the Rhodamine B retention in water and water/solvent mixtures is discussed for some of the membranes treated in this thesis.

Finally, in **Chapter 7**, the synthesis methods and the performance of the various membranes developed in this work are evaluated, and suggestions for further research are provided.

1.5. References

(1)   Lively, R. P.; Sholl, D. S. *From Water to Organics in Membrane Separations*; 2017. https://doi.org/10.1038/nmat4860.

(2)   Drioli, E.; Romano, M. Progress and New Perspectives on Integrated Membrane Operations for Sustainable Industrial Growth. *Industrial and Engineering Chemistry Research*. American Chemical Society March 7, 2001, pp 1277–1300. https://doi.org/10.1021/ie0006209.

(3)   Dong, G.; Nagasawa, H.; Yu, L.; Guo, M.; Kanezashi, M.; Yoshioka, T.; Tsuru, T. Energy-Efficient Separation of Organic Liquids Using Organosilica Membranes via a Reverse Osmosis Route. *J. Memb. Sci.* **2020**, *597*, 117758. https://doi.org/10.1016/j.memsci.2019.117758.

(4)   Kelly, R. M. General Processing Considerations. In *Handbook of Separation Process Technology*; Rousseau, R. W., Ed.; Wiley , 1987; pp 197–225.

(5)   Marchetti, P.; Solomon, M. F. J.; Szekely, G.; Livingston, A. G. Molecular Separation with Organic Solvent Nanofiltration: A Critical Review. *Chem. Rev.* **2014**, *114*, 10735–10806. https://doi.org/10.1021/cr500006j.

(6)   Van der Bruggen, B.; Curcio, E.; Drioli, E. Process Intensification in the Textile Industry: The Role of Membrane Technology. *J. Environ. Manage.* **2004**, *73* (3), 267–274. https://doi.org/10.1016/j.jenvman.2004.07.007.

(7)   Buekenhoudt, A.; Beckers, H.; Ormerod, D.; Bulut, M.; Vandezande, P.; Vleeschouwers, R. Solvent Based Membrane Nanofiltration for Process Intensification. *Chemie Ing. Tech.* **2013**, *85* (8), 1243–1247. https://doi.org/10.1002/cite.201200247.

(8)   Peeva, L.; Burgal, J. da S.; Valtcheva, I.; Livingston, A. G. Continuous Purification of Active Pharmaceutical Ingredients Using Multistage Organic Solvent Nanofiltration Membrane Cascade. *Chem. Eng. Sci.* **2014**, *116*, 183–194. https://doi.org/10.1016/j.ces.2014.04.022.

(9)   Fodi, T.; Didaskalou, C.; Kupai, J.; Balogh, G. T.; Huszthy, P.; Szekely, G. Nanofiltration-Enabled In Situ Solvent and Reagent Recycle for Sustainable Continuous-Flow Synthesis. *ChemSusChem* **2017**, *10* (17), 3435–3444. https://doi.org/10.1002/cssc.201701120.

(10)   Razali, M.; Didaskalou, C.; Kim, J. F.; Babaei, M.; Drioli, E.; Lee, Y. M.; Szekely, G. Exploring and Exploiting the Effect of Solvent Treatment in Membrane Separations. **2017**. https://doi.org/10.1021/acsami.7b01879.

(11)   Robinson, J. P.; Tarleton, E. S.; Millington, C. R.; Nijmeijer, A. Solvent Flux through Dense Polymeric Nanofiltration Membranes. *J. Memb. Sci.* **2004**, *230* (1–2), 29–37. https://doi.org/10.1016/J.MEMSCI.2003.10.027.

(12)   Jimenez Solomon, M. F.; Bhole, Y.; Livingston, A. G. High Flux Membranes for Organic Solvent Nanofiltration (OSN)-Interfacial Polymerization with Solvent Activation. *J. Memb. Sci.* **2012**, *423–424*, 371–382. https://doi.org/10.1016/j.memsci.2012.08.030.

(13)   Karan, S.; Jiang, Z.; Livingston, A. G. Sub-10 Nm Polyamide Nanofilms with Ultrafast Solvent Transport for Molecular Separation. *Science* **2015**, *348* (6241), 1347–1351. https://doi.org/10.1126/science.aaa5058.

(14)   Van Der Bruggen, B.; Braeken, L.; Vandecasteele, C. Flux Decline in Nanofiltration Due to Adsorption of Organic Compounds. *Sep. Purif. Technol.* **2002**, *29* (1), 23–31. https://doi.org/10.1016/S1383-5866(01)00199-X.

(15)   Tempelman, K.; Casanova, S.; Benes, N. E. The Effect of Hydrocarbon

Pollution on Polysulfone-Based Membranes in Aqueous Separations. *Sep. Purif. Technol.* **2019**, *224*, 348–355. https://doi.org/10.1016/j.seppur.2019.05.013.

(16) Xia, L.; Ren, J.; Weyd, M.; McCutcheon, J. R. Ceramic-Supported Thin Film Composite Membrane for Organic Solvent Nanofiltration. *J. Memb. Sci.* **2018**, *563*, 857–863. https://doi.org/10.1016/J.MEMSCI.2018.05.069.

(17) Goh, K. S.; Chen, Y.; Chong, J. Y.; Bae, T. H.; Wang, R. Thin Film Composite Hollow Fibre Membrane for Pharmaceutical Concentration and Solvent Recovery. *J. Memb. Sci.* **2021**, *621*, 119008. https://doi.org/10.1016/J.MEMSCI.2020.119008.

(18) Yi Li; Sha Li; Junyong Zhu; Alexander Volodine; Bruggen, B. V. der. Controllable Synthesis of a Chemically Stable Molecular Sieving Nanofilm for Highly Efficient Organic Solvent Nanofiltration. *Chem. Sci.* **2020**, *11* (16), 4263–4271. https://doi.org/10.1039/D0SC00056F.

(19) Karan, S.; Jiang, Z.; Livingston, A. G. Sub-10 Nm Polyamide Nanofilms with Ultrafast Solvent Transport for Molecular Separation. *Science (80-.).* **2015**, *348* (6241), 1347–1351. https://doi.org/10.1126/science.aaa5058.

(20) Bastin, M.; Raymenants, J.; Thijs, M.; Vananroye, A.; Koeckelberghs, G.; Vankelecom, I. F. J. Epoxy-Based Solvent-Tolerant Nanofiltration Membranes Prepared via Non-Solvent Induced Phase Inversion as Novel Class of Stable Membranes. *J. Memb. Sci.* **2021**, *626*, 119206. https://doi.org/10.1016/J.MEMSCI.2021.119206.

(21) Meyer, E. E.; Rosenberg, K. J.; Israelachvili, J. Recent Progress in Understanding Hydrophobic Interactions. *Proc. Natl. Acad. Sci.* **2006**, *103* (43), 15739–15746. https://doi.org/10.1073/PNAS.0606422103.

(22) Vanherck, K.; Koeckelberghs, G.; Vankelecom, I. F. J. Crosslinking Polyimides for Membrane Applications: A Review. *Prog. Polym. Sci.* **2013**, *38* (6), 874–896. https://doi.org/10.1016/j.progpolymsci.2012.11.001.

(23) Maaskant, E.; Tempelman, K.; Benes, N. E. Hyper-Cross-Linked Thin Polydimethylsiloxane Films. *Eur. Polym. J.* **2018**, *109*, 214–221. https://doi.org/10.1016/J.EURPOLYMJ.2018.09.052.

(24) Jimenez-Solomon, M. F.; Song, Q.; Jelfs, K. E.; Munoz-Ibanez, M.; Livingston, A. G. Polymer Nanofilms with Enhanced Microporosity by Interfacial Polymerization. **2016**. https://doi.org/10.1038/NMAT4638.

(25) Ding, M.; Cai, X.; Jiang, H.-L. Improving MOF Stability: Approaches and

34

Applications. **2019**. https://doi.org/10.1039/c9sc03916c.

(26) Yang, C. H.; Chang, J. S.; Lee, D. J. Chemically Stable Covalent Organic Framework as Adsorbent from Aqueous Solution: A Mini-Review. *Journal of the Taiwan Institute of Chemical Engineers*. Taiwan Institute of Chemical Engineers May 1, 2020, pp 79–91. https://doi.org/10.1016/j.jtice.2020.02.008.

(27) Khan, N. A.; Zhang, R.; Wu, H.; Shen, J.; Yuan, J.; Fan, C.; Cao, L.; Olson, M. A.; Jiang, Z. Solid−Vapor Interface Engineered Covalent Organic Framework Membranes for Molecular Separation. *J. Am. Chem. Soc* **2020**, *142*, 13450–13458. https://doi.org/10.1021/jacs.0c04589.

(28) Drelich, J.; Chibowski, E. Superhydrophilic and Superwetting Surfaces: Definition and Mechanisms of Control. *Langmuir* **2010**, *26* (24), 18621–18623. https://doi.org/10.1021/LA1039893.

(29) Pujari, S. P.; Scheres, L.; Marcelis, A. T. M.; Zuilhof, H. Covalent Surface Modification of Oxide Surfaces. *Angew. Chemie - Int. Ed.* **2014**, *53* (25), 6322–6356. https://doi.org/10.1002/anie.201306709.

(30) Merlet, R. B.; Pizzoccaro-Zilamy, M. A.; Nijmeijer, A.; Winnubst, L. Hybrid Ceramic Membranes for Organic Solvent Nanofiltration: State-of-the-Art and Challenges. *J. Memb. Sci.* **2020**, *599*, 117839. https://doi.org/10.1016/j.memsci.2020.117839.

(31) Kishor, R.; Ghoshal, A. K. APTES Grafted Ordered Mesoporous Silica KIT-6 for CO2 Adsorption. *Chem. Eng. J.* **2015**, *262*, 882–890. https://doi.org/10.1016/J.CEJ.2014.10.039.

(32) Issa, A. A.; Luyt, A. S. Kinetics of Alkoxysilanes and Organoalkoxysilanes Polymerization: A Review. *Polym. 2019, Vol. 11, Page 537* **2019**, *11* (3), 537. https://doi.org/10.3390/POLYM11030537.

(33) Liu, Y.; Li, Y.; Li, X.-M.; He, T. Kinetics of (3-Aminopropyl)Triethoxylsilane (APTES) Silanization of Superparamagnetic Iron Oxide Nanoparticles. *Langmuir* **2013**, *29* (49), 15275–15282. https://doi.org/10.1021/LA403269U.

(34) Minko, S. Grafting on Solid Surfaces: Grafting to and Grafting from Methods. In *Polymer Surfaces and Interfaces: Characterization, Modification and Applications*; Sramm, M., Ed.; Springer Berlin Heidelberg, 2008; pp 215–234. https://doi.org/10.1007/978-3-540-73865-7_11.

(35) Merlet, R. B.; Amirilargani, M.; de Smet, L. C. P. M.; Sudhölter, E. J. R.; Nijmeijer, A.; Winnubst, L. Growing to Shrink: Nano-Tunable Polystyrene Brushes inside 5 Nm Mesopores. *J. Memb. Sci.* **2019**, *572*, 632–640.

https://doi.org/10.1016/j.memsci.2018.11.058.

(36) Brittain, W. J.; Minko, S. A Structural Definition of Polymer Brushes. *J. Polym. Sci. Part A Polym. Chem.* **2007**, *45* (16), 3505–3512. https://doi.org/10.1002/pola.22180.

(37) Zhou, Q.; Xu, S.; Zhu, C.; Cao, B.; Kausar, F.; Xu, A.; Yuan, W. Z.; Zhang, Y. Towards High-Performance Hybrid Hydrophilic Membranes: Chemical Anchoring of Hydroxyl-Rich Nanoparticles on PVDF Membranes via a Silane Coupling Agent. *J. Mater. Sci. 2017 5219* **2017**, *52* (19), 11737–11748. https://doi.org/10.1007/S10853-017-1313-1.

(38) Lu, J.; Xue, Y.; Shi, R.; Kang, J.; Zhao, C.-Y.; Zhang, N.-N.; Wang, C.-Y.; Lu, Z.-Y.; Liu, K. A Non-Sacrificial Method for the Quantification of Poly(Ethylene Glycol) Grafting Density on Gold Nanoparticles for Applications in Nanomedicine. *Chem. Sci.* **2019**, *10* (7), 2067–2074. https://doi.org/10.1039/C8SC02847H.

(39) Pinheiro, A. F. M.; Hoogendoorn, D.; Nijmeijer, A.; Winnubst, L. Development of a PDMS-Grafted Alumina Membrane and Its Evaluation as Solvent Resistant Nanofiltration Membrane. *J. Memb. Sci.* **2014**, *463*, 24–32. https://doi.org/10.1016/J.MEMSCI.2014.03.050.

(40) Tanardi, C. R.; Pinheiro, A. F. M.; Nijmeijer, A.; Winnubst, L. PDMS Grafting of Mesoporous γ-Alumina Membranes for Nanofiltration of Organic Solvents. *J. Memb. Sci.* **2014**, *469*, 471–477. https://doi.org/10.1016/j.memsci.2014.07.010.

(41) Tanardi, C. R.; Vankelecom, I. F. J.; Pinheiro, A. F. M.; Tetala, K. K. R.; Nijmeijer, A.; Winnubst, L. Solvent Permeation Behavior of PDMS Grafted γ-Alumina Membranes. *J. Memb. Sci.* **2015**, *495*, 216–225. https://doi.org/10.1016/J.MEMSCI.2015.08.004.

(42) Tanardi, C. R.; Nijmeijer, A.; Winnubst, L. Coupled-PDMS Grafted Mesoporous γ-Alumina Membranes for Solvent Nanofiltration. *Sep. Purif. Technol.* **2016**, *169*, 223–229. https://doi.org/10.1016/J.SEPPUR.2016.05.057.

(43) Merlet, R. B.; Tanardi, C. R.; Vankelecom, I. F. J.; Nijmeijer, A.; Winnubst, L. Interpreting Rejection in SRNF across Grafted Ceramic Membranes through the Spiegler-Kedem Model. *J. Memb. Sci.* **2017**, *525*, 359–367. https://doi.org/10.1016/J.MEMSCI.2016.12.013.

(44) Tanardi, C. R.; Catana, R.; Barboiu, M.; Ayral, A.; Vankelecom, I. F. J.; Nijmeijer, A.; Winnubst, L. Polyethyleneglycol Grafting of Y-Alumina

Membranes for Solvent Resistant Nanofiltration. *Microporous Mesoporous Mater.* **2016**, *229*, 106–116. https://doi.org/10.1016/J.MICROMESO.2016.04.024.

(45) Buekenhoudt, A.; Wyns, K.; Meynen, V.; Maes, B.; Cool, P. SURFACE MODIFIED INORGANIC MATRIX AND METHOD FOR PREPARATION THEREOF. WO2O10/106167, 2015.

(46) Hosseinabadi, S. R.; Wyns, K.; Meynen, V.; Buekenhoudt, A.; Van der Bruggen, B. Solvent-Membrane-Solute Interactions in Organic Solvent Nanofiltration (OSN) for Grignard Functionalised Ceramic Membranes: Explanation via Spiegler-Kedem Theory. *J. Memb. Sci.* **2016**, *513*, 177–185. https://doi.org/10.1016/J.MEMSCI.2016.04.044.

(47) Van Heetvelde, P.; Beyers, E.; Wyns, K.; Adriaensens, P.; Maes, B. U. W.; Mullens, S.; Buekenhoudt, A.; Meynen, V. A New Method to Graft Titania Using Grignard Reagents †. *This J. is Cite this Chem. Commun* **2013**, *49*, 6998. https://doi.org/10.1039/c3cc43695k.

(48) Hosseinabadi, S. R.; Wyns, K.; Buekenhoudt, A.; Van der Bruggen, B.; Ormerod, D. Performance of Grignard Functionalized Ceramic Nanofiltration Membranes. *Sep. Purif. Technol.* **2015**, *147*, 320–328. https://doi.org/10.1016/J.SEPPUR.2015.03.047.

(49) Mustafa, G.; Wyns, K.; Buekenhoudt, A.; Meynen, V. Antifouling Grafting of Ceramic Membranes Validated in a Variety of Challenging Wastewaters. *Water Res.* **2016**, *104*, 242–253. https://doi.org/10.1016/J.WATRES.2016.07.057.

(50) Mustafa, G.; Wyns, K.; Vandezande, P.; Buekenhoudt, A.; Meynen, V. Novel Grafting Method Efficiently Decreases Irreversible Fouling of Ceramic Nanofiltration Membranes. *J. Memb. Sci.* **2014**, *470*, 369–377. https://doi.org/10.1016/j.memsci.2014.07.050.

(51) Fard, A. K.; McKay, G.; Buekenhoudt, A.; Al Sulaiti, H.; Motmans, F.; Khraisheh, M.; Atieh, M. Inorganic Membranes: Preparation and Application for Water Treatment and Desalination. *Materials*. Multidisciplinary Digital Publishing Institute January 5, 2018, p 74. https://doi.org/10.3390/ma11010074.

(52) Hosseinabadi, S. R.; Wyns, K.; Meynen, V.; Buekenhoudt, A.; Van der Bruggen, B. Solvent-Membrane-Solute Interactions in Organic Solvent Nanofiltration (OSN) for Grignard Functionalised Ceramic Membranes: Explanation via Spiegler-Kedem Theory. *J. Memb. Sci.* **2016**, *513*, 177–185.

https://doi.org/10.1016/J.MEMSCI.2016.04.044.

(53) Rezaei Hosseinabadi, S.; Wyns, K.; Meynen, V.; Carleer, R.; Adriaensens, P.; Buekenhoudt, A.; Van der Bruggen, B. Organic Solvent Nanofiltration with Grignard Functionalised Ceramic Nanofiltration Membranes. *J. Memb. Sci.* **2014**, *454*, 496–504. https://doi.org/10.1016/J.MEMSCI.2013.12.032.

(54) Amirilargani, M.; Merlet, R. B.; Nijmeijer, A.; Winnubst, L.; de Smet, L. C. P. M.; Sudhölter, E. J. R. Poly (Maleic Anhydride-Alt-1-Alkenes) Directly Grafted to γ-Alumina for High-Performance Organic Solvent Nanofiltration Membranes. *J. Memb. Sci.* **2018**, *564*, 259–266. https://doi.org/10.1016/J.MEMSCI.2018.07.042.

(55) Amirilargani, M.; Yokota, G. N.; Vermeij, G. H.; Merlet, R. B.; Delen, G.; Mandemaker, L. D. B.; Weckhuysen, B. M.; Winnubst, L.; Nijmeijer, A.; Smet, L. C. P. M.; Sudhölter, E. J. R. Melamine-Based Microporous Organic Framework Thin Films on an Alumina Membrane for High-Flux Organic Solvent Nanofiltration. *ChemSusChem* **2020**, *13* (1), 136–140. https://doi.org/10.1002/cssc.201902341.

(56) Amelio, A.; Sangermano, M.; Kasher, R.; Bernstein, R.; Tiraferri, A. Fabrication of Nanofiltration Membranes via Stepwise Assembly of Oligoamide on Alumina Supports: Effect of Number of Reaction Cycles on Membrane Properties. *J. Memb. Sci.* **2017**, *543*, 269–276. https://doi.org/10.1016/j.memsci.2017.08.067.

(57) Fan, H.; Gu, J.; Meng, H.; Knebel, A.; Caro, J. High-Flux Membranes Based on the Covalent Organic Framework COF-LZU1 for Selective Dye Separation by Nanofiltration. *Angew. Chemie Int. Ed.* **2018**, *57* (15), 4083–4087. https://doi.org/10.1002/anie.201712816.

(58) Lishun TEchnology Co.,Ltd. http://www.lishunkeji.com/en/product_mo.asp?title="Hao Yu"Single channel Ceramic Membrane Filtration (accessed Aug 25, 2021).

(59) Li, X.; Zhang, C.; Cai, S.; Lei, X.; Altoe, V.; Hong, F.; Urban, J. J.; Ciston, J.; Chan, E. M.; Liu, Y. Facile Transformation of Imine Covalent Organic Frameworks into Ultrastable Crystalline Porous Aromatic Frameworks. *Nat. Commun.* **2018**, *9* (1), 2998. https://doi.org/10.1038/s41467-018-05462-4.

(60) Wang, Z.; Si, Z.; Cai, D.; Shufeng Li, G. L.; Qin, P. Synthesis of Stable COF-300 Nanofiltration Membrane via in-Situ Growth with Ultrahigh Flux for Selective Dye Separation. *J. Memb. Sci.* **2020**, *615*, 118466. https://doi.org/10.1016/j.memsci.2020.118466.

(61) Szczepanski, V.; Vlassiouk, I.; Smirnov, S. Stability of Silane Modifiers on Alumina Nanoporous Membranes. *J. Memb. Sci.* **2006**, *281* (1–2), 587–591. https://doi.org/10.1016/J.MEMSCI.2006.04.027.

(62) Kujawa, J.; Cerneaux, S.; Kujawski, W. Investigation of the Stability of Metal Oxide Powders and Ceramic Membranes Grafted by Perfluoroalkylsilanes. *Colloids Surfaces A Physicochem. Eng. Asp.* **2014**, *443*, 109–117. https://doi.org/10.1016/J.COLSURFA.2013.10.059.

(63) Buekenhoudt, A.; Wyns, K.; Mustafa, G.; Meynen, V. Method for increasing the fouling resistance of norganic membranes by grafting with organic moeties. US 2017/0065936A1, March 9, 2017.
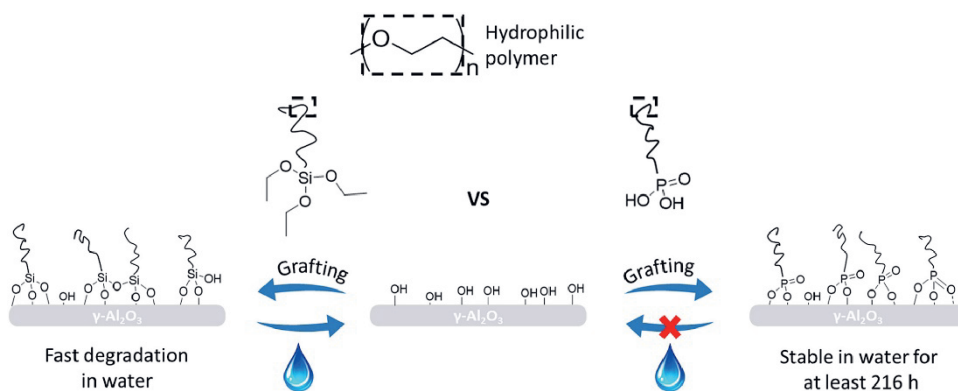
Chapter 2

Hydrolytic stability of PEG-grafted γ-alumina membranes: Alkoxysilane vs Phosphonic acid linking groups

ABSTRACT

Small polyethylene glycol (PEG) molecules were grafted on ceramic γ-alumina membranes, by making use of organo-alkoxysilanes or organo-phosphonic acids as linking groups. It was proven by FTIR that the short PEG brushes are chemically grafted into the pores of a 5 nm γ-alumina mesoporous support, which results in a decrease of the pore diameter as measured by cyclohexane permporometry (reduction of 2.1 nm). The stability of these PEG-grafted membranes was investigated in water for 216 hours. Permeability and liquid state ^{1}H NMR were used to show that PEG-modified membranes with an alkoxysilane linking group degrade rapidly during exposure to water. On the contrary, the phosphonic acid linking group remained grafted on γ-alumina supports for at least 216 hours in water. In conclusion, this work shows a promising and simple method for the fabrication in a green solvent (water) of hydrophilic organically-modified ceramic membranes, which can be successfully applied for wastewater treatment.

2.1. Introduction

Nanofiltration (NF) processes were first introduced in the 1980s for the removal of small organics and divalent ions from water, achieving a molecular weight cut-off (MWCO) in the range of 200 - 1000 Da.[1,2] The development of solvent-stable polymeric membranes makes it possible for the chemical industry to use them as alternatives to conventional separation methods, like distillation, which are energy, material, and capital intensive.[3] To broaden the application of membranes in the chemical industry, membranes must show high stability under pressures, temperatures, and in the presence of aggressive solvents. However, many polymeric membranes, while under high pressures (compaction) and/or in apolar solvents (swelling), suffer from performance drop.

Ceramic membranes can offer a solution due to their high mechanical, chemical, and thermal stability, which makes them applicable in organic solvent nanofiltration (OSN),[4,5] desalination, and wastewater treatment.[6-9] Most pristine ceramic membranes are, in general, unable to remove small organic molecules (< 400 Da) and dissolved salts, which makes them unsuitable for NF applications. To reduce the pore size of the respective membrane, polymers with low molecular weight can be chemically tethered via a linking group on porous γ-alumina,[4,5,10] silica,[11] titania[12,] or zirconia[13] supports.

Tanardi et al.,[14] used alkoxysilanes as linking groups to graft polydimethylsiloxane (PDMS) on mesoporous γ-alumina supports, resulting in higher rejections of small molecular weight polyethylene glycols (PEGs) in comparison to pristine γ-alumina membranes (MWCO of 400 to 600 Da instead of 7500 Da). In another paper,[10] γ-alumina porous supports were modified with PEG-alkoxysilane with various functional groups (e.g., bis-linking group, ureido group) and different ethylene glycol units (between 10 and 45) and it is proven, by using a combination of characterization techniques (FTIR, ^{29}Si NMR, TGA, N$_2$ sorption), that surface modification can be achieved in one step under an inert atmosphere. These membranes showed higher permeabilities for hexane than for ethanol and Sudan Black (456 Da) rejections of 54 and 89 % respectively for each solvent. However, in these works, no spectroscopic analysis of the modified membranes was conducted, to confirm chemical grafting of the polymer with the inorganic surface. Additionally, the stability of the layer during extended solvent permeation measurements was not studied.

The field of metal-oxides surface modification is dominated by alkoxysilane linking groups. However, several studies indicate that alkoxysilane grafted oxides are hydrolytically unstable.[15,16] Szczepanski et al.,[15] assessed the hydrolytic stability of (3-aminopropyl)trimethoxysilane (APS) and 3-(2- aminoethyl)aminopropyl trimethoxysilane (AEAPS) modified anodized aluminium oxide (AAO) membranes.

The primary amines, on the grafted surface, were further reacted with a succinnimidyl ester substance leading to amide bond formation. Then, the grafted membranes were treated with a phosphate buffer saline solution (pH = 7.6) and post-treatment analysis showed a decrease in the concentration of the grafted material, on the surface, over time in the buffer solution. The effect was found to be most dramatic with the AEPAS, which has a free secondary amine that according to Szczepanski affects the pH near the grafted surface where the Si-O-Al bond is located. Therefore, the authors claim that the stability of the Si-O-Al bond depends on the pH surrounding the grafted surface and thus implying that alkoxysilane grafted alumina should be relatively stable under neutral aqueous conditions.

Kujawa et al.,[16] assessed the stability under hydrolytic conditions in pure water and in 1M NaOH (pH ≥ 12) of a series of hydrophobic polymer brushes (perfluoroalkyl-triethoxysilane), grafted on alumina, as well as titania and zirconia powders. The authors followed the degradation of the polymeric layer via TGA analysis before and after the modified materials were treated in the air or aqueous solution. Small degradation (5 – 8%) was observed in water after a prolonged time (1 to 2 years). However, significant degradation (30%) was observed under basic conditions (pH ≥ 12) within 2 hours of immersion, demonstrating the good stability of alkoxysilane grafted oxides in pure water, as compared to their rapid degradation under extreme pH's.

Moreover, Debrassi et al.[17] compared the stability of different linking groups (hexadecyl -alkoxysilane, -phosphonic acid, -carboxylic acid, -alkyne, and -alkene) in water at pH 7. Utilizing contact angle measurements, the authors identified the alkoxysilane (and phosphonic acid) linking group as stable in water.

It must be emphasized that studies on the stability of alkoxysilane modified alumina materials in water were focussed on either reactive (e.g. primary or secondary amines) functional groups[15] or hydrophobic layers.[16,17] Up to date, no research was performed on the stability of the Si-O-Al in neutral water and in the presence of a hydrophilic inert polymeric layer.

Grignard reagents are well-established alternatives to alkoxysilanes. Mustafa et al.,[18] hydrophobized porous titania nanofiltration membranes ($\varnothing_{pore} \approx 0.9$ nm) to mitigate irreversible fouling in wastewater treatment, by using Grignard reagents. Grignard grafting results in a single bond formation between the graft and the titanium centre, resulting in a highly stable graft. The authors[18] observed that methyl and phenyl Grignard grafted membranes showed lower water permeabilities (8 - 9 L h^{-1} m^{-2} bar^{-1}) compared to pristine membranes (20 L h^{-1} m^{-2} bar^{-1}) but higher resistance to irreversible fouling. Even though, Grignard grafting on the titania surface offers a good and stable alternative to alkoxysilanes, the strict conditions (i.e., multiple
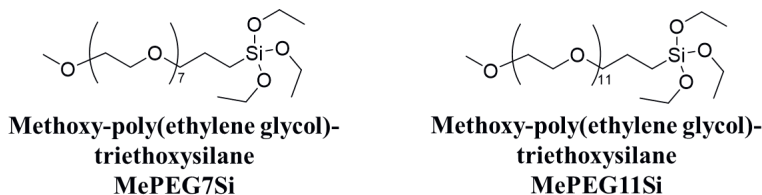
reaction steps, oxygen and water-free) can be troublesome for large scale applications.[12]

Organo-phosphonic acids were successfully used for surface modification of a wide range of ceramics providing a stable and easy-to-synthesize graft.[17-19] The phosphonic acid (PA) linking group can react even under aqueous conditions by condensation (P-OH) and/or coordination (P=O) with the support surface to form up to three P-O-M bonds per molecule.[20] Mustafa et al.,[18] used methyl and phenyl phosphonic acid grafts to modify titania membranes with a pore size of 0.9 nm. The resulted membranes exhibited slightly lower permeabilities compared to the pristine ceramic support (15 instead of 20 L h^{-1} m^{-2} bar^{-1}) and a similar PEG MWCO ($\approx$ 500 Da). However, a smaller degree of irreversible fouling was found compared to the unmodified titania membrane. Up to date, the surface modification of micro or mesoporous ceramic supports with phosphonic acid linking groups was reported using small molecules (e.g., ethyl, phenyl, etc.).[18,21-24]
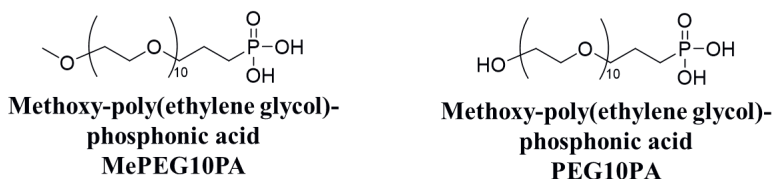
The preparation of hydrolytic-stable polymeric/ceramic hybrid membranes requires a precise selection of the linking group and the composition of the graft. In this work, we explore the hydrolytic stability of modified polyethylene glycol (PEG)/γ-Al$_2$O$_3$ membranes and the influence on the chemical nature of the linking group. Two types of linking groups were selected, namely the trimethoxysilane and phosphonic acid linking groups, with various short chains (between 7 and 11 units) of polyethylene glycols (PEGs). A PEG layer, grafted on a porous ceramic support to reduce its pore size, has the potential to improve the membrane performance in water, due to its hydrophilic nature. Furthermore, the PEG polymers used have no reactive functional groups and thus cannot promote any Si-O-Al bond activation, contrary to previous findings.[15] This, allows us to observe the stability of the Si-O-Al bond in pure water for the first time. Details and sample codes of the precursor materials used are given in Figure 2.1. The phosphonic acid-grafted membranes are prepared in water under ambient atmosphere, while for the alkoxysilane grafted-membranes toluene was used as a solvent and a water-free environment (nitrogen flow) is necessary. The chemisorption of the linking groups is investigated using a set of characterization techniques, such as FTIR, permporometry, and water contact angle. Finally, the stability of the chemical bond between the precursor and the ceramic is tested at room temperature in water and evidenced by water permeation measurements and ^{1}H liquid NMR.

Alkoxysilane precursor molecules

Methoxy-poly(ethylene glycol)-
triethoxysilane
MePEG7Si

Methoxy-poly(ethylene glycol)-
triethoxysilane
MePEG11Si

Phosphonic acid precursor molecules

Methoxy-poly(ethylene glycol)-
phosphonic acid
MePEG10PA

Methoxy-poly(ethylene glycol)-
phosphonic acid
PEG10PA

Figure 2.1: Chemical structures of precursor materials used for the fabrication of membranes and code names of the fabricated membranes.

2.2. Experimental

2.2.1. Materials

The alpha-alumina (α-Al$_2$O$_3$) substrates (disc: 21 mm of diameter, 2 mm of thickness, 80 nm pore diameter) were supplied from Pervatech B.V., the Netherlands. These ceramic substrates comprise primarily of macroporous α-alumina (> 99 %), which ensures mechanical stability under pressure. The polished side of these supports were dip-coated with a boehmite sol and subsequently calcined at 650 °C for 3 hours. The procedure was performed twice to eliminate any defects on the surface of the inorganic membrane, yielding a thin inorganic layer of 3 μm in total thickness and an average pore diameter of 5 nm (as determined by cyclohexane permporometry). Further details for the fabrication and the characteristics of the γ-Al$_2$O$_3$ layer can be found elsewhere.[25,26] Mesoporous γ-Al$_2$O$_3$ flakes were prepared using 30 mL of the same boehmite sol as used for dip-coating, obtaining the same calcination procedure as described above.

Methoxy-PEG10-phosphonic acid ethyl ester (MePEG10PE, 650 g/mol), PEG10-phosphonic acid ethyl ester (PEG10PE, 588.1 g/mol), Methoxy-PEG11-triethoxysilane (MePEG11Si, 720.96 g/mol), MethoxyPEG7-triethoxysilane (MePEG7Si, 544.75 g/mol) starting materials were purchased from Specific Polymers and used as received. Anhydrous toluene (99.8%), anhydrous dichloromethane (99.8%), ethanol (absolute), sodium hydroxide (0.1 M), and the

bromotrimethylsilane (TMSBr 97%) were supplied by Sigma-Aldrich and used without further purification. Ultrapure MilliQ water was used in all reactions.

2.2.2. Synthesis of the PEG phosphonic acids

The MethoxyPEG10-phosphonic acid (MePEG10PA) and the PEG10-phosphonic acid (PEG10PA) were synthesized by the method as described by McKenna et al.[27] The under anhydrous condition reaction between bromotrimethylsilane (TMSBr), and phosphonate esters (MePEG10PE or PEG10PE) results in the formation of the corresponding trimethylsilyl phosphonate esters. Hydrolysis of these trimethylsilyl phosphonate esters afforded the desired phosphonic acids in the form of brown viscous liquids with 98% yield. The detailed experimental procedure and the spectroscopic analysis (FTIR, ^{1}H, and ^{13}C NMR) are provided in the supporting information and are in good agreement with the literature data.

2.2.3. Grafting procedure

Prior to grafting, the γ-alumina mesoporous supports or flakes were soaked at room temperature in an ethanol/water (2:1) mixture to ensure a clean surface and to provide additional hydroxyl groups (remove leftover impurities from sintering) on the pore surface. Then, the solution was decanted for the membranes, whereas the flakes were centrifuged. The materials were then dried at 50 °C under a vacuum for 12 h.

Preparation of the PEG-alkoxysilane grafted γ-alumina membranes and flakes

The PEG-alkoxysilane modified membranes were prepared by adapting the grafting procedure from Tanardi and co-workers,[10] using similar γ-alumina discs. Under an inert atmosphere, 0.1 mmol of either MePEG7Si or MePEG11Si was placed in a reaction flask and dissolved in 100 mL of anhydrous toluene. Subsequently, the γ-alumina mesoporous support was immersed in the solution and stirred for 24 h at 110 °C. After this time, the solution was cooled to room temperature, and the resulting PEG-alkoxysilane/γ-alumina grafted membranes were washed in a sonicated bath with 5 mL of toluene (1x) and subsequently with 5 mL of ethanol (3x) for the total duration of 2 h. The samples, denoted MePEG7Si or MePEG11Si reflecting the polymer used, were dried under vacuum for 12 h at 50 °C. For the preparation of the PEG-alkoxysilane grafted γ-alumina flakes, the same procedure was employed except that 500 mg of powder were immersed in 50 mL 4.8 mM PEG-alkoxysilane solution.

Preparation of the PEG-phosphonic acid grafted γ-alumina membranes and flakes

Here 0.1 mmol of the PEG phosphonic acid (either MePEG10PA or PEG10PA) was added to a reaction flask and dissolved in 100 mL of water. The pH of the solution, which was initially ~3, was adjusted to 4 by dropwise addition of 0.1 M NaOH

47

solution. The pH of the reaction solution was adjusted to 4 in order to avoid any possible degradation of the γ-alumina surface during the grafting reaction. Subsequently, the γ-alumina mesoporous support was placed in the solution, and it was refluxed for 24h at 100 °C. The resulting PEG-phosphonic acid grafted γ-alumina membranes were washed with 5 mL water (1x) and 5 mL ethanol (3x) in a sonicated bath for 2 hours. Finally, the modified ceramics, denoted MePEG10PA or PEG10PA, were dried for 12h under a vacuum at 50 °C. For the preparation of the PEG-phosphonic acid grafted γ-alumina flakes, the same procedure was employed, except that 500 mg of powder were immersed in 50 mL of a PEG-alkoxysilane solution at 4.8 mM.

2.2.4. Characterization

FTIR analyses on pristine and grafted γ-alumina membranes were conducted using a Perkin Elmer Spectrum 100 spectrometer. Spectra were recorded in the 4000-600 cm^{-1} range using 10 scans at a resolution of 4 cm^{-1} (γ-alumina spectrum was used as background).

TGA analyses on grafted and non-grafted γ-alumina flakes were conducted by a coupled TGA-MS 2960 from TA Instruments. γ-Alumina flakes were used instead of membrane samples due to the low relative amount of γ-alumina compared to the whole ceramic support, leading to low concentrations of grafted material in the membrane. As a result, the low weight of the polymer in the membrane sample can significantly affect the quality of the measurements. In all cases, a two-step program was utilized; room temperature to 150 °C at a heating rate of 10 °C/min under nitrogen and dwell 1 hour (drying step), subsequently heated to 1000 °C at a heating rate of 2 °C/min under nitrogen and dwell for 1 hour in the air to remove any remaining organic material. Each test was performed with approximately 40 mg of material.

Water contact angle data, using the sessile drop method, were collected on grafted γ-Al$_2$O$_3$ membranes by a QCM Optical Contact Angle instrument. For individual samples, six spots on the surface were measured and averaged. Three samples were tested for each reaction condition, i.e., 18 data points were used to calculate the average contact angle and the standard deviation.

Cyclohexane permporometry measurements were performed on pristine and grafted γ-alumina membranes to evaluate the pore size distribution before and after grafting. In this test, first, the filling of the pores takes place via capillary condensation of a volatile substance (cyclohexane). During a stepwise decrease of the cyclohexane partial pressure, the pores open in order of decreasing diameter. Simultaneously, the pore size distribution is calculated from flux measurements of non-condensable

gases (oxygen and nitrogen) through the free pores using the Kelvin equation. Dead-end pores are excluded from this measurement. Further details are given in 28.

For the study of the hydrolytic stability of the grafted materials, ^{1}H liquid-state NMR spectra were acquired using a Bruker Ascend 400 MHz NMR spectrometer at frequencies of 400 MHz. Prior to the analysis, the grafted flakes were placed overnight in an oven at 150 °C under a nitrogen atmosphere to obtain well-dried materials. Typically, 10 mg of grafted powder were added in a borosilicate 5 mm NMR tube with 2-3 mL of deuterium oxide NMR solvent. Finally, the tube was sealed with a polypropylene cap, and spectra were recorded as a function of time. Between measurements, the samples were shaken at 1500 rpm on an IKA™ VXR Basic Vibrax™ Vortex Shaker. For the purpose of this test, the samples were kept sealed from the initial addition of reagents to the last recorded spectrum.

2.2.5. Water permeability

Water permeability experiments were performed on a dead-end high throughput setup incorporating 8 units in a single measurement. Prior to the experiment, membranes were soaked in water for ~1h to hydrate the active layer. The stainless steel cell was filled with the feed solution, and nitrogen was used to pressurize the cell. Permeate fluxes were obtained by measuring the permeate weight as a function of time. All measurements were conducted on three samples for each type of membrane. At every pressure point, 3 data sets were recorded every 0.5 – 1h and averaged to find the water flux of the membrane.

2.3. Results and Discussion

With the aim to develop hybrid ceramic membranes for aqueous waste treatments, polyethylene glycol (PEG) brushes were grafted on the pore surface of γ-alumina mesoporous substrates with a native pore diameter of 5 nm. According to Dohmen et al.,[29] the radius of gyration of PEG polymers in solution, having similar Mw as the ones used in our study, is approximately 0.5 nm for MePEG7Si and between 0.6 - 0.7 nm for the other PEG polymers used. The alkoxysilane linking group is calculated to have a radius of approximately 0.3 - 0.4 nm, whereas the phosphonic acid is a more compacted group and has a calculated radius of 0.1 - 0.2 nm. Thus, it is expected that in the reaction mixture, the molecules exhibit a minimum diameter (considering that in solution, the molecules form spheres) of 1.6 nm and a maximum of 2.2 nm. This means that the molecules can infiltrate from the bulk solution into the 5 nm pores of the γ-alumina layer and graft the pore surface. Nevertheless, the grafting reaction was performed for 24h under reflux to allow for higher grafting densities inside the ceramic pores.

Water contact angle results of both the unmodified γ-alumina substrate and the grafted membranes are shown in Table 2.1. For each set of membranes, identical

water contact angle values were obtained at different locations on the membranes, suggesting a homogeneous grafting over the entire surface. Independently of the linking function used, the water contact angles increased after grafting from 0° for γ-alumina to values around 35 - 50° for the grafted membranes. An increase in water contact angle is correlated with a change in surface properties of the membranes. According to Tanardi et al., PEG-alkoxysilane modified membranes exhibit water contact angles of about 40°, which is in accordance with the results provided here. It must be noted that values lower than 90° correspond to surfaces with high wettability. Thus, PEG grafted membranes show hydrophilic properties.[30]

To study the pore size of the hybrid membranes, cyclohexane permporometry measurements were conducted (Table 2.1). Independently of the type of PEG used (either 7 or 11 units), the alkoxysilane-modified membranes show a pore shrinkage, compared to the bare γ-alumina membrane, of approximately 2 nm. On the other hand, the phosphonic acid-modified membranes show a smaller decrease in pore size, varying between 1.1 and 1.5 nm. For identical PEG unit lengths (compare MePEG10PA and MePEG11Si), a large difference in pore size is observed. This can be explained by homocondensation reactions occurring between trifunctional alkoxysilanes, which does not occur with phosphonic acid linking groups.[31] This homocondensation means that the relatively reactive alkoxysilane group can condense with other alkoxysilanes on the ceramic surface forming a multilayer. Besides, alkoxysilane homocondensation can lead to denser monolayers, resulting in the polymer chains extended away from the inorganic surface.[32] Both cases can result in significant pore shrinkage. In addition, Tanardi et al.,[10] showed by means of solid-state NMR that polymeric chains can limit the uncontrolled homocondensation reactions that can occur between alkoxysilanes near the ceramic surface. This means that multilayer formation is also limited which means that under our grafting conditions, monolayer formation is promoted whereas multilayer formation is significantly restricted.

The phosphonic acid, on the other hand, exhibits two distinctive reaction pathways.[20] The first reaction pathway involves the hydroxyl groups (Al-OH) on the ceramic surface which act as nucleophiles and attack on the electrophilic phosphorus atom of the phosphoryl group (P=O). As a result, a P-OH group can acquire a free proton (H$^+$) and expel a water molecule leading to the consumption of the P-OH groups under grafting conditions. The second reaction pathway involves the coordination of the electron-rich oxygen atom of the phosphoryl group (P=O) to a Lewis acid centre. Thus, the activation occurs via the formation of a phosphoryl-aluminum complex with which neighbouring hydroxyl groups can react, yielding a stable Al-O-P bond.[33] The fastest reactivity of the alkoxysilane, as compared to the phosphonic acid, with the ceramic surface, as well as the slow homocondensation reactions that can occur,

could potentially explain the pore size differences occurring, after grafting, between the two linking groups.

Table 2.1: Water contact angle and pore diameter of the γ-alumina unmodified substrate and the grafted membranes as well as grafting performance (= reaction yield). The standard deviation is determined from the results obtained from three samples prepared under similar conditions. The pore shrinkage was obtained using the average pore diameter of the γ-alumina and the grafted membranes.

Membrane	N° PEG units	Contact angle (°)	Pore diameter (nm)	Pore shrinkage (nm)	Weight loss PEG (%)	Reaction yield[*] (%)
γ-Al$_2$O$_3$	-	0	5.5 ± 0.1	-	-	-
MePEG7Si	7	51 ± 1.6	3.7 ± 0.2	1.8	10	62
MePEG11Si	11	52 ± 5.0	3.4 ± 0.2	2.1	10	42
MePEG10PA	10	34 ± 9.0	4.4 ± 0.0	1.1	6	26
PEG10PA	10	42 ± 4.0	4 ± 0.1	1.5	5	22

[*]The yields were calculated using the TGA results and by assuming that the weight loss is only related to the decomposition of the organic part. Details on the calculation can be found in the Supplementary Information.

TGA analysis was performed on PEG-modified γ-alumina flakes to assess the amount of grafted species on the ceramic support (or reaction yield). For TGA analyses, γ-alumina flakes were used (see experimental section 2.4). The TGA curves of unmodified and modified γ-alumina flakes are shown in Figure S2.8 of the supporting information (Section C), while the resulting weight losses are given in Table 2.1. At temperatures above 200 °C, the PEG-modified flakes show a more significant drop in weight compared to the unmodified γ-alumina flakes, which is attributed to the presence of PEG on the ceramic surface. Alkoxysilane-modified flakes show a 10 % weight loss, whereas phosphonic acid-modified flakes show a loss of ~5 % organics by weight compared to unmodified γ-alumina. Tanardi et al.,[10] showed similar weight losses (10%) for PEG-alkoxysilane-modified flakes. From the weight loss data, a qualitative analysis of the reaction yield (grafting density) is made, and the results are provided in Table 2.1. The alkoxysilane grafted flakes show higher reaction yields than the phosphonic acid PEG derivatives (50 – 60% difference). As mentioned before, this is attributed to the higher reactivity of the alkoxysilane linking group in toluene compared to the reactivity of the phosphonic

acid in water and in agreement with the smaller pore shrinkage observed for the phosphonic acid derivatives.

A large difference in reaction yields is also observed between the two alkoxysilane grafted flakes. The MePEG7Si graft has approximately 50% more yield than the MePEG11Si, while for both alkoxysilane derivatives, a pore shrinkage of about 2 nm was observed by cyclohexane permporometry (see Table 2.1). According to well-established polymer chemistry rules, the polymer chain height, H, which correlates with layer thickness and thus pore-size reduction, depends on the nature of the medium, i.e., the solvent. In "good" solvents, the height of the brush is linearly correlated to the polymer length, n, and the grafting density, σ. In "poor" solvents, the height relates linearly with the length, n, but shows a lower dependency with the grafting density, $\sigma^{0.33}$.[33] Thus, in cyclohexane (a "poor" solvent used for permporometry), the polymer length, rather than grafting density, will have a larger effect on the brush height and thus to the pore size measured by cyclohexane permporometry. Therefore, from permporometry and TGA results, we can assume that alkoxysilanes are forming monolayers under the grafting conditions used herein.

FTIR analyses provide insight into the reactions of the linking groups with the inorganic surface. The high resolution of the ATR-FTIR equipment used allows us to perform detailed measurements on the grafted membranes, as given in Figure 2.2. Reports in the literature show that grafting can result in the formation of different grafted states with varying stabilities. Brodard-Severac et al.[34] found, by means of ^{17}O MAS NMR, that phosphonic acid-grafted titania contained approximately 5% of unreacted acidic sites (P-**OH**), implying the presence of multiple species. In addition, FTIR analyses can be used to evidence the presence of physisorbed species, which remain on the surface after thoroughly washing and affect the stability of the polymeric layer and the performance of the membrane. Figure 2.2A shows the FTIR spectra in the range of 700 and 1500 cm^{-1} for the pure molecules. In each spectrum, a high-intensity band at 1095 cm^{-1} is visible and is attributed to the etheric unit (**-C-O-C-**) of the polymer.[35] The same band is visible for all the grafted ceramic membranes (Figure 2.2B), which confirms the integrity of the PEG polymer after grafting.

Concerning the bands related to the linking group, the pure alkoxysilane (MePEG7/11Si) molecules exhibit two characteristic peaks at 1080 and 815 cm^{-1} which correspond to the stretching vibrations of the unhydrolyzed Si-O-C bonds.[36,37] Moreover, the band at 952 cm^{-1} is attributed to the asymmetrical stretching of the three ethoxy leaving groups (Si-**OC$_2$H$_5$**), appended on the alkoxysilane functional group.[38] Grafting of the PEG-alkoxysilane on alumina surfaces leads to significant changes for both cases (MePEG7/11Si) observed via FTIR. Accordingly, the broad band centred at 1090 cm^{-1} is ascribed to the formation of a Si-O-Al bond after

52

grafting.[39,40] This is further confirmed by the disappearance of the Si-O-C (1080 and 815 cm^{-1}) bands and the absence of the ethoxy leaving groups at 952 cm^{-1} after grafting.[32-35]

The FTIR spectra of the pure phosphonic acid (PA) molecules, as displayed in Figure 2.2A, show a band at 1250 cm^{-1}, which is attributed to the stretching vibration of the phosphoryl group (**P=O**), whereas the stretching of the acidic groups (P-**OH**) is visible at ~980 cm^{-1}.[24,31] The modified PA membranes (Fig 2B) exhibit a broad band centred at ~1100 cm^{-1} which is ascribed to the formation of the desired P-O-Al bond.[24,41,42] The P=O bond seems unchanged for the grafted materials; however, the disappearance of the P-OH band after grafting indicates bidentate attachment with the surface.[41,42] In conclusion, FTIR analysis suggests that in both cases, grafting has been successfully performed with no or no significant amounts of physisorbed material on the surface of the ceramic support.
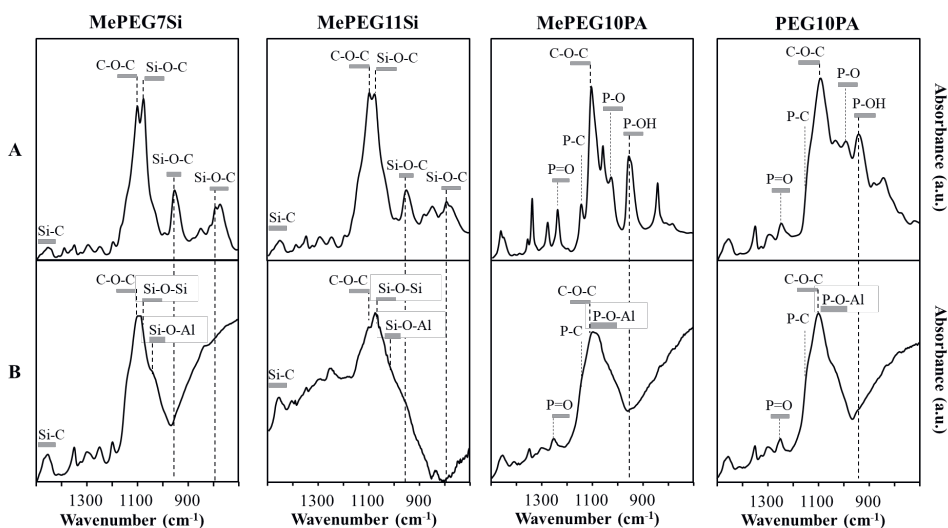
Figure 2.2: FTIR spectra of the pure molecules (A) and the grafted membranes (B). The complete spectra from 4000 – 650 cm^{-1} can be found in SI.

2.3.1. Membrane behaviour in water

The stability in water of the chemical bonding between the PEG molecule and alumina surface was investigated by ^{1}H NMR and water flux experiments as a function of time.

Liquid ^{1}H NMR was used to identify the potential products of the hydrolysis reaction between the modified γ-alumina support and deuterated water (D_2O). For this experiment, it was not possible to use the grafted membranes directly, due to the low amount of grafted species compared to the bulk (see also TGA discussion).

Therefore, γ-alumina flakes, modified in the same way as was done for the membranes, were used instead. The flakes were immersed in D_2O at room temperature, and ^1H NMR spectra were recorded in D_2O on each sample at specific times (1 h, 96 h, 288 h for the alkoxysilane and 1 h, 96 h, 408 h for phosphonic acid-modified alumina flakes). Only the hydrolyzed species that diffuse in the solvent during the liquid NMR experiments are detected. Because the NMR analyses were conducted in the same tube for each condition, the peak of the etheric unit at 3.69 ppm was used as a reference to follow the appearance of hydrolysed species in the D_2O solvent, and for this reason, the spectra were plotted from 3 to 4 ppm. The ^1H NMR spectra of the pure molecules and the hydrolysed products of grafted alumina flakes are provided in Figure 2.3. ^1H NMR spectra of the pristine alkoxysilane and phosphonic acid PEG present a very intense peak at 3.69 ppm ascribed to the repetitive etheric unit (-**CH₂OCH₂-**). The methoxy end-group of the PEG chain is visible with low intensity at 3.36 ppm. For the PEG-phosphonic acid with the hydroxyl end-group (PEG10PA), this peak at 3.36 ppm is not observed. PEG-polymers are known as hydrolytically stable materials, and thus is expected that hydrolytic stability tests will affect only the linking groups.[43] After a short exposure to D_2O (≤ 1h), both types of alkoxysilane-grafted flakes (MePEG7/11Si) exhibit two distinctive chemical shifts at 3.69 and 3.36 ppm, which can be respectively attributed to the etheric unit of the polymeric chain and the methoxy end-group as a result of the hydrolysis reaction. Moreover, the intensities of these peaks are increasing over time which is due to a higher concentration of hydrolysed species in the solution. Thus, the ^1H NMR analysis indicates a fast hydrolytic degradation at room temperature of the alkoxysilane graft on γ-alumina materials. Similarly, ^1H NMR spectra were recorded for phosphonic acid PEG-modified flakes. The ^1H NMR study clearly shows that the phosphonic acid-modified flakes are not affected by the presence of water even after 408 hours. Hence, we have clear indications that PEG phosphonic acid-modified materials do not exhibit hydrolysis after a long period in water at room temperature.
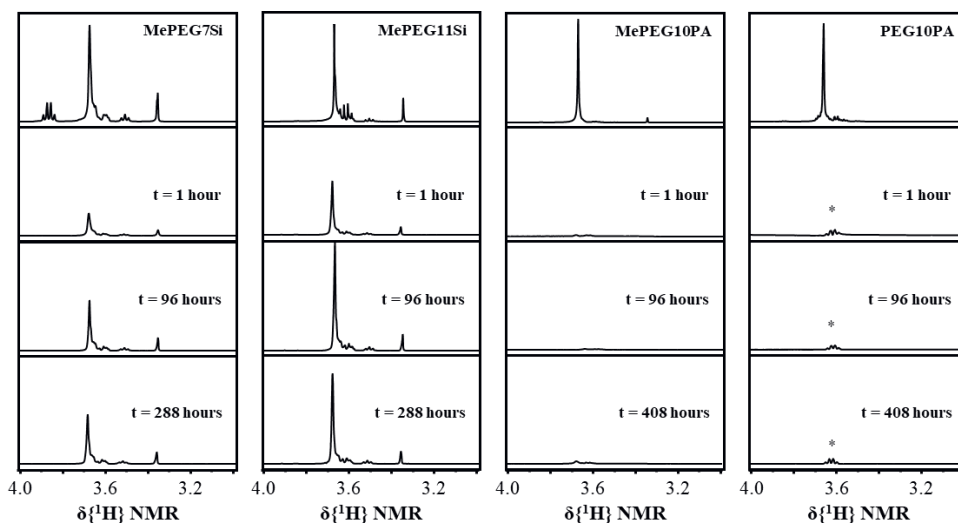
Figure 2.3: Liquid ^{1}H NMR of the precursor molecules (top spectra) and the hydrolysed products of the modified γ-alumina flakes after a specified time in deuterated water. The asterisk (*) denotes solvent contamination. The complete spectra from 0 – 5 ppm can be found in SI.

The behaviour of the γ-alumina membranes, in pristine and grafted form, was investigated by water flux measurements at 5 different pressures, as shown in Figure 2.4. The data were recorded after the flux reached equilibrium, which was achieved between 0.5 and 1h after starting the experiment. The pristine γ-alumina supports, tested under similar conditions, show permeabilities of 8 – 9 L m^{-2} h^{-1} bar^{-1} (Figure S2.9), whereas grafted membranes exhibit an almost 10-fold drop in permeability (Table 2). Tanardi et al.[10] studied the permeability of PEG grafted membranes with apolar (hexane) and polar (ethanol) solvents. The pristine γ-alumina supports support showed hexane and ethanol permeabilities of 8.4 and 3.4 L m^{-2} h^{-1} bar^{-1}. PEG grafting on the support resulted in lower permeabilities (hexane = 3.4 L m^{-2} h^{-1} bar^{-1}, ethanol = 0.8 L m^{-2} h^{-1} bar^{-1}), showing higher resistance to the polar solvent and thus a larger drop in permeability compared with the γ-alumina support (factor 4 drop for ethanol, while a factor 2.5 for hexane). The authors related this permeability trend of the PEG membranes with the swelling degree of the PEG brushes in each solvent. The more polar ethanol swells significantly more than the polymers resulting in lower permeabilities. For the same reason, the water permeability of the PEG grafted membranes is expected to be significantly lower than the pristine support. Thus, the 10-fold drop in water permeability observed in our study is probably related to a strong swelling degree of the grafted PEG brushes in the pores of the support.

According to permporometry results (Table 1), the PEG-alkoxysilane grafted membranes have smaller pore diameters than the PEG-phosphonic acid membranes

and should result in lower water permeabilities,[45] which seems to be in contradiction with the results in Figure 2.4. However, as seen from the behaviour of the grafted materials in water by ^{1}H NMR, we can assume that the alkoxysilane graft degrades fast. Even after one hour, some of the grafted species are hydrolysed (see Figure 2.3). As we used an equilibrium time of 0.5 – 1h for determining the water flux prior to the first measurement, it is expected that within that period, already a reasonable amount of the alkoxysilane graft is hydrolysed. Therefore, the difference between the permporometry and permeability results can be attributed to the fast hydrolysis of the grafted PEG-alkoxysilane species in water. Further investigation on the behaviour of the alumina-modified membranes is needed to assess the assumptions of the hydrolysis of alkoxysilane grafts in water.
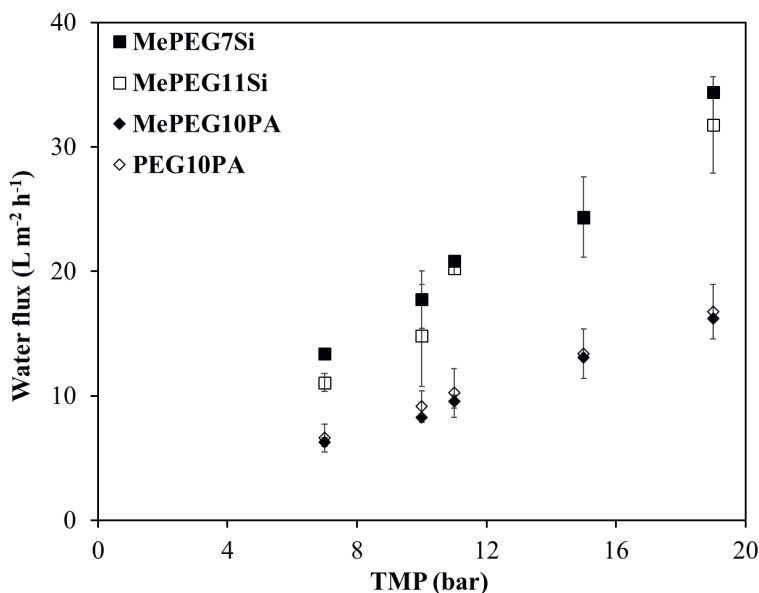
Figure 2.4: Water flux as a function of pressure for grafted membranes. Error bars indicate the standard deviation between three membranes prepared under similar conditions.

To further assess the stability of the grafted membranes under hydrolytic conditions, membranes were immersed at room temperature in MilliQ water for a certain period (24 – 216 hours), dried at 70 °C under vacuum, and reused to repeat the water permeability measurements. Figure 2.5 presents the water permeability of the grafted membranes, including an equilibrium time in water of 0.5-1h (0 h in Figure 2.5) and after 24, 72, and 216 h of immersion in water. The two types of membranes (alkoxysilane and phosphonic acid-modified) show significant differences in water permeability. Namely, alkoxysilane-modified membranes show an increase of 28%

56

for MePEG7Si and 59 % for MePEG11Si in water permeability after 24h. After three days (72h) in water, the permeability of both alkoxysilane-modified membranes show a further increase of 41% for MePEG7Si and 69% for MePEG11Si, which can be correlated to the degradation of the polymeric layer. On the other hand, the phosphonic acid-modified membranes show almost no change in permeability, even after 216 hours of immersion in water. The increasing permeability observed solely with alkoxysilane membranes can be correlated with the degradation of the polymeric layer. Degradation of the polymeric layer could also occur due to the presence of physisorbed species at the ceramic pore surface. However, FTIR analysis confirmed the absence of unreacted $Si-OCH_2CH_3$ and Si-OH groups on the grafted alumina membrane (see Figure 2.2B and S2.10 – S2.13). This, along with the permeability results, suggests that the alkoxysilane-modified membranes exhibit very low hydrolytic stability. In contrast, the phosphonic acid-modified membranes seem to present good hydrolytic stability, which is in agreement with the ^{1}H NMR results indicating a stable grafted species even after 408 hours (Figure 2.3). Furthermore, our findings are confirmed by studies on the poisoning of zeolitic materials (high concentration of Si-O-Al bonds) with phosphoric acid (H_3PO_4).[46] In that work, it is shown that the P-O-Al bond in the presence of water is not only stable but is also favoured over the Si-O-Al bond (hydrolysed to form P-O-Al). This indicates that the grafting reaction in a green solvent, such as water, is favoured when phosphonic acid is used, and additionally, the grafted species formed is hydrolytically stable under process conditions involving aqueous streams.
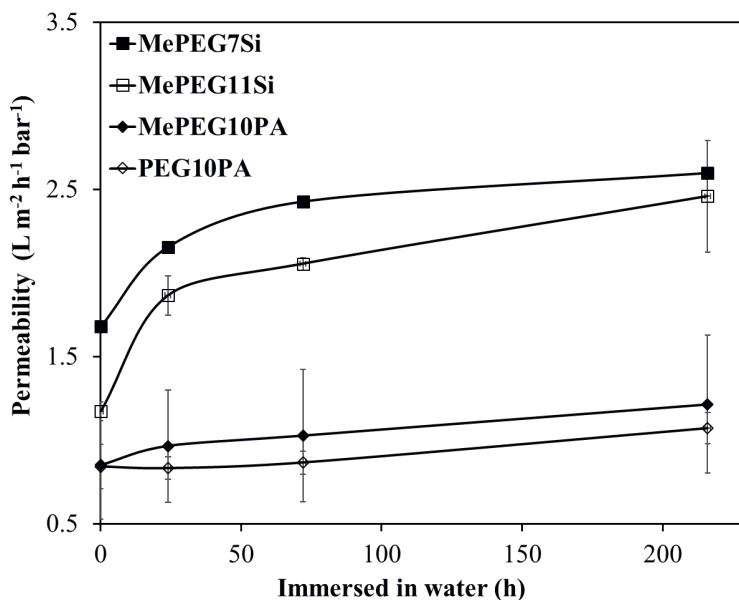
Figure 2.5: Water permeability results of the PEG-grafted membranes after grafting (0 hours) and after hydrolytic treatments for 216 hours. Error bars indicate standard deviation, obtained over three samples prepared under the same conditions and immersed in water for the same time.

2.4. Conclusion

In this work, the pore diameter of γ-alumina membranes with a size of 5.5 nm were reduced by 1 - 2 nm through grafting with small PEG molecules, having either trimethoxysilane or phosphonic acid as linking groups. The phosphonic acid graft, in contrast to the alkoxysilane graft, showed stable behaviour in water even after 216 h in water, and no hydrolysis was observed with liquid NMR analysis. In contrast, it was shown that γ-alumina, covalently-grafted with PEG-alkoxysilanes, easily hydrolysed after contact with water. This shows that Szczepanski's[15] claims on alkoxysilane-modified oxides degradation being depended on the organic layer and its functionality is not entirely true, and it should be expanded to hydrophilic layers in pure water, in general. So, even under neutral aqueous conditions use of alkoxysilanes should be avoided when the modified surface is hydrophilic. In addition, liquid-state NMR, in combination with other techniques, was utilized to assess the physical interaction between liquid and solid. We showed that NMR has the potential use for an easy qualitative evaluation on the effects of a solvent in contact with a solid material, such as hydrolysis reactions on the surface of a membrane.
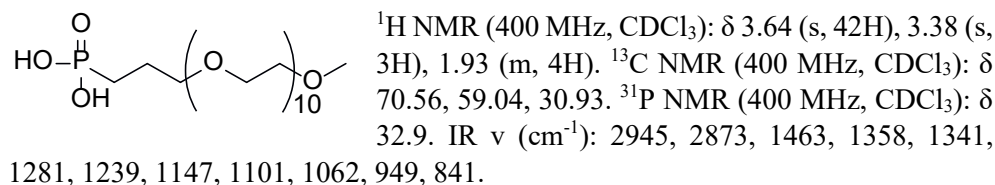
Finally, a promising and simple fabrication method for the fabrication of hydrophilic, phosphonic acid PEG-modified ceramic nanofiltration membranes is shown in this work for use in industrial wastewater treatment for the removal of small organic solutes. Due to the materials involved in the fabrication step, these PEG membranes are suitable for industrial fabrication and use.
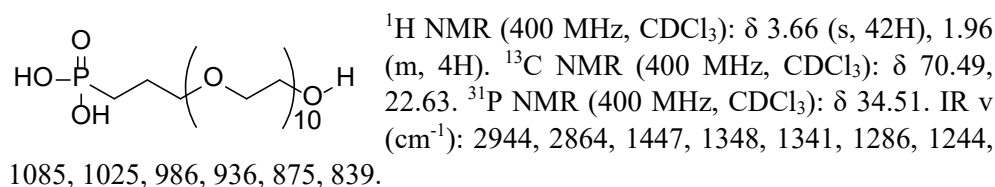
2.5. Supporting information
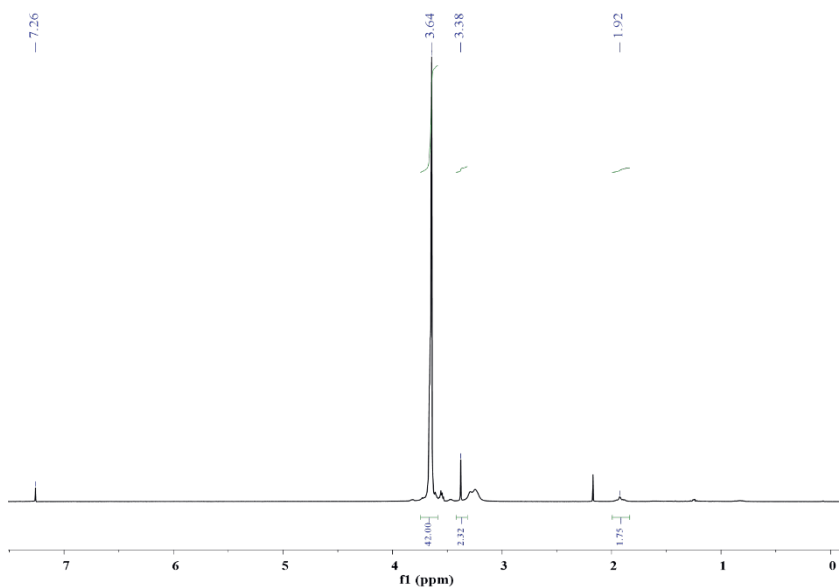
1. Synthesis of the PEG-phosphonic acids

Methoxy-PEG10-phosphonic acid (MePEG10PA) and PEG10-phosphonic acid (PEG10PA) were synthesized according to McKenna's method[27] utilizing the reaction conditions from Xu et al.[46] Namely, 5 g (1 eq.) of PEG-phosphonate (either MePEG10PE or PEG10PE) were dissolved in 30 mL of anhydrous dichloromethane under inert conditions. Subsequently, 3 eq. of bromotrimethylsilane was added to the solution under stirring at room temperature. Then, the solution was stirred for 24 hours under a nitrogen atmosphere. Subsequently, the volume was reduced under vacuum, leading to the expected trimethylsilyl phosphonate ester PEG as a brown viscous liquid in quantitative yields (98%, 6 g). Afterward, the resulting liquid was mixed with 50 mL of a water/methanol (1:1 v/v) solution under stirring for 15 minutes. Finally, the solvent was removed under reduced pressure to afford PEG10PA ($\delta\{CDCl_3\}$ ^{31}P = 34.57 ppm) or MePEG10PA ($\delta\{CDCl_3\}$ ^{31}P = 32.9 ppm) as brown viscous liquid (99%, 5 g).

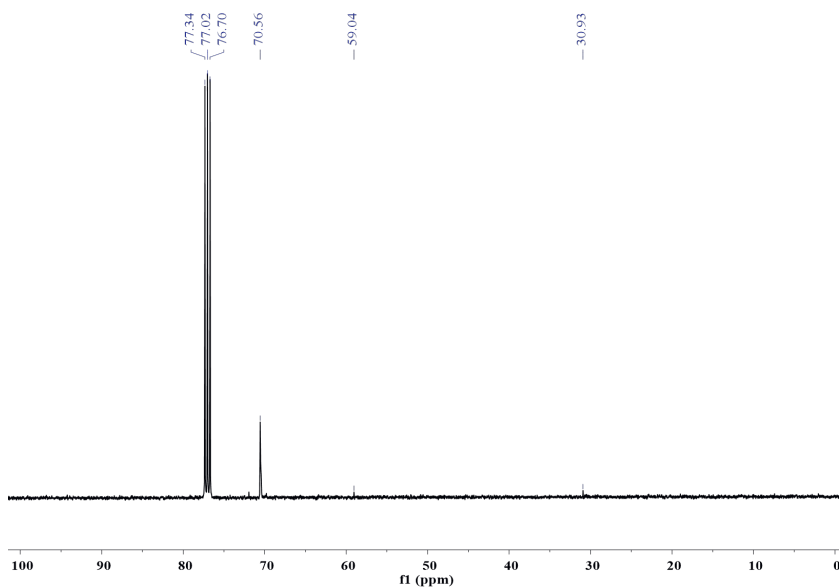**Methoxy-poly(ethylene glycol)-phosphonic acid (MePEG10PA)**:

^1H NMR (400 MHz, CDCl$_3$): δ 3.64 (s, 42H), 3.38 (s, 3H), 1.93 (m, 4H). ^{13}C NMR (400 MHz, CDCl$_3$): δ 70.56, 59.04, 30.93. ^{31}P NMR (400 MHz, CDCl$_3$): δ 32.9. IR v (cm^{-1}): 2945, 2873, 1463, 1358, 1341, 1281, 1239, 1147, 1101, 1062, 949, 841.

Poly(ethylene glycol)-phosphonic acid (PEG10PA):

^1H NMR (400 MHz, CDCl$_3$): δ 3.66 (s, 42H), 1.96 (m, 4H). ^{13}C NMR (400 MHz, CDCl$_3$): δ 70.49, 22.63. ^{31}P NMR (400 MHz, CDCl$_3$): δ 34.51. IR v (cm^{-1}): 2944, 2864, 1447, 1348, 1341, 1286, 1244, 1085, 1025, 986, 936, 875, 839.
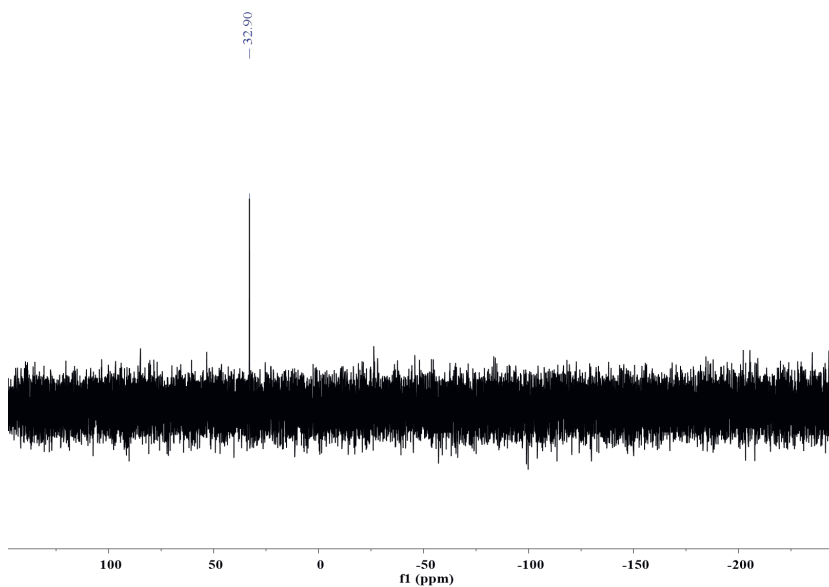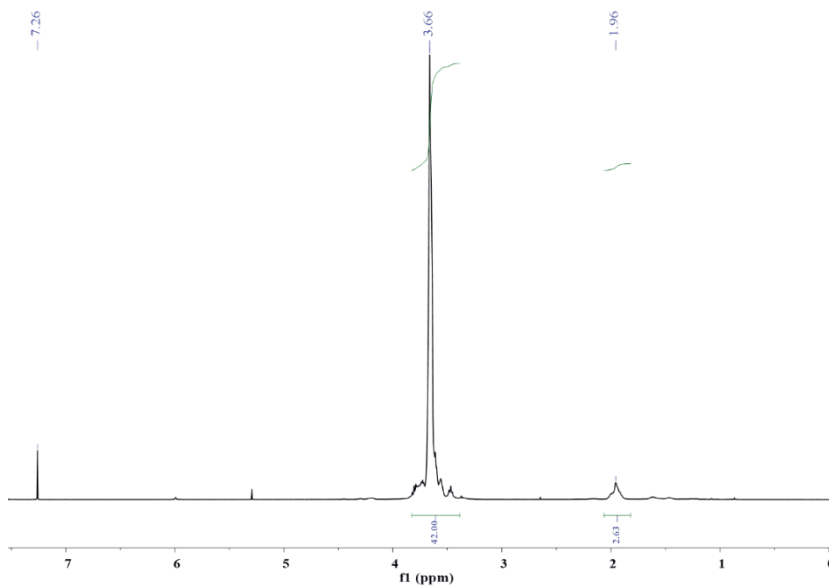
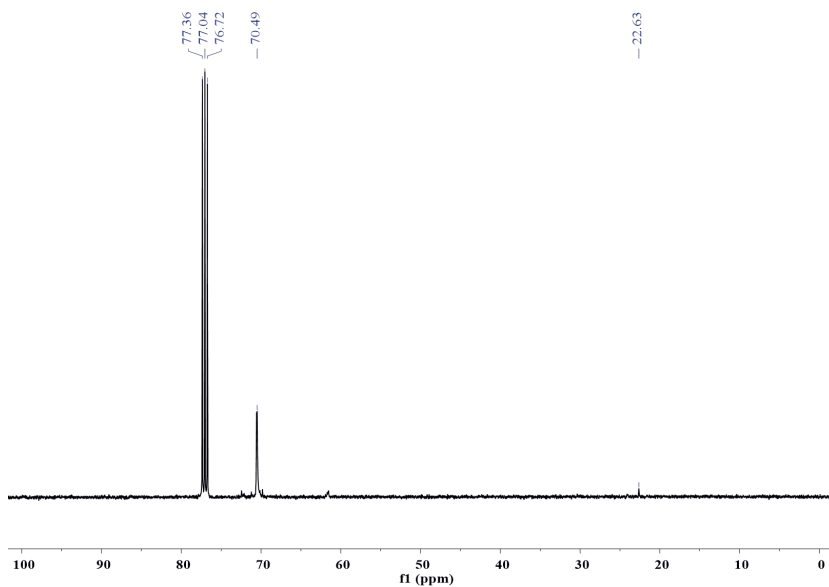**Figure S2.1:** ^{1}H NMR of the MePEG10PA as synthesized in deuterated chloroform.

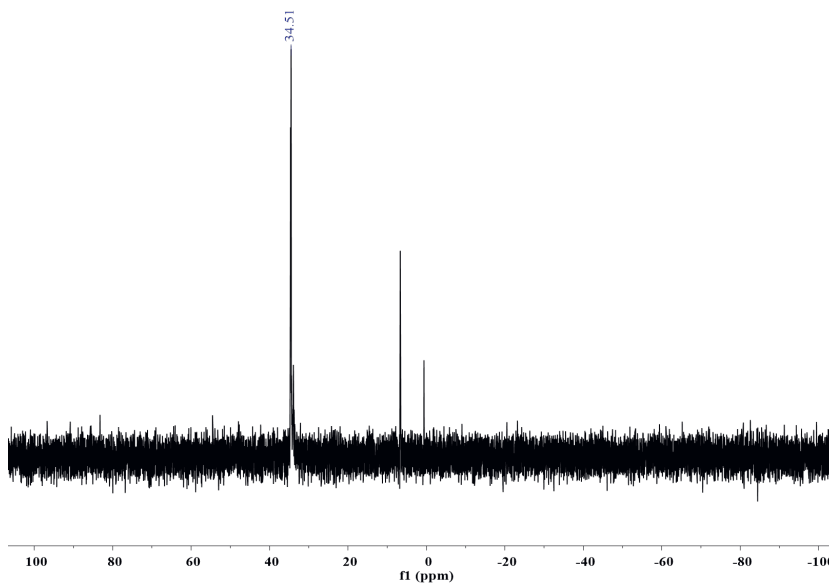**Figure S2.2:** ^{13}C NMR of the MePEG10PA as synthesized in deuterated chloroform.

60

Figure S2.3: ^{31}P NMR of MePEG10PA as synthesized in deuterated chloroform.

**Figure S2.4:** ^{1}H NMR of the PEG10PA as synthesized in deuterated chloroform.

Figure S2.5: ^{13}C NMR of the PEG10PA as synthesized in deuterated chloroform.

Figure S2.6: ^{31}P NMR of PEG10PA as synthesized in deuterated chloroform.

## 2. Pore size distribution (PSD) via cyclohexane permporometry of the unmodified and PEG modified γ-alumina discs

The average pore diameters for each sample are 5.5, 3.7, 3.4, 4.4 and 4 nm for the unmodified γ-alumina, MePEG7Si, MePEG11Si, MePEG10PA and PEG10PA membranes, respectively.
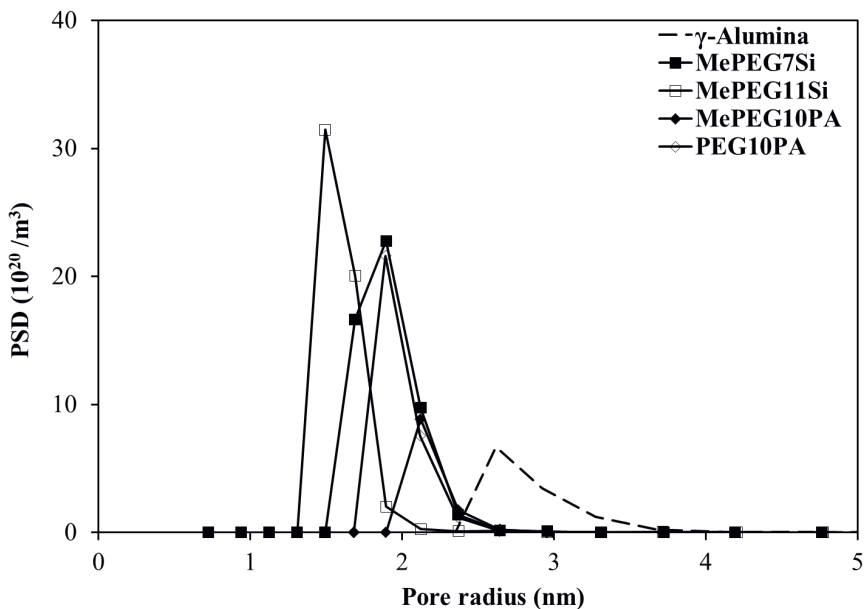
Figure S2.7: Pore size distribution of the unmodified and modified γ-alumina membranes.

3. Thermogravimetric analysis conducted on unmodified and PEG modified γ-alumina particles

The data are provided starting from 200 °C because between 40 and 200 °C water is released.[10]
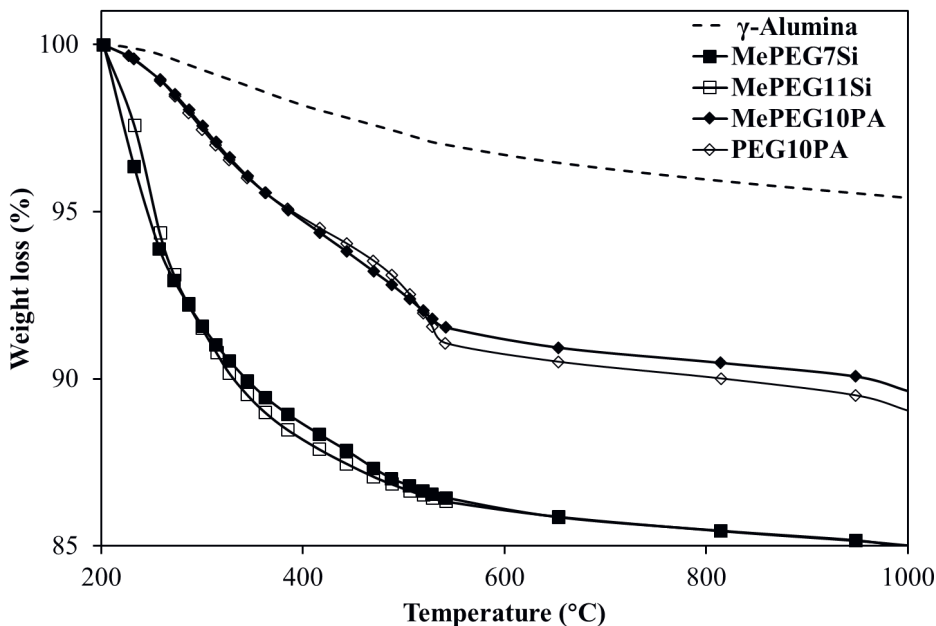
Figure S2.8: TGA graphs of unmodified and grafted alumina flakes.

The reaction yields were calculated from the TG analysis as follows:

The amount (in mol) of grafted PEG is found by:

$$mol_{PEG} = \frac{Mass_{PEG}}{MW_{PEG}}$$

where $Mass_{PEG}$ is the weight of combusted material as measured by TG analysis and MW_{PEG} is the molecular weight of the grafted species minus the inorganic part (PO_3H_2 and SiO_3Et_3).

The mass of γ-alumina is calculated by:

$$Mass_{Al} = 100 - mol_{PEG} \times MW_{FG} - Mass_{PEG},$$

where MW_{FG} is the molar mass of the non-combustible material remaining on the alumina (PO_3 and SiO_3).

The reaction yields is calculated by:
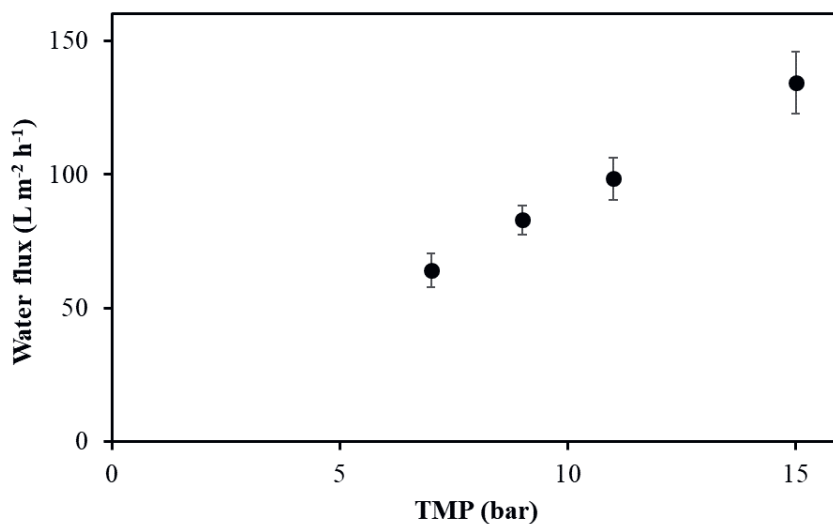
$$Yield(\%) = 100 \times \frac{mol_{PEG} \times Mass_{Al,exp}}{Mass_{Al} \times mol_{PEG,exp}}$$

where $Mass_{Al,exp}$ is the weight of γ-alumina used in the reaction and $mol_{PEG,exp}$ the starting amount used in the reaction.

4. Water permeability of pristine γ-alumina support

A water permeability of 9 L m^{-2} h^{-1} bar^{-1} was calculated from water flux results as function of Trans Membrane Pressure (TMP)
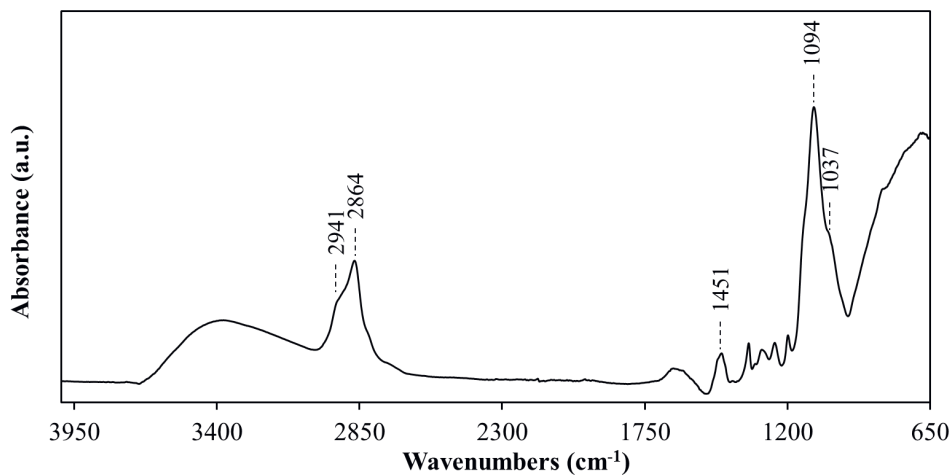

Figure S2.9: Water flux of the γ-alumina support as function of trans membrane pressure.

5. FTIR spectra of the pure PEG polymers and the PEG-modified ceramic membranes
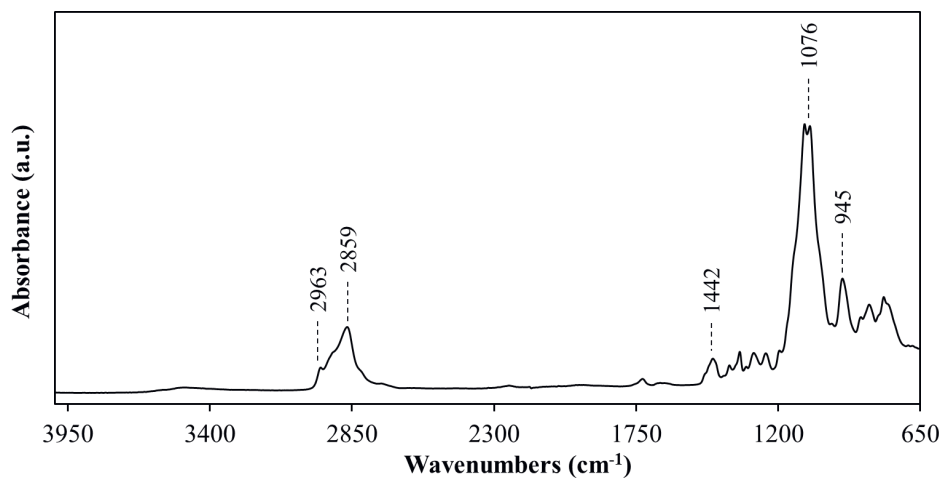
In the case of the modified ceramic membrane, the unmodified γ-alumina support was used as background.
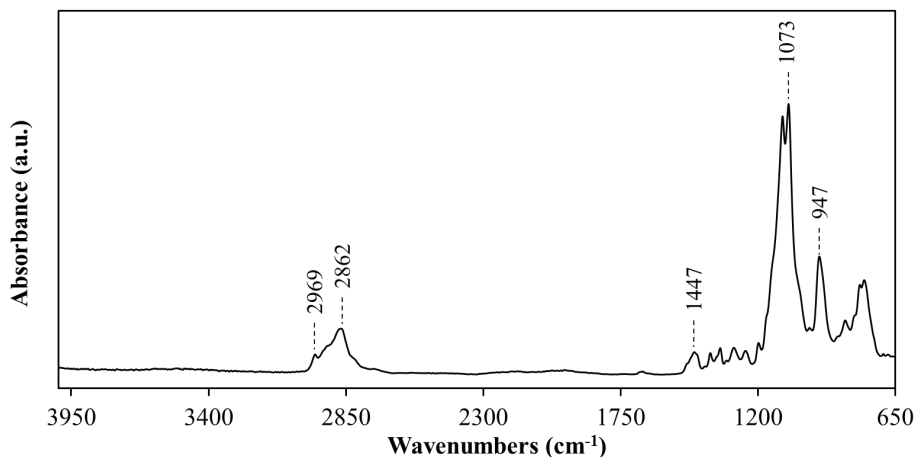
Figure S2.10: FTIR spectrum of the as received MePEG7Si.

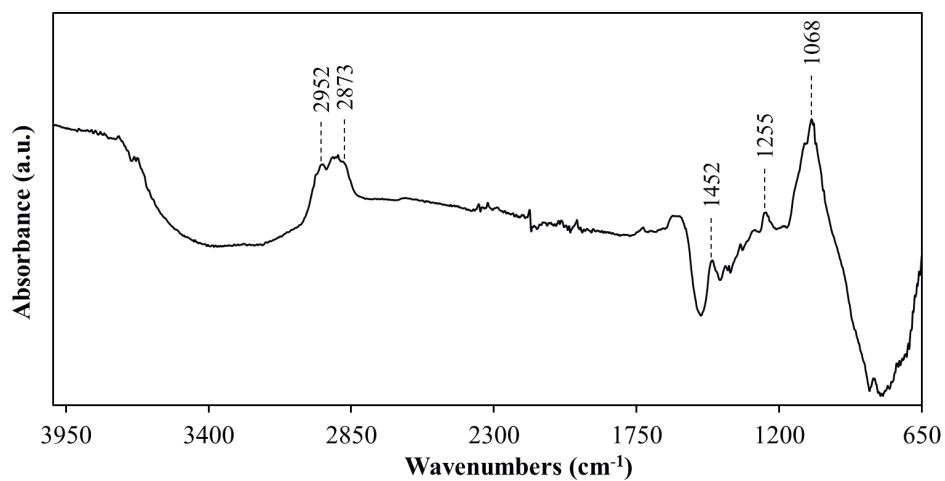**Figure S2.11:** FTIR spectrum of the MePEG7Si modified γ-alumina membrane.

Figure S2.12: FTIR spectrum of the as received MePEG11Si.

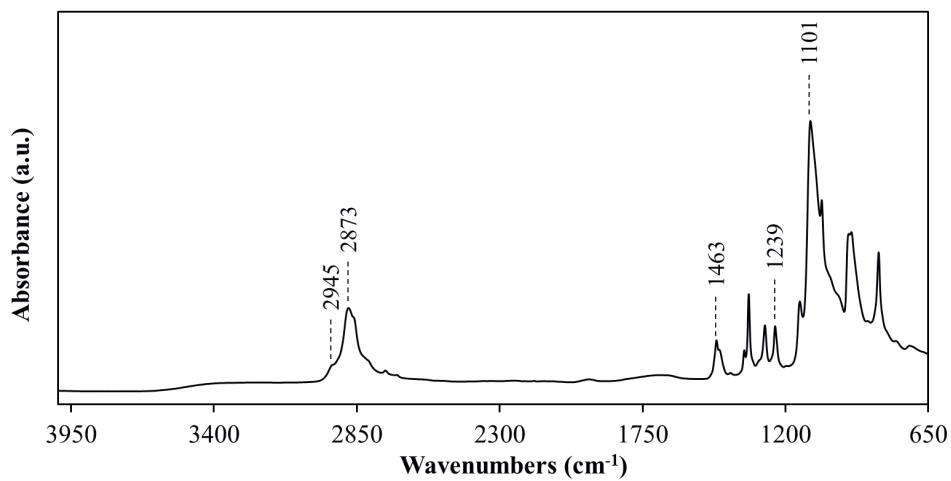**Figure S2.13:** FTIR spectrum of the MePEG11Si modified γ-alumina membrane.

Figure S2.14: FTIR spectrum of the as synthesized MePEG10PA.
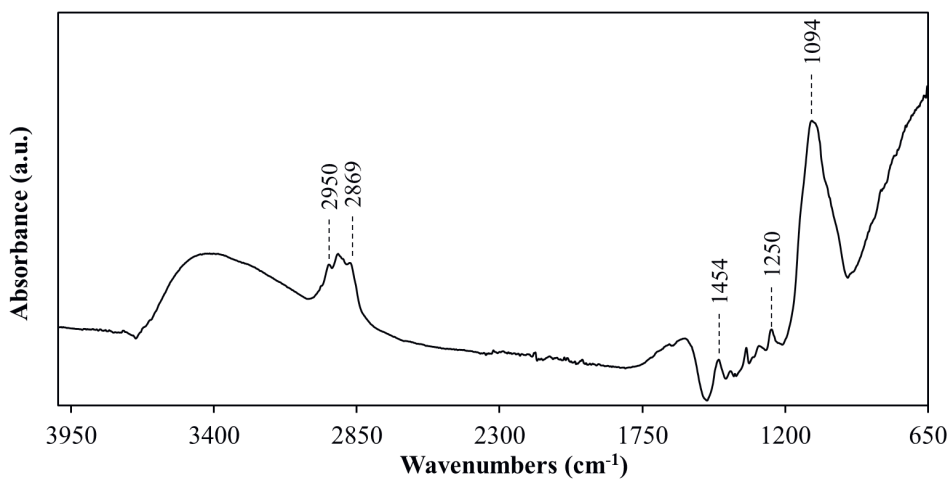
Figure S2.15: FTIR spectrum of the MePEG10PA modified γ-alumina membrane.
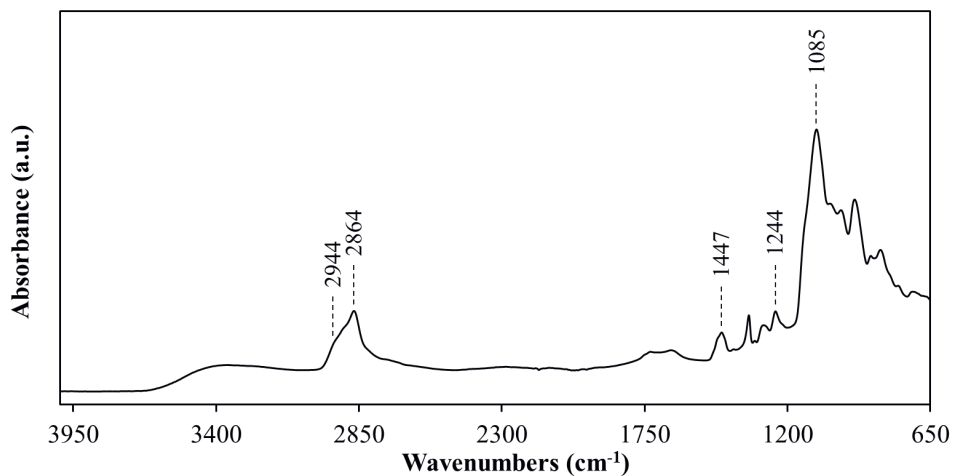
Figure S2.16: FTIR spectrum of the as synthesized PEG10PA.
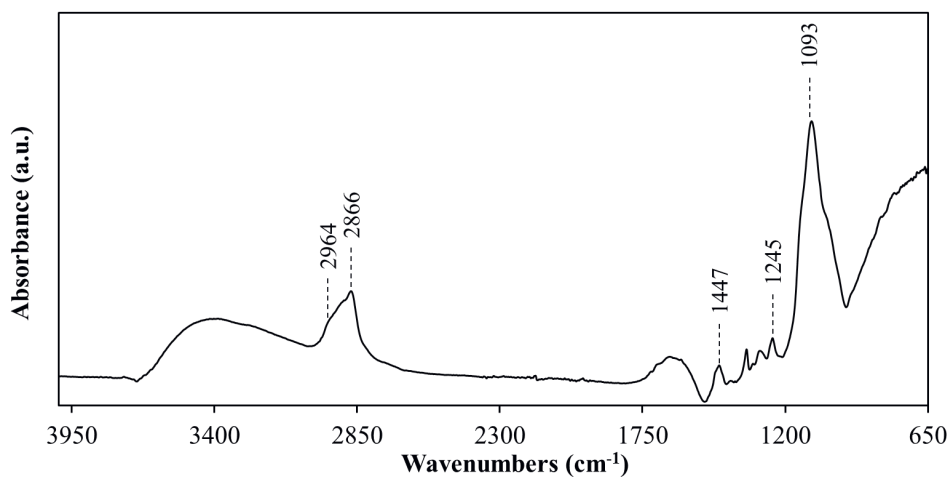
Figure S2.17: FTIR spectrum of the PEG10PA modified γ-alumina membrane.

6. NMR spectra of the as received PEG-alkoxysilane and the as prepared PEG-phosphonic acids as well as the modified γ-alumina particles under hydrolytic conditions as recorded in different time intervals
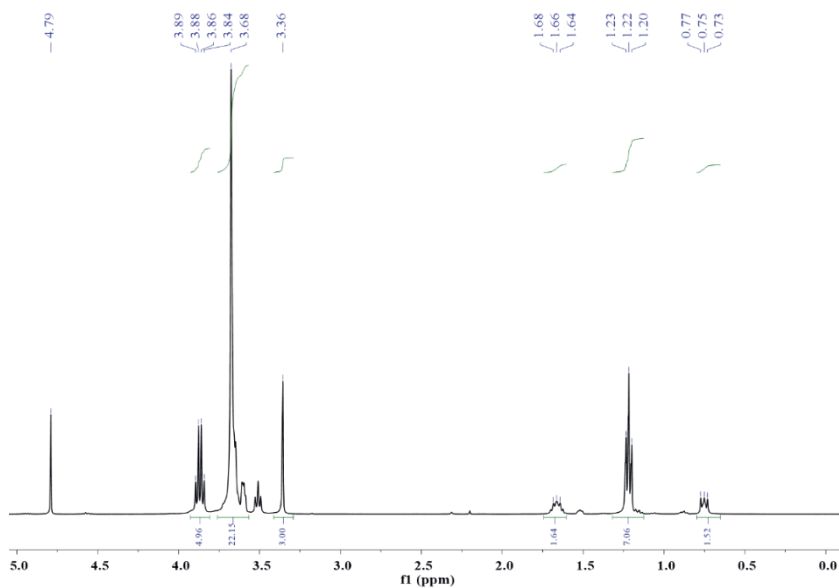
Figure S2.18: ^{1}H NMR spectrum of the as received MePEG7Si in deuterated water.
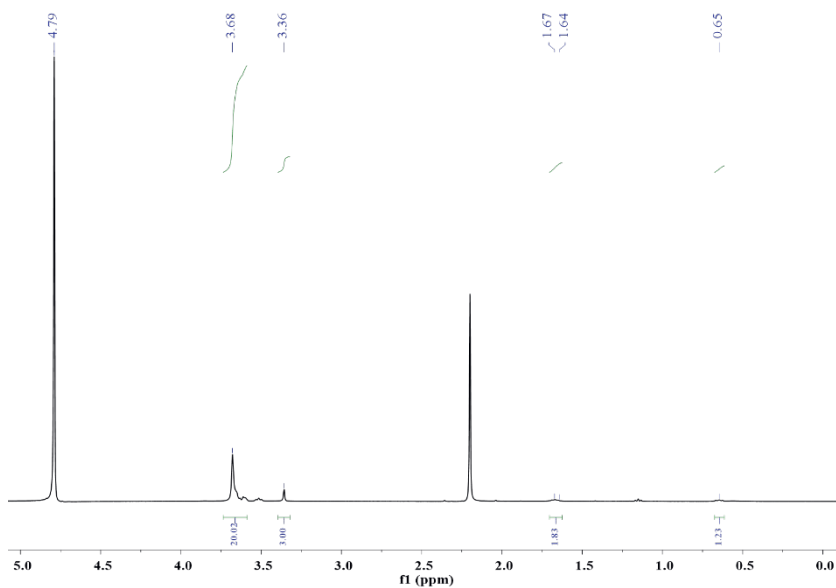
Figure S2.19: ^{1}H NMR spectrum of the MePEG7Si grafted γ-alumina flakes immersed in deuterated water for 1h.
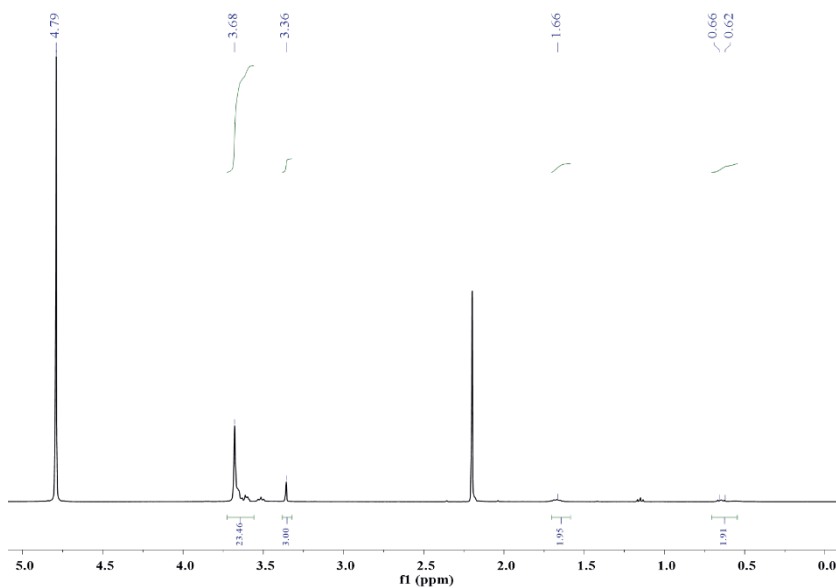
Figure S2.20: ^{1}H NMR spectrum of the MePEG7Si modified γ-alumina flakes immersed in deuterated water for 96h.
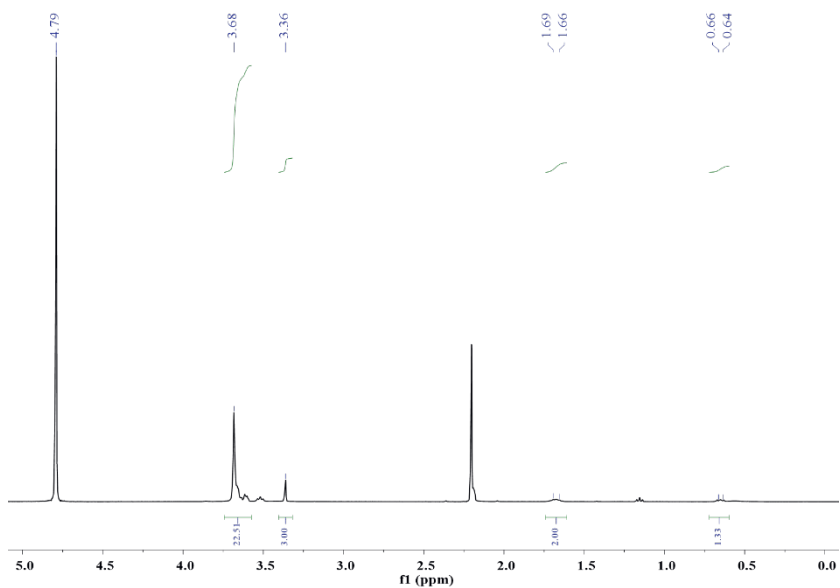
Figure S2.21: ^{1}H NMR spectrum of the MePEG7Si modified γ-alumina flakes immersed in deuterated water for 288h.
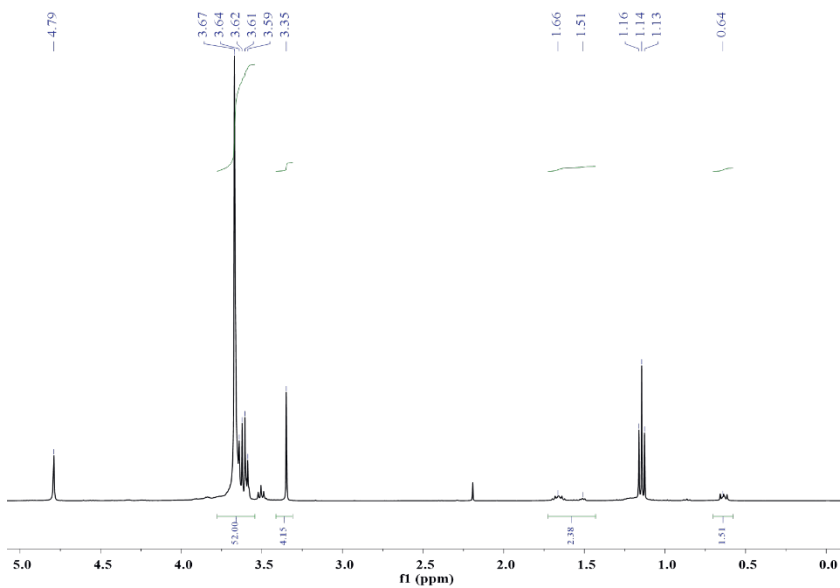
Figure S2.22: ^{1}H NMR spectrum of the as received MePEG11Si in deuterated water.

Figure S2.23: ^{1}H NMR spectrum of the MePEG11Si modified γ-alumina flakes immersed in deuterated water for 1h.

Figure S2.24: ^{1}H NMR spectrum of the MePEG11Si modified γ-alumina flakes immersed in deuterated water for 96h.
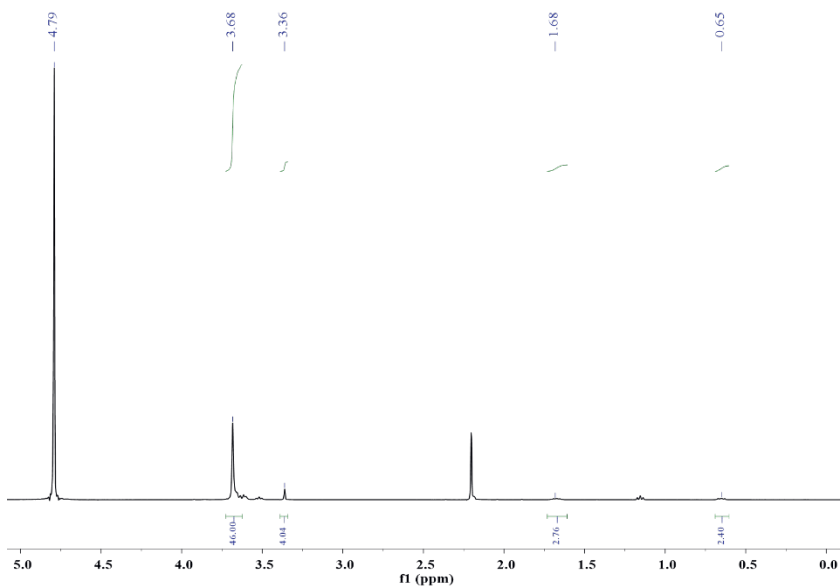
Figure S2.25: ^{1}H NMR spectrum of the MePEG11Si modified γ-alumina flakes immersed in deuterated water for 288h.
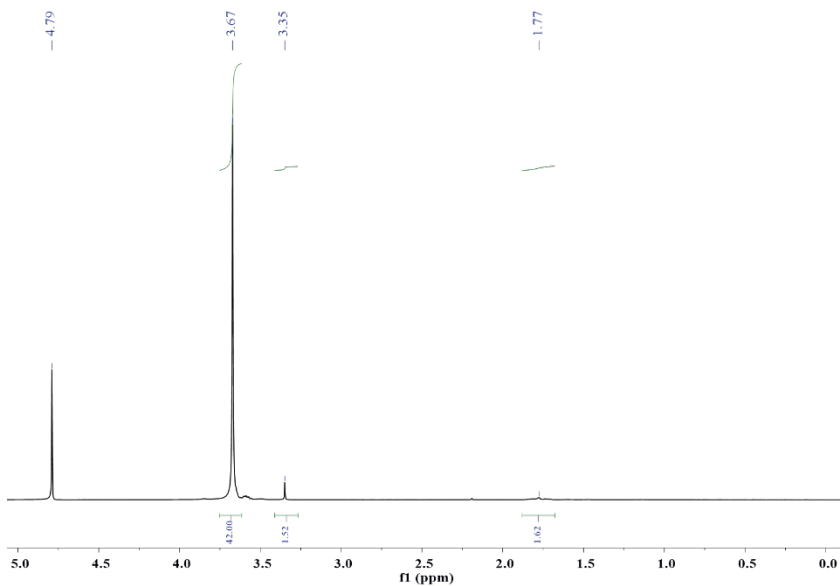
Figure S2.26: ^{1}H NMR spectrum of the as prepared MePEG10PA in deuterated water.

74
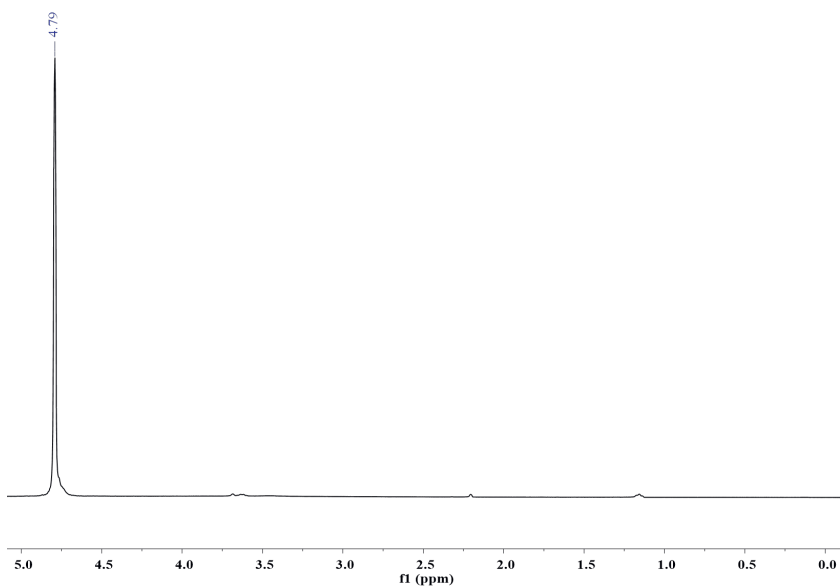
Figure S2.27: ^{1}H NMR spectrum of the MePEG10PA modified γ-alumina flakes immersed in deuterated water for 1h.
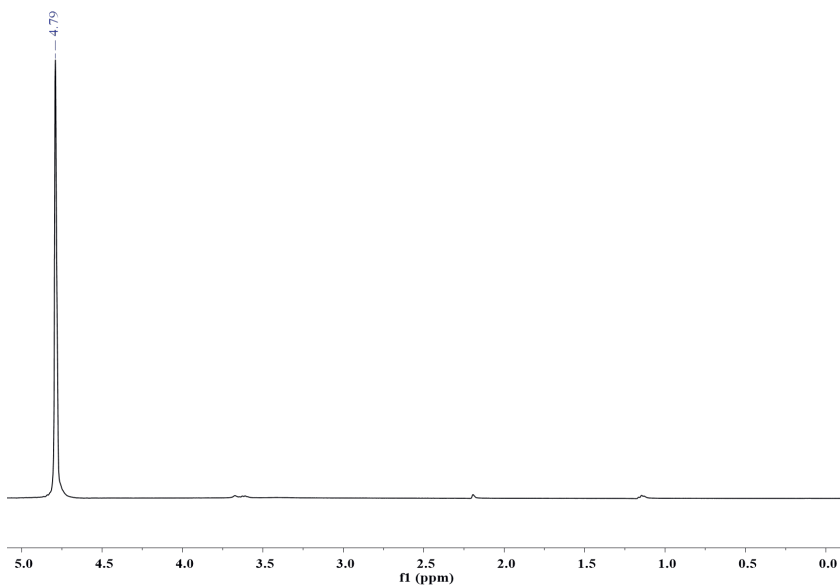
Figure S2.28: ^{1}H NMR spectrum of the MePEG10PA modified γ-alumina flakes immersed in deuterated water for 96h.
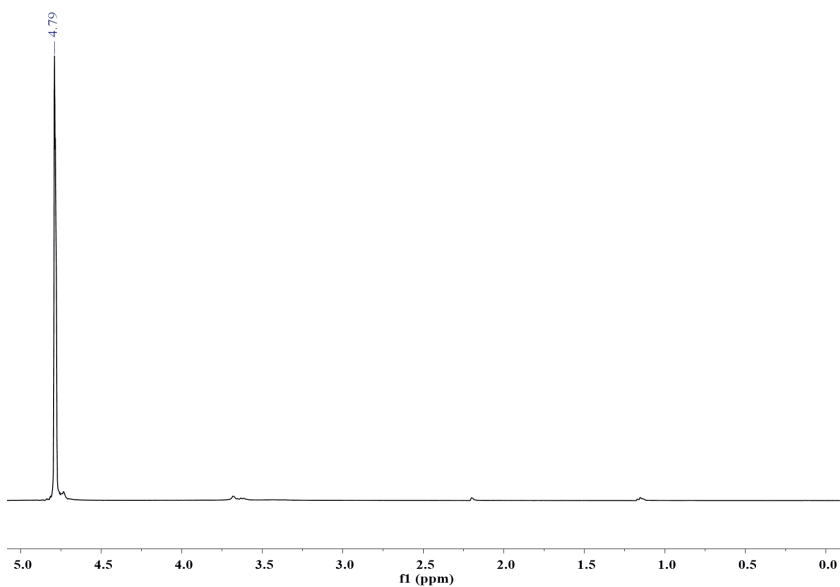
Figure S2.29: ^{1}H NMR spectrum of the MePEG10PA modified γ-alumina flakes immersed in deuterated water for 408h.
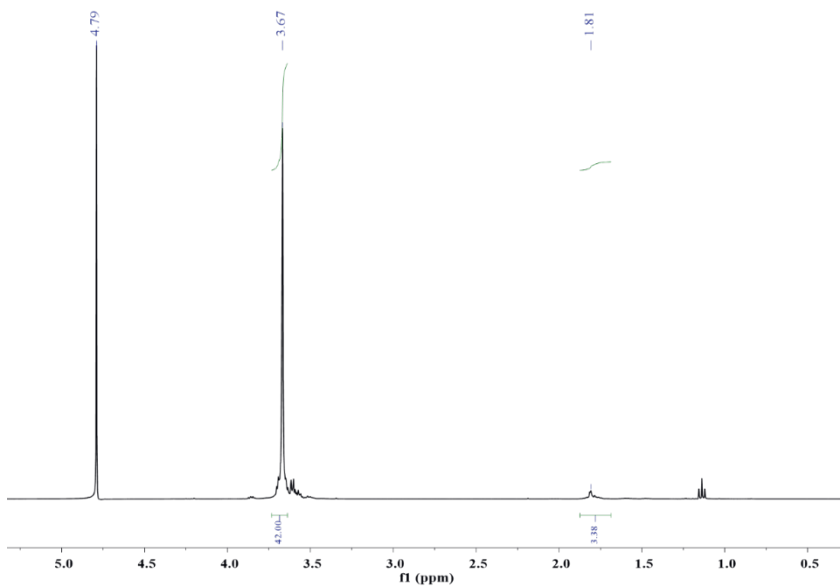
Figure S2.30: ^{1}H NMR spectrum of the as prepared PEG10PA in deuterated water.
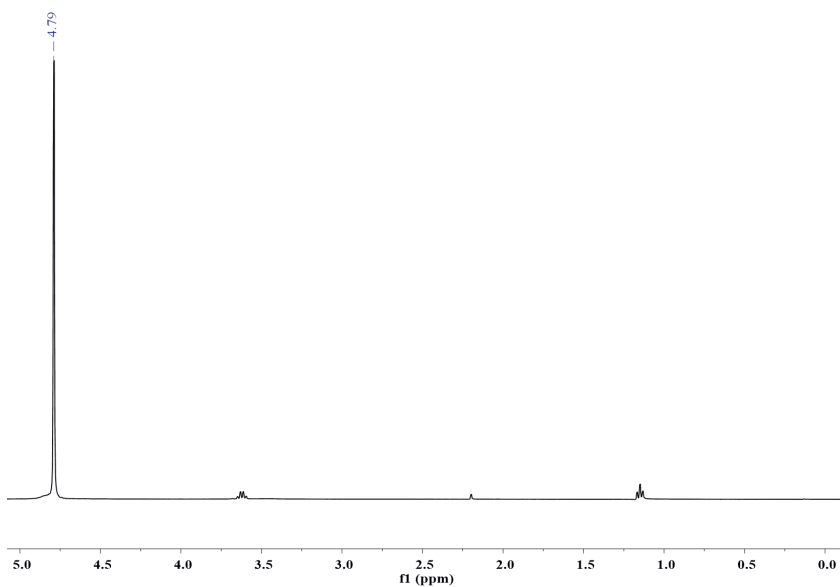
Figure S2.31: ^{1}H NMR spectrum of the PEG10PA modified γ-alumina flakes immersed in deuterated water for 1h.
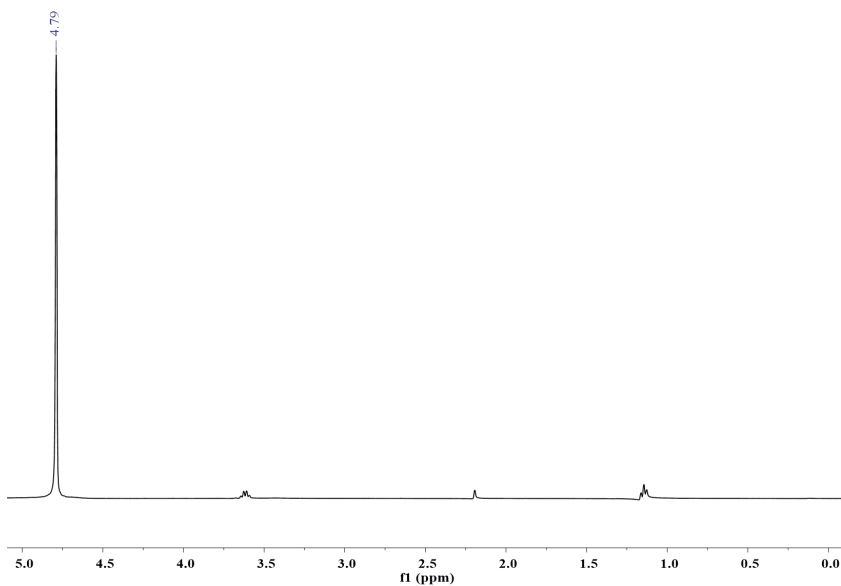
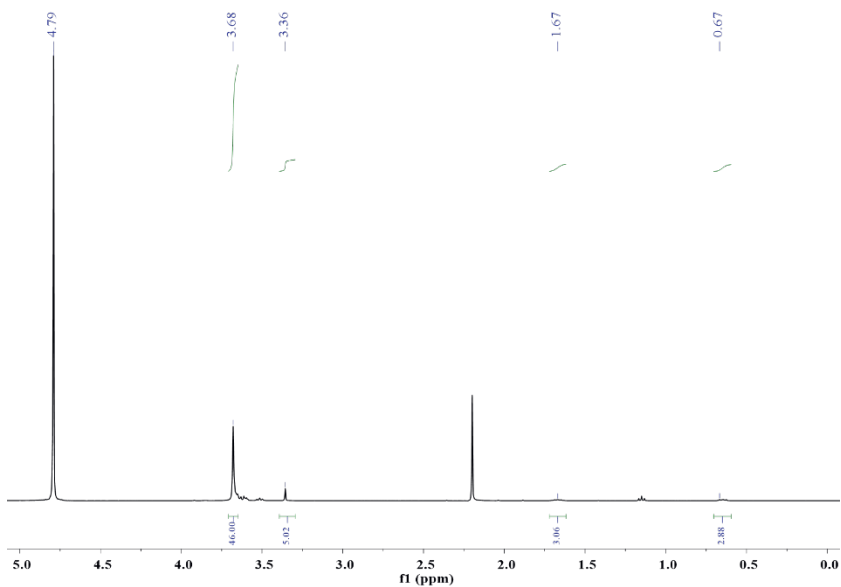**Figure S2.32:** ^{1}H NMR spectrum of the PEG10PA modified γ-alumina flakes immersed in deuterated water for 288h.

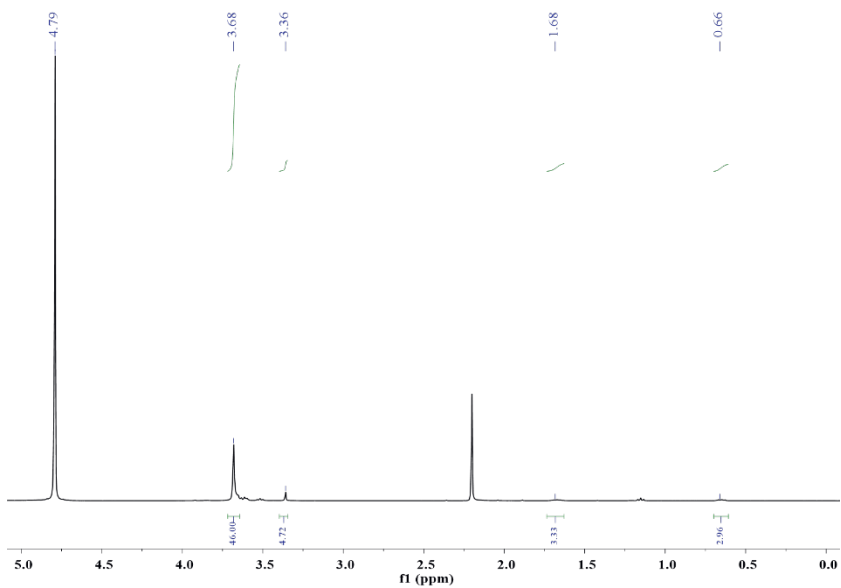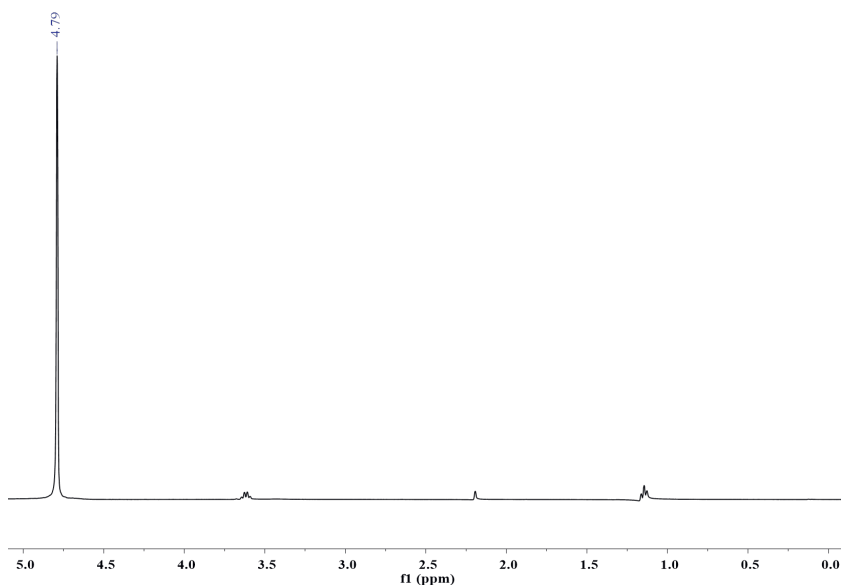**Figure S2.33**: ¹H NMR spectrum of the PEG10PA modified γ-alumina flakes immersed in deuterated water for 408h.

2.6. References

(1)   P. Eriksson, Nanofiltration extends the range of membrane filtration, Environ. Prog. 7 (1988) 58–62. doi:10.1002/ep.3300070116.

(2)   P. Marchetti, M.F.J. Solomon, G. Szekely, A.G. Livingston, Molecular Separation with Organic Solvent Nanofiltration: A Critical Review, Chem. Rev. 114 (2014) 10735–10806. doi:10.1021/cr500006j.

(3)   E.M. Rundquist, C.J. Pink, A.G. Livingston, Organic solvent nanofiltration: a potential alternative to distillation for solvent recovery from crystallisation mother   liquors,   Green   Chem.   14   (2012)   2197–2205. doi:10.1039/C2GC35216H.

(4)   M. Amirilargani, R.B. Merlet, A. Nijmeijer, L. Winnubst, L.C.P.M. de Smet, E.J.R. Sudhölter, Poly (maleic anhydride-alt-1-alkenes) directly grafted to γ-alumina for high-performance organic solvent nanofiltration membranes, J. Memb. Sci. 564 (2018) 259–266. doi:10.1016/J.MEMSCI.2018.07.042.

(5)   R.B. Merlet, M. Amirilargani, L.C.P.M. de Smet, E.J.R. Sudhölter, A. Nijmeijer, L. Winnubst, Growing to shrink: Nano-tunable polystyrene brushes inside   5 nm   mesopores,   J.   Memb.   Sci.   572   (2019)   632–640. doi:10.1016/J.MEMSCI.2018.11.058.

(6)   S.M. Samaei, S. Gato-Trinidad, A. Altaee, The application of pressure-driven ceramic membrane technology for the treatment of industrial wastewaters – A review, Sep. Purif. Technol. 200 (2018) 198–220. doi:10.1016/J.SEPPUR.2018.02.041.

(7)   T. Fujioka, A. Hoang, T. Okuda, H. Takeuchi, H. Tanaka, L. Nghiem, T. Fujioka, A.T. Hoang, T. Okuda, H. Takeuchi, H. Tanaka, L.D. Nghiem, Water Reclamation Using a Ceramic Nanofiltration Membrane and Surface Flushing with Ozonated Water, Int. J. Environ. Res. Public Health. 15 (2018) 799. doi:10.3390/ijerph15040799.

(8)   D. Das, S. Baitalik, B. Haldar, R. Saha, N. Kayal, Preparation and characterization of macroporous SiC ceramic membrane for treatment of waste water, J. Porous Mater. 25 (2018) 1183–1193. doi:10.1007/s10934-017-0528-5.

(9)   A. Kayvani Fard, G. McKay, A. Buekenhoudt, H. Al Sulaiti, F. Motmans, M. Khraisheh, M. Atieh, A. Kayvani Fard, G. McKay, A. Buekenhoudt, H. Al Sulaiti, F. Motmans, M. Khraisheh, M. Atieh, Inorganic Membranes: Preparation and Application for Water Treatment and Desalination, Materials (Basel). 11 (2018) 74. doi:10.3390/ma11010074.

(10)   C.R. Tanardi, R. Catana, M. Barboiu, A. Ayral, I.F.J. Vankelecom, A. Nijmeijer, L. Winnubst, Polyethyleneglycol grafting of y-alumina membranes for solvent resistant nanofiltration, Microporous Mesoporous Mater. 229 (2016) 106–116. doi:10.1016/J.MICROMESO.2016.04.024.

(11)   Y.-F. Lin, J.-M. Chang, Q. Ye, K.-L. Tung, Hydrophobic fluorocarbon-modified silica aerogel tubular membranes with excellent CO2 recovery ability in membrane contactors, Appl. Energy. 154 (2015) 21–25. doi:10.1016/J.APENERGY.2015.04.109.

(12)   P. Van Heetvelde, E. Beyers, K. Wyns, P. Adriaensens, B.U.W. Maes, S. Mullens, A. Buekenhoudt, V. Meynen, A new method to graft titania using Grignard reagents, Chem. Commun. 49 (2013) 6998–7000. doi:10.1039/C3CC43695K.

(13)   S.K. Hubadillah, M.H.D. Othman, T. Matsuura, M.A. Rahman, J. Jaafar, A.F. Ismail, S.Z.M. Amin, Green silica-based ceramic hollow fiber membrane for seawater desalination via direct contact membrane distillation, Sep. Purif. Technol. 205 (2018) 22–31. doi:10.1016/J.SEPPUR.2018.04.089.

(14)   C.R. Tanardi, I.F.J. Vankelecom, A.F.M. Pinheiro, K.K.R. Tetala, A. Nijmeijer, L. Winnubst, Solvent permeation behavior of PDMS grafted γ-

alumina membranes, J. Memb. Sci. 495 (2015) 216–225. doi:10.1016/J.MEMSCI.2015.08.004.

(15) V. Szczepanski, I. Vlassiouk, S. Smirnov, Stability of silane modifiers on alumina nanoporous membranes, J. Memb. Sci. 281 (2006) 587–591. doi:10.1016/J.MEMSCI.2006.04.027.

(16) J. Kujawa, S. Cerneaux, W. Kujawski, Investigation of the stability of metal oxide powders and ceramic membranes grafted by perfluoroalkylsilanes, Colloids Surfaces A Physicochem. Eng. Asp. 443 (2014) 109–117. doi:10.1016/J.COLSURFA.2013.10.059.

(17) A. Debrassi, A. Ribbera, W.M. De Vos, T. Wennekes, H. Zuilhof, Stability of (Bio)Functionalized Porous Aluminum Oxide, Langmuir. 30 (2014) 1311–1320. doi:10.1021/la403525z.

(18) G. Mustafa, K. Wyns, P. Vandezande, A. Buekenhoudt, V. Meynen, Novel grafting method efficiently decreases irreversible fouling of ceramic nanofiltration membranes, J. Memb. Sci. 470 (2014) 369–377. doi:10.1016/j.memsci.2014.07.050.

(19) P.H. Mutin, G. Guerrero, A. Vioux, Hybrid materials from organophosphorus coupling molecules, J. Mater. Chem. 15 (2005) 3761–3768. doi:10.1039/b505422b.

(20) G. Guerrero, P.H. Mutin, A. Vioux, Organically modified aluminas by grafting and sol–gel processes involving phosphonate derivatives, J. Mater. Chem. 11 (2001) 3161–3165. doi:10.1039/b104411g.

(21) J. Randon, R. Paterson, Preliminary studies on the potential for gas separation by mesoporous ceramic oxide membranes surface modified by alkyl phosphonic acids, J. Memb. Sci. 134 (1997) 219–223. doi:10.1016/S0376-7388(97)00110-5.

(22) J. Randon, P. Blanc, R. Paterson, Modification of ceramic membrane surfaces using phosphoric acid and alkyl phosphonic acids and its effects on ultrafiltration of BSA protein, J. Memb. Sci. 98 (1995) 119–129. doi:10.1016/0376-7388(94)00183-Y.

(23) J. Caro, M. Noack, P. Kölsch, Chemically modified ceramic membranes, Microporous Mesoporous Mater. 22 (1998) 321–332. doi:10.1016/S1387-1811(98)00107-3.

(24) M.-A. Pizzoccaro, M. Drobek, E. Petit, G. Guerrero, P. Hesemann, A. Julbe, Design of Phosphonated Imidazolium-Based Ionic Liquids Grafted on γ-

Alumina: Potential Model for Hybrid Membranes, Int. J. Mol. Sci. 17 (2016) 1212. doi:10.3390/ijms17081212.

(25)   P. Karakiliç, C. Huiskes, M.W.J. Luiten-Olieman, A. Nijmeijer, L. Winnubst, Sol-gel processed magnesium-doped silica membranes with improved H_2/CO_2 separation, J. Memb. Sci. 543 (2017) 195–201. doi:10.1016/J.MEMSCI.2017.08.055.

(26)   R.J.R. Uhlhorn, M.H.B.J.H.I. Veld, K. Keizer, A.J. Burggraaf, Synthesis of ceramic membranes, J. Mater. Sci. 27 (1992) 527–537. doi:10.1007/BF00543947.

(27)   C.E. Mckenna, M.T. Higa, N.H. Cheung, M.-C. Mckenna, The facile dealkylation of phosphonic acid oialkyl esters by bromotrimethylsilane (1), Tetrahedron Lett. (1977) 155–158.

(28)   G.Z. Cao, J. Meijerink, H.W. Brinkman, A.J. Burggraaf, Permporometry study on the size distribution of active pores in porous ceramic membranes, J. Memb. Sci. 83 (1993) 221–235.

(29)   M.P.J. Dohmen, A.M. Pereira, J. Martin, K. Timmer, N.E. Benes, J.T.F. Keurentjes, Hydrodynamic Radii of Polyethylene Glycols in Different Solvents Determined from Viscosity Measurements, (n.d.). doi:10.1021/je700355n.

(30)   Y. Yuan, T.R. Lee, Contact Angle and Wetting Properties, in: Springer, Berlin, Heidelberg, 2013: pp. 3–34. doi:10.1007/978-3-642-34243-1_1.

(31)   S.P. Pujari, L. Scheres, A.T.M. Marcelis, H. Zuilhof, Covalent surface modification of oxide surfaces, Angew. Chemie - Int. Ed. 53 (2014) 6322–6356. doi:10.1002/anie.201306709.

(32)   J.J. Keating, J. Imbrogno, G. Belfort, Polymer Brushes for Membrane Separations: A Review, ACS Appl. Mater. Interfaces. 8 (2016) 28. doi:10.1021/acsami.6b09068.

(33)   P.G. de Gennes, Conformations of Polymers Attached to an Interface, Macromolecules. 13 (1980) 1069–1075. doi:10.1021/ma60077a009.

(34)   F. Brodard-Severac, G. Guerrero, J. Maquet, P. Florian, C. Gervais, P.H. Mutin, High-Field 17 O MAS NMR Investigation of Phosphonic Acid Monolayers on Titania, Chem. Mater. 20 (2008) 5191–5196. doi:10.1021/cm8012683.

(35)   G. Long, X.-L. Yang, Y. Zhang, J. Pu, L. Liu, H.-B. Liu, Y.-L. Li, F. Liao,

Facile one-step coating approach to magnetic submicron particles with poly(ethylene glycol) coats and abundant accessible carboxyl groups, Int. J. Nanomedicine. 8 (2013) 791–807. doi:10.2147/IJN.S41411.

(36) M. Marrone, T. Montanari, G. Busca, L. Conzatti, G. Costa, M. Castellano, A. Turturro, A Fourier Transform Infrared (FTIR) Study of the Reaction of Triethoxysilane (TES) and Bis(3-triethoxysilylpropyl)tetrasulfane (TESPT) with the Surface of Amorphous Silica, J . Phys. Chem. B. 108 (2004) 3563–3572. doi:10.1021/jp036148x.

(37) G.S. Ahmed, M. Gilbert, S. Mainprize, M. Rogerson, FTIR analysis of silane grafted high density polyethylene, Plast. Rubber Compos. 38 (2009) 13–20. doi:10.1179/174328909X387711.

(38) S.R. Kunst, L. Vanessa, R. Beltrami, H. Ribeiro, P. Cardoso, M.R. Ortega Veja, E. Knopp, K. Baldin, T. Lemos Menezes, C. De, F. Malfatti, Effect of Curing Temperature and Architectural (Monolayer and Bilayer) of Hybrid Films Modified with Polyethylene Glycol for the Corrosion Protection on Tinplate, Mater. Res. 17 (2014) 1071–1081. doi:10.1590/1516-1439.284614.

(39) L.A.S.A. Prado, M. Sriyai, M. Ghislandi, A. Barros-Timmons, K. Schulte, Surface Modification of Alumina Nanoparticles with Silane Coupling Agents, J. Braz. Chem. Soc. 21 (2010) 2238–2245. doi:10.1591/S0103-50532010001200010.

(40) K. Sinkó, R. Mezei, J. Rohonczy, P. Fratzl, Gel structures containing Al(III), Langmuir. 15 (1999) 6631–6636. doi:10.1021/la980686x.

(41) P. Thissen, A. Vega, T. Peixoto, Y.J. Chabal, Controlled, Low-Coverage Metal Oxide Activation of Silicon for Organic Functionalization: Unraveling the Phosphonate Bond, Langmuir. 28 (2012) 17494–17505. doi:10.1021/la3038457.

(42) M.-A. Pizzoccaro-Zilamy, M. Drobek, E. Petit, D. Toteé, G. Silly, G. Guerrero, M.G. Cowan, A. Julbe, Initial Steps toward the Development of Grafted Ionic Liquid Membranes for the Selective Transport of CO 2, Ind. Eng. Chem. Res. 57 (2018) 16027–16040. doi:10.1021/acs.iecr.8b02466.

(43) B.D. Ulery, L.S. Nair, C.T. Laurencin, Biomedical applications of biodegradable polymers, J. Polym. Sci. Part B Polym. Phys. 49 (2011) 832–864. doi:10.1002/polb.22259.

(44) S. Murad, L.C. Nitsche, The effect of thickness, pore size and structure of a nanomembrane on the flux and selectivity in reverse osmosis separations: a

molecular dynamics study, Chem. Phys. Lett. 397 (2004) 211–215. doi:10.1016/j.cplett.2004.08.106.

(45) H.E. Van Der Bij, B.M. Weckhuysen, Phosphorus promotion and poisoning in zeolite-based materials: synthesis, characterisation and catalysis, Chem. Soc. Rev. 44 (2015) 7406. doi:10.1039/c5cs00109a.

(46) Y. Xu, L. Qian, G.D. Prestwich, Synthesis of r-Fluorinated Phosphonates from r-Fluorovinylphosphonates: A New Route to Analogues of Lysophosphatidic Acid, (n.d.). doi:10.1021/ol034597+.

Chapter 3

Solid-state grafting via vacuum infiltration of organo-phosphonic acids into mesoporous alumina supports

ABSTRACT

Organophosphonic acids of both hydrophilic and hydrophobic character were grafted via a solid-state reaction on inorganic γ-alumina flakes. The grafting reaction was studied through FTIR, TGA, and solid-state NMR analysis to understand the type of grafting as well as the grafting density at different reaction temperatures. FTIR confirmed the formation of covalent bonding with only the hydrophobic, n-octadecyl phosphonic acid (ODPA) on the flakes, while the hydrophilic, polyethylene glycol (PEG), grafted samples were not able to directly confirm the formation of a covalent bond. TGA analysis revealed that hydrophobic polymer brushes (ODPA) favour the reaction between phosphonic acid and the inorganic surface, whereas hydrophilic brushes resulted in significantly lower grafting densities. Flat-sheet membrane supports were grafted under solid-state conditions to better understand the grafting reaction between PEG-phosphonic acids and γ-alumina. The membranes were investigated with a series of analytical techniques, including FTIR, water contact angle, and membrane performance tests in water. All these tests showed that reactive groups on the polymeric chain of the organophosphonic acids can gravely influence the reactivity between the phosphonic acids and the inorganic surface. The method used was a more sustainable, simple alternative way to graft the pores of an inorganic support by using a minimal amount of starting materials and minimizing waste production.

3.1. Introduction

Inorganic materials are known for their durability against temperature, mechanical stress, and reactive chemicals. For that reason, they are widely used in a/o heterogeneous catalysis[1,2] and energy storage.[3] Their long lifespan and stability render them appealing also for separations in the chemical industry when shaped, for example, as porous inorganic membranes. However, due to their physical nature and pore sizes, typically in the mesoporous and macroporous range, the applicability of such membranes in separation processes, particularly in the nanofiltration range (retention of 200 – 1000 Da or 0.5 – 2 nm solutes), is limited.[4] Surface modification of porous inorganic membranes with small or large (polymers) organic molecules can tailor the surface properties and shrink the pores to fit the requirements of various applications, including nanofiltration (NF).[4]

Typically, grafting is done through a condensation reaction, resulting in, for example, a covalent bond between a functional group and a hydroxyl group on the surface of a metal oxide.[5] Such functional groups include organosilanes, carboxylic acids, phosphonic acids (PA), and Grignard reagents.[5] Organosilanes, due to their ease of reactivity with a plethora of metal oxides under mild conditions, are the most widely used functional groups for functionalizing inorganic supports.[4,5] Furthermore, organosilanes are prone to homocondensation reactions, which can lead to dense monolayers. On the other hand, this homocondensation can result in multilayer formation. These multilayers are usually hydrolytically unstable[5] and can have a detrimental effect on the grafting density and homogeneity of the final organic-inorganic hybrid material.[5] While these problems are mitigated by controlling the grafting conditions (water content, temperature, reagent concentration, etc.), metal oxides grafted with organosilanes have shown low hydrolytic stability in water and thus are not suitable for aqueous applications.[5,6] Conversely, functional groups such as phosphonic acid demonstrated the formation of strong, hydrolytically stable, and up to three covalent bonds with metal oxides such as alumina, titania, and zirconia.[4,6–8] Additionally, in comparison with the organosilanes, homocondensation reactions with phosphonic acids occur at highly dehydrating conditions,[9] preventing, therefore, the formation of multilayers during grafting. Hence, the application of organophosphonic acids in the fabrication of hybrid inorganic membrane materials is of high significance.

By utilizing phosphonic acids (PA) as a linking group, one can attach a variety of polymers to an inorganic support to match the properties of the hybrid material to the application. For demanding membrane applications, the grafting of phosphonic acid molecules/oligomers on inorganic supports has been used sporadically in membrane technology to either adjust the surface properties of inorganic supports[10–12] or to reduce the pore size.[6] Most of these studies used kinetic control, diffusion of

PA-functional molecules from the bulk solution in the pore to graft the inorganic surface, grafting the top surface of the support, while the pore surface remained primarily not functionalized. However, to increase the retention performance of the membrane, the functionalization of inorganic pores is more crucial. The effect of kinetic control was also observed by Merlet et al.[13] when they attempted to grow (grafting-from) polystyrene brushes from an inorganic alumina support via a living radical polymerization (SI-ATRP). The authors first grafted the support with a small initiator molecule via vapor grafting. Then, the polymer was grown by simple kinetic control resulting in primarily the polymer growth at the outer surface rather than on the pore surface, which was evident by the relatively low separation performance. When the polymer was forced to grow only inside the pores through deactivating the initiator at the top surface, the membrane performance was significantly improved, indicating that the pores were functionalized with the polystyrene. However, for a grafting-to method to overcome the kinetic control, a different approach is needed. As the issue arises primarily due to the diffusion limitation from the bulk to the pore of the support, then by first confining the desirable amount of polymer in the pore can be a viable solution. In the solid state, the coordination of solvent molecules on the inorganic surface is eliminated, and thus the grafting reaction can be enhanced. Additionally, confinement and grafting in the solid state of PA-functional molecules can lower the amount of chemicals needed to graft the pore surface compared to solution-phase grafting and can offer better control on the grafting density, as only the necessary amount is used. This translates to a more cost-effective and sustainable grafting method for the preparation of hybrid inorganic membranes.

In this work, we studied a solid-state grafting method to functionalize γ-alumina surfaces with various organophosphonic acid compounds (Figure 3.1). The grafting method was firstly applied on γ-alumina flakes (solid particles), which allowed us to investigate the influence of the polymeric chain (i.e., alkyl vs. ether; apolar vs. polar) on the solid-state reaction. The investigation was done through a series of analytical techniques, including Fourier-transform infrared spectroscopy (FTIR), nuclear magnetic resonance (NMR), and thermogravimetric analysis (TGA).

n-Octadecyl phosphonic acid
ODPA

Polyethylene glycol ω-phosphonic acid
PEGPA

Poly(ethylene oxide), α-methoxy, ω-phosphonic acid
MPEGPA
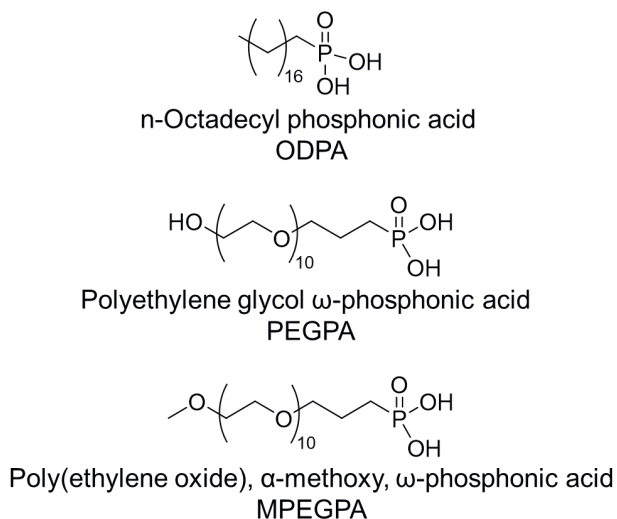
Figure 3.1: Chemical structures of the precursor polymers used in this work, with their corresponding names and abbreviations.

Furthermore, the influence of the confinement and temperature on the solid-state reaction was explored by applying the solid-state reaction on a defined and rigid porous inorganic matrix, which bears similar chemical properties to the γ-alumina flakes. Hence, a mesoporous (pore diameter 5.5 nm) γ-alumina layer supported on an α-alumina macroporous supports was utilized. As porous inorganic layers bear significantly higher (inner) pore surface in relation to the top surface (flakes exhibit larger outer to pore surface), and there are no grafted molecules at the pore entrance to limit the diffusion of the polymer solution inside the pores (steric hindrance), most of the organophosphonic acid molecules will end up inside the inorganic pores, creating a crowded, confined space. Here, two polyethylene glycol (PEG)-phosphonic acids oligomers (Figure 3.1, PEGPA and MPEGPA) which bear different end groups (methyl or hydroxyl), were compared. Through a combination of analytical techniques, including contact angle, water permeability, and dye retentions, we could confirm that the confinement effect is more pronounced at higher reaction temperatures.

3.2. Materials and methods

3.2.1. Materials

Solvents methanol (analytical, 99%, Merck), ethanol (analytical, 99.9%, Merck), ethanol (technical, Boom B.V.), and acetone (technical, Boom B.V.) were used as received. Polyethylene glycol ω-phosphonic acid (PEGPA, n = 10, 580 g/mol) and Poly(ethylene oxide), α-methoxy, ω-phosphonic acid (MPEGPA, n = 10, 590 g/mol)

were prepared as reported in [6]. n-Octadecyl phosphonic acid (ODPA, 334.5 g/mol, Apollo scientific), Rhodamine B (RB, 99%, Merck) and Brilliant yellow (BY, 70%, Sigma Aldrich) were used as received. Milli-Q water (18.2 MΩ cm) was used in all experiments.

α-Alumina (α-Al$_2$O$_3$ > 99 %) flat-sheet supports (disc with diameter 21 mm, thickness 2 mm, and 80 nm pore diameter) with one side polished were purchased from Pervatech B.V., the Netherlands. The polished side was dip-coated with a boehmite sol (prepared in-house) and subsequently calcined at 650 °C for 3 hours. The dip-coating procedure was performed twice to remove any defects remaining in the first layer, resulting in a γ-alumina layer of 3 μm in total thickness and 5.5 nm mean pore diameter. Further details for the fabrication of the γ-alumina layer can be found elsewhere.[14] Calcined supports were washed with a water/ethanol solution (2:1 v/v) for at least 8h at room temperature and then dried overnight in a vacuum oven at 50 °C. For the γ-alumina flakes, the same boehmite sol and the calcination procedure was used as with the membrane preparation.

3.2.2. Grafting procedure

Preparation of the γ-alumina flakes PEGPA/MPEGPA-grafted samples: 744 mg (1.3 mmol) PEGPA or 570 mg (0.9 mmol) of MPEGPA were dissolved with 2-3 mL of methanol (used to transport the polymer in the pores) at room temperature. Then, 1 g of γ-alumina flakes was added to the solution, and the mixture was placed under vacuum (rotavapor) and swirled for 1h at room temperature while the pressure was lowered gradually until the solvent was removed. The impregnated flakes (ImFP and ImFM) were then heated to 60 °C (5 °C/min) to remove any remaining solvent from the pores of the supports. The grafting reaction was done by thermally treating the impregnated samples at or above 150 °C (up to 200 °C) for 12 h under a nitrogen atmosphere (heating/cooling 5 °C/min). After the grafting reaction, the flakes were washed with water followed by ethanol in a sonicated bath for 0.5h. The washing step was repeated 3 times with each solvent. Flakes grafted with PEGPA/MPEGPA are denoted as GFP/GFM150 and GFP/GFM200 for samples thermally treated at 150 and 200 °C, respectively.

Grafting γ-alumina flakes with ODPA: 435 mg (1.3 mmol) ODPA was dissolved in 450 mL of ethanol at 60 °C. Then, in a round bottom flask containing 1 g of γ-alumina flakes, the ethanolic solution of ODPA was added, and the mixture was placed on a rotavapor and swirled for 1h at 60 °C. The pressure was lowered gradually until the solvent was removed. The impregnated flakes (ImFO), obtained in this way, were then heated to 60 °C (5 °C/min) to remove any remaining solvent from the pores of the supports. The grafting reaction was done by thermally treating the impregnated samples at or above 150 °C (up to 200 °C) for 12 h under a nitrogen atmosphere (heating/cooling 5 °C/min). After the grafting reaction, the flakes were washed with

water followed by ethanol in a sonicated bath for 0.5h. The washing step was repeated 3 times with each solvent. Flakes grafted with ODPA are denoted as GFO150 and GFO200 for samples thermally treated at 150 and 200 °C, respectively.

Grafting porous γ-alumina supported α-alumina samples with PEGPA or MPEGPA: 290 mg (0.5 mmol) of PEGPA or 297.7 mg (0.5 mmol) of MPEGPA were dissolved in 5 mL of methanol (100 mM) at room temperature. Cleaned and dried supports were placed in a custom-made impregnation setup with the γ-alumina layer facing upwards, and a hose connected to a vacuum pump was attached to the impregnation setup (Figure S3.1). The impregnation of the solution was done by transferring the PEGPA/MPEGPA solution on top of the support and applying a vacuum for 0.5 h at room temperature. Then, the remaining solution (~ 4 mL) was removed with a Pasteur pipet, and the wet membrane was left to dry at room temperature for 1 h. Subsequently, the membranes were transferred to an oven where the impregnated supports were heated to 60 °C (5 °C/min) to remove any remaining methanol inside the pores of the supports. The grafting reaction was done by thermally treating the supports at or above 150 °C (up to 200 °C) for 12 h under a nitrogen atmosphere (heating/cooling 5 °C/min). After the grafting reaction, the membranes were backwashed (pressure applied on the α-alumina side) in a dead-end permeation setup with water at 30 bar transmembrane pressure (TMP). Washing of the membranes was monitored via UV analysis (λ_{max} = 200 nm) of the permeate, which was performed (3-5 days) until no polymer was observed in the permeate. Membranes grafted with PEGPA will be abbreviated as GP150, GP170, and GP200 for membranes treated at 150, 170, and 200 °C, accordingly. Membranes grafted with MPEGPA will be abbreviated as GM150 and GM200 for membranes treated at 150 and 200 °C, accordingly.

3.2.3. Characterization

Fourier Transform Infrared spectroscopy (FTIR) measurements on both membrane and flake samples were done using a Perkin Elmer UATR Spectrum Two. Wavenumbers between 4000 and 400 cm^{-1} were scanned in reflectance mode at a resolution of 4 cm^{-1} for a minimum of 16 scans. High-resolution scanning electron microscopy (HR-SEM) micrographs of membrane samples were obtained with a Hitachi S-4800 field-emission scanning electron microscope (Japan) using an accelerating voltage of 2 kV. Samples were metalized with platinum to favour charge release. The change in pore diameter of the membrane samples as a function of the grafting procedure was determined by permporometry using cyclohexane as condensable vapor. The experimental procedure is described in detail elsewhere.[15] X-ray diffraction (XRD) analysis was performed on a Bruker D2 phaser at the wavelength of Cu Kα (λ = 1.5405 Å; X-ray power: 40 kV, 40 mA) in Bragg-Brentano scanning mode between the angles 5 and 40° (2θ) were scanned with a step size of

0.05°. ^{27}Al solid-state nuclear magnetic resonance (ssNMR) analysis was acquired using the quantitative Single Pulse technique with ^{1}H decoupling, with a recycle delay of 1 s and a $\pi/12$ pulse of 1 µs (~15°). Aluminium nitrate was used as a secondary reference (peak at 0.0 ppm). The width of the spectral window is 250 kHz, and the line broadening is 50 or 100 Hz. Water contact angles were measured using the sessile drop method, with 2 µL drops of Milli-Q water. Thermogravimetric analysis (TGA) was conducted using an STA 449 F3 Jupiter (Netzsch). Measurements were performed under 55 mL min^{-1} N$_2$ and 15 mL min^{-1} O$_2$ flow with a heating rate of 5 °C min^{-1} from 40 to 800 °C. Temperature calibrations were made using melting standards. Measurements were run sample-temperature controlled. The sample masses were determined using an internal balance 30 min after inserting the sample.

3.2.4. Membrane performance

Permeability and retention data were collected with a custom-made, dead-end filtration setup connected through a pressure regulator valve to a nitrogen tank for pressurizing the solutions. Permeability (L m^{-2} h^{-1} bar^{-1}) is expressed as the flux (L h^{-1}) of water or a solvent across a membrane per unit of driving force per square meter of exposed membrane area (2.4 cm^2). Flux data were collected by weighing the mass of permeate at four-time intervals, while permeability was determined from flux data at three applied transmembrane pressures between 5 and 20 bar by taking the slope of a linear fit of the collected flux data. All slopes were found to be linear unless otherwise noted. Membranes were determined as impermeable (0 L m^{-2} h^{-1} bar^{-1}) to water after being tested at 31 bar (applied pressure) overnight.

Retentions (R) of Brilliant Yellow (BY, Mw = 624.55 g mol^{-1}, 50 ppm) and Rhodamine B (RB, Mw = 479.02 g mol^{-1}, 50 ppm) were calculated by the equation:

$$R = 1 - c_p/c_f \qquad (1)$$

where c_p and c_f are the permeate and feed solute concentrations, respectively. Retention samples were obtained at recoveries between 35 and 50%. Starting volumes used were between 250 and 300 mL. Dye adsorption during filtration tests was assessed by calculating the dye concentration in the feed solution and permeate solution after the end of the experiment. In all cases, the dye mass balance accounts for no or insignificant dye adsorption on the surface of the membranes. Solute concentrations of BY and RB were calculated from Perkin-Elmer λ12 UV-Vis spectrophotometer results at the characteristic wavelength of 401.5 (BY) and 543 (RB/water) nm.

3.3. Results and Discussion

To achieve the overall aim of the study, first, the solid-state reaction between organophosphonic acids (PAs) and the γ-alumina surface (flakes) was investigated. Two different types of organophosphonic acids were used that differ significantly in hydrophilicity; ODPA, due to its alkyl chain (CH_2-CH_2), is considered hydrophobic, whereas both PEGPA and MPEGPA, due to their hydrogen acceptor etheric units (CH_2-O-CH_2),[16] are considered hydrophilic.

For grafting γ-alumina flakes, a homogeneous polymer solution was swirled with anhydrous γ-alumina flakes. The impregnation was done by gradually reducing the pressure while mixing. This way, the solvent was evaporated, and the polymer was impregnated in the inorganic matrix. Then, after removing the solvent, the solid-state reaction was performed by thermally treating the impregnated flakes at 150 or 200 °C for 12h under nitrogen to avoid decomposition of the organic chain in the air.

FTIR analysis was used to investigate the grafting reaction of γ-alumina with ODPA, PEGPA, and MPEGPA, and the results are given in Figure 3.2. FTIR analysis of the pristine materials (ODPA, PEGPA, and MPEGPA) shows the alkyl groups (C-H) between 1500 and 1250 cm^{-1}.[17] In the ODPA spectrum, two strong bands appear in this region which are attributed to the symmetrical alkyl repetitive unit. This differs significantly from the two PEG polymers, as here, the signals appear less intense and at a lower wavenumber. Furthermore, in ODPA, a strong band at 1215 cm^{-1} is attributed to the phosphoryl group (P=O) of the phosphonic acid functional group.[17,18] However, the PEGPA exhibits no observable vibration band for the P=O group, while for MPEGPA, the P=O vibration band is scarcely visible (SI Figure S3.5). This low and almost invisible vibration band is attributed to the presence of the P-OH and C-OH, present in PEGPA, groups which can intermolecularly interact with the P=O group via a hydrogen bond resulting in a broader and lower frequency band.[19] In the FTIR spectra of PEGPA and MPEGPA, the strong vibrational band at 1090 cm^{-1}, accompanied by a small signal at 1034 cm^{-1}, is assigned to the asymmetric and symmetric vibration bands of the etheric repetitive unit. Furthermore, the bands appearing between 980 and 930 cm^{-1} for ODPA and both PEGPA and MPEGPA are attributed to the phosphonic acid group (P-OH).[19,20]

For the impregnated flakes (ImFO/P/M), the spectra are relatively similar to the pristine polymers. Only the ImFP sample differs from the PEGPA spectrum in the region between 980 and 930 cm^{-1}, associated with the acid P-OH vibration band. Here, the P-OH bond is only visible as a shoulder, while for both ImFO and ImFM, the phosphonic acid vibration band is clearly observed. From the aforementioned, it can be hypothesized that the P-OH groups of PEGPA interact intermolecularly with both the hydroxyl-terminal groups of other PEG chains and the hydroxyl groups on the γ-alumina surface. So, the presence of a polar protic group, like the hydroxyl,

interferes between the reactive sites on the inorganic surface and the phosphonic acid affecting, in turn, the reactivity between PA and the inorganic surface.

Grafting of the different polymers through a temperature treatment results in all cases in significant differences with the FTIR results compared to the pristine and impregnated samples. Grafting of ODPA (GFO150/200) leads to a narrower P=O band which is downshifting from 1215 to 1190 cm^{-1}. The shifting of the P=O band suggests a change in the chemical environment around the functional group. Narrowing of the same band indicates that the newly formed chemical environment around the P=O group is more symmetrical. Furthermore, the disappearance of the P-OH band, along with a newly formed band at 1126 cm^{-1}, indicates the formation of a covalent bond between the alumina surface and the phosphonic acid (P-O-Al).[17] This confirms the successful grafting of ODPA on the γ-alumina surface for both GFO150 and GFO200. However, for GFO150, the P=O band exhibits a narrower shape, and smaller downshift than for GFO200. This indicates that at 150 °C, the grafted species have, in the majority, a similar chemical environment (i.e., are attached on the surface in a similar manner or via a single binding mode, either mono-, bi-, or tri-dentate). On the other hand, at 200 °C, the reactivity of PAs with the inorganic surface can be increased either due to a temperature dependency, as shown by others,[21] a dissolution-precipitation phenomenon, or due to an increase in the polymeric chain mobility. Increased reactivity leads to higher grafting densities and, thus, denser monolayers. Denser monolayers imply less available space for each PA molecule leading to grafted species with a combination of binding modes; therefore, PA molecules (in this case, the P=O bond) can have different chemical environments in their vicinity and thus leading to the broadening of the P=O band on the FTIR spectrum of GFO200. On the other hand, this can also be due to the formation of aluminium phosphate or phosphonate phases.

Grafting of PEGPA and MPEGPA results in FTIR spectra that show similar absorption bands with different intensities in the region between 1250 and 900 cm^{-1}. The P-OH bands on all PEG-grafted samples disappear. However, no new bands are visible near the 1190 cm^{-1} IR region where the P-O-Al bond is expected. The lack of visibility of the P-O-Al band in the FTIR spectrum can be caused by the strong C-O-C absorption band and overlaps with the P-O-Al. As no P-OH bands are present after grafting, and the spectra were recorded after thoroughly washing of the samples (TGA shows a measurable change in the amount of polymer before grafting and after washing of the grafted materials), it is concluded that for all samples, a covalent bond was formed. Comparing the different reaction temperatures, a more intense C-O-C band appears for the samples prepared at 200 °C compared to 150 °C. This can be related to additional material grafted on the inorganic surface with increasing temperature. Still, with solely FTIR, we cannot study the influence of the temperature

on the reactivity between PA and the inorganic surface and the resulting binding modes formed under different temperatures.
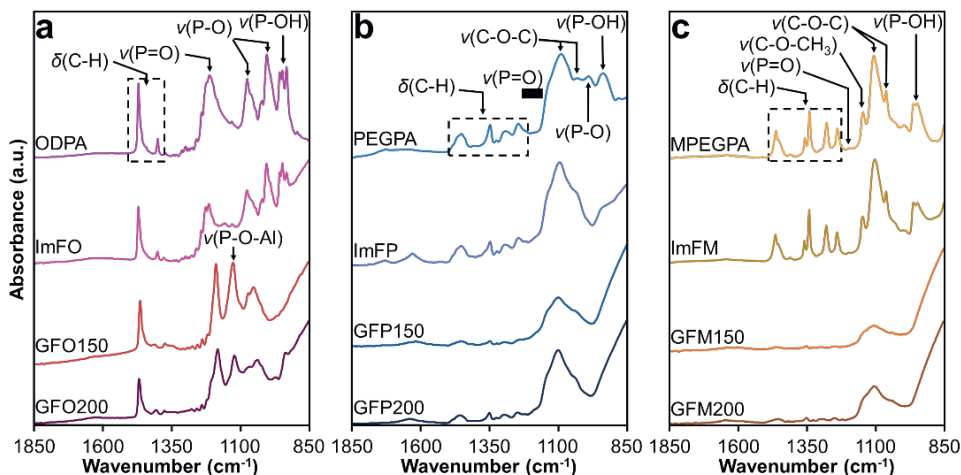
Figure 3.2: FTIR spectra of ODPA (a), PEGPA (b), and MPEGPA (c) in their pristine form, impregnated (ImF) on γ-alumina flakes and grafted on γ-alumina flakes at 150 °C (GFO/GFP/GFM150) and 200 °C (GFO/GFP/GFM200). For the P=O absorption band in PEGPA, which is not observed, a range is given with a black bar where it should appear according to the literature.[22]

After successfully grafting the γ-alumina flakes, the samples were further characterized with thermogravimetric analysis (TGA). TGA can provide information on the surface coverage of the γ-alumina flakes with the different polymers. TGA results of the impregnated and grafted samples are provided in Figures S3.1-S3.3 and Table S3.1. Analysis of the impregnated samples shows a surface coverage of 3.4, 2.8, and 2.7 P nm^{-2} (= number of P atoms per nm^2) for ODPA, PEGPA, and MPEGPA, respectively. ODPA grafted samples show relatively high surface coverage of 3.2 P nm^{-2} and an overall grafting yield of more than 90%, independent of grafting temperature. This demonstrates the effectiveness of the solid-state reaction for ODPA. However, high grafting densities of the ODPA grafted alumina samples could suggest the formation of crystalline aluminium phosphonate phases by a dissolution–precipitation mechanism.[23] XRD analysis (Figure S3.10) of the ODPA grafted samples were conducted, and the results indicate that at temperatures exceeding 170 °C, a different phase (17 – 26°) appears, which becomes dominant at 200 °C.

For PEGPA, the surface coverage increases with the reaction temperature from 1.6 P nm^{-2}, for GFP150, to 1.8 P nm^{-2}, for GFP200, resulting in reaction yields of 58 and 65%, respectively. The MPEGPA samples show even lower surface coverage of 0.5

and 0.6 P nm^{-2} and reaction yields of 17 and 24% for GFM150 and GFM200, accordingly. For both PEGPA and MPEGPA samples, no aluminium phosphonate phases were detected by either ^{27}Al solid-state NMR analysis (Figure S3.8) or XRD (Figure S3.9). The difference in grafting yield, or grafting efficiency, between the polymers could be due to their size, as ODPA has only 18 methyl groups (18 elements) in the polymeric chain, whereas both PEGs (PEGPA and MPEGPA) have 10 ethyl glycols in their polymeric chain (30 elements) and thus occupy more space per molecule on the inorganic surface leading to lower grafting densities (molecule per nm^2). However, the size of the polymer cannot explain the difference in grafting yield observed between the PEGPA/MPEGPA samples and in comparison to the ODPA-grafted samples.

A noteworthy difference between the polymers used is the hydrophilicity, or polarity, of their organic (polymeric) chain. PEGPA shows the most hydrophilic character among the two PEG polymers as the protic hydroxyl-terminal group is a strong hydrogen bond donor and can strongly adsorb on hydroxyl-rich inorganic surfaces. As a result, the coordination of the different polymers with the γ-alumina surface differs and, thus, their reactivity with the inorganic surface. As schematically illustrated in Figure 3.3, we assume that in the case of the ODPA grafted samples, the PA does not interact with the apolar alkyl chain of the ODPA, but it will coordinate preferentially towards the hydroxyl-rich inorganic (alumina) surface as represented by the blue arrow (Figure 3.3a, top). In contrast, in the case of PEGPA and MPEGPA, both the PA and the etheric polymers can interact with one another and the inorganic surface via hydrogen bonds (green arrow, Figure 3.2b, and c, top). Furthermore, the protic hydroxyl group of the PEGPA can strongly adsorb on the inorganic surface and uses reactive sites that otherwise would have been available for reacting with the PA (Figure 3.3b). As a result, ODPA has the most favourable coordination with the inorganic surface, leading to high reaction yields and grafting densities and validating the TGA results (SI, section 3.5.2). In contrast, PEG chains can interfere intermolecularly with other PEGs as well as with the inorganic surface (covering reactive sites or aluminols), leading to lower reaction yields as well as grafting densities. Based on this discussion, PEGPA, due to the hydroxyl-terminal group, is expected to result in lower grafting densities than MPGEPA. However, TGA results indicate a significantly higher grafting density for PEGPA than for MPEGPA. This rather contradictory result may be the product of a side, or self-condensation reaction that occurs between the hydroxyl-terminal group of PEGPA and the PA group, similarly to the grafting reaction, as shown in Figure 3.3b (bottom). The side reaction with PEGPA would lead to additional material attached to the inorganic surface and hence higher grafting densities (compared to MPEGPA).
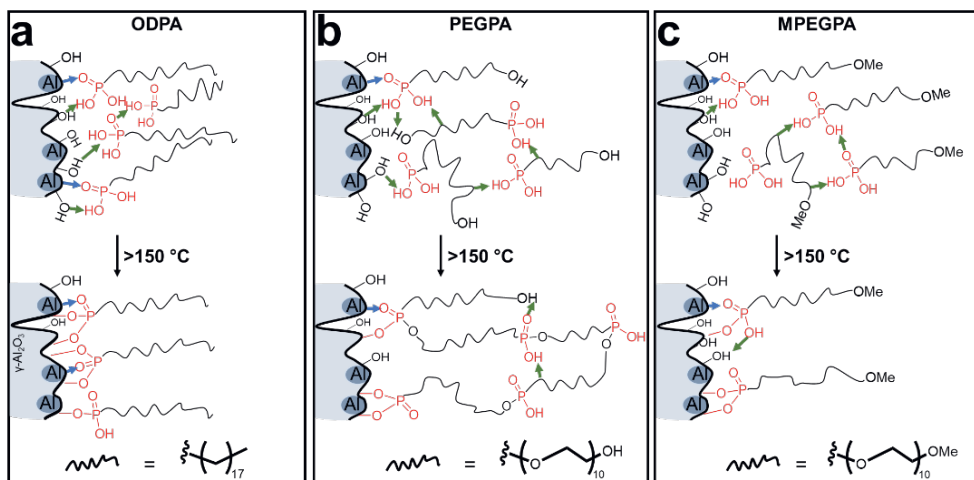
Figure 3.3: Schematic representation of the ODPA (a), PEGPA (b), and MPEGPA (c) after impregnation (top) and after thermal treatment in the solid state (bottom). (Al) denotes Lewis acid site on the inorganic surface, ➡ denotes coordination with the surface, and ➡ denotes hydrogen bonding.

To directly confirm that indeed a self-condensation reaction takes place for PEGPA, the pristine polymers (PEGPA and MPEGPA) were treated under the grafting conditions, meaning a temperature treatment of 200 °C under a nitrogen atmosphere. The resulting materials were compared optically and chemically (FTIR) with the pristine polymers. Figure 3.4 shows images of the PEGPA and MPEGPA before and after thermally treating the polymers and further immersing them in dimethylformamide (DMF). PEGPA, in its pristine form, is a brown viscous liquid (Figure 3.4, PEGPA). However, after thermal treatment at 200 °C, the liquid PEGPA formed a brown film, as shown in Figure 3.4 (PEG200). Interestingly, the PEG200 sample was not soluble in any solvents tested, such as water, DMF (Figure 3.4), or chloroform. On the other hand, MPEGPA, after the thermal treatment, optically looked similar to the pristine material (Figure 3.4, MPEG200) and was soluble in all solvents tested (water, DFM, and chloroform). Additionally, FTIR analysis of the pristine PEGPA and MPEGPA before and after thermal treatment (Figure S3.5) shows that only for PEGPA the doublet band, attributed to the asymmetric and symmetric vibration bands P-OH at 988 cm^{-1}, start to merge. Besides, FTIR analysis of the PEGPA indicates the consumption of the P-OH bond and hence the esterification of the acid (P-O-C, 1035 cm^{-1}). Therefore, these experiments confirm that the PEGPA can undergo an intermolecular self-condensation reaction to form a phosphonate ester (Figure S3.7), leading to higher grafting densities (determined via TGA) than MPEGPA. Finally, it should be noted that at lower temperatures, the self-

condensation reaction of PEGPA is significantly slower, as shown in Figure S3.6, where the pristine PEGPA is still in liquid form after thermal treatment at 150 °C. Therefore, the higher grafting densities observed with PEGPA compared to MPEGPA cannot only be attributed to its self-condensation reaction. This will be discussed in the next section.
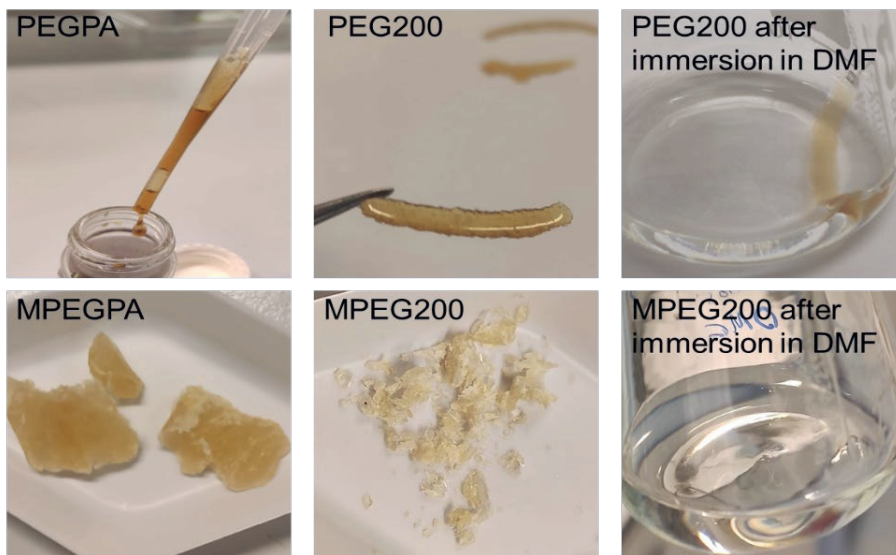
Figure 3.4: Images of PEGPA (top) and MPEGPA (bottom) before (PEGPA/MPEGPA), after thermal treatment at 200 °C for 12h under nitrogen atmosphere (PEG200/MPEG200), and after subsequent immersion in DMF.

3.3.1. Membrane characteristics

Grafted inorganic membranes on supported γ-alumina layers were then prepared using a similar solid-state approach as developed on the flakes. The γ-alumina layer used in this work exhibits a thickness of 3 μm with a pore diameter of 5.5 nm and a porosity of ~60 % and is supported on an α-alumina macroporous layer ($\varnothing_{pore} \approx 80$ nm, thickness ≈ 2 mm). Here, only the grafting of PEG and MPEGPA were studied as the grafting of ODPA led to high grafting densities but also with phase change in the γ-alumina layer, which could potentially lead to a defected membrane layer. Furthermore, the apolar character of ODPA will result in a hydrophilic membrane surface and will resist the water permeability significantly and thus is not suitable for aqueous applications. In addition, two PEG-PAs were selected to conduct a direct comparison with PEG grafted membranes prepared via solution phase grafting.[24] It is known that upon confinement, the properties of a molecule can change. Therefore here, we also aim to get a better insight into the influence of temperature on the solid-

state grafting reaction upon confinement. This should allow us to determine the best conditions to control and achieve high separation performance.

FTIR analysis was performed on the pristine γ-alumina layer (γ-Al$_2$O$_3$) as well as the grafted membranes, and the results are provided in Figure 3.5. The FTIR spectrum of the pristine γ-alumina shows no significant absorption bands in the region provided. Overall, the spectra of the grafted samples (GP/GM150 and GP/GM200) exhibit similar absorption bands and are similar to the spectra obtained from the grafted γ-alumina flakes (Figure 3.2). Only minor differences in intensity are observed between the two PEG polymers in the region where the PEG chain absorbs (1200 to 970 cm^{-1}). These differences are attributed to the hydroxyl-terminal group of PEGPA and the self-condensation reaction that is exclusive to PEGPA. The self-condensation of PEGPA molecules can lead to higher concentrations of PEG on the support (as shown for flakes by TGA), increasing the intensity of the C-O-C bond in the IR spectrum. Similarly to the grafted flakes, the P-O-Al bond overlaps with the C-O-C absorption band and hence is not visible with FTIR. The membranes were thoroughly washed with water under the constant pressure of 30 bars to ensure that the observed bands belong only to grafted PEGs. The washing procedure took place until no more PEGs were observed in the permeate solution of each membrane via UV analysis (Figure S3.1, step 3).
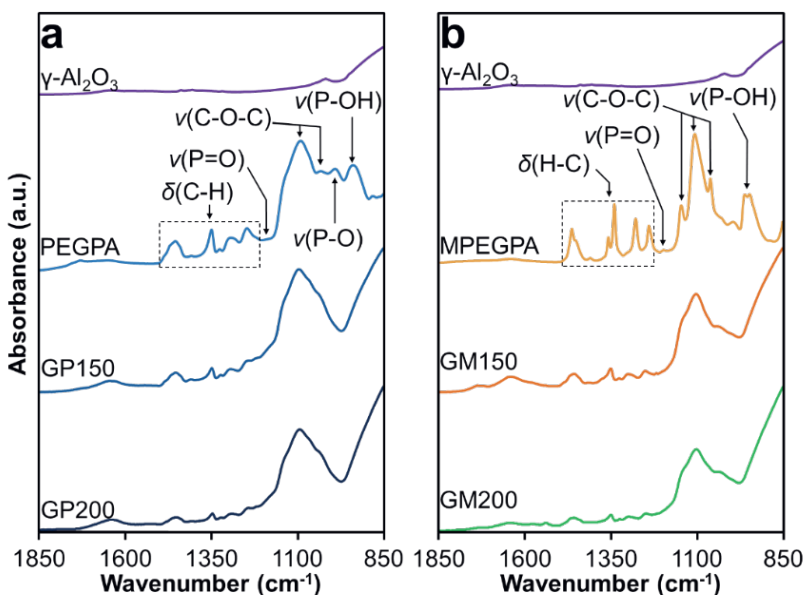
Figure 3.5: FTIR spectra of the γ-alumina layer (γ-Al$_2$O$_3$), pure and grafted PEGPA (a) and MPEGPA (b) at 150 (GP/GM150) and 200 °C (GP/GM200).

The distribution of the PEGPA polymer in the inorganic support was analysed by SEM, and further analysing the P/Al ratio by means of EDS. By analysing the cross-section of the PEGPA membranes grafted at different temperatures, we can qualitatively observe the distribution of the polymer (through the presence of P) over the γ-alumina layer and understand the effect of the impregnation step. The SEM-EDS results of the PEGPA grafted membranes and the SEM micrographs of each sample are provided in Figure 3.5. Overall, the membranes exhibit a similar distribution of phosphorus over the γ-alumina layer. Furthermore, all samples showed no phosphorus in the α-alumina support. The phosphorus distribution is uniform to penetration depths of 1.5 – 2 μm, and at higher depths, the phosphorus concentration significantly drops and reaches 0 in the α-alumina layer. This illustrates that the impregnation step is, indeed, forcing the polymer towards the inner pore surface. Even though TGA analysis showed an increase in the grafting density with higher temperature, still the SEM-EDS analysis indicates a similar distribution of PEG over the γ-alumina surface unrelated to temperature. This can be related to the limitation of the measurement as SEM-EDS analysis is a qualitative analysis and can only provide rough estimations on the amount of material on the samples. Finally, the thermal treatment shows no influence on the penetration depth of the polymer in the pores of the γ-alumina layer. As a result, the penetration depth at which the polymer is grafted seems to be related to the impregnation step rather than the grafting step (reaction temperature).
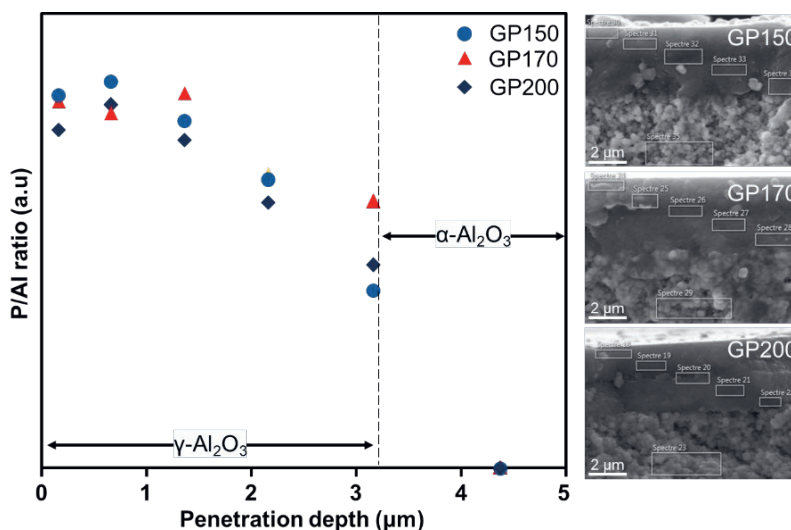
Figure 3.6: SEM-EDS analysis of the cross-section of PEGPA grafted membranes at 150 (GP150), 170 (GP170), and 200 °C (GP200). The atomic ratio between phosphorous (P) and aluminium (Al) is provided over the depth (left), which is the distance from the top surface (γ-Al$_2$O$_3$) of the membrane towards the bottom side (α-Al$_2$O$_3$). The SEM micrographs (right) for each sample are provided along with the spots analysed with EDS for the estimation of the P and Al content of each sample.

The surface properties of membranes were studied with water contact angle analysis and the results are provided in Figure 3.6. The PEG brushes contain etheric units and a hydrogen bond acceptor (C-O-C) and therefor show a hydrophilic character, but significantly less than the pristine inorganic surface, containing hydroxyl groups. Overall, the grafted membranes show higher contact angles than the pristine support, which can be attributed to the functionalization and "masking" of the superficial hydroxyl groups (aluminols) of the γ-alumina layer. For the PEGPA grafted membranes (GP), the water contact angle is decreasing, from 83 to 46°, with increasing grafting temperature from 150 to 200 °C. On the other hand, the MPEGPA grafted membranes (GM) show similar contact angles (~40°) at both 150 (GM150) and 200 °C (GM200) grafting temperatures. The difference between the two types of membranes, GP and GM, could be attributed to the self-condensation reaction between PEGPA molecules. During the grafting reaction, PEGPA molecules can react with the surface and themselves via the terminal hydroxyl group, which leads to the formation of a phosphonate ester (P-O-C). Compared to its hydroxyl precursor, the phosphonate ester is less hydrophilic and can lead to higher water contact angles.

Interestingly, the water contact angle of PEGPA-grafted membranes decreases with increasing grafting temperature. This is because, at higher temperatures, the self-condensation reaction increases, leading to the intermolecular linkage between the polymers. Thus more available hydrophilic groups (C-OH and/or P-OH) at the surface of the membrane lead to lower water contact angles. However, we still have no clear indication of whether the grafting conditions can significantly affect the membrane performance.
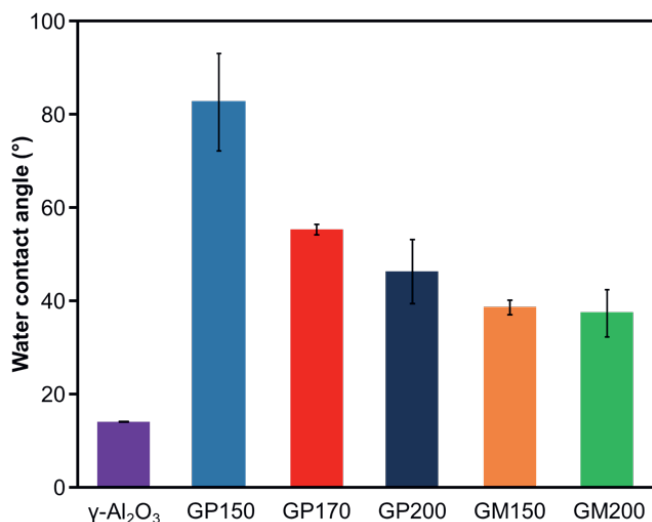
Figure 3.7: Water contact angle of the pristine γ-alumina (γ-Al$_2$O$_3$) and PEG grafted membranes prepared at different grafting temperatures.

Further analysis of the membrane samples, such as pore size distribution and retention tests, can allow us to evaluate and identify the optimal separation performance in function of the grafting temperature for the two PEGs.

Cyclohexane permporometry was employed to get more insight into the influence of grafting conditions on pore size. Before the analysis, the applicability of the Knudsen equation during cyclohexane capillary condensation was confirmed by conducting single gas permeation tests on the grafted membrane samples (SI). A comparative analysis of the pore diameter between the pristine and grafted inorganic membranes is given in Figure 3.8. The pristine inorganic support (Figure 3.8, γ-Al$_2$O$_3$) shows a relatively narrow pore diameter distribution with a mean pore diameter of 5.5 nm. Overall grafting of PEG on the γ-alumina support results in smaller pore diameters compared to the pristine support. With Increasing grafting temperature (from 150 to 200 °C) a decrease in pore diameter is observed with both PEGPA and MPEGPA. PEGPA samples prepared at 150 and 170 °C (GP150 and GP170) result in a less steep transition in the oxygen permeance (Figure 3.8a), which translates to a

102

broadening in the pore size distribution, while for MPEGPA, a steeper transition is observed, indicting a narrower pore size distribution. As discussed before, the broadening in pore size distribution for GP150/170 samples is probably due to the phosphonate ester formation (via self-condensation reaction). Samples treated at 200 °C with PEGPA (GP200) and MPEGPA (GM200) exhibit no transition point in the oxygen permeance (Figure 3.8a and b), which means that the pore diameters are below the detection limit of the permporometry equipment (< 2 nm). Interestingly, the significant pore shrinkage from 150 to 200 °C with PEGPA was rather expected due to the self-condensation reaction of the precursor molecules. However, with MPEGPA, no homocondensation or self-condensation reactions of the precursor molecules are expected. As increasing temperatures increase the mobility of the polymeric chains, these chains can stretch more (from mushroom to brush-like), and additional PEG molecules can fit next to each other on the γ-alumina pore surface. Due to these stretched PEG chains, the pore size of the grafted membranes can significantly shrink, as observed with permporometry. Therefore, we observe a synergistic effect between the nanoconfinement of the polymer in the pores and higher grafting temperatures on the grafting density of inorganic membrane layers. Contrary to SEM-EDS results, cyclohexane permporometry indicates that higher grafting densities can be achieved at higher temperatures. As mentioned before, the resolution of SEM-EDS analysis is low and, therefore can only be used to indicate the polymer's distribution over the inorganic matrix.
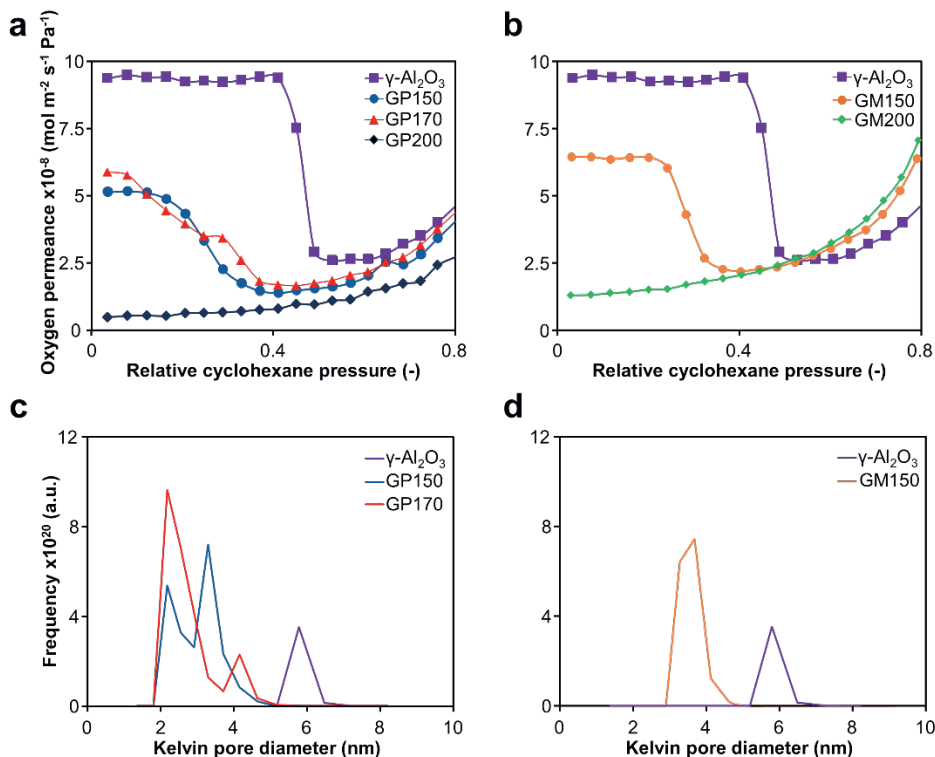
Figure 3.8: Cyclohexane permporometry analysis results. Oxygen permeance over the relative cyclohexane pressure of the pristine γ-alumina (γ-Al$_2$O$_3$) and the PEGPA (a) and MPEGPA (b) grafted membranes at 150 (GP/M150), 170 (GP170), and 200 °C (GP/M200). Estimated Kelvin pore diameter distributions of the pristine and PEGPA (c) and MPEGPA (d) grafted inorganic membranes. For sample GP/GM200, the pore diameter is smaller than 2 nm and does not allow cyclohexane capillary condensation to occur in the pores. Therefore, GP/GM200's pore diameter is below the method's limit and is not provided here.

3.3.2. Performance of PEGPA and MPEGPA grafted γ-alumina membranes

The homogeneity of the grafting over the pore surface of the inorganic support for the PEG grafted membranes was further studied through water permeability and dye retention tests (Figure 3.9). Lower water permeabilities relate to higher flow resistance to water which can be attributed to smaller pores as well as to a less hydrophilic character of the grafted membranes compared to the pristine support (see Figure 3.7). A comparison of the GP150 with the GM150 membranes shows that GP150 has a smaller pore size (Figure 3.8) and a less hydrophilic character (Figure 3.7) than GM150, while the water permeability is the same as that of GM150 (Figure 3.9). Therefore, it can be assumed that the main contribution to the drop in water

104

permeability for the grafted membranes is due to the denser pores of the grafted membranes rather than their lesser hydrophilic character compared to the pristine γ-alumina. Besides, by considering the PEGPA-grafted membranes (GP), a decrease in contact angle is observed with increasing reaction temperature, while there is a strong decrease in permeability.

Furthermore, retention tests were performed with Brilliant Yellow (BY, 629 Da) and Rhodamine B (RB, 479 Da) in water on the pristine PEGPA and MPEGPA grafted inorganic membranes. The results are given in Figure 3.9b. Compared to the pristine support, all grafted membranes showed an increase in the retention of BY, with all grafted membranes exceeding 90% solute retention. GP170 and GM150, and GM200 exhibited better RB retentions than the pristine membrane, while the GP150 membrane almost showed no difference in retention compared with the pristine support. GP170 samples were able to retain, on average, 52% RB, whereas MPEGPA grafted membranes showed significantly higher retentions of 84% (GM150) and 75% (GM200). Evidently, the best PEGPA grafted membrane (GP170) exhibited a factor 2.5 higher RB retention as compared to the pristine support. On the other hand, the best MPEGPA grafted membrane (GM150) showed almost 6 times higher RB retention than both the pristine and GP150 membranes.

Interestingly, GP150 and GP170 show relatively smaller pore diameters than GM150 (Figure 3.8), but RB retention is significantly higher with GM150. This can only be attributed to the interference and self-condensation reaction of PEGPA. Here, it is important to mention that permporometry was done using cyclohexane which is an apolar solvent, and the brush-like chains (flexible), due to their polar character, can behave different in apolar (cyclohexane) and polar (water) solvents, which can explain the differences observed between permporometry and dye retention. Additionally, solute retention is not only depended on pore size, as other mechanisms, such as Donnan exclusion, can affect the retention of charged dyes in water. GM200 shows lower RB retention than GM150 and lower water permeability. Therefore, with water permeability and dye retention tests, we observe that the solid-state grafting reaction between PA and the inorganic surface results in a stable covalent bonding. Furthermore, by increasing the reaction temperature, the grafting density increases as the permeability decrease significantly. Finally, at higher temperatures (200 °C), the reaction seems to lead to an inhomogeneous grafting and thus leading to lower RB retentions. Thus, the results indicate that at relatively low temperatures (150 – 170 °C), the grafting reaction is the optimum for homogeneously grafting the pore surface of inorganic layers.
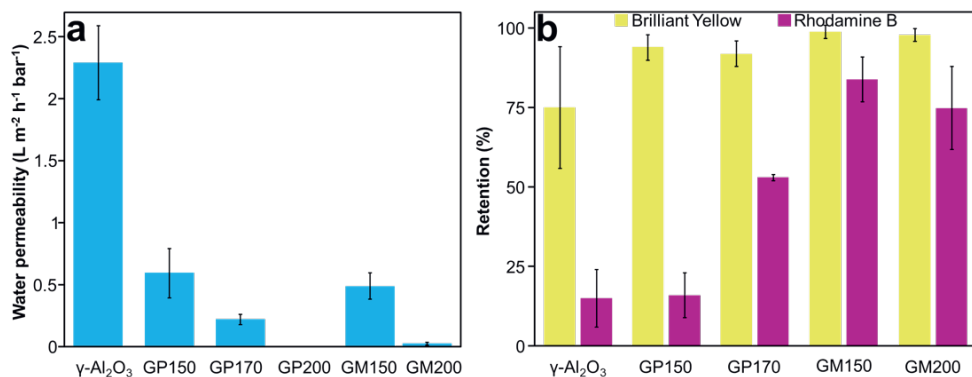
Figure 3.9: Water permeability (a) and dye retention (b) of the pristine, PEGPA, and MPEGPA grafted membranes. 50 ppm of Brilliant Yellow (624 Da) and Rhodamine B (479 Da) in water were used for the nanofiltration tests. Dye retention tests were not performed on GP200 membranes as they showed no water permeability.

Overall, with this work, we showcase the potential and better understand a simple method for confining a small polymer inside the mesopores of an inorganic support to fabricate stable organic-inorganic hybrid materials. This method can be expanded to different polymers but also different support types, such as titania, and shapes, such as tubular inorganic membranes depending on the application.

3.4. Conclusion

A simple method is described to graft the pore surface of mesoporous γ-alumina supports with organo-phosphonic acid polymers. The grafting of the polymers on the pore surface was achieved by impregnating the inorganic supports with a methanolic solution of the polymer under vacuum, followed by a solid-state grafting reaction at temperatures varying from 150 to 200 °C. Utilizing FTIR, the covalent bonding between organo-phosphonic acid and the inorganic surface was confirmed. In addition, TGA results indicated an influence on the polarity of the polymers, where apolar polymers result in significantly higher grafting densities. Furthermore, we identified a secondary self-condensation reaction during grafting with the hydroxyl-terminated PEG-phosphonic acid. However, this secondary reaction was avoided when employing a methoxy-terminated PEG-phosphonic acid.

Grafting of the PEGPA and MPEGPA at 200 °C resulted in larger pore shrinkages than grafting at 150 °C. This indicated a synergistic effect between polymer nanoconfinement and reaction temperature on the grafting density on the pore surface. In addition, membrane performance tests (water permeability and dye retention) indicated that PEGPA and MPEGPA grafting results in different microstructures in the mesopores of γ-alumina layers.

The grafting method described here is a simple method that potentially can be expanded to different organophosphonic acids (polystyrene, polydimethylsiloxane, polymethyl methacrylates etc.), and inorganic supports for the fabrication of materials with varying surface and pore properties. Examples of these include the grafting of hydrophobic ODPA that potentially can be used to increase the stability of an inorganic support in acidic or basic conditions,[25] for catalysis, and more. Furthermore, the simplicity of the method allows for easy upscaling of the technology to commercial supports, such as tubular inorganic membranes, by utilizing available techniques such as simple vacuum pumps or liquid permeation setups to force the solution into the pores.

3.5. Supporting information

1. Schematic representation for membrane fabrication
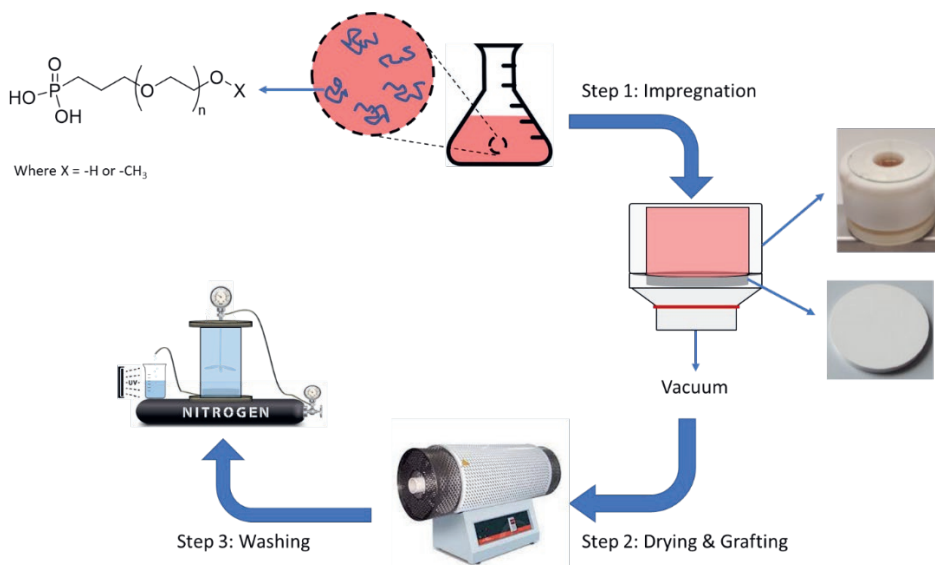
Figure S3.1: Schematic representation of the impregnation method used to graft the pores of the γ-alumina layer supported on a macroporous α-alumina supports. Firstly, a solution of PEGPA or MPEGPA in methanol is poured on top of the γ-alumina layer, which is sealed inside a specialized mould. Then vacuum is applied from the side of the α-alumina layer, which forces the polymer solution to impregnate the support. After the impregnated sample is dried, then the grafting reaction takes place under nitrogen at temperatures above 150 °C. Finally, the unreacted polymer was removed by pushing water through the pores of the membrane at 30 bar until no more polymer is observed via UV analysis of the permeate solution.

2. Thermogravimetric analysis (TGA) of impregnated and grafted γ-alumina flakes

TGA analysis was conducted from 30 to 800 °C in air at a heating rate of 5 °C/min. The amount of powder used was exceeding 30 mg for each run.
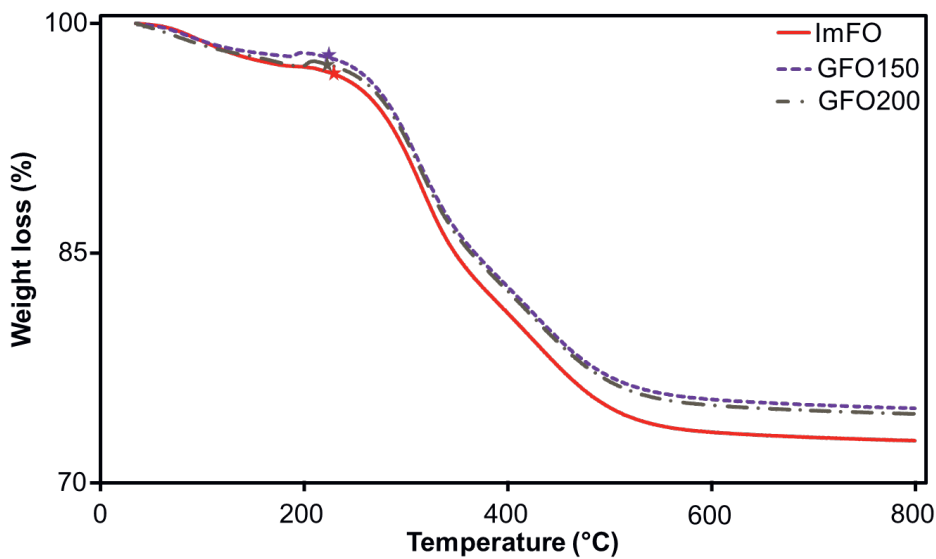
Figure S3.2: Weight loss over temperature for impregnated and grafted γ-alumina flakes with ODPA.
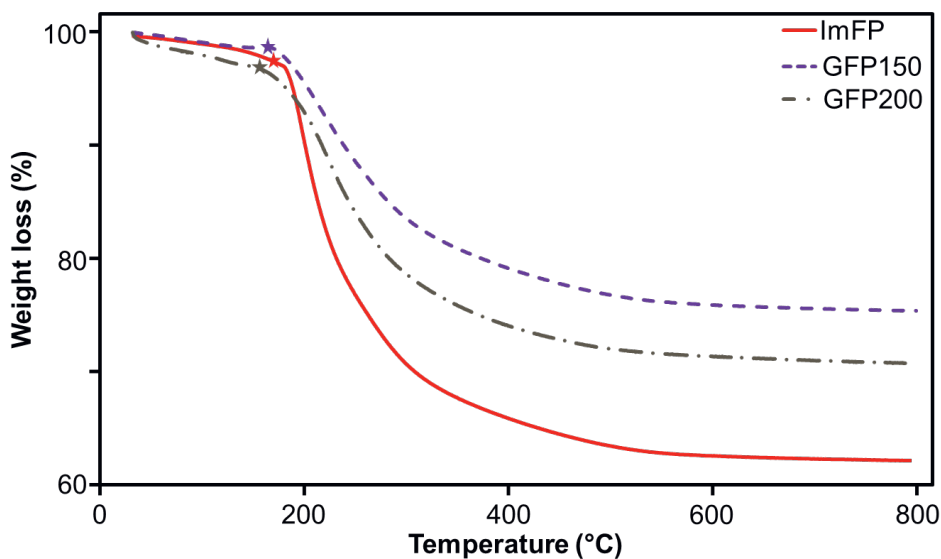
Figure S3.3: Weight loss over temperature for impregnated and grafted γ-alumina flakes with PEGPA.
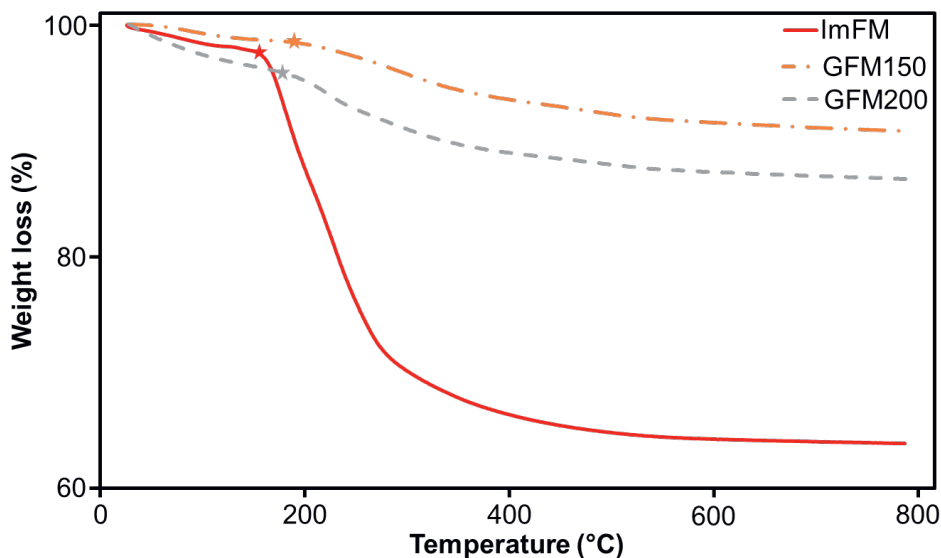
Figure S3.4: Weight loss over temperature for impregnated and grafted γ-alumina flakes with MPEGPA.

Table S3.1: Values obtained from the TG analysis of the γ-alumina flakes impregnated with ODPA, PEGPA or MPEGPA and after treatment at different temperatures.

Sample	Weight loss organics (%)	Inorganic mass (mg)	* P (mmol g^{-1})	**Grafting density (P nm^{-2})	***Reaction yield (%)
ImFO	25	76	1.3	3.4	-
GFO150	23	77	1.2	3.2	93
GFO200	23	77	1.2	3.2	92
ImFP	34	66	1.0	2.8	-
GFP150	23	77	0.6	1.6	58
GFP200	25	75	0.7	1.8	65
ImFM	34	66	1.0	2.7	-
GFM150	8	92	0.2	0.5	18
GFM200	10	90	0.2	0.6	22

The weight loss was calculated for each sample by subtracting the weight loss before the steep part of the curve (shown with an asterisk, ≈ 200 °C) with the weight loss at the end of the TG curve, where the decomposition of the organics took place.

* For the calculation of P (PEG) mmol g^{-1} equation (1) was used:

$$\frac{P \; mmol}{g} = \frac{Weight \; loss \; (g)}{MW_{org}\left(\frac{g}{mol}\right) * mass_{\gamma+PA}(g)} * 1000 \qquad (1)$$

Where, MW$_{org}$ is the molecular weight of only the organic part of each organo-phosphonic acid (ODPA, PEGPA, and MPEGPA) used to graft γ-alumina flakes, calculated by subtracting the molecular weight of the whole molecule from the inorganic part (phosphonic acid). For the calculation, the following molecular weights were used: MW$_{OD}$ = 253 g mol^{-1} MW$_{MPEG}$ = 513 g mol^{-1}, MW$_{PEG}$ = 499 g mol^{-1}. The inorganic mass was calculated according to the formula mass$_{\gamma+PA}$ = 100 – Weight loss.

** For the surface coverage of PEG molecules per nm^2 of γ-alumina (P nm^{-2}), equation (2) was used:

$$\frac{P}{nm^2} = \frac{\frac{mmol}{g} * Avogadro \; \#(\frac{P}{mmol})}{SA_\gamma \; (\frac{nm^2}{g})} \qquad (2)$$

Where, Avogadro's # = 6.022*10^{20} P mmol^{-1} and SA$_\gamma$ = 2.25*10^{20} nm^2 g^{-1}.

*** The reaction yields were calculated with equation (3):

$$Reaction \; yield \; (\%) = \frac{\frac{P \; mmol_{gr}}{g}}{\frac{P \; mmol_{im}}{g}} * 100\% \qquad (3)$$

Where, the P mmol$_{gr}$ g^{-1} is the amount of mmol PEG that remained after the grafting reaction per gram of γ-alumina, and P mmol$_{im}$ g^{-1} is the is the amount of mmol PEG after impregnation per gram of γ-alumina.

3. FTIR analysis of pure and thermally treated pristine PEG brushes

Pristine PEGPA and MPEGPA were thermally treated at 150 and 200 °C, similarly to membrane preparation. The materials before and after the thermal treatment were characterized with FTIR
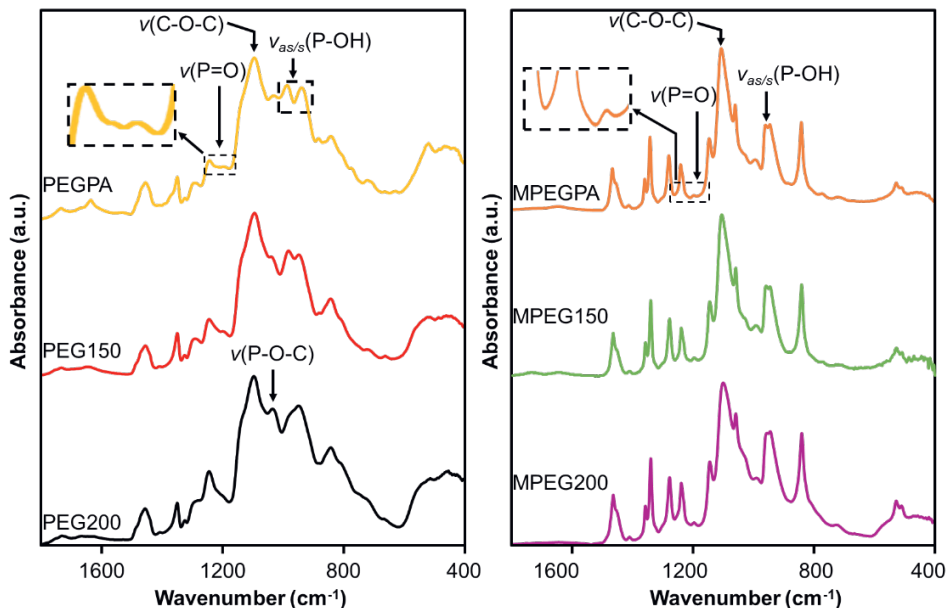
Figure S3.5: FTIR spectra of the pristine and thermally treated PEGPA and MPEGPA at 150 and 200 °C. The indentations are used to show clearly the absorption band of P=O.

4. Images of PEGPA after thermal treatment

The viscous liquid PEGPA was placed in the oven at different temperatures under the same conditions used for grafting. At 150 °C, PEGPA became more viscous but remained liquid (PEG150). At 170 °C, PEGPA became solid with little to no liquid remaining. However, the material was still sticky (PEG170). Finally, at 200 °C, PEGPA completely solidified, and the material was not sticky anymore but more of a solid material (PEG200). The solidification of the polymer was attributed to the intermolecular self-condensation reaction (Figure S3.7) between the phosphonic acid and the hydroxyl-terminal group of the polymeric chain leading to the formation of phosphonate ester.
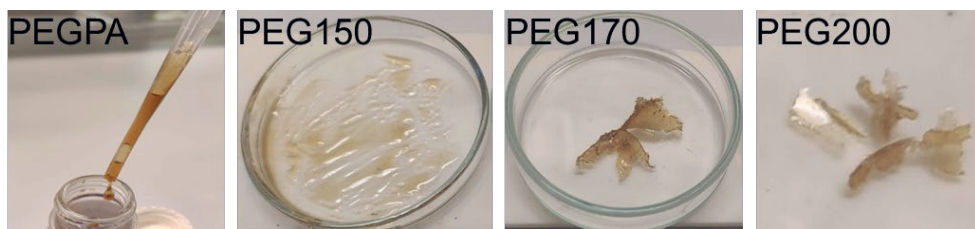
Figure S3.6: Pure PEGPA after thermally treated at 150 (PEG150), 170 (PEG170) and 200 °C (PEG200) for 12h under nitrogen.
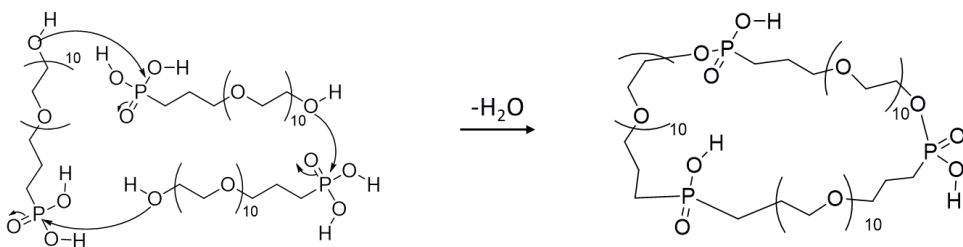
Figure S3.7: Schematic representation of the self-condensation reaction between three molecules of PEGPA, which can lead to a cross-linked polymer. Cross-linking leads to formation of solid as shown in Figure S3.6.

5. Solid-state nuclear magnetic resonance (ssNMR) analysis
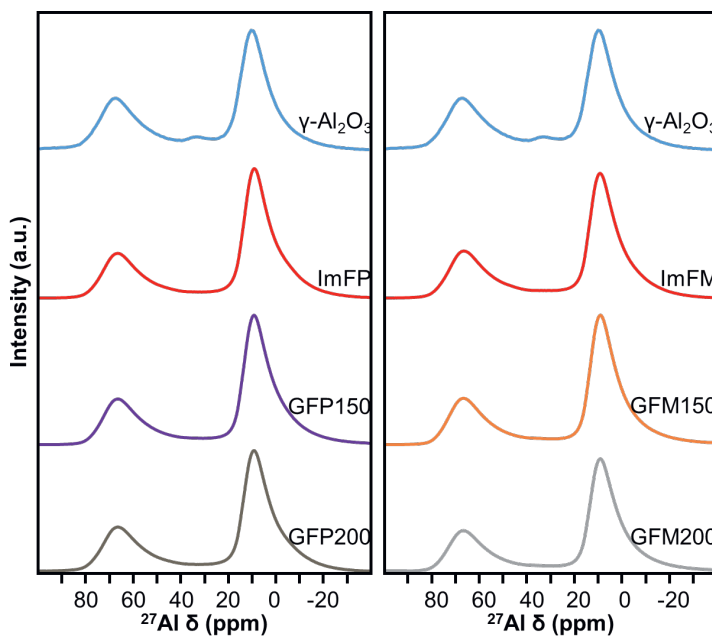
Figure S3.8: ^{27}Al NMR spectra of the pristine γ-alumina (γ-Al$_2$O$_3$), PEGPA/MPEGPA impregnated (ImFP/M) and grafted γ-alumina flakes at 150 and 200 °C.

6. X-ray diffraction (XRD) analysis
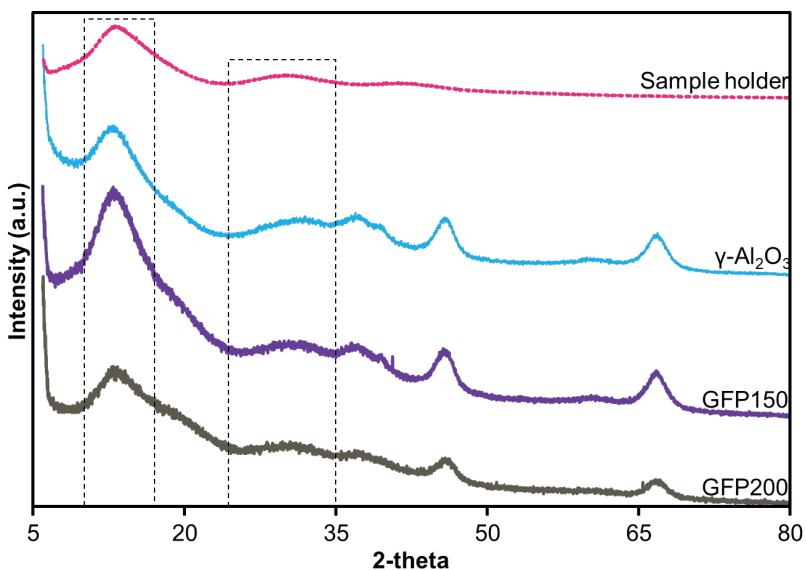
Figure S3.9: XRD diffractograms of the pristine γ-alumina flakes (γ-Al₂O₃) and PEGPA grafted at 150 (GFP150) and 200 °C (GFP200). The XRD diffractogram of the sample holder was also included as the two large diffraction between 5-20 and 25-35° are due to the diffraction of the sample holder.
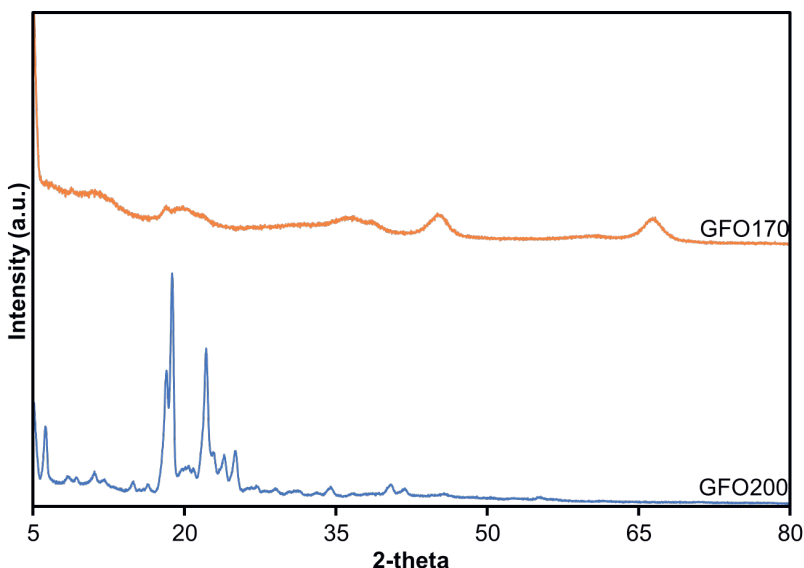
Figure S3.10: XRD diffractograms of the ODPA grafted γ-alumina flakes at 170 (GFO170) and 200 °C (GFO200).

3.6. References

(1) Terra, J. C. S.; Moores, A.; Moura, F. C. C. Amine-Functionalized Mesoporous Silica as a Support for on-Demand Release of Copper in the A3-Coupling Reaction: Ultralow Concentration Catalysis and Confinement Effect. *ACS Sustain. Chem. Eng.* **2019**, *7* (9), 8696–8705. https://doi.org/10.1021/ACSSUSCHEMENG.9B00576/SUPPL_FILE/SC9B0 0576_SI_001.PDF.

(2) Bui, H. M.; Fischer, R.; Szesni, N.; Tonigold, M.; Achterhold, K.; Pfeiffer, F.; Hinrichsen, O. Development of a Manufacturing Process for Binder Jet 3D Printed Porous Al2O3 Supports Used in Heterogeneous Catalysis. Addit. Manuf. 2022, 50, 102498. https://doi.org/10.1016/J.ADDMA.2021.102498.

(3) Ji, S.; Wang, X.; Li, K.; Huan, Y.; Ma, G.; Su, Y.; Wei, T.; Ji, S.; Wang, X.; Li, K.; Huan, Y.; Ma, G.; Su, Y.; Wei, T. 3D Vertically Aligned Microchannel Three-Layer All Ceramic Lithium Ion Battery for High-Rate and Long-Cycle Electrochemical Energy Storage. Small 2022, 2107442. https://doi.org/10.1002/SMLL.202107442.

(4) Merlet, R. B.; Pizzoccaro-Zilamy, M. A.; Nijmeijer, A.; Winnubst, L. Hybrid Ceramic Membranes for Organic Solvent Nanofiltration: State-of-the-Art and Challenges. J. Memb. Sci. 2020, 599, 117839. https://doi.org/10.1016/j.memsci.2020.117839.

(5)   Pujari, S. P.; Scheres, L.; Marcelis, A. T. M.; Zuilhof, H. Covalent Surface Modification of Oxide Surfaces. Angew. Chemie – Int. Ed. 2014, 53 (25), 6322–6356. https://doi.org/10.1002/anie.201306709.

(6)   Kyriakou, N.; Pizzoccaro-Zilamy, M.-A.; Nijmeijer, A.; Luiten-Olieman, M.; Winnubst, L. Hydrolytic Stability of PEG-Grafted γ-Alumina Membranes: Alkoxysilane vs Phosphonic Acid Linking Groups. Microporous Mesoporous Mater. 2020, 307, 110516. https://doi.org/10.1016/j.micromeso.2020.110516.

(7)   Roevens, A.; Van Dijck, J. G.; Geldof, D.; Blockhuys, F.; Prelot, B.; Zajac, J.; Meynen, V. Aqueous or Solvent Based Surface Modification: The Influence of the Combination Solvent – Organic Functional Group on the Surface Characteristics of Titanium Dioxide Grafted with Organophosphonic Acids. Appl. Surf. Sci. 2017, 416, 716–724. https://doi.org/10.1016/J.APSUSC.2017.04.143.

(8)   Roevens, A.; Van Dijck, J. G.; Tassi, M.; D'Haen, J.; Carleer, R.; Adriaensens, P.; Blockhuys, F.; Meynen, V. Revealing the Influence of the Solvent in Combination with Temperature, Concentration and PH on the Modification of TiO2 with 3PA. Mater. Chem. Phys. 2016, 184, 324–334. https://doi.org/10.1016/J.MATCHEMPHYS.2016.09.059.

(9)   Mutin, P. H.; Guerrero, G.; Vioux, A. Hybrid Materials from Organophosphorus Coupling Molecules. J. Mater. Chem. 2005, 15, 3761–3768. https://doi.org/10.1039/b505422b.

(10)   Pizzoccaro-Zilamy, M.-A.; Drobek, M.; Petit, E.; Toteé, D.; Silly, G.; Guerrero, G.; Cowan, M. G.; Julbe, A. Initial Steps toward the Development of Grafted Ionic Liquid Membranes for the Selective Transport of CO 2. Ind. Eng. Chem. Res. 2018, 57, 16027–16040. https://doi.org/10.1021/acs.iecr.8b02466.

(11)   Mustafa, G.; Wyns, K.; Vandezande, P.; Buekenhoudt, A.; Meynen, V. Novel Grafting Method Efficiently Decreases Irreversible Fouling of Ceramic Nanofiltration Membranes. J. Memb. Sci. 2014, 470, 369–377. https://doi.org/10.1016/j.memsci.2014.07.050.

(12)   Randon, J.; Blanc, P.; Paterson, R. Modification of Ceramic Membrane Surfaces Using Phosphoric Acid and Alkyl Phosphonic Acids and Its Effects on Ultrafiltration of BSA Protein. J. Memb. Sci. 1995, 98 (1–2), 119–129. https://doi.org/10.1016/0376-7388(94)00183-Y.

(13)   Merlet, R. B.; Amirilargani, M.; de Smet, L. C. P. M.; Sudhölter, E. J. R.; Nijmeijer, A.; Winnubst, L. Growing to Shrink: Nano-Tunable Polystyrene

Brushes inside 5 Nm Mesopores. J. Memb. Sci. 2019, 572, 632–640. https://doi.org/10.1016/j.memsci.2018.11.058.

(14) Uhlhorn, R. J. R.; Veld, M. H. B. J. H. I.; Keizer, K.; Burggraaf, A. J. Synthesis of Ceramic Membranes. J. Mater. Sci. 1992, 27 (2), 527–537. https://doi.org/10.1007/BF00543947.

(15) Cuperus, F. P.; Bargeman, D.; Smolders, C. A. Permporometry. The Determination of the Size Distribution of Active Pores in UF Membranes. J. Membr. Sczence 1992, 71 (1–2), 57–67. https://doi.org/10.1016/0376-7388(92)85006-5.

(16) Kozlowska, M.; Goclon, J.; Rodziewicz, P. Intramolecular Hydrogen Bonds in Low-Molecular-Weight Polyethylene Glycol. ChemPhysChem 2016, 17 (8), 1143–1153. https://doi.org/10.1002/CPHC.201501182.

(17) Luschtinetz, R.; Seifert, G.; Jaehne, E.; Adler, H. J. P. Infrared Spectra of Alkylphosphonic Acid Bound to Aluminium Surfaces. Macromol. Symp. 2007, 254 (1), 248–253. https://doi.org/10.1002/MASY.200750837.

(18) Wurmbrand, D.; Rg, J.; Fischer, W. A.; Rosenberg, R.; Boldt, K.; Morphogenesis of Anisotropic Nanoparticles: Self-Templating via Non-Classical, Fibrillar Cd2Se Intermediates. Chem. Commun. 2018, 54 (53), 7358–7361. https://doi.org/10.1039/C8CC02058B.

(19) Lin-Vien, D.; Colthup, N. B.; Fateley, W. G.; Grasselli, J. G. Organophosphorus Compounds. Handb. Infrared Raman Charact. Freq. Org. Mol. 1991, 263–276. https://doi.org/10.1016/B978-0-08-057116-4.50022-5.

(20) Vega, A.; Thissen, P.; Chabal, Y. J. Environment-Controlled Tethering by Aggregation and Growth of Phosphonic Acid Monolayers on Silicon Oxide. 2012. https://doi.org/10.1021/la300709n.

(21) Pizzoccaro, M.-A.; Drobek, M.; Petit, E.; Guerrero, G.; Hesemann, P.; Julbe, A. Design of Phosphonated Imidazolium-Based Ionic Liquids Grafted on γ-Alumina: Potential Model for Hybrid Membranes. Int. J. Mol. Sci. 2016, 17 (8), 1212. https://doi.org/10.3390/ijms17081212.

(22) Pretsch, E.; Bühlmann, P.; Affolter, C. Structure Determination of Organic Compounds; 2000. https://doi.org/10.1007/978-3-662-04201-4.

(23) Guerrero, G.; Mutin, P. H.; Vioux, A. Organically Modified Aluminas by Grafting and Sol–Gel Processes Involving Phosphonate Derivatives. J. Mater. Chem. 2001, 11 (12), 3161–3165. https://doi.org/10.1039/b104411g.

(24) Jang, S.; Son, D.; Hwang, S.; Kang, M.; Lee, S.-K.; Jeon, D.-Y.; Bae, S.; Lee, S. H.; Lee, D. S.; Kim, T.-W. Hybrid Dielectrics Composed of Al2O3 and Phosphonic Acid Self-Assembled Monolayers for Performance Improvement in Low Voltage Organic Field Effect Transistors. Nano Converg. 2018, 5, 20. https://doi.org/10.1186/s40580-018-0152-3.

(25) Kujawa, J.; Cerneaux, S.; Kujawski, W. Investigation of the Stability of Metal Oxide Powders and Ceramic Membranes Grafted by Perfluoroalkylsilanes. Colloids Surfaces A Physicochem. Eng. Asp. 2014, 443, 109–117. https://doi.org/10.1016/J.COLSURFA.2013.10.059.

Chapter 4

A new method towards a robust covalently attached cross-linked nanofiltration membrane

ABSTRACT

As nanofiltration applications increase in diversity, there is a need for new fabrication methods to prepare chemically and thermally stable membranes with high retention performance. In this work, thio-bromo "click" chemistry was adapted for the fabrication of a robust covalently attached and ultrathin nanofiltration membrane. The selective layer was formed on a pre-functionalized porous ceramic surface via a novel, liquid-vapor interfacial polymerization method. No harmful solvents and a minimal amount of reagents were used. The properties of the membrane selective-layer and its free-standing equivalent were characterized by complementary physico-chemical analysis. The stability of the thin selective layer was established in acid, base, hypochlorite, non-polar solvents, and up to 150°C. The potential as a nanofiltration membrane was confirmed through solvent permeability tests (water, ethanol, hexane, toluene), PEG-in-water molecular weight cut-off measurements ($\approx$700 g mol^{-1}), and dye retention measurements.
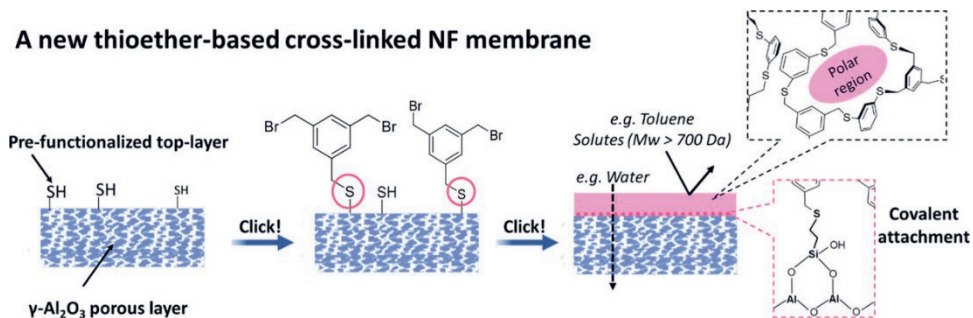
A new thioether-based cross-linked NF membrane

4.1. Introduction

The industry's separation, recovery, and disposal of liquid mixtures account for at least 40 – 70% of capital and operating costs.[1,2] Membrane-based technologies have shown potential as alternative or complement to conventional separation and purification processes thanks to their easy operation, high separation efficiency, low energy consumption, and eco-friendliness.[3] This has been observed particularly for the purification of water or organic solvents under extreme process conditions (e.g., high pressure and/or temperature),[1] where nanofiltration (NF) membranes are ideal for the removal of small organic solutes with a molecular size between 0.5 and 2 nm (like antibiotics, catalysts etc.).

Interfacial polymerization (IP) is extensively used for the preparation of NF membranes. This method allows the formation of ultrathin-dense polymeric networks on porous substrates by a controlled polymerization process at the interface of two immiscible phases (e.g., water-toluene).[4,5] Unfortunately, the fabrication of NF membranes with good separation performance by IP implies the use of solvents and monomers in a large excess[6] (e.g., at least 1 – 3 wt.%) due to the low monomer to polymer conversions[7] and by-product formation. As a result, large quantities of waste are produced, which is one of the major drawbacks of the IP method.[8]

Also, despite the excellent performance reported for the NF membranes prepared by the IP method, the resulting polymeric layers present low mechanical and chemical stability under severe conditions (i.e., extreme pH values, bleach, and other reactive chemicals).[9,10] This correlates to the monomers used, which are usually composed of halogenated acids, such as trimesoyl chloride (TMC), and diamine benzene-derivatives (DAB). A combination of these types of monomers facilitates the formation of crosslinked polymeric networks at short reaction times, which leads to enhanced chemical stability in polar and apolar solvents. However, the amide bonds formed during the reaction between these two types of monomers (TMC and DABs) are very sensitive to hydrolysis and cannot thus withstand strong acids, bases, or hypochlorite-based cleaning treatments.[11,12] Additionally, swelling and detachment of the membrane from the porous substrates can occur during the cleaning treatment as the conventional IP process does not involve a covalent attachment between the membrane and the substrate surface. Therefore, there is a need to adjust the IP reaction process to mitigate waste production and to increase the chemical and mechanical stability of the NF membranes produced.

To overcome the challenges of conventional IP methods, "click" chemistry can be used instead of amidization reactions. "Click" chemistry is a tool used for the fabrication of highly cross-linked and chemically stable polymers. This method is characterized by a high reaction yield and low waste production.[13] Besides, "click" reactions can promote the formation of chemical linkages that are chemically inert

even under extreme conditions. Among the existing possibilities, the thio-bromo "click" reaction, which occurs at room temperature under basic conditions (pH < 9), results in stable thioether bonds, which can be used as an alternative to conventional amidization reactions used in conventional IP methods.

In 2005, Timmerman et al.[14] established the first thio-bromo "click" reaction synthesis to prepare cyclic peptides in high yields and more rapidly than conventional synthesis methods. The resulting products were made via the reaction of cysteine-based peptides as thiol substituted with benzylic bromides under mild basic conditions (pH ~8).[15] The method was expanded to the preparation of polymers by Monnereau et al. in 2015.[16] Hyper-crosslinked thioether-based porous polymers were formed under similar conditions. These networks were shown to be insoluble in common organic solvents and were thermally stable up to 500 °C. Such methods have the potential to be used in membrane technology due to the simplicity, the high yields of the reaction conditions, and the resulting chemical stability of the polymers formed. Therefore, by adapting the IP method with the "click" reactions, ultrathin and selective membrane layers can be formed. A proof of concept was shown by Rapakousiou et al. in 2017,[17] where the liquid/liquid IP method in combination with the "click" reaction of copper-catalysed azide-alkyne cycloaddition (CuAAC) was used to form an ultrathin polymer with a thickness of 5 nm. Even if "click" chemistry has proven itself over the years, there are no cases where "click" reactions have been used in membrane fabrication.

In this work, we propose a novel method towards the formation in two steps of an ultrathin cross-linked NF membrane composed of stable thioether bonds. Starting from the top surface of a pre-functionalized porous ceramic support, two successive thio-bromo "click" reactions are conducted to form the NF separation layer. Here, the "click" reaction is also used to covalently attach the polymeric layer on top of a porous ceramic support. Ceramic supports, which exhibit high thermal and chemical stability, do not suffer from plasticization issues, swelling, or thermal degradation, phenomena observed with common porous polymeric supports. In addition, ceramic supports can be easily functionalized with a wide range of small organic molecules[18,] including thiol-terminated ones.[19] Even though IP layers have been successfully formed on ceramic supports in the past,[20] only conventional IP (polyamides predominantly) procedures were used, and to date, no covalent attachment between the selective layer and the ceramic support has been reported. In this work, the second "click" reaction is done via a vapor phase reaction without the use of a catalyst. For the first time, we report a selective layer made completely via "click" chemistry. A special effort is devoted to understanding the impact of each reaction step on the final layer and the network's thermal and chemical stability. The system reported here can serve as a proof-of-concept for developing thioether-based layers for a wide range of applications such as in membrane science, coatings, optoelectronics, and many more.

124

4.2. Materials & methods

4.2.1. Materials

Solvents used were ethanol (technical grade > 95%), anisole (>99%, Merck, NL), and water (MilliQ). Chemicals used were glycerol (anhydrous, Merck, NL), 1,3,5-tris(bromomethyl)benzene (3Br) (> 97%, Fluorochem, UK), (3-mercaptopropyl)trimethoxysilane (MPTMS) (> 95%, Merck, NL), 1,3-benzenedithiol (2SH) (> 99%, Merck, NL), triethanolamine (TEOA) (> 99.5%, Merck, NL), Brilliant Yellow (70%, Sigma Aldrich, NL), Rhodamine B (> 99%, Merck, NL), Sudan Black B (> 99%, Sigma-Aldrich, NL), polyethylene glycol (Merck, NL). The chemical structures and abbreviations can be found in Figure S4.1 of the Supporting Information. The α-alumina (α-Al$_2$O$_3$) substrates (disc: 21 or 39 mm of diameter, 2 mm of thickness, 80 nm pore diameter) were purchased from Pervatech B.V., the Netherlands. These ceramic substrates are comprised primarily of macroporous α-alumina (> 99 %), which ensures mechanical stability under pressure. The polished side of these supports was dip-coated with a boehmite sol and subsequently calcined at 650 °C for 3 hours. The procedure was performed twice to eliminate any defects on the surface of the porous support and led to the formation of a thin γ-alumina layer of 3 μm in total thickness (Figure S4.2B of the Supporting Information). Further details for the fabrication of the γ-alumina layer can be found elsewhere.[21,22]

4.2.2. Thioether-based cross-linked NF membrane preparation

Prior to use the mesoporous γ-alumina supports, these were soaked in a water/ethanol mixture (v/v = 2:1) for 8 h before drying under vacuum at 50 °C. The synthesis of the thioether-based cross-linked membrane is divided in three steps as described in Scheme 1.
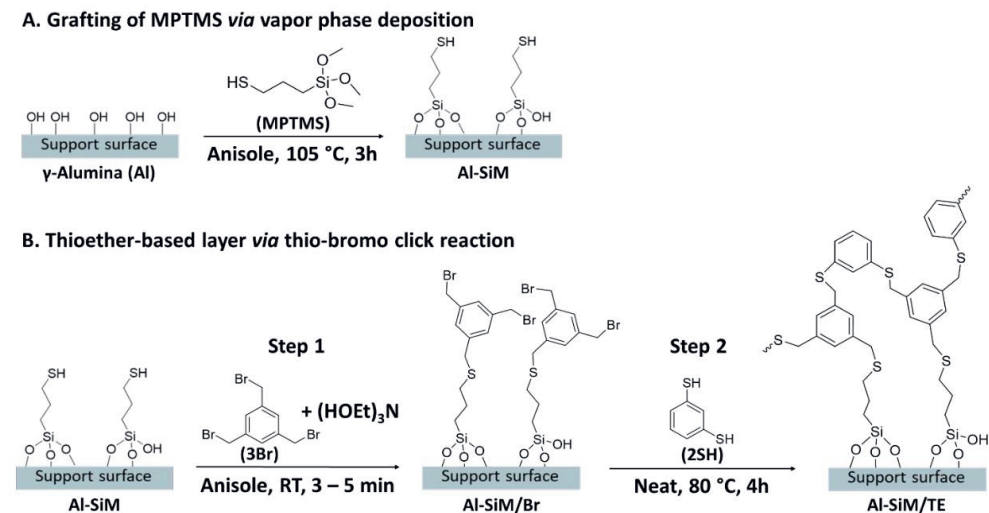
Scheme 4.1: Schematic representation of the grafting of MPTMS via vapor phase deposition (A) and the stepwise thioether-based membrane formation (B)

Porous support pre-functionalization: The grafting of (3-mercaptopropyl)trimethoxysilane (MPTMS) was conducted using the vapor phase grafting method. Before the synthesis, γ-alumina support was filled with glycerol by rubbing a drop (≈ 1 mL) onto the substrate surface and dabbed with a tissue after 10 min stand time. Vapor phase grafting was conducted by placing glycerol-filled γ-alumina support (top-surface facing down) 2 – 3 cm above 50 mL of a 25 mM anisole solution of MPTMS at 105 °C for 3h (Figure S4.4). After cooling to room temperature, the pre-functionalized porous support was washed with 20 mL anisole for 1h under sonication to remove the physisorbed species and dried overnight at 50 °C under vacuum. Samples obtained at this stage were denoted Al-SiM.

Liquid phase "click" reaction: Following the MPTMS grafting step, the pre-functionalized porous support was soaked for 3 – 5 min in a solution containing 0.22 mmol of 1,3,5-tris(bromomethyl)benzene (3Br) and 0.16 mmol of triethanolamine (TEOA) in 10 mL of anisole (Figure S4.4). After removing from the solution, compressed air was gently blown across the surface of the support to remove any solvent visible to the eye. Samples obtained at this stage were denoted Al-SiM/Br.

126

Vapor phase "click" reaction: The thioether-based cross-linked membrane was then prepared by placing the Al-SiM/Br samples (top-surface facing down) 1 – 2 cm above 25 µL (0.17 mmol) of 1,3-benzenedithiol (2SH) pure precursor at 80 °C for 4h under stirring (Figure S4.4). After cooling to room temperature, the resulting membrane was washed twice in 20 mL of ethanol for 30 min under sonication and dried at 50°C under vacuum. Samples obtained at this stage were denoted Al-SiM/TE.

4.2.3. Characterization

Fourier Transform Infrared spectroscopy (FTIR) measurements were done using a Perkin Elmer UATR Spectrum Two. Wavenumbers between 4000 and 550 cm^{-1} were scanned in reflectance mode at a resolution of 4 cm^{-1} for a minimum of 16 scans. Field-emission scanning electron microscopy (FE-SEM) images were obtained with a Zeiss MERLIN high-resolution scanning electron microscope using an accelerating voltage of 1.4 kV. FE-SEM samples were sputtered with 2 nm of chromium to avoid sample charging. Thermogravimetric analysis (TGA) coupled with differential scanning calorimetry (DSC) and mass spectroscopy (MS) was conducted using an STA 449 F3 Jupiter (Netzsch), equipped with a dual TG/DSC sample/reference holder. Measurements were performed under 55 mL min^{-1} N$_2$ and 15 mL min^{-1} O$_2$ flow with a heating rate of 10 °C min^{-1} from 40 to 800 °C. Calibrations were made using melting standards. Measurements were run sample-temperature controlled. The sample masses were determined using an internal balance 30 min after inserting the sample. The gases that evolved during TGA analysis were transferred to a mass spectrometer (QMS 403 D Aëolos, Netzsch). TGA and MS start times were synchronized, but no correction was applied for the time offset caused by the transfer line time (estimated < 30 s, systematic offset). A bar graph scan for m/z = 1–110 amu was recorded for all samples to determine the evolving m/z numbers. TGA/DSC crucible correction can be found in SI, Figure S4.12. The pore size of the mesoporous alumina membranes was determined by permporometry using cyclohexane as condensable vapor. The experimental procedure is described in detail elsewhere.[23]

X-ray fluorescence spectroscopy (XRF) measurements were conducted on a Bruker SS Tiger using membrane samples prepared via the stepwise membrane method described above. Complete elemental analysis is provided in the Supporting Information. Spectroscopic ellipsometry was performed using a J.A. Woollam M-2000 ellipsometer on silicon wafer (one side polished, CZ test grade, Silchem) samples coated in a fashion identical to the prepared Al-SiM, Al-SiM/Br, and Al-SiM/TE membrane samples without the glycerol pre-treatment step. First, a piece of a silicon wafer (30x30 mm) with a native oxide layer was cleaned in an oxygen plasma chamber for 10 min at 100 watts. Next, any residual organics were washed off with ethanol, and then the wafer was dried under vacuum at 50 °C overnight. The

preparation of the coatings followed the stepwise protocol developed for the preparation of the thioether-based membrane, except that no pore-filling agent was used. After each reaction step, a part of the substrate was preserved for analysis (Figure S4.13). Each sample was rinsed with ethanol multiple times, dried under vacuum overnight at 50 °C, and stored under N_2 at room temperature. The detailed parameters to assess the layer thickness can be found in the Supporting Information.

4.2.4. Membrane screening and performance tests

Permeability and retention data were collected with a custom-made, dead-end filtration setup, consisting of a nitrogen tank pressurizing a feed vessel with a valve to regulate pressure. Permeability is expressed as the flux of water or a solvent across a membrane per unit of driving force, here as litters per square meter of exposed membrane area (2.4 or 9.1 cm^2) per hour per bar of pressure applied across the membrane (L m^{-2} h^{-1} bar^{-1}). Permeability data were collected by weighing the flow of permeate at timed intervals and at three applied transmembrane pressures between 8 and 15 bar and by taking the slope of a linear fit of the collected data. All slopes were found to be linear unless otherwise noted. A permeability of 0.0 indicates no detected solvent flux during 17 h of operation at a transmembrane pressure of 15 bar.

Retentions I of Brilliant Yellow (BY, Mw = 624.55 g mol^{-1}, 50 ppm), Rhodamine B (RB, Mw = 479.02 g mol^{-1}, 50 ppm), Sudan Black B (SBB, Mw = 457 g mol^{-1}, 50 ppm) or PEG oligomers (Mw = 300, 600, 1000, 1500 g mol^{-1}) were calculated by the equation

$$R = 1 - c_p/c_f \qquad (1)$$

where c_p and c_f are the permeate and feed solute concentrations, respectively. Retention samples were obtained at recoveries between 15-25%. Solute concentrations of BY, RB, and SBB were calculated from Perkin-Elmer λ12 UV-Vis spectrophotometer results at the characteristic wavelength of 401.5 (BY), 554 (RB), and 604 (SBB) nm. PEG concentrations were determined by gel permeation chromatography (GPC). The GPC setup consisted of two SUPREMA 100 Å columns from PSS Polymer Standards Service GmbH (Germany), an HPLC pump from Waters (Millipore B.V., The Netherlands), and a Shodex RI-Detector from Showa Denko GmbH (Germany). The columns were calibrated using the same PEG standards.

4.2.5. Chemical resistance tests

Thioether-based cross-linked films, prepared as described in the Supporting Information (section 4), were used to conduct the chemical resistance tests. The films were subjected to soaking in either 1M sodium hydroxide (NaOH), 1M nitric acid (HNO$_3$), or 10% hypochlorite (NaOCl) solution for 5 days, then dried at 50 °C under

vacuum. FTIR analysis was used before and after exposure to the aforementioned chemicals to assess the chemical integrity of the film.

4.3. Results and Discussion

4.3.1. Porous support pre-functionalization with MPTMS

The porous γ-alumina top-surface was pre-functionalized with 3-(mercaptopropyl)trimethoxysilane (MPTMS), a precursor for the thioether-based network, using a vapor phase deposition grafting method (Scheme 1A). Here, the alkoxysilane linking groups of the precursor react with the hydroxyl-rich surface of the γ-alumina support via a condensation reaction, yielding a homogeneous monolayer coverage without poly(homo)condensation reactions.[18]

FTIR analysis was used to demonstrate the grafting of the MPTMS precursor on the top-surface of the porous γ-alumina support. The FTIR spectrum of the pre-functionalized support (Al-SiM) in the range $3800 – 2300$ cm^{-1} and $1800 – 960$ cm^{-1} is presented in Figures 4.1A and 4.1B. The bands visible between 2840 and 2950 cm^{-1} correspond to the symmetric and antisymmetric C–H stretching vibrations of the precursor's aliphatic group. The grafting is suggested by the disappearance of a sharp vibration band at 2840 cm^{-1} which corresponds to the Si-O**CH₃** group of the MPTMS precursor (Figure S4.11, Supporting Information, section 5). This is also confirmed by the presence of a broad vibration band centred at 1050 cm^{-1}, which can be ascribed to the newly formed Si-O-Al bond.[24] Compared to the FTIR spectrum of the precursor, the weak stretching vibration band of the thiol group (**S-H**) located at 2565 cm^{-1} is not visible for the Al-SiM sample. This can be due to the low concentration of grafted molecules on the pre-functionalized surface and the weak absorbance of the S-H group in this IR region.[25]
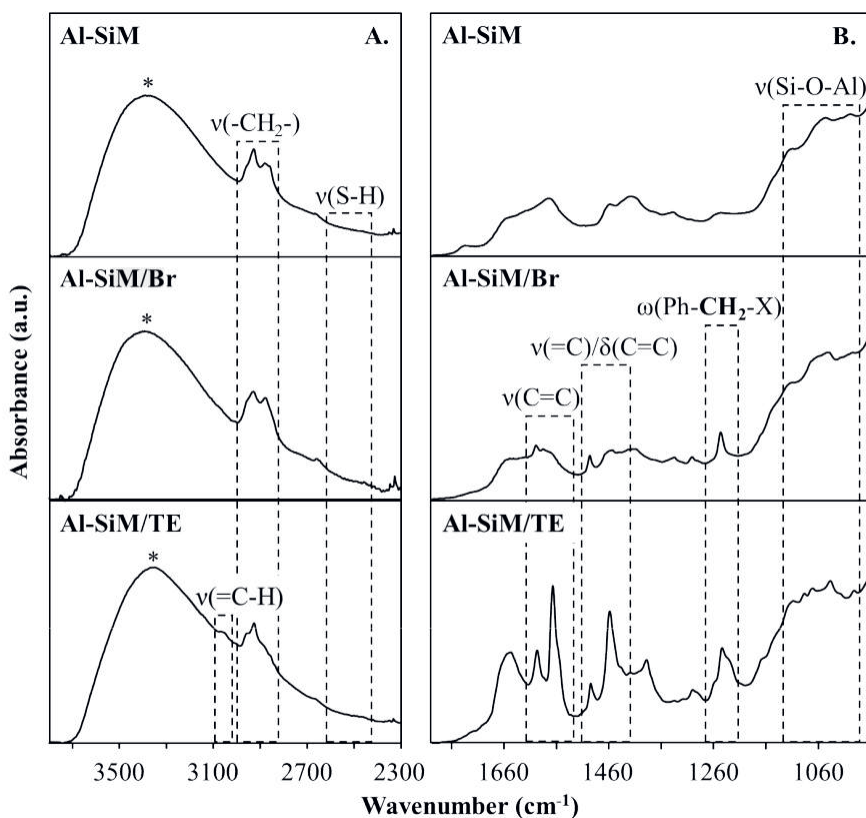
Figure 4.1: FTIR spectra of the Al-SiM, Al-SiM/Br and Al-SiM/TE samples between 3800 – 2300 cm^{-1} (A) and 1800 – 960 cm^{-1} (B). The symbol (*) denotes the vibration band attributed to physisorbed water.[23]

XRF was used to further confirm the presence and conservation of the side chain of the MPTMS precursor after grafting. The results are presented in Table S4.1 (Supporting Information, section 6). The analysis revealed the presence of silicon and sulphur, respectively 0.3% and 0.3%, thus, confirming along with the FTIR results that the support has been successfully functionalized.

Cyclohexane permporometry was used to investigate the possible blocking of the support pores due to poly(homo)condensation reactions of the MPTMS precursor. Indeed, the presence of precursors in the pores can affect the formation and properties of the resulting NF thioether-based membrane. The oxygen flux through the Al-SiM and the unmodified γ-alumina support as a function of the relative cyclohexane pressure during the desorption step of the permporometry analysis is shown in Figure S4.13A (Supporting Information, section 7). At the beginning of the desorption step, all the pores are blocked with condensed cyclohexane, and there is no oxygen flux.

130

In the interval $0.5 > P/P_0 > 0.3$, the oxygen permeance increases with the increase in the number of open pores. By considering that the capillary condensation process takes place in this interval, Kelvin diameters of ~5.5 and ~5 nm (Supporting Info, section 7) were calculated for the unmodified γ-alumina support and the Al-SiM sample (5.5 ± 0.03 and 4.8 ± 0.07, accordingly). The results are very similar, and we can thus conclude the successful grafting of MPTMS on the support's top-surface without poly(homo)condensation reactions into the pores.

4.3.2. Formation of the thioether-based hyper cross-linked membrane

Prior to the membrane fabrication, thioether-based free-standing films were prepared as a proof-of-concept via the liquid-liquid IP (LIP) method. The LIP method, in contrast to a single solvent system, allows for the formation of a well-defined organic network.[26] Preparation of LIP free-standing films was proven to be crucial in determining potential side reactions by ^{1}H liquid NMR and the physicochemical properties of the membrane layer, such as thermal and chemical stability. The preparation procedure and the physicochemical characterizations of the film is reported in the Supporting Information (section 4).

Thioether-based cross-linked membranes were prepared on the pre-functionalized support (Al-SiM) in two steps, as shown in Scheme 1B. The first step consisted of the deposition of a basic solution of the 1,3,5-tris(bromomethyl)benzene (3Br) monomer onto the pre-functionalized porous ceramic support. Under these solution phase conditions, the thiol surface groups of the grafted precursors can react with the 3Br monomer via the thio-bromo "click" reaction, forming a thioether bond (Al-SiM/Br). The base catalyst (TEOA, $pK_a \approx 11$)[27] was added to the 3Br monomer solution to minimize the formation of disulphide bonds, which were detected by ^{1}H liquid NMR during the preparation of the film (Figure S4.9 and S4.10, Supporting Information, section 4). Disulphide bonds are generally weaker than thioether bonds since they can be cleaved under mild conditions[28,29]; thus, their presence in the final membrane layer is viewed as defects. Subsequently, the support surface was exposed to 1,3-benzenedithiol (2SH) monomer vapours, forming a thioether-based cross-linked membrane (Al-SiM/TE, Scheme 1B, step 2). This second step was done without the use of a base catalyst since the nucleophile in the vapor phase has enough energy to overcome the kinetic barrier of the "click" reaction.[30,31] Therefore, the 2SH monomer in the vapor phase is expected to react with the 3Br monomer in contact with the liquid phase. Thus, we expect that the "click" polymerization reaction occurs at the liquid-vapor interface, and thus an interfacial polymerization should take place on top of the ceramic support. The reaction parameters for the preparation of Al-SiM/TE sample (Scheme 1B) were selected by screening through different reaction conditions (reaction times and monomer concentrations). A combination of Sudan Black B (Mw = 457 g mol^{-1}) retention tests and solvent permeability measurements

were conducted to identify the samples showing the presence of a distinct selective and permeable layer on top of the support. The results of this preliminary study are summarized in the Supporting Information (section 8).

To confirm the formation of the thioether-based cross-linked network, FTIR analysis was conducted after each reaction step, on the respective samples Al-SiM/Br and Al-SiM/TE. The FTIR spectra in the range 3800 – 2300 cm^{-1} and 1800 – 960 cm^{-1} are presented in Figures 4.1A and 4.1B, respectively. The presence of aromatic rings for these samples is confirmed by the quadrant stretching vibration band observed at 1602 cm^{-1} (ν(C=C)). Moreover, this assumption is also verified by the multiple bands appearing at 1484, 1450, 1440, and 1412 cm^{-1} which are associated with the stretching and bending vibrations of the aromatic rings (ν(C=C) and δ(=CH)).[25,32] The good signal resolution of these vibration bands in the case of the Al-SiM/TE sample suggests the presence of a high concentration of aromatic rings and, thus, the formation of a network. The absorption band at 1249 cm^{-1}, appearing in both samples, is attributed to the wagging vibration of the methyl group at the benzylic position, Ph-**CH₂**-X, where X is either a sulphur or a bromine atom.[33] To determine if this vibration band resulted from the formation of thioether bonds or unreacted 3Br monomers, the spectra were compared to the spectrum of the pure 3Br monomer (Figure S4.14, Supporting Information, section). Even though in the spectrum of the 3Br monomer, the vibration of the methyl group (Ph-**CH₂**-Br) appears at 1209 cm^{-1}, the presence of the bromine in the Al-SiM/Br or /TE cannot be excluded, and further in-depth analysis is required. Moreover, the disappearance of the C-Br absorption band at 704 cm^{-1} would indicate full conversion of the benzylic bromides to thioethers in the membrane layer. However, no specific signals can be observed below 900 cm^{-1} in the case of the Al-SiM/TE membrane due to the high intensity of the signal attributed to the alumina support (Figure S4.14, Supporting Information, section 9). Here, the free-standing film can be used since it is spectroscopically identical to the Al-SiM/TE. According to the FTIR of the film, an absorption band at 710 cm^{-1} is present, which can be attributed to both unreacted methyl bromides (C-Br)[25] or the desirable thioether bonds (C- S-C).[34,35] Thus, from the FTIR results, thioether-bond formation is indicated. However, the presence of bromide in the sample cannot be excluded, and further investigation is necessary.

XRF analysis was conducted to determine the amount of sulphur and the presence of any residual bromine in the final thioether-based membrane. The results are given in Table S4.1 (Supporting Information, section 4.5.6). The weight concentration of sulphur is increasing by 1.3% between the Al-SiM and Al-SiM/TE samples which confirms the increase concentration of thioether bonds on the surface (Al-SiM: 0.3 wt%; Al-SiM/TE: 2.0 wt%). Less than 0.1 wt% of bromine was detected in the Al-SiM/TE sample, which suggests the predominance of the thioether-based bond formation.

To study the pore size of the membrane and to confirm the formation of a defect-free layer as suggested by the preliminary SBB retention tests, cyclohexane permporometry experiments were conducted. The oxygen flux through the Al-SiM/Br and Al-SiM/TE samples as a function of the relative cyclohexane pressure during the desorption step is shown in Figures S4.13A and B of the Supporting Information (section 7). Pore diameter of ~4 nm is determined for the Al-SiM/Br sample, indicating a pore shrinkage of ~1 nm compared to the unmodified γ-alumina support. This decrease in pore diameter can be attributed to the presence of the 3Br monomers, which have reacted in step 1 with the thiol surface groups present at the entrance of the pore (Scheme 4.1B). The Al-SiM/TE sample obtained oxygen permeance of 1×10^{-8} mol s^{-1} m^{-2} Pa^{-1} (Figure S4.13A). This value corresponds to the detection limit of the setup. The absence of a clear transition point in the cyclohexane permporometry curve suggests the complete coverage of the γ-alumina porous support with the thioether-based network and that the Al-SiM/TE sample is mainly composed of micropores (pore diameter < 2 nm).

According to literature [36–38,] the pore size of the layer can also be estimated using retention tests of a series of PEG molecules with different molecular weights (Mw). It is known that PEG molecules can form spheres in the solution of a certain radius, which can be estimated via the Stokes-Einstein equation (2):

Molecular radius (Å) = $0.1673 \times (M_w \text{ (g/mol)})^{0.557}$ (2)

where M_W is the molecular weight of the PEG, which is 90% retained by the membrane. Figure S4.15 in the Supporting Information (section 4.5.10) shows the PEG retention obtained for the Al-SiM/TE sample. A molecular weight cut-off (MWCO) of ≈700 g mol^{-1} was obtained, which is much lower than the MWCO of unmodified γ-alumina support (2500 g mol^{-1}),[39] and well in the nanofiltration range[1]. Using the MWCO and equation (2), a hydrodynamic diameter of 1.3 nm was calculated. This value is in accordance with the pore diameter suggested by the cyclohexane permporometry measurements (pore diameter below 2 nm) and in the pore range needed for NF applications.

FE-SEM analysis was used to investigate the morphology, location, and homogeneity of the Al-SiM/TE membrane. Figure 4.2A shows a cross-section image of the membrane with part of the α-alumina support and the γ-alumina layer consistent with reported characteristics.[21,22] No organic layer was observed on the top surface until higher magnification was used, as shown in Figure 4.2B, where a thin organic layer is indicated. The organic layer seems to be in direct contact with the γ-alumina support. However, as shown in Figure 4.2B, the top layer also appears in a different location in the form of thin flakes detached from the supports. The detachment can be artifacts induced either by the primary electron beam or the high

vacuum of the SEM equipment. Based on these observations, the layer thickness should not be more than 50 nm.
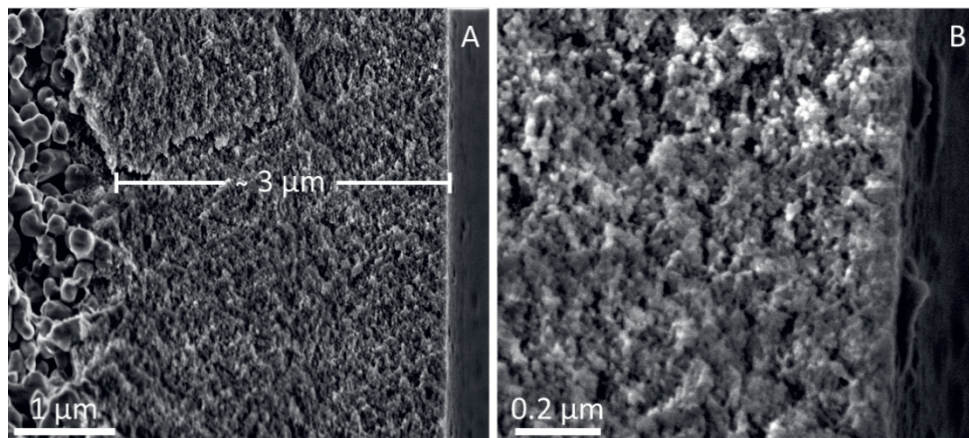
Figure 4.2: FE-SEM cross-section images of the thin thioether-based membrane layer covalently attached to a mesoporous γ-alumina support with a magnification of 63k (A) and 260k (B).

For insight into the thickness of the thioether-based layer, spectroscopic ellipsometry measurements were performed. Ellipsometry has been used to measure the thickness of polymeric film prepared by conventional LIP.[40] However, due to the roughness and porosity of the γ-alumina support, it is impossible to apply this analysis to the Al-SiM/TE membrane. Thus, the membrane synthesis was transposed onto silicon wafer substrates to study layer formation after each reaction step. Grafting of MPTMS on the silicon wafer yields a thin layer of 1.0 ± 0.1 nm. This thickness value is in accordance with MPTMS layers prepared by Gothe et al.[41] After the first "click" reaction with the 3Br monomer, an increase in thickness of ~0.3 nm was measured. Finally, after the second "click" reaction with the 2SH monomer by VIP, an ultrathin thioether-based layer is formed with a thickness of 7.8 ± 0.4 nm. We expect that when prepared on the porous membrane support, the thickness of the thioether-based layer would be higher than the one shown by ellipsometry due to the inherent porosity of the γ-alumina support. Even though the pores of the support are filled with glycerol, monomers are expected to be able to infiltrate the porous ceramic during the VIP step and form a thicker layer than the one observed with ellipsometry. Nevertheless, the thickness of the membrane separation layer is expected to be very thin and thus would not be observed by FE-SEM.

4.3.3. Stability of the thioether-based cross-linked membrane

The stability of the thioether-based network was assessed first through exposure to different solvents. Permeability tests were conducted with solvents of different

134

polarities (water, ethanol, toluene, and hexane) under the same conditions. Thermal treatment was included in the test to study any potential degradation of the structure caused by the temperature or the solvent tested. As shown in Figure 4.3, the water permeability of the Al-SiM/TE membrane is approximately 0.6 L m^{-2} h^{-1} bar^{-1} and similar to ethanol permeability (0.5 L m^{-2} h^{-1} bar^{-1}). Compared to the water flux of the pristine support (6 L m^{-2} h^{-1} bar^{-1}),[36,] the thioether-based membrane exhibits approximately one order of magnitude lower permeability, suggesting a layer on top of the support. The Al-SiM/TE membrane was found impermeable to apolar solvents, such as toluene and hexane. This suggests that either the organic layer has collapsed and a (non-porous) dense network has formed in contact with the apolar medium, or the organic layer has a rigid hydrophilic structure, impermeable to apolar solvents. As shown in Figure 4.3, the membrane was then dried and re-tested with water, and the water permeability remained constant (0.60 ± 0.05 L m^{-2} h^{-1} bar^{-1}), thus suggesting the formation of a rigid hydrophilic network via the VIP method.
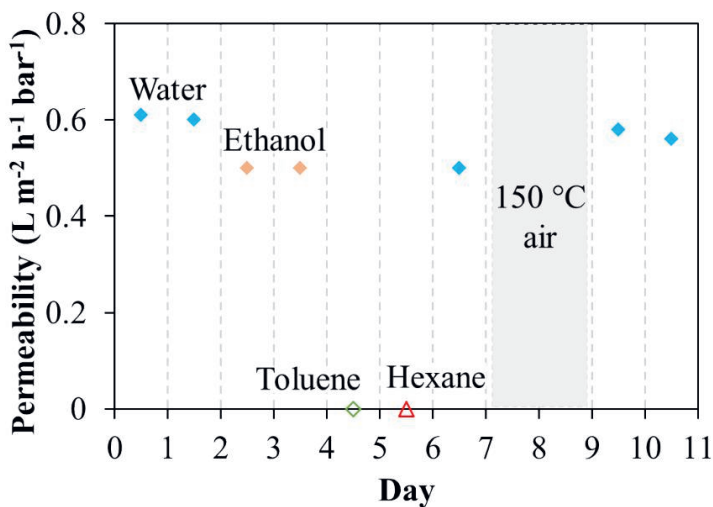
Figure 4.3: The permeability of various solvents through the same membrane over consecutive tests. The same membrane was exposed to heat for 2 days, and then the water permeability was tested for 2 consecutive days. Between each permeability test, the sample was dried overnight at 50 °C under a vacuum.

Following the solvent permeability tests, the thermal stability of Al-SiM/TE membrane was further investigated. The sample was thermally treated at 150 °C for 48h, and water permeability of 0.57 ± 0.01 L m^{-2} h^{-1} bar^{-1} was measured. This value is identical to the value obtained before the thermal treatment (0.57 ± 0.06 L m^{-2} h^{-1} bar^{-1}).

To further confirm the integrity of the network, a free-standing film was analysed by TGA-MS and FTIR spectroscopy. The TGA results indicate that the thioether-based layer is thermally stable below 300 °C, where no weight loss was observed (Figure S4.19, Supporting Info, section 4.5.14). Above 310 °C, thermal degradation occurs with a significant weight loss above 460 °C. FTIR analysis confirmed this observation. Compared to the FTIR spectrum of the free-standing film, the thermally treated sample shows small differences in vibration bands. New weak bands at 2500, 1500, and 1150 cm^{-1} could be denoted, possibly due to slight oxidation of the film. Overall, these results confirm that the thioether-based membrane prepared via the novel VIP method bears a highly dense and hydrophilic network thermally stable until at least 150 °C.

Preservation of the thioether-based network's integrity in different media (basic, neutral and acidic) was also studied. Unfortunately, the γ-alumina layer is not resistant to highly acidic or basic environments[42;] therefore, the membrane could not be tested in those media. However, the chemical resilience of the thioether-based film could be investigated. This was done by placing a piece of the film in a vial containing either 1 M HCl (pH ≈ 1), 1M NaOH (pH ≈ 14), or 10% sodium hypochlorite (bleach, pH ≈ 13.2) for 5 days at room temperature. These chemicals are commonly used in the industry for disinfecting and cleaning membranes.[43–45] FTIR results, obtained before and after exposure to the aforementioned chemicals, are shown in Figure S4.20. The spectra show no significant changes after exposure to the chemicals, thus the high chemical stability of this new thioether-based network.

4.3.4. Membrane performance

A series of retention tests were conducted on the Al-SiM/TE membrane using an aqueous solution of Brilliant Yellow (BY, 625 g mol^{-1}), Rhodamine B (RB, 479 g mol^{-1}), and an ethanolic solution of Sudan Black B (SBB, 457 g mol^{-1}). The results are given in Table 4.2. Both aqueous solutions result in high retention values, $99 \pm 0.4\%$ for BY and $90 \pm 7\%$ for RB. However, SBB retention in ethanol averaged $50 \pm 2\%$, which can be attributed to the neutral character of the SBB dye as compared to the charged BY or RB. This and the fact that the membrane was impermeable to apolar solvents indicate that the Al-SiM/TE membrane bears a dense charged surface. Thus, we expect that the Al-SiM/TE membranes can find use in the removal of dyes from water.

Table 4.2: Solute rejection tests performed on the Al-SiM/TE membrane. The tests were performed under constant pressure (11 bar), using nitrogen gas and stirring at 700 – 800 rpm. Each test was reproduced three times, of which the presented retention is the average, and the error refers to the standard deviation of 3 samples.

Solute	Solvent	Charge	M_W (g mol^{-1})	Retention (%)
Brilliant Yellow	Water	Negative	625	100 ± 0.4
Rhodamine B	Water	Positive	479	93 ± 7
Sudan Black B	Ethanol	Neutral	457	50 ± 2
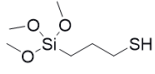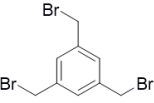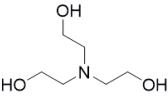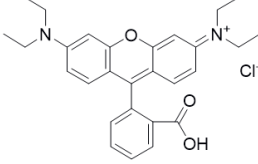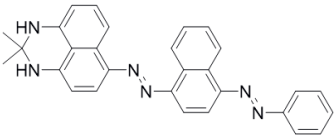
4.4. Conclusion

A "click" reaction approach within a novel liquid-vapor IP method was used to prepare ultrathin selective thioether-based cross-linked NF membranes. Typically, LIP methodologies used in membrane technology rely on a biphasic liquid system. However, our novel liquid-vapor system relies on a single green solvent and minimal reactant usage. As a result, the monomer amounts used in this work are minimal (from 0.05 to 0.2 wt.%) compared to concentrations of a typical IP procedure (from 1 to 3 wt.%).[6] We demonstrated that the thioether layer exhibits, via spectroscopic and solvent permeation tests, high chemical stability under a range of conditions, including organic solvents (ethanol, hexane, toluene), extreme pH values (0 or 14), and in sodium hypochlorite solution (10% aqueous). In addition, the performance (permeability) was not affected by thermal treatment (150°C for two days), and the degradation of the layer occurred above 300 °C.

Preliminary nanofiltration tests show permeabilities of 0.6 and 0.5 L m^{-2} h^{-1} bar^{-1} in water and ethanol, respectively, with a PEG MWCO of 700 g mol^{-1} as well as good retention of charged dyes in water. The membrane was found to be impermeable yet stable to two apolar solvents, toluene, and hexane. Based on this proof-of-concept, the development of thioether-based cross-linked networks can be expanded to a variety of NF and separation applications.[16] The liquid-vapor interfacial polymerization method presented is highly effective and facile, showing significant advantages over the liquid-liquid IP method.

4.5. Supporting Information

1. Chemical structures and abbreviations of the compounds used in this study

Figure S4.1: Chemical structures and abbreviations of the compounds used in this study: 1,3-benzenedithiol (2SH),1,3,5-tris(bromomethyl)benzene (3Br), (3-mercaptopropyl)trimethoxysilane (MPTMS), triethanolamine (TEOA), trimethylamine (TEA), Brilliant Yellow (BY), Sudan Black B (SBB), Rhodamine B (RB), and polyethylene glycol (PEG).

2. Porous ceramic support
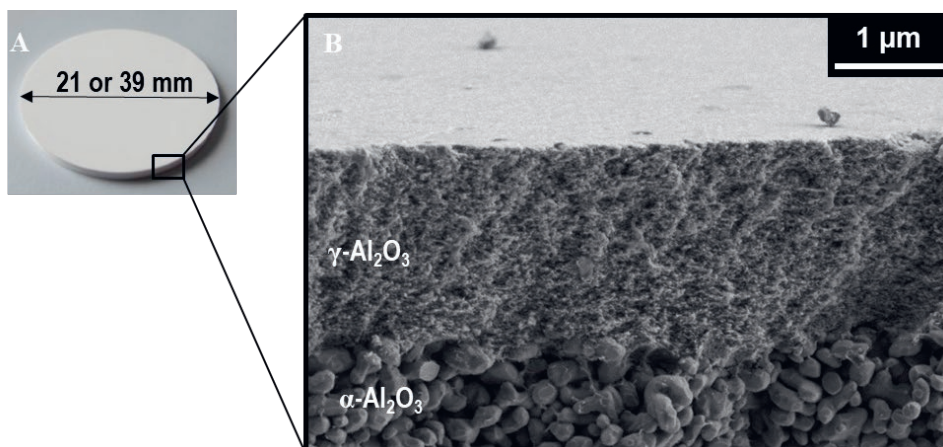
Figure S4.2: (A) Image of the porous ceramic support, (B) FE-SEM picture of a cross-section of the top layer of the support, showing a γ-alumina layer ($\varnothing_{pores}$ = 5 nm, 3 µm in thickness) and a part of the α-alumina substrate ($\varnothing_{pores}$ = 80 nm, 2 mm in thickness).
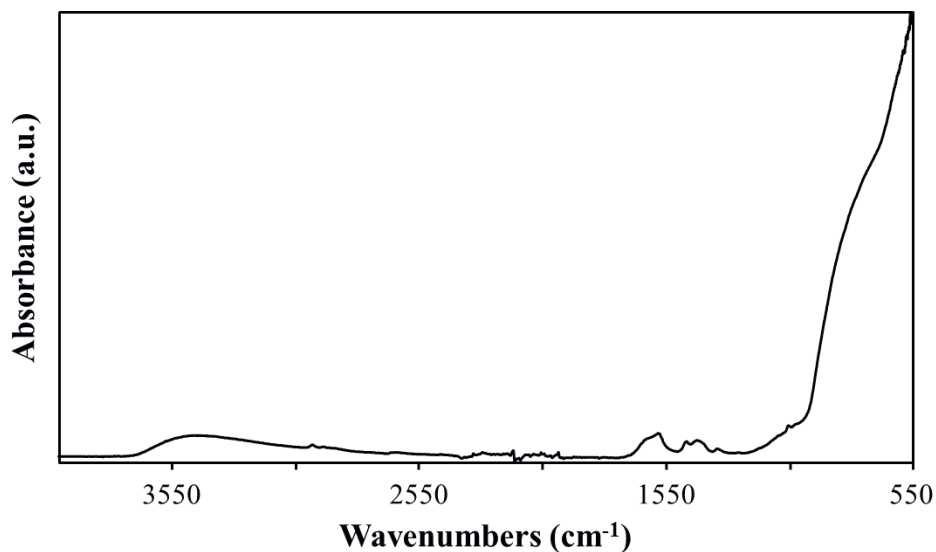
Figure S4.3: FTIR spectrum of the unmodified γ-alumina layer on the α-alumina support.

3. Schematic illustration for the thioether-based cross-linked nanofiltration membrane synthesis
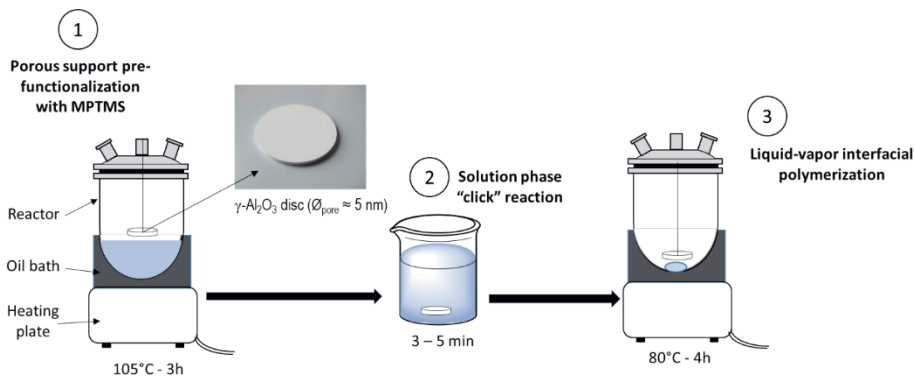
Figure S4.4: Schematic illustration for the thioether-based cross-linked nanofiltration membrane synthesis.

4. Thioether-based cross-linked free-standing film preparation

The thioether-based free-standing film was prepared as a proof-of-concept as well as to determine some physico-chemical properties of the final membrane. Compared to a synthesis in a single solvent, the liquid interfacial polymerization method allows the formation of a well-defined organic network.[26] Prior to the film preparation, a ${}^1H$ liquid NMR study was conducted to evidence potential side reactions. The film preparation procedure, and the results of the ${}^1H$ liquid NMR study can be found below. The FTIR analysis of the film is discussed in the manuscript and the spectrum can be found in Figure S4.14 (Section 4.5.9).

Film preparation procedure: In a glass vial, 17 mg (0.12 mmol, 1 eq) of 2SH and 20 μL (0.14 mmol, 0.6 eq) of TEA were dissolved in 10 mL of MilliQ water under well stirring. In a separate vial, 26 mg (0.073 mmol, 0.9 eq) of 3Br was dissolved in 10 mL of toluene. Then, on top of the aqueous solution, a small amount of toluene was added slowly to prevent mixing of the two phases (≈ 1 mL). Subsequently, the organic solution was added dropwise in the vial containing the aqueous phase. A thin layer appeared after 15 min, however the biphasic mixture was left over night to ensure the formation of a thick homogeneous layer (Figure S4.5). Afterwards, the layer was removed with a pincer and washed sequentially with 5 mL of water, ethanol and acetone, in a sonicated bath for 30 min. Finally, the film was dried at 50 °C under vacuum.
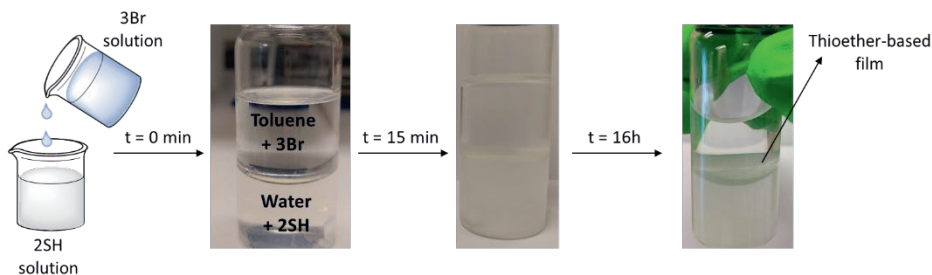
Figure S4.5: Schematic representation of the thioether-based cross-linked film preparation by liquid interfacial polymerization.

5. ^{1}H liquid NMR study

A Bruker Ascend^{TM} 400 MHz NMR spectrometer was used to perform ^{1}H liquid-state nuclear magnetic resonance (NMR) measurements in either D_2O or toluene d8. Chemical shifts were expressed in parts per million (ppm, δ) downfield from tetramethyl silane.

NMR sample preparation procedure: In NMR tubes containing a small amount of 2SH (~15 mg) either anhydrous toluene-d8 or deuterium oxide (D_2O) was added and shaken to form a mixture (Figure S4.7 for D_2O, Figure S4.8 for toluene d8). For the reaction mixtures in both organic and aqueous phase, a small amount of triethylamine (~1.2 eq) was added in each NMR tube. The ^{1}H NMR spectra were recorded 15 min after preparation of the solutions.

As can be seen in Figure S4.9, the newly appeared peaks (compared to Figure S4.7) were attributed to the formation of disulphide bonds, in the presence of a base and oxygen. These peaks are more visible in D_2O (Figure S4.9 vs. Figure S4.10). Unfortunately, due to the random configuration of these molecules, the elucidation of the spectrum is impossible with merely ^{1}H NMR. However, these results provide information on the reaction occurring during the interfacial polymerization process. The possible reactions are schematically represented in Figure S4.6. We assume that initially in the aqueous phase, the base catalyst activates the 2SH monomer via deprotonation (A). Then, two reactions can occur in presence of oxygen (O_2): at the interface between the two liquid phases, the thio-bromo "click" reaction occurs forming the desired thioether-based film (B); In the aqueous phase, the thiolate anions can be oxidized by the dissolved O_2 which leads to the undesirable disulphide bond formation (C).[46] The latter is demonstrated by ^{1}H NMR spectra in Figure S4.9 and S4.10.
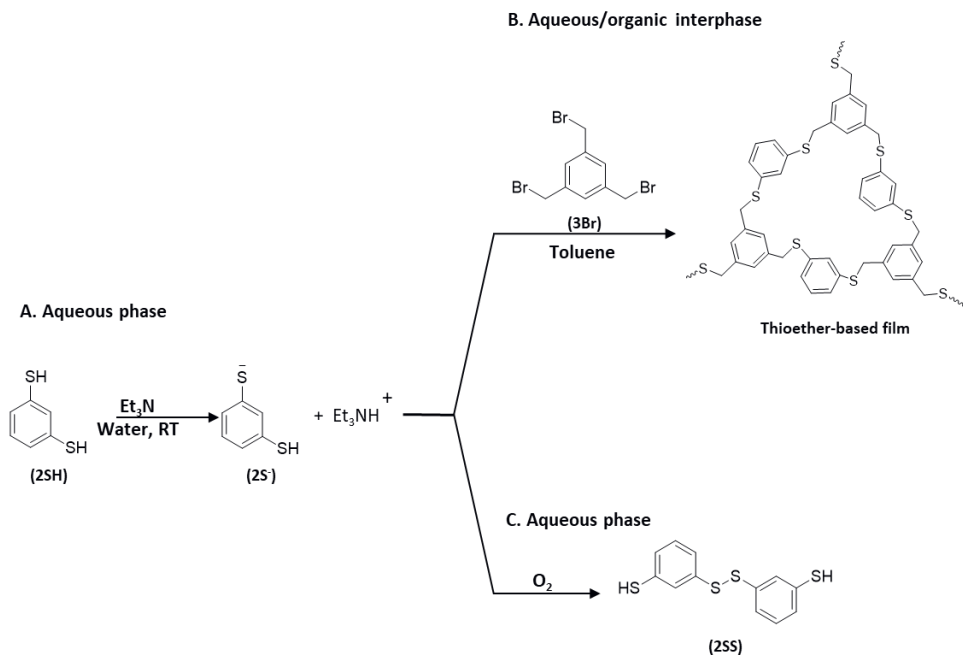
Figure S4.6: Schematic representation of the reactions occurring during the liquid-liquid interfacial polymerization (LIP) of the thioether-based cross-linked film. (A) Activation of the 2SH monomer under basic conditions leading to thiolate ion formation. (B) The thio-bromo "click" reaction resulting in polymerization and film formation at the aqueous-organic interphase. (C) Side reaction occurring in the presence of oxygen, leading to the undesirable disulphide (2SS).
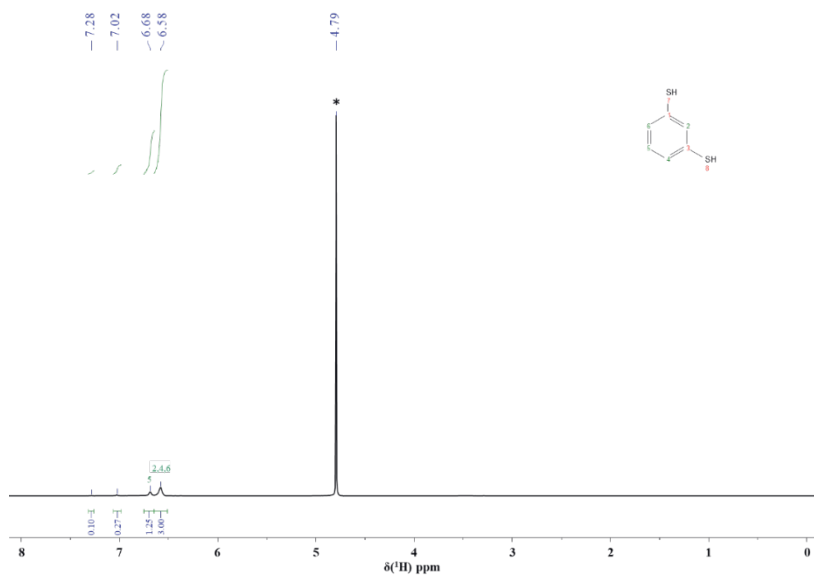
Figure S4.7: ^{1}H liquid NMR spectrum of 2SH in water. Asterisk (*) denotes solvent peak (D$_2$O).
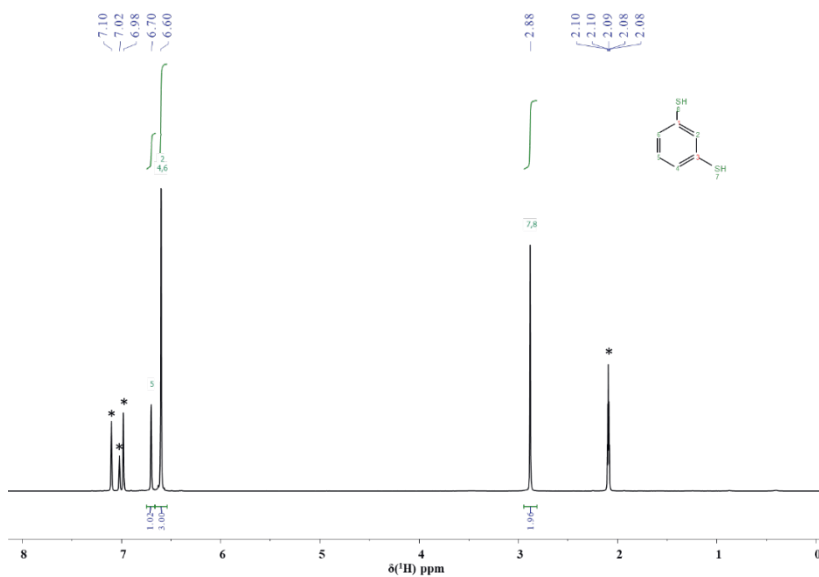
Figure S4.8: ^{1}H NMR spectrum of 2SH in toluene. Asterisks (*) denote solvent peaks (C$_7$D$_8$).
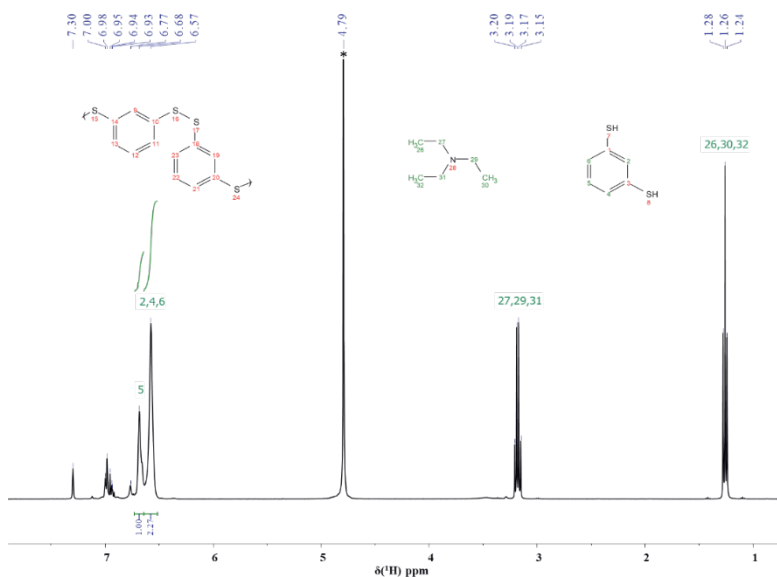
Figure S4.9: ^{1}H liquid NMR Spectrum of the reaction product of 2SH and TEA in deuterium oxide. Asterisks (*) denote solvent peaks (D$_2$O).
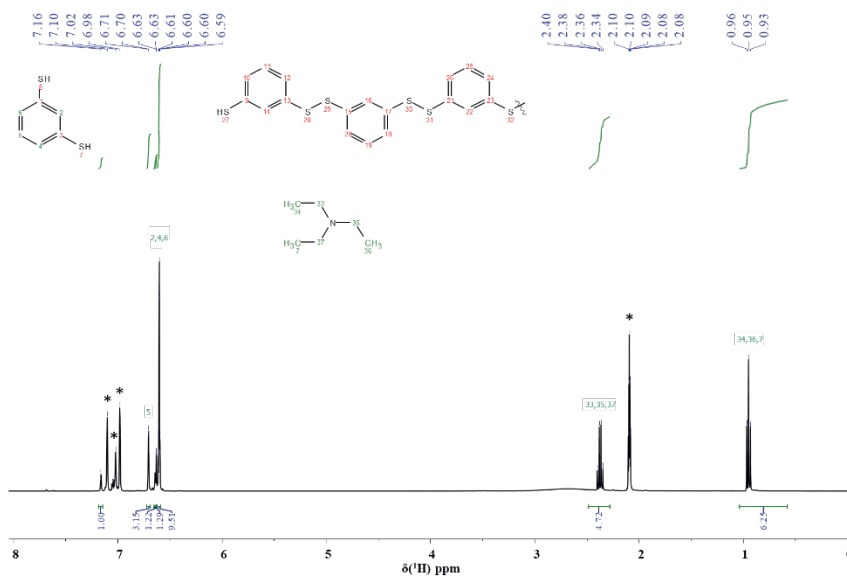
Figure S4.10: ^{1}H-NMR Spectrum of 2SH and TEA in deuterated toluene. Asterisks (*) denote solvent peaks (C$_7$D$_8$).

6. FTIR analysis of the MPTMS precursor used for the vapor phase grafting of the ceramic support
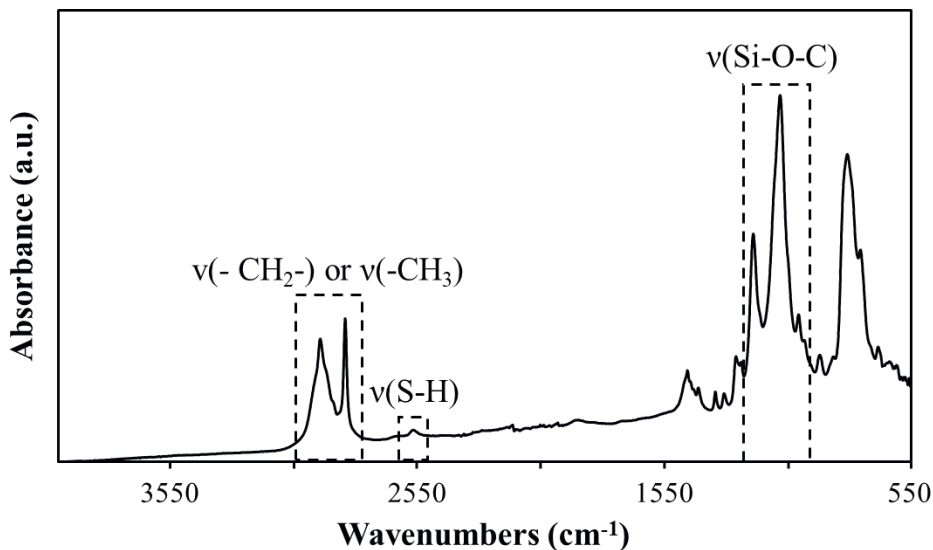
Figure S4.11: FTIR of the MPTMS precursor.

7. X-ray fluorescence spectroscopy (XRF)

Table S4.1: Weight compositions of the Al-SiM, and Al-SiM/TE samples. Chloride is observed due to cross contamination during measurement.

Samples / Element	Al-SiM	Al-SiM/TE
Al	53.2	44.1
Si	0.3	0.5
S	0.3	2.0
Cl	0.2	1.1
Br	0	0.03
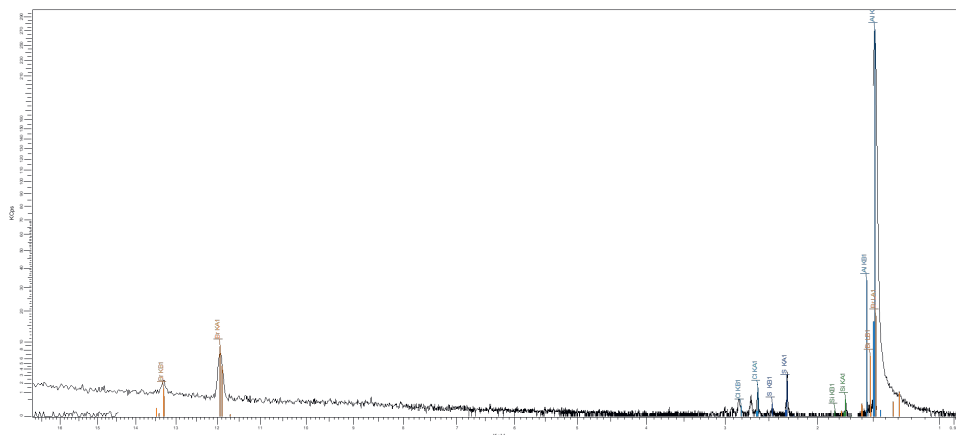
Figure S4.12: XRF spectrum of the Al-SiM/TE sample.

4.6. References

(1)   Marchetti, P.; Solomon, M. F. J.; Szekely, G.; Livingston, A. G. Molecular Separation with Organic Solvent Nanofiltration: A Critical Review. *Chem. Rev.* **2014**, *114*, 10735– 10806. https://doi.org/10.1021/cr500006j.

(2)   Vandezande, P.; Gevers, L. E. M.; Vankelecom, I. F. J. Solvent Resistant Nanofiltration: Separating on a Molecular Level. *Chem. Soc. Rev.* **2008**, *37* (2), 365–405. https://doi.org/10.1039/b610848m.

(3)   Szekely, G.; Jimenez-Solomon, M. F.; Marchetti, P.; Kim, J. F.; Livingston, A. G. Sustainability Assessment of Organic Solvent Nanofiltration: From Fabrication to Application. *Green Chem.* **2014**, *16* (10), 4440–4473. https://doi.org/10.1039/c4gc00701h.

(4)   Wittbecker, E. L.; Morgan, P. W. Interfacial Polycondensation. I. *J. Polym. Sci. Part A Polym. Chem.* **1996**, *34* (4), 521–529. https://doi.org/10.1002/pola.1996.815.

(5)   Gong, G.; Wang, P.; Zhou, Z.; Hu, Y. New Insights into the Role of an Interlayer for the Fabrication of Highly Selective and Permeable Thin-Film Composite Nanofiltration Membrane. *ACS Appl. Mater. Interfaces* **2019**, *11* (7), 7349–7356. https://doi.org/10.1021/acsami.8b18719.

(6) Raaijmakers, M. J. T.; Benes, N. E. Current Trends in Interfacial Polymerization Chemistry. *Prog. Polym. Sci.* **2016**, *63*, 86–142. https://doi.org/10.1016/j.progpolymsci.2016.06.004.

(7) Song, Y.; Fan, J. B.; Wang, S. Recent Progress in Interfacial Polymerization. *Mater. Chem. Front.* **2017**, *1* (6), 1028–1040. https://doi.org/10.1039/c6qm00325g.

(8) Mehta, P. P.; Pawar, V. S. Electrospun Nanofiber Scaffolds: Technology and Applications. In *Applications of Nanocomposite Materials in Drug Delivery*; Elsevier, 2018; pp 509–573. https://doi.org/10.1016/B978-0-12-813741-3.00023-6.

(9) Lee, K. P.; Bargeman, G.; de Rooij, R.; Kemperman, A. J. B.; Benes, N. E. Interfacial Polymerization of Cyanuric Chloride and Monomeric Amines: PH Resistant Thin Film Composite Polyamine Nanofiltration Membranes. *J. Memb. Sci.* **2017**, *523*, 487–496. https://doi.org/10.1016/J.MEMSCI.2016.10.012.

(10) Jye, L. W.; Ismail, A. F. *Nanofiltration Membranes*; CRC Press, 2016. https://doi.org/10.1201/9781315181479.

(11) Do, V. T.; Tang, C. Y.; Reinhard, M.; Leckie, J. O. Degradation of Polyamide Nanofiltration and Reverse Osmosis Membranes by Hypochlorite. *Environ. Sci. Technol.* **2012**, *46* (2), 852–859. https://doi.org/10.1021/es203090y.

(12) Ma, Q.; Shuler, P. J.; Aften, C. W.; Tang, Y. Theoretical Studies of Hydrolysis and Stability of Polyacrylamide Polymers. *Polym. Degrad. Stab.* **2015**, *121*, 69–77. https://doi.org/10.1016/j.polymdegradstab.2015.08.012.

(13) Kolb, H. C.; Finn, M. G.; Sharpless, K. B. Click Chemistry: Diverse Chemical Function from a Few Good Reactions. *Angew. Chemie Int. Ed.* **2001**, *40* (11), 2004–2021. https://doi.org/10.1002/1521-3773(20010601)40:11<2004::AID-ANIE2004>3.0.CO;2-5.

(14) Timmerman, P.; Beld, J.; Puijk, W. C.; Meloen, R. H. Rapid and Quantitative Cyclization of Multiple Peptide Loops onto Synthetic Scaffolds for Structural Mimicry of Protein Surfaces. *ChemBioChem* **2005**, *6* (5), 821–824. https://doi.org/10.1002/cbic.200400374.

(15) Richelle, G. J. J.; Ori, S.; Hiemstra, H.; van Maarseveen, J. H.; Timmerman, P. General and Facile Route to Isomerically Pure Tricyclic Peptides Based on Templated Tandem CLIPS/CuAAC Cyclizations. *Angew. Chemie Int. Ed.* **2018**, *57* (2), 501–505. https://doi.org/10.1002/anie.201709127.

(16) Monnereau, L.; Grandclaudon, C.; Muller, T.; Bräse, S. Sulfur-Based Hyper Cross-Linked Polymers. *RSC Adv.* **2015**, *5* (30), 23152–23159. https://doi.org/10.1039/c5ra01463h.

(17) Rapakousiou, A.; Sakamoto, R.; Shiotsuki, R.; Matsuoka, R.; Nakajima, U.; Pal, T.; Shimada, R.; Hossain, A.; Masunaga, H.; Horike, S.; Kitagawa, Y.; Sasaki, S.; Kato, K.; Ozawa, T.; Astruc, D.; Nishihara, H. Liquid/Liquid Interfacial Synthesis of a Click Nanosheet. *Chem. – A Eur. J.* **2017**, *23* (35), 8443–8449. https://doi.org/10.1002/chem.201700201.

(18) Pujari, S. P.; Scheres, L.; Marcelis, A. T. M.; Zuilhof, H. Covalent Surface Modification of Oxide Surfaces. *Angew. Chemie – Int. Ed.* **2014**, *53* (25), 6322–6356. https://doi.org/10.1002/anie.201306709.

(19) Zheng, Z.; Zhao, H.; Fa, W.; He, W.; Wong, K. W.; Kwok, R. W. M.; Lau, W. M. Construction of Cross-Linked Polymer Films Covalently Attached on Silicon Substrate via a Self-Assembled Monolayer. *RSC Adv.* **2013**, *3* (29), 11580–11585. https://doi.org/10.1039/c3ra40949j. Maaskant, E.; de Wit, P.; Benes, N. E. Direct Interfacial Polymerization onto Thin Ceramic Hollow Fibers. *J. Memb. Sci.* **2018**, *550*, 296–301. https://doi.org/10.1016/j.memsci.2018.01.009.

(21) R.J.R. Uhlhorn, M.H.B.J. Huis In't Veld, K. Keizer, A. J. B. Synthesis of Ceramic Membranes Synthesis of Non-Supported and Supported y-Alumina. *J. Mater. Sci.* **1992**, *27*, 527–537.

(22) ten Hove, M.; Luiten-Olieman, M. W. J.; Huiskes, C.; Nijmeijer, A.; Winnubst, L. Hydrothermal Stability of Silica, Hybrid Silica and Zr-Doped Hybrid Silica Membranes. *Sep. Purif. Technol.* **2017**, *189*, 48–53. https://doi.org/10.1016/j.seppur.2017.07.045.

(23) Cuperus, F. P.; Bargeman, D.; Smolders, C. A. Permporometry: The Determination of the Size Distribution of Active Pores in UF Membranes. *J. Memb. Sci.* **1992**, *71* (1–2), 57–67. https://doi.org/10.1016/0376-7388(92)85006-5.

(24) Yang, D.; Paul, B.; Xu, W.; Yuan, Y.; Liu, E.; Ke, X.; Wellard, R. M.; Guo, C.; Xu, Y.; Sun, Y.; Zhu, H. Alumina Nanofibers Grafted with Functional Groups: A New Design in Efficient Sorbents for Removal of Toxic Contaminants from Water. *Water Res.* **2010**, *44* (3), 741–750. https://doi.org/10.1016/j.watres.2009.10.014.

(25) Coates, J. Interpretation of Infrared Spectra, A Practical Approach. In *Encyclopedia of Analytical Chemistry*; John Wiley & Sons, Ltd: Chichester, UK, 2006. https://doi.org/10.1002/9780470027318.a5606.

(26) Maaskant, E.; Gojzewski, H.; Hempenius, M. A.; Vancso, G. J.; Benes, N. E. Thin Cyclomatrix Polyphosphazene Films: Interfacial Polymerization of Hexachlorocyclotriphosphazene with Aromatic Biphenols. *Polym. Chem.* **2018**, *9* (22), 3169–3180. https://doi.org/10.1039/c8py00444g.

(27) Khalili, F.; Henni, A.; East, A. L. L. PK a Values of Some Piperazines at (298, 303, 313, and 323) K. *J. Chem. Eng. Data* **2009**, *54*, 2914–2917. https://doi.org/10.1021/je900005c.

(28) Pepels, M.; Filot, I.; Klumperman, B.; Goossens, H. Self-Healing Systems Based on Disulfide-Thiol Exchange Reactions. *Polym. Chem.* **2013**, *4* (18), 4955–4965. https://doi.org/10.1039/c3py00087g.

(29) Carrion-Vazquez, M.; Oberhauser, A. F.; Fowler, S. B.; Marszalek, P. E.; Broedel, S. E.; Clarke, J.; Fernandez, J. M. Mechanical and Chemical Unfolding of a Single Protein : *Proc. Natl. Acad. Sci.* **1999**, *96* (March), 3694–3699.

(30) Saric, I.; Peter, R.; Kolympadi Markovic, M.; Jelovica Badovinac, I.; Rogero, C.; Ilyn, M.; Knez, M.; Ambrožić, G. Introducing the Concept of Pulsed Vapor Phase Copper-Free Surface Click-Chemistry Using the ALD Technique. *Chem. Commun.* **2019**, *55* (21), 3109–3112. https://doi.org/10.1039/C9CC00367C.

(31) Gao, F.; Aminane, S.; Bai, S.; Teplyakov, A. V. Chemical Protection of Material Morphology: Robust and Gentle Gas-Phase Surface Functionalization of ZnO with Propiolic Acid. *Chem. Mater.* **2017**, *29* (9), 4063–4071. https://doi.org/10.1021/acs.chemmater.7b00747.

(32) Lin-Vien, D.; Colthup, N. B.; Fateley, W. G.; Grasselli, J. G. *The Handbook of Infrared and Raman Characteristic Frequencies of Organic Molecules*; Daimay Lin-Vien, Colthup Norman B., Fateley William G., G. J. G., Ed.; Academic Press, 1991. https://doi.org/doi:10.1021/ac60293a718.

(33) Colthup, N. B.; Daly, L. H.; Wiberley, S. E. METHYL AND METHYLENE GROUPS. In *Introduction to Infrared and Raman Spectroscopy*; Elsevier, 1990; pp 215–233. https://doi.org/10.1016/b978-0-08-091740-5.50008-9.

(34) Benevides, P. J. C.; Young, M. C. M.; Giesbrecht, A. M.; Roque, N. F.; Da Bolzani, V. S. Antifungal Polysulphides from Petiveria Alliacea L.

150

Phytochemistry **2001**, *57* (5), 743–747. https://doi.org/10.1016/S0031-9422(01)00079-6.

(35) Benzyl sulfide https://webbook.nist.gov/cgi/cbook.cgi?ID=C538749&Type=IR-SPEC&Index=2#IR-SPEC (accessed Apr 8, 2020).

(36) Pizzoccaro-Zilamy, M. A.; Huiskes, C.; Keim, E. G.; Sluijter, S. N.; Van Veen, H.; Nijmeijer, A.; Winnubst, L.; Luiten-Olieman, M. W. J. New Generation of Mesoporous Silica Membranes Prepared by a Stöber-Solution Pore-Growth Approach. ACS Appl. Mater. Interfaces 2019, 11 (20), 18528–18539. https://doi.org/10.1021/acsami.9b03526.

(37) Puhlfürß, P.; Voigt, I.; Weber, R.; Morbé, M. Microporous TiO2membranes with a Cut off <500 Da. J. Memb. Sci. 2000, 174 (1), 123–133. https://doi.org/10.1016/S0376-7388(00)00380-X.

(38) Singh, S.; Khulbe, K. C.; Matsuura, T.; Ramamurthy, P. Membrane Characterization by Solute Transport and Atomic Force Microscopy. J. Memb. Sci. 1998, 142 (1), 111–127. https://doi.org/10.1016/S0376-7388(97)00329-3.

(39) Pinheiro, A. F. M.; Hoogendoorn, D.; Nijmeijer, A.; Winnubst, L. Development of a PDMS-Grafted Alumina Membrane and Its Evaluation as Solvent Resistant Nanofiltration Membrane. J. Memb. Sci. 2014, 463, 24–32. https://doi.org/10.1016/J.MEMSCI.2014.03.050.

(40) Maaskant, E.; Vogel, W.; Dingemans, T. J.; Benes, N. E. The Use of a Star-Shaped Trifunctional Acyl Chloride for the Preparation of Polyamide Thin Film Composite Membranes. J. Memb. Sci. 2018, 567, 321–328. https://doi.org/10.1016/j.memsci.2018.09.032.

(41) Gothe, P. K.; Gaur, D.; Achanta, V. G. MPTMS Self-Assembled Monolayer Deposition for Ultra-Thin Gold Films for Plasmonics Related Content. J. Phys. Commun. 2018, 2 (3), 035005. https://doi.org/10.1088/2399-6528/aaaedd.

(42) Roelofs, F.; Vogelsberger, W. Dissolution Kinetics of Nanodispersed γ-Alumina in Aqueous Solution at Different PH: Unusual Kinetic Size Effect and Formation of a New Phase. J. Colloid Interface Sci. 2006, 303 (2), 450–459. https://doi.org/10.1016/j.jcis.2006.08.016.

(43) Li, K.; Li, S.; Huang, T.; Dong, C.; Li, J.; Zhao, B.; Zhang, S. Chemical Cleaning of Ultrafiltration Membrane Fouled by Humic Substances: Comparison between Hydrogen Peroxide and Sodium Hypochlorite. Int. J.

Environ. Res. Public Health 2019, 16 (14), 2568. https://doi.org/10.3390/ijerph16142568.

(44) Madaeni, S. S.; Mohamamdi, T.; Moghadam, M. K. Chemical Cleaning of Reverse Osmosis Membranes. Desalination 2001, 134 (1–3), 77–82. https://doi.org/10.1016/S0011-9164(01)00117-5.

(45) Membrane chemical cleaning: why is it required and how is it performed? https://www.sterlitech.com/blog/post/membrane-chemical-cleaning (accessed May 15, 2020).

(46) Saeed Abaee, M.; Mojtahedi, M. M.; Navidipoor, S. Diethylamine-Catalyzed Dimerization of Thiols: An Inexpensive and Green Method for the Synthesis of Homodisulfides Under Aqueous Conditions. Synth. Commun. 2011, 41 (9), 170–176. https://doi.org/10.1080/00397911.2015.1005631.

(47) Amirilargani, M.; Merlet, R. B.; Nijmeijer, A.; Winnubst, L.; de Smet, L. C. P. M.; Sudhölter, E. J. R. Poly (Maleic Anhydride-Alt-1-Alkenes) Directly Grafted to γ-Alumina for High-Performance Organic Solvent Nanofiltration Membranes. J. Memb. Sci. 2018, 564, 259–266. https://doi.org/10.1016/J.MEMSCI.2018.07.042.

(48) Gothe, P. K.; Gaur, D.; Achanta, V. G. MPTMS Self-Assembled Monolayer Deposition for Ultra-Thin Gold Films for Plasmonics Related Content. J. Phys. Commun. 2018, 2 (3), 035005. https://doi.org/10.1088/2399-6528/aaaedd.

(49) Bhagat, S. D.; Chatterjee, J.; Chen, B.; Stiegman, A. E. High Refractive Index Polymers Based on Thiol-Ene Cross-Linking Using Polarizable Inorganic/Organic Monomers. Macromolecules 2012, 45 (3), 1174–1181. https://doi.org/10.1021/ma202467a.

(50) Zhang, G.; Xing, X. J.; Li, D. S.; Wang, X. J.; Yang, J. Effects of Thioether Content on the Solubility and Thermal Properties of Aromatic Polyesters. Ind. Eng. Chem. Res. 2013, 52 (47), 16577–16584. https://doi.org/10.1021/ie401750e.

(51) Monnereau, L.; Grandclaudon, C.; Muller, T.; Bräse, S. Sulfur-Based Hyper Cross-Linked Polymers. RSC Adv. 2015, 5 (30), 23152–23159. https://doi.org/10.1039/c5ra01463h.

(52) Merlet, R. B.; Pizzoccaro-Zilamy, M. A.; Nijmeijer, A.; Winnubst, L. Hybrid Ceramic Membranesfor Organic Solvent Nanofiltration: State-of-the-Art and Challenges. Journal of Membrane Science. Elsevier B.V. April 1, 2020, p 117839. https://doi.org/10.1016/j.memsci.2020.117839.

152

(53) Merlet, R. B.; Tanardi, C. R.; Vankelecom, I. F. J.; Nijmeijer, A.; Winnubst, L. Interpreting Rejection in SRNF across Grafted Ceramic Membranes through the Spiegler-Kedem Model. J. Memb. Sci. 2017, 525, 359–367. https://doi.org/10.1016/J.MEMSCI.2016.12.013.

(54) Tanardi, C. R.; Nijmeijer, A.; Winnubst, L. Coupled-PDMS Grafted Mesoporous γ-Alumina Membranes for Solvent Nanofiltration. Sep. Purif. Technol. 2016, 169, 223–229. https://doi.org/10.1016/J.SEPPUR.2016.05.057.

Chapter 5

Controlled Nanoconfinement of Polyimide Networks in Mesoporous γ-Alumina Membranes for the Molecular Separation of Organic Dyes

ABSTRACT

Polyimide networks are key in the development of stable, resilient, and efficient membranes for separation applications under demanding conditions. To this aim, the controlled design of the network's nanostructure and its properties are needed. However, such control remains a challenge with currently available synthesis methods. Here, we present a simple nanofabrication approach that allows the controlled nanoconfinement, growth and covalent attachment of polyimide (PI) networks inside the mesopores of γ-alumina layers. The attachment of the PI network on the γ-alumina layer was initiated via different pre-functionalization steps that play a pivotal role in inducing the in-situ polymerization reaction at the pore entrance and/or at the inner pore surface. The nanoconfinement was found to be limited to maximal the1.5 μm-thick γ-alumina supporting layer at maximum, and the resulting hybrid PI/ceramic membranes showed stable performance in a variety of solvents. These PI/ceramic membranes were found to be very efficient in the challenging separation of small organic dye molecules such as Rhodamine B (479 g mol^{-1}) from toxic solvents such as dimethylformamide or dioxane. Therefore, this technique opens up possibilities for a multitude of separations. Moreover, the PI synthesis approach can be applied to other applications that also rely on porosity and stability control, such as for advanced insulation and anticorrosion.

Nanoconfined Polyimide Network into mesopores
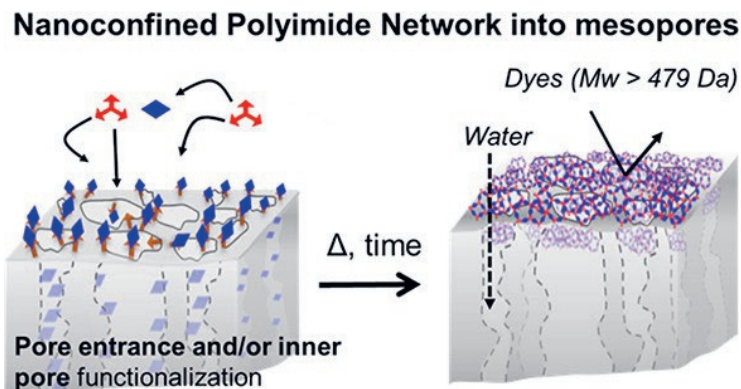
This chapter has been published as:

5.1. Introduction

The industry relies heavily on separation methods, from the purification of primary materials to the isolation of polymers, pharmaceuticals, and many other products.[1]Conventional separation methods, such as distillation, are principally thermally driven. As a result, they can be costly, energy-intensive, and inefficient in separating thermally sensitive intermediates or products.[1–3] As an alternative, nanofiltration membrane-based separation technologies are increasingly implemented in the industry either in combination with distillation or extraction as hybrid processes or by totally replacing these conventional methods. The term "nanofiltration" (NF) refers to a pressure-driven membrane-based separation process in which particles and dissolved molecules smaller than 2 nm are rejected. By replacing the high energy-demanding thermally-driven separation methods (e.g., distillation) with low energy-demanding pressure-driven NF membranes, one can get more energy-efficient and environmentally-friendly processes.[1–3] Nevertheless, current membrane materials, which are often polymeric, are not always compatible with industrial streams, particularly mixtures of water and organic solvents, causing membrane failure due to the degradation or dissolution of the material itself. Therefore, when designing a membrane for complex applications, one should consider not only the mixture of solutes but also the nature of the solvents involved. Nowadays, membranes developed for such challenging applications are called solvent-tolerant nanofiltration (STNF) membranes.[2,4]

The most common materials used to prepare STNF membranes are polymers, such as polyamide–imides,[5] polydimethylsiloxanes,[6] etc. These polymeric membranes have generally shown high permeability and stable rejection with polar organic solvents such as alcohols or tetrahydrofuran. However, the performance of these membranes is unsatisfactory telepresence of apolar solvents, mainly due to the degradation of the supporting layer.[4] As a result, the permeability often decreases, and the rejection becomes unpredictable. Hence, such behaviour hinders the implementation of this membrane technology in water/solvent streams. The combination of a chemical-inert porous ceramic support functionalized with polyimides (PI) can overcome the instability issue of the support. PIs are among the most resilient polymeric membrane-based materials used nowadays. PIs are polymers characterized by a stable imide ring as a repetitive unit that exhibits good mechanical properties, chemical solvent resistance, heat resistance, and electrical properties.[7]

Polyimides (PIs) are prepared by the polycondensation reaction between (di)anhydrides and (di or tri)amines at temperatures between 180 and 300 °C. Due to their high thermal (> 400°C) and chemical resistance, polyimides are extensively used as membrane materials for gas separation, solvent exchange, and many others.[8]

Commercial PI membranes such as Puramem were well adapted for specific STNF applications in solvents such as toluene and heptane, but only in operating conditions up to 50°C.[9] To prevent dissolution and to increase the hydrophilicity (imide group to amic acid) of the PI membrane material in polar aprotic or chlorinated solvents; it has been reported that additional cross-linking steps are often needed.[8] Even though the amic acids are more hydrophilic than imides, they are less chemically stable.[10] Therefore, in membrane technology, it is crucial to combine a highly stable material, such as polyimides, which are also potentially processable to membranes. Therefore, different approaches were explored to overcome the problems associated with material stability and processability.[11] For example, Kuttiani Ali et al.[12] developed hydrophilic nanocomposite membranes for ultrafiltration by adding silica nanoparticles, pre-functionalized with deep-eutectic solvents, into a polyimide solution prior to casting. The membranes containing 2 wt.% of nanoparticles presented the best mechanical and phenol retention under a wide pH range. Moreover, Wei et al.[13] prepared an ultrathin polyimide/silica nanofiltration membrane by in-situ hydrolysis and condensation of tetraethoxysilane. The resulting membrane presented improved hydrophilicity, mechanical strength, and thermal stability compared to the pure PI-NF membrane. Using a similar approach, Qiang et al. [14] formed a resistant STNF membrane. Despite the promising performances, the potential leaching of nanoparticles is not negligible and can lead to potential human and environmental exposure.[15] Thus far, many researchers have focused on introducing inorganic nanoparticles into the PI matrix. The opposite approach in which PI networks are confined in an inorganic matrix could also be employed.

Following this latter strategy, Isaacson et al.[16,17] nanoconfined a PI network in a mesoporous tortuous organosilica matrix. The preparation procedure involved infiltrating polyamic acid oligomers into the porous matrix and subsequent cross-linking of the polymer units. As a result, the composite film/layer prepared showed enhanced resistance to fracture compared to the pristine mesoporous support due to a so-called confinement-induced molecular bridging mechanism. Such confined polyimide systems could be used as a thermal barrier coating for high-temperature operations (at least up to 350°C) and superior lightweight materials for aerospace applications. However, the possibility of using this confined PI network as a separation layer is unknown.

Studies have shown that the nanoconfinement of a crystallized polymer within nano porous anodic aluminium oxide (AAO) templates is suitable for preparing innovative systems for biosensing and optical and electrical-related applications.[18] When a polymer is confined within a micrometre-thick rigid AAO template, comprising of vertically oriented large pores (10 – 100 nm) that are not tortuous, the crystallization behaviour experiences dramatic changes as the pore size is reduced. This approach allows modulation of the polymer nanostructures for specific applications. However,
158

it is not suitable for practical separation applications in the industry due to the limited surface area of the AAO supports when dealing with cubic meters of water and their fragility when exposed to harsh conditions.[19] In contrast to previous studies done on AAO supports or mesoporous organosilica layers; we looked at defined and rigid mesoporous ceramic membranes with relatively low tortuosity. Alumina (γ-, or α-phase) membranes are commercially predominant in the market and are available in the shape of discs and tubes.[20,21] Compared to AAO templates, mesoporous γ-Al$_2$O$_3$ membranes are supported on millimetre-thick α-alumina supports and commercialized in the form of modules, making them suitable for real separations under demanding conditions (high pressure and temperature).[22,23] However, their relatively large pores (~ 5 nm) are not selective in the nanofiltration range. Nevertheless, the γ-alumina surface is rich in free hydroxyl groups that can be used to modify the pore entrance and inner pore surface by covalently attaching molecules, oligomers, and polymer brushes to prepare hybrid membranes.[4,24–27]

In fact, it has been shown that grafting-to and grafting-from reactions can be applied to modify dense substrates[28] and the pore entrance and inner pore surface of γ-alumina mesoporous layers.[4,24–27] Sun et al.[28] used the grafting-from method to grow polyglycidyl methacrylate brushes from silicon wafers' surface (-induced). These brushes were used as an adhesive interlayer to attach a polyimide film on silicon wafers chemically. As a result, improved friction and wear resistance was observed compared to the polyimide films on bare silicon wafers. However, the possibility of simultaneous pore confinement and covalent attachment of across-linked PI network onto the ceramic support has not been demonstrated yet. Furthermore, the growth of a crystalline polymer in one step from the surface of aceramic support as well as the applicability of such material under membrane conditions, is still not shown in the literature.

In this work, we have initiated for the first time the in-situ polymerization reaction of a PI network directly from an inorganic surface and controlled the nanoconfinement inside rigid and well-defined, tortuous γ-alumina mesoporous γ-alumina mesoporous layers as indicated in Scheme 1. Our strategy is to use two different precursors that promote the confinement of the PI network in the ceramic support. The first precursor, bearing an amino-functional group, is located at the top surface and pore entrance, while the second one, consisting of an anhydride-functional group, is present on both the surface and within the mesopores of the γ-alumina layer. Indeed, the above functional groups induce a surface polyimidization reaction that controls the location of the network formation either at the pore entrance or inside the γ-alumina layer. Furthermore, we show that by increasing the reaction time from 1 to 5 days, the membrane performance was significantly improved due to the increase in the concentration of the polyimide network into/on the mesoporous layer. A combination of different surface and pore characterization techniques were

employed to demonstrate the successful growth and confinement of the polymer inside the mesoporous layer. In addition, the nanoconfined PI-based membranes were tested in different model mixtures where their potential as solvent-resistant nanofiltration (NF) membrane was demonstrated. The concept described in this work illustrates how across-linked polyimide can grow in a nanoconfined space, such as the tortuous but defined mesopores of our alumina membranes. This can be achieved by simply controlling the grafting of the initiator for the surface-induced in-situ polymerization from the surface of the alumina support. This approach can be expanded in other fields where controlled nanoconfinement of across-linked crystalline polymer is desired for different applications.
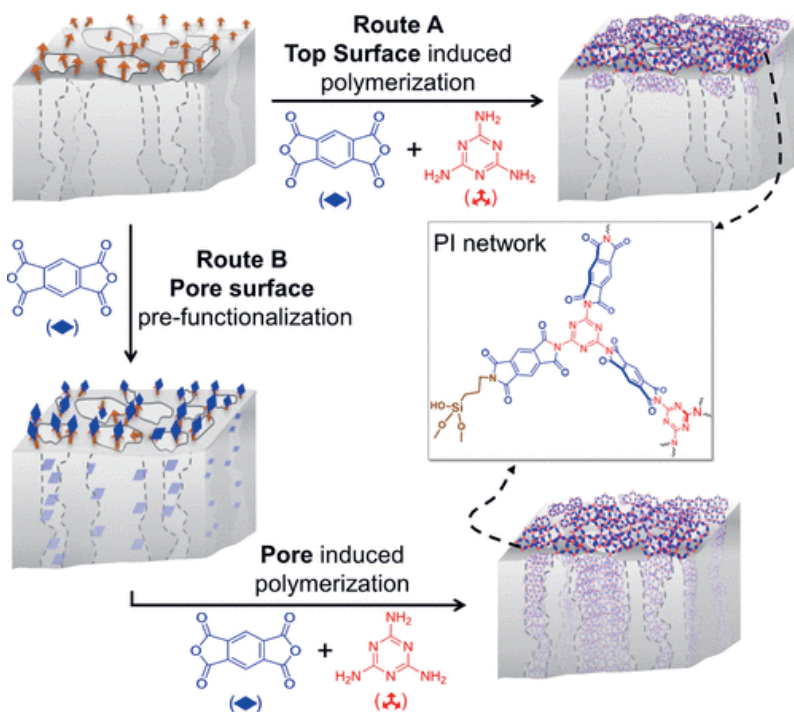
Scheme 1: Schematic illustration of the two fabrication routes, a and b, used for the controlled nanoconfinement of the PI network in a tortuous but defined, rigid mesoporous γ-alumina layer matrix. Both routes originate from pre-functionalized supports with (3-aminopropyl)triethoxysilane (APTES, dark orange arrow) molecules grafted at the top surface of the support. In route A, direct PI growth occurs between pyromellitic dianhydride (PMDA, blue diamond), melamine (MA, red triple arrow), and the superficial amino functionality, leading to the formation of the PI network at the top surface and pore entrance. In route B, an additional pre-functionalization of the APTES modified support (top and pore surface) is conducted only with PMDA (blue diamond). The subsequent PI network formation is also extended (favoured) in the γ-alumina mesopores.

5.2. Methods

5.2.1. Materials

Solvents ethanol (technical grade > 95%), anisole (>99%, Merck, NL), N-methyl-2-pyrrolidone (NMP) (>99%, anhydrous, Merck, NL), mesitylene (>99%, Acros Organics, NL), isoquinoline (95%, TCI, Europe), acetone (technical grade, >95%), 1,4-dioxane (anhydrous, Sigma Aldrich, NL), dimethylformamide (>99%, Sigma Aldrich, NL), and ethanol (analytical grade, Merck, NL) were used as received.

161

Water was purified through a Milli-Q Reference Water Purification System. Glycerol (anhydrous, Merck, NL), 3-aminopropyl triethoxysilane (>98%, Sigma Aldrich, NL), pyromellitic dianhydride (PMDA) (97%, Sigma Aldrich, NL), melamine (MA) (99%, Sigma Aldrich, NL), Brilliant Yellow (70%, Sigma Aldrich, NL), and Rhodamine B (>99%, Merck, NL) were used as received. The chemical structures and abbreviations can be found in Figure S5.1 of the Supporting Information. Support Fabrication. The α-alumina (α-Al2O3 > 99%) flat-sheet substrates (disc: diameter, 21 mm; thickness, 2 mm; pore diameter, 80 nm) with one polished side were purchased from Pervatech B.V., the Netherlands. The polished side was dip-coated with a boehmite sol (prepared in-house) and subsequently calcined at 650 °C for 3 h to form a γ-alumina layer of 1.5 μm in total thickness and 5.5 nm in mean pore diameter. Further details for the fabrication of the γ-alumina layer can be found elsewhere.[23,49] The calcined supports were washed by immersion in a 2:1 v/v water/ethanol solution for at least 8 h at room temperature and then dried overnight in a vacuum oven at 50 °C.

5.2.2. Pre-functionalization of the Top Surface and Pore Entrance

The γ-alumina layer was first filled with 1−2 mL of glycerol by rubbing the viscous liquid onto the surface and letting it soak for >10 min. The top surface of the substrate was dabbed clean with a fibreless tissue. Then, 21 μL of 3-aminopropyl trimethoxysilane (APTES) was dissolved in anisole (anhydrous) and transferred into a reaction vessel with the glycerol-filled γ-alumina layer suspended above the solution. The solution was heated to 105 °C for 3 h in a sealed vessel. After grafting, the functionalized porous support was washed with 20 mL of anisole for 1 h and 20 mL of water for 20 min under sonication and dried overnight at 50 °C under vacuum. Amino-functionalized supports obtained at this stage were denoted as A.

5.2.3. Pre-functionalization of the γ-Alumina Layer's Inner Pore Surface

Under an inert atmosphere in a 50 mL reaction vessel charged with 40 mg (0.18 mmol) of PMDA, 20 mL of mesitylene was added and stirred for 1−2 min. A sample was then immersed in the solution, and the mixture was heated to 160 °C overnight. The mixture was cooled to room temperature, and the sample was washed with n-methyl-2-pyrrolidone (NMP) and acetone in a sonicated bath for 30 min. Finally, the sample (denoted as B) was dried in a vacuum oven at 50 °C overnight. Pore Surface-Induced Polyimidization Reaction. In a 50 mL reaction vessel, 530 mg (2.43 mmol) of PMDA and 260 mg (2.06 mmol) MA were added. Under an inert atmosphere, 9 mL of anhydrous NMP, 9 mL of mesitylene, and 0.9 mL of isoquinoline were added in the reaction vessel and stirred for a few minutes. Afterward, the pre-functionalized sample (A or B) was added in the mixture and was heated to 200 °C for either 1 or 5 days. After the reaction was completed, the dark brown mixture was cooled to room temperature, and the membrane was removed from the solution and washed with 20

162

mL of NMP in a sonicated bath for 1 h. Then, the membrane was immersed in 20 mL of fresh NMP and left for 3 days at room temperature to remove unreacted monomers or ungrafted polymers. Finally, the membrane was sonicated in 20 mL of acetone and dried in a vacuum oven at 50 °C overnight. Membrane samples prepared via route A (Scheme 1) are denoted as A-1 and A-5 (or A-1/ 5) for 1 and 5 days of reaction. Samples prepared via route B (Scheme 1) are denoted as B-1 and B-5 (or B-1/5). After the preparation of each membrane, the remaining reaction solution was collected and filtered under a vacuum to yield a dark brown powder. These powders were then washed with 50 mL of NMP and 50 mL of acetone. Finally, the powders were dried in a vacuum oven at 50 °C overnight. Powder samples collected from the solution are denoted as I-1 and I-5. Detailed information on the spectroscopic characterization of the PI powders can be found in the SI.

5.2.4. Characterization

Fourier transform infrared spectroscopy (FTIR) measurements on both membrane and powder samples were done using a PerkinElmer UATR Spectrum Two. Wavenumbers between 4000 and 550 cm^{-1} were scanned in reflectance mode at a resolution of 4 cm^{-1} for a minimum of 16 scans. Powder X-ray diffraction (XRD) patterns were recorded using a PANanalytical X'Pert PRO diffractometer at the wavelength of Cu Kα (λ = 1.5405 Å) (X-ray power: 40 kV, 40 mA) in Bragg−Brentano scanning mode. The program scanned angles (2θ) from 5 to 55° with a 0.026° step and a step time of 158s. Scanning electron microscopy (SEM) images of powder and membrane samples and energy-dispersive X-ray spectroscopy (EDS) were obtained using a JEOL JSM-6010LA scanning electron microscope using an accelerating voltage of 5 kV. SEM samples were sputtered with 5 nm of palladium/platinum layer to avoid sample charging. High-resolution scanning electron microscopy (HR-SEM) micrographs of membrane samples were obtained with a Hitachi S-4800 field-emission scanning electron microscope (Japan) using an accelerating voltage of 2 kV. Samples were metalized with platinum to favour charge release. The change in the pore diameter of the membrane samples was determined by permporometry using cyclohexane as condensable vapor. The experimental procedure is described in detail elsewhere.[49] Water contact angles were measured using the sessile drop method with 2 μL drops of Milli-Q water. Atomic force microscopy (AFM) imaging was carried out in intermittent-contact mode in the air with AFM instrument Bruker Dimension ICON. The average roughness profile of the samples was determined by imaging 1 μm^2 of each sample.

5.2.5. Membrane Performance

Permeability and retention data were collected with a custom-made, dead-end filtration setup connected via a pressure regulator valve to a nitrogen tank for pressurizing the solutions. Permeability (L m^{-2} h^{-1} bar^{-1}) is expressed as the flux (L h^{-1}) of water or a solvent across a membrane per unit of driving force per square meter of exposed membrane area (2.4 cm^2). Flux data were collected by weighing the mass of the permeate at four-time intervals, while permeability was determined from flux data at three applied transmembrane pressures between 8 and 20 bar by taking the slope of a linear fit of the collected flux data. All slopes were found to be linear unless otherwise noted. Retentions I of Brilliant Yellow (BY, Mw = 624.55 g mol^{-1}, 50 ppm) and Rhodamine B (RB, Mw = 479.02 g mol^{-1}, 50 ppm) were calculated with the equation

$$R = 1 - c_p/c_f \qquad (1)$$

where c_p and c_f are the permeate and feed solute concentrations, respectively. Retention samples were obtained at recoveries between 35 and 50%. The dye adsorption during retention measurements was calculated with the equation

$$M_{Ads} = M_f - M_R - M_p \qquad (2)$$

where M_{Ads} is the amount of dye adsorbed on each membrane, M_f is the total amount of dye used at the beginning of each separation test (feed solution), M_R is the amount of dye in the retentate, and M_p is the amount of dye in the permeate. In all cases, the dye concentration of BY and RB was increased in the retentate to account for limited adsorption of 2 – 3% for the PI-nanoconfined ceramic membranes. Solute concentrations of BY and RB were calculated from PerkinElmer λ12 UV−Vis spectrophotometer results at the characteristic wavelengths of 401.5 (BY), 543 (RB/water), 554 (RB/water, and RB/1,4-dioxane), and 560 (RB/DMF) nm.

5.3. Results and Discussion

5.3.1. Synthesis and Characterization of the Pre-functionalized γ-Alumina Layer and Polyimide Membranes

Our strategy to pre-functionalize supports and subsequently form polyimide (PI)-based membranes is presented in Scheme 1. The PI-nanoconfined membranes were prepared by pre-functionalizing the mesoporous γ-alumina layer with 3-aminopropyl trimethoxysilane (APTES). A reliable vapor phase grafting procedure has been developed by our research group to covalently attach APTES molecules at the pore surface of the γ-alumina layer. Indeed, carefully selecting the grafting conditions and a suitable pore filling agent can lead to a homogeneous monolayer of APTES molecules without the problem of homocondensation reactions occurring between

164

the alkoxysilane linking group.[24] The primary amine group of APTES can react via a condensation reaction with the dianhydride precursor of the PI network during the subsequent polyimidization reaction between pyromellitic dianhydride (PMDA) and melamine (MA). This reaction should lead to the covalent attachment of the polyimide network exclusively on the top surface and pore entrance of the mesoporous γ-alumina layer (Scheme 1, route A). Here, we employed a pore blocking agent, allowing us to graft only the top surface and pore entrance of the γ-alumina layer. Hence, we assume that the rapid PI network formation from the functionalized pore entrance will limit the diffusion of monomers as well as any PI oligomer units formed in the bulk solution into the pristine pores. This way, a PI concentration gradient is induced along the mesoporous layer with the highest concentration close to the pore entrance. Samples were modified in solution with only PMDA before the in situ polycondensation (Scheme 1, route B) to allow the PI network formation to also occur inside the mesopores of the support. Here, PMDA can react not only with the amino group of the grafted APTES molecules but also with free hydroxyl groups at the inner pore surface of the γ-alumina layer.[29] Thus, the PI network formation takes place uniformly from the whole surface, including the pore entrance and pore surface, of the mesoporous γ-alumina layer.
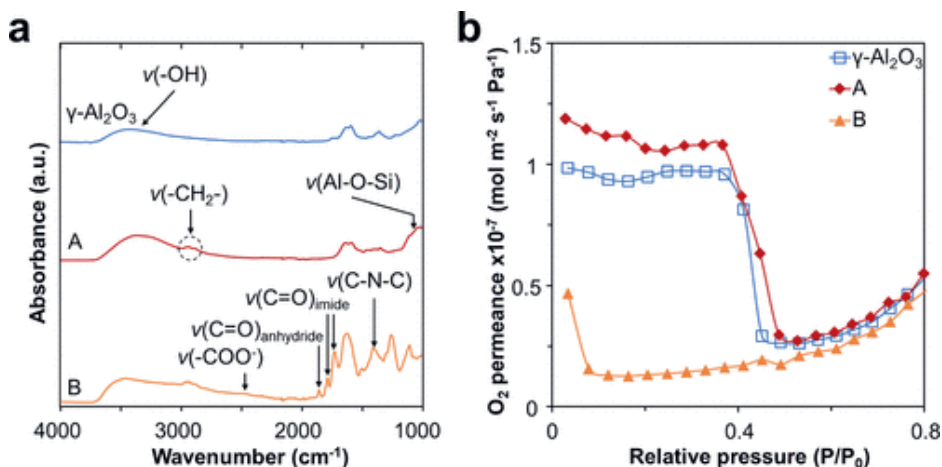
Figure 5.1: (a) FTIR spectra of the pre-functionalized samples (A, red and B, orange) and comparison with the pristine γ-alumina layer (γ-Al2O3) in the interval between 1000 and 4000 cm^{-1}. (b) Oxygen permeance as a function of the relative cyclohexane vapor pressure for the pristine γ-alumina layer, sample A, and sample B. The oxygen flux is measured only through active pores in the range of 2−50 nm. Using the Kelvin equation, the pore diameter distribution can be estimated for the pristine γ-alumina layer and sample A as shown in Figure S5.19. However, the pore diameter of sample B is below the molecular size of cyclohexane (condensable liquid). Thus, pore size distribution cannot be estimated in this way.

Fourier transform infrared (FTIR) analysis was employed to demonstrate the pre-functionalization of the mesoporous γ-alumina layer. The spectra of the pristine γ-alumina layer and the layers pre-functionalized respectively with APTES (sample A) and APTES + PMDA (sample B) are shown in Figure 5.1a. The FTIR spectrum of the pristine mesoporous layer shows a broad band centred at 3420 cm^{-1}, which can be attributed to the stretching vibration of adsorbed water and surface hydroxyl groups.[30,31] Functionalization of the γ-alumina layer with APTES results in the appearance of primarily a broad band between 1180 and 970 cm^{-1}, which is associated with the formation of the Al-O-Si bond and confirms the grafting of the APTES at the top surface and pore entrance. This finding is further confirmed by the presence of the asymmetric and symmetric stretching vibration bands at 2927 and 2886 cm^{-1}, which can be attributed to the alkyl groups (−CH2−) of the grafted APTES molecules. In addition, the sharp vibration band at 2974 cm^{-1} (Figure S5.4) attributed to the linking function (CH3CH2O-Si) is not present in the spectrum of sample A, suggesting complete hydrolysis of the functional group during the grafting reaction and thus confirming the formation of the desired Si-O-Al bond again.[24] In comparison with sample A, the interpretation of the FTIR spectrum of sample B is more difficult due to the number of bands. Only the most important ones are discussed here. The formation of the imide functional group and attachment of PMDA is confirmed first by the vibration bands at 1787 and 1727 cm^{-1}, which is ascribed to the C=O bond, and the band at 1365 cm^{-1}, which is related to the C-N-C bond. In addition, the anhydride group is also apparent at 1856 cm^{-1}, which suggests either the partial reaction of PMDA with the amino-functionalized support (A) and/or the presence of unreacted and physically adsorbed PMDA on the ceramic support. The band at 2460 cm^{-1} attributed to the carboxylate groups (COO−)[32] in the sample is due to the formation of an amic acid group or PMDA grafting at the pore surface.[29,32]

Cyclohexane permporometry was used to study the effect of pre-functionalization on the pore size distribution of the support. This dynamic characterization technique allows measuring the pore diameter of active pores present in the pre-functionalized γ-alumina layer. The stepwise analysis will enable one to follow the change in pore diameter starting from the pristine γ-alumina layer and moving toward the functionalized samples (A and B in Figure 5.1b). The pristine γ-alumina layer exhibits a mean pore diameter of ~ 5.5 nm, and the support pre-functionalized with APTES (sample A) shows no pore size diminution. This last result differs from published reports where a pore shrinkage of 0.5 nm was observed, and no glycerol or other pore-blocking agents were used.[33] This means that glycerol, used as the pore-blocking agent, has allowed us to control the grafting reaction and to functionalize only the top surface of the γ-alumina layer. However, subsequent functionalization with PMDA (sample B) resulted in a significant reduction of the pore diameter.

Compared to pristine γ-alumina and sample A, the oxygen permeation curve of sample B presented in Figure 5.1b suggests that the pore opening occurs at low cyclohexane relative pressures during the desorption step (~0.1 instead of 0.4 P/P_0). Considering the data acquired via cyclohexane permporometry, we cannot determine the exact pore diameter since the Kelvin equation is not valid since no clear transition point is obtained for this sample. Nevertheless, knowing the limit of the measurement, which corresponds to the molecular diameter of cyclohexane (~0.5 nm), one can assume that the pore diameter of sample B must be lower than 1 nm. Overall, the cyclohexane permporometry results indicate the presence of PMDA in the pores of the γ-alumina layer, which can be physically or chemically adsorbed at the pore entrance and inner pore surface.
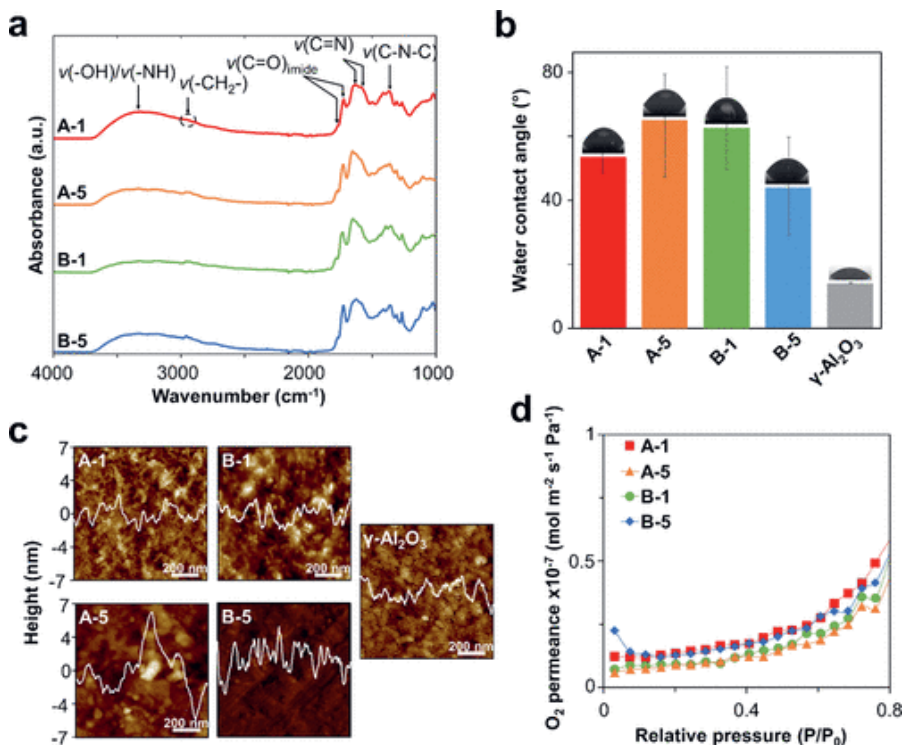
Figure 5.2: (a) FTIR analysis of the PI-nanoconfined samples. The complete spectra between 4000 and 400 cm⁻¹ are provided in the SI. (b) Water contact angles of the PI-nanoconfined samples. (c) AFM micrographs of the top surface of the PI-nanoconfined samples and the pristine γ-alumina layer. The line represents the averaged roughness profile of each sample. (d) Oxygen permeation as a function of cyclohexane partial pressure of the PI-nanoconfined membranes.

As explained before, the attachment, growth, and molecular confinement of the PI network in the γ-alumina layer was performed via two different approaches; first, by the direct formation of the PI network from the pre-functionalized surface of sample A, where the functional groups were at the top surface and pore entrance of the γ-alumina layer, and second, from sample B, where the functional groups were located at the top and pore surface of the γ-alumina layer. FTIR analysis was performed on the nanoconfined PI membranes to assess the spectroscopic characteristics of the network formed after in situ polymerization. Figure 5.2a displays the spectra of the four PI nanoconfined membrane samples (A-1/5 and B-1/5). All samples exhibit similar spectroscopic characteristics with minor differences in the intensity of certain bands for the two different reaction times (1 and 5 days) and both reaction routes. The two bands at ∼1780 and ∼1720 cm^{-1} are ascribed to the C=O bond of the imide and are more intense, with longer reaction times for both routes. The bands at 1565 and 1453 cm^{-1} are attributed to the stretching vibration of the triazine ring and appear in all membranes.[34] The band at 1660 cm^{-1} could indicate the presence of amic acid on the γ-alumina layer. However, no other absorption bands confirm the presence of amide. Therefore, to get a better insight into this observation, the powders (I-1 and I-5) collected from the reaction mixture were used to indirectly gain information on the nature of the material, confined in the mesopores (Figures S5.13 and S5.14). The FTIR spectra of the powders, formed in the bulk solution during in situ polymerization of membrane samples, clearly show the formation of an amino-terminated imide network. Hence, in situ polymerization seems to promote imide formation for 1 and 5 days of reaction time without any indication of amic acid presence. Finally, the band between 1390 and 1360 cm^{-1} is ascribed to the absorption of the C−N−C group.[35–37] Thus, this leads to the conclusion that the FTIR analysis strongly suggests the presence of a polyimide network in the γ-alumina layer.

The high crystallinity of aromatic polyimides has been demonstrated in the literature by powder X-ray diffraction (XRD) analysis.[7] In our work, no diffraction peaks corresponding to crystalline aromatic polyimides could be detected in the membrane samples (Figure S5.15). The XRD pattern obtained revealed the presence of the highly intense diffraction peaks of the α-alumina macroporous support, which can be explained by the X-rays' penetration depth (being more than 3 μm in the XRD configuration used). The absence of diffraction peaks correlated with the γ-alumina phase where the polyimide network is confined can be explained by the nanosized nature of this layer. Kim and Nam[38] described a decrease in the diffraction peaks of the α-alumina phase when different polyimide/α-alumina film composites were prepared using an amorphous polymer. Interestingly, the diffraction peaks of the α-alumina phase were identical to our pristine support, thus suggesting either small amounts or even the absence of the PI network in the α-alumina pores. To shed more light into the confined network's nature, XRD analysis was conducted on the powder

extracted from the bulk solution at the end of the synthesis of the membranes. The powder XRD patterns between 5 and 50° 2θ are provided in Figure S5.16 for the powder samples obtained after 1 or 5 days of reaction time (denoted as I-1 and I-5). The analysis revealed the formation of polycrystalline materials with an amorphous background observed in small proportion. The comparison of the diffractograms between samples I-1 and I-5 shows a clear relationship between increasing reaction time and improved crystallinity, evidenced by the narrowing of the diffraction peaks and a decrease in the baseline broadening. These results are corroborated by the scanning electron microscopy (SEM) analysis of the powders (Figure S5.20), which also shows changes in morphology as a function of reaction time. The sample I-1 appeared to consist of a mixture of platelet crystallites of several micrometre wide, cauliflower-like aggregates and clustered (random) spherical porous phases (ranging from nanometres to micrometres in diameter). Increasing reaction time led to the growth of a fascinating morphology consisting of defined flower-shaped crystallites, as observed with sample I-5, decorated with smaller crystallites. Similar results were obtained by Baumgartner et al.,[7,39,] who observed an "amorphous" baseline while analysing the produced polyimide crystalline samples under hydrothermal conditions using p-phenylenediamine and PMDA as monomers. Comparison with published records of polyimide powders prepared using the same precursors (PMDA and MA) but under different experimental conditions (temperature and solvent) shows different crystal structures. Li et al.[35] described the preparation of a PI powder between PMDA and MA below 200 °C leading to a relatively amorphous material (two broad peaks between 10 and 50°), whereas at 200 °C or above,[40] a semicrystalline structure was observed. Thus, the powder XRD results provided here confirm that the organization of the material depends both on the temperature of the polycondensation reaction and the reaction times. However, when the PI powder was treated at 300 °C for several hours, a new diffraction peak at 44° was observed, which is possibly related to the degradation by-products. Thermal treatment of the PI powders at 400 °C resulted in an almost complete loss of crystallinity and an increase in the diffraction peak intensity at 44° (Figure S5.17). The observed thermal degradation evidenced by powder XRD is also corroborated by the thermogravimetric analysis (TGA) provided in Figure S5.18. A slight weight loss for both I-1 and I-5, 2.2 and 1.4%, respectively, occurred upon heating from room temperature to 300 °C. However, above 300 °C, a significant weight loss occurs, particularly for sample I-1. Thus, we can assume that the PI network remains stable at temperatures below 300 °C, which is ideal for membrane applications.

It must be noted that the confinement of a polyimide network in the γ-alumina layer should lead to an enhancement of the physicochemical stability of the polyimide network, as shown by Isaacson et al.[17] Based on the powders' crystallinity and morphology, one can assume that the PI membrane samples exhibit similar structural

characteristics as the polyimide powders. If our assumptions are confirmed, it would mean that by simply varying the reaction time, we can engineer the membrane's micropores and thus enhance the membrane separation performance. Therefore, it is crucial to look closer at the PI network inside the support and describe the nanoconfinement effect well.

5.3.2. PI Network Nanoconfinement Characteristics

A series of analytical techniques were employed to investigate the influence of the supports' pre-functionalization on the extent of the PI nanoconfinement. First, water contact angle analysis was done on the PI-nanoconfined samples and the pristine support to evaluate (indirectly) the polymerization effect on the support surface properties. The results are given in Figure 5.2b. Compared to the pristine layer, which presents a water contact angle of 14° (disappearing in 6 – 7s), characterizing a porous hydrophilic surface, the PI-nanoconfined samples show an increased water contact angle (40 – 65°). This observation suggests that the membrane surface is still hydrophilic (water contact angles < 90°) but certainly less hydrophilic than the pristine support. Interestingly, different water contact angles were obtained for the samples prepared via routes A and B, respectively, 63° (±16°) and 54° (±5°) for the same reaction time (1 day). Nevertheless, with the increase in the reaction time, a rise of 11° was measured for the samples prepared via route B, while a decrease of 19° was measured for the samples made via route A. As for porous hydrophilic surfaces, accurately estimating a descending water contact angle is challenging. Still, the difference between the two routes can be inherent to the pre-functionalization step.

Further investigation and comparison of the PI-nanoconfined membrane surface morphology with that of the γ-alumina layer were conducted by atomic force microscopy (AFM) analysis, and the results are shown in Figure 5.2c. From the average roughness profiles, it is apparent that the surface morphology of the PI-nanoconfined membranes changes with increasing reaction time. Compared with the pristine γ-alumina layer, polymerization for 1 day for both routes does not seem to affect the surface roughness (~3 nm). Samples reacted for 5 days show only a slight increase in surface roughness, with the A-5 samples exhibiting more considerable differences in height on the surface (~4 nm) compared to B-5 samples (~3 nm) as shown in Figure 5.2c. The empirical information gained from water contact angle and AFM analyses postulates a fundamental difference between the two routes, which becomes more prevalent after longer reaction times. The influence of reaction conditions on the pore diameter of the PI-nanoconfined membranes was investigated by means of cyclohexane permporometry. The results are provided in Figure 5.2d. During the analysis, no oxygen permeation was measured at low cyclohexane partial pressures (< 1.5 nm) or even in a dense sample. This suggests a pore diameter

170

shrinkage of more than 4 nm. Indeed, the permporometry analysis demonstrates that the presence of the PI network affects the pore size of the mesoporous γ-alumina layer.

All the results described above showed that the polymer network changes the morphology of the surface only in a subtle manner. However, the pore sizes are significantly affected, indicating either an ultrathin top layer or a confined polymer in the mesoporous layer. To better understand this finding and to observe the PI network on the γ-alumina layer directly, we proceeded with HR-SEM analyses of the studied membrane samples.

The top surface and cross-sectional high-resolution SEM pictures of the PI-nanoconfined membranes are given in Figure 5.3a, together with photographs of the membrane samples. Compared to the pristine γ-alumina layer, which is naturally white (Figure S5.21), the PI-nanoconfined membrane samples appear to be substantially covered by the polymeric network as denoted by brownish coloration, which is typical for a polyimide material. The comparison of the top-surface micrographs of membrane samples prepared by the two fabrication routes (A and B) does not show any significant differences at first glance. One day of reaction leads to the formation of small particles with a sheet-like structure visible on both A-1 and B-1 samples. Increasing the reaction time to 5 days leads to the disappearance of the sheet structure, suggesting the formation of a thin homogeneous layer. From the SEM analysis of PI powders (Figure S5.20), we observed that the 5 day long reaction yields a clear platelet-like structure, whereas the 1 day reaction results in a mixture of aggregates and crystallites. One can observe similar sheet-like structures from the HR-SEM analysis of the top surface of both A-1 and B-1 samples. This indicates that the PI networks that are growing on the surface of the γ-alumina layer and those growing in the bulk solution exhibit similar characteristics. Hence, we expect that the PI network growth, induced from the ceramic surface, will have similar morphology with smaller particles mainly when infiltrated in the pores. Finally, it is expected that such platelet-like particles should ensure good coverage of the support surface, as seen on the micrographs of both A-5 and B5 samples.
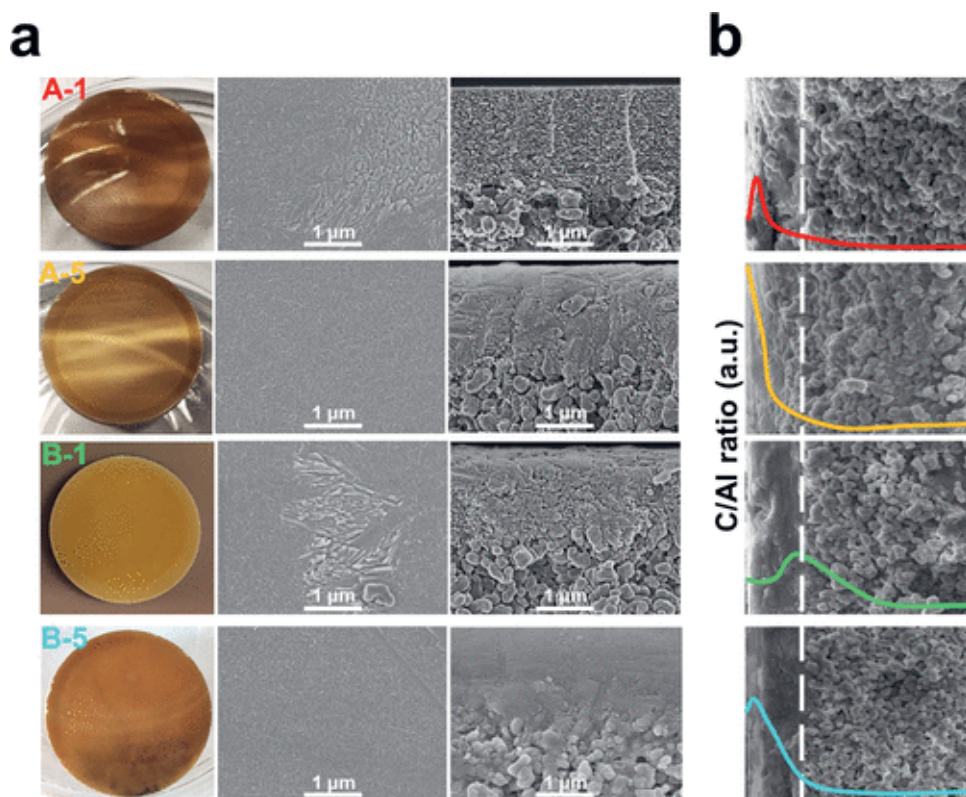
Figure 5.3: (a) Images of the PI-nanoconfined membranes (left) accompanied by HR-SEM micrographs of the top surfaces (middle) and the cross sections (right). (b) Evolution of the carbon/aluminium ratio (wt.% by EDS) along the membrane cross-section. The dashed white line denotes the limit between the γ-alumina layer (left) and the α-alumina support (right).

In comparison, the HR-SEM cross-sectional analysis of the membranes shows a clear difference between the two synthesis routes after 1 day of reaction. For the A-1 sample, the PI network seems to be located at the γ-alumina layer top surface. In contrast, for the B-1 sample, infiltration of the PI network in the γ-alumina layer could be observed. The samples A-5 and B5, after 5 days of reaction time, also present extended infiltration of the PI network in the γ-alumina layer. This finding thus strongly indicates that longer reaction times of polymerization on pre-functionalized γ-alumina layers promoted the nanoconfinement of the PI network in the 5 nm pores of the γ-alumina layer. Evidently, the difference between membranes A-1 and B-1 suggests that the choice of pre-functionalization can affect the extent of the PI nanoconfinement in the γ-alumina layer.

In complement, energy-dispersive X-ray spectroscopy (EDS) analysis can offer qualitative elemental information over a membrane's cross-section (Figure 5.3b). By measuring the ratio of carbon over aluminium along the cross-section of the different membrane samples, one can define the influence of the preparation route and, indirectly, the pre-functionalization steps on the nanoconfinement of the PI network. Overall, the EDS analysis reveals that organic (polymeric) material resides in the γ-alumina layer. In route A, the network accumulates near the pore entrance, whereas in route B (samples B-1 and B-5), a spread distribution of the PI network inside the γ-alumina layer is observed. These results clearly indicate a link between the pre-functionalization step and the nanoconfinement of PI networks inside the γ-alumina layer. On the other hand, the reaction time merely affects the concentration of the polymeric network.

In conclusion, by combining the knowledge gained from HR-SEM and EDS, we can ensure that the functionalization of the support promotes the growth of the PI network during polymerization. Based on these results, a membrane formation mechanism was drawn (Scheme 1). The membranes prepared via route A, thanks to the presence of the amino group (APTES) at the top surface of the support, exhibit a higher concentration of PI near the pore entrance. Alternatively, with route B, a homogeneous polymer distribution is observed throughout the γ-alumina layer, which is attributed to the functionalization of the inner pore surface with anhydride functional groups (PMDA). These differences in membrane architecture can significantly affect their membrane performance due to an increase in the thickness of the separating layer, as schematically shown in Scheme 1. Additionally, longer reaction times lead to higher concentrations of polymer inside the γ-alumina layer, which could potentially promote the formation of smaller pore diameters and, thus, better separation performance. A series of membrane separation tests have been performed with model aqueous solutions described hereafter to confirm our interpretation from the HR-SEM and EDS analysis.

5.3.3. PI-Nanoconfined Membrane Performance

The PI nanoconfined membranes were tested first in aqueous solutions of Brilliant Yellow (BY, 625 g mol^{-1}) or Rhodamine B (RB, 479 g mol^{-1}) and compared with the pristine γ-alumina layer. The retention and water permeability results are summarized in Figure 5.4. All four PI-nanoconfined membranes show retentions above 90% of BY (627 g mol^{-1}) in water, which significantly increases compared to the pristine γ-alumina layer (76%). However, with Rhodamine B (RB, 479 g mol^{-1}), the retentions for the A-1 and B-1 samples were between 70 and 80%. With increasing the polyimidization reaction time, the membranes (A-5 and B-5) show RB retentions well over 90%. This can be attributed to the increasing PI concentration in the pores of the γ-alumina layer. Compared with the pristine γ-alumina layer (14%

retention for RB), the separation performance of the PI-nanoconfined membranes thus displays a significant improvement. These results also suggest that, despite this increase in the concentration of the polymeric network in the tortuous mesopores, there are still many open pores that are either smaller than the Rhodamine B molecule (sieving effect) or are small and charged (Donnan effect) and thus have a direct influence on the separation performance of the membranes.
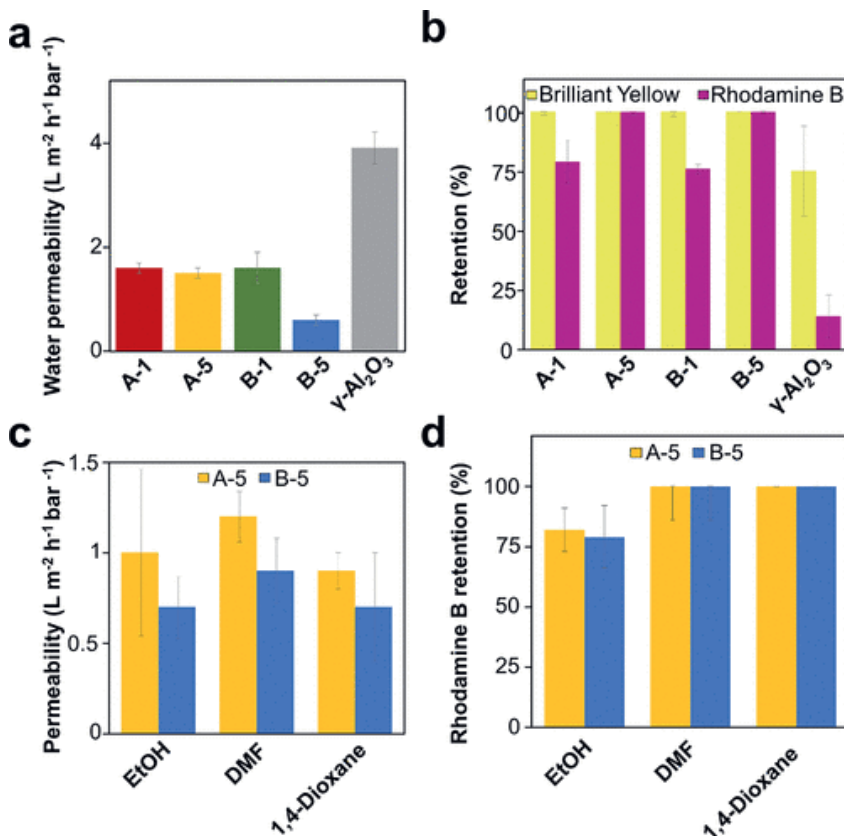
Figure 5.4: (a) Water permeability of the PI-nanoconfined membranes and the pristine layer (γ-Al$_2$O$_3$). (b) Retention of Brilliant Yellow (BY) and Rhodamine B in water for PI-nanoconfined membranes and the pristine layer (γ-Al$_2$O$_3$). Each test was repeated three times (the presented permeation and retention are averages, and the errors refer to the standard deviation from the average value of three samples). (c) Performance of A-5 and B-5 samples in different solvents. (d) RB retention in different solvents for A-5 and B-5 samples.

The water permeability results, on the other hand, suggest a clear difference between routes A and B, particularly for samples treated for 5 days. It is evidenced from the increase in RB retention for sample A-5 compared to A-1 that for route A, the

polymer amount in the γ-alumina pores is increasing; hence, the pores are shrunk significantly. However, since the water permeability for A-5 remains comparable to that of A-1, this can indicate that the polymer concentration is only increasing at the pore entrance, leading to thin selective barriers. For sample B-5, the RB retention is also increasing compared to B-1; here, decreasing permeability suggests a thicker selective barrier. These preliminary results indicate that the polymer concentration is increasing with increasing reaction time (A-5 and B-5), but the location where the polymer concentration is increased depends on the pre-functionalization of the support. This means that for route A, the polymer grows only at the top surface and pore entrance, positively influencing the membrane's retention but evidently leaving the water permeability unaffected. On the other hand, for route B, the polymer grows in the whole or part of the γ-alumina layer, as also indicated by EDS analysis. Hence, from this series of water permeation tests accompanied by permporometry, HR-SEM, and EDS analyses, we have evidence that in the synthesis of PI-nanoconfined membranes, the pre-functionalization step controls the extent of polymerization inside the mesoporous support.

Sample A-5 was also tested for 5 days in RB/water solution to assess the stability of the PI-nanoconfined ceramic membranes. The results are provided in Figure S5.27. As shown, the RB retention remains stable at approximately 98 – 99%. Furthermore, the water flux increases slightly after the first day (from 8 to 10 L m^{-2} h^{-1}) but remains relatively stable in the following 4 days. Therefore, this preliminary result shows that the method used to prepare the PI-nanoconfined membranes results in relatively stable membranes.

The two membranes showing the best rejection, the B-5 and A-5 samples, were subsequently tested in different solvents containing RB. The results for the solvent permeability and RB retention in solvents are accordingly given in Figure 5.4c, d. Three different organic solvents were selected based on their polarity: ethanol, DMF, and 1,4-dioxane, with polarity values of 0.654, 0.386, and 0.164, respectively. Indeed, by testing the membranes in different liquid media, we gain more insight into the membrane layer's properties. As shown in Figure 5.4c, the membranes perform well in all solvents. Only in ethanol is the retention performance of the PI-nanoconfined membranes lower than 90% (79% for B-5 and 83% for A-5). The results can be attributed to the nature and solubility of RB in different solvents. According to Hinckley et al.,[41] RB in a solution can be present in two forms, the lactone (L) and the zwitterionic (Z) form, which are in equilibrium, and the most dominant form depends on the solvent. Hinckley et al.[41] showed that the ratio zwitterionic:lactone (charged:neutral) in water (Z:L = 4.4) and formamide (Z:L = 7.67) is higher than in ethanol (Z:L = 2.4). Since ethanol favours the neutral form of RB compared to water and DMF, we expect that the zwitterion rejection might be

175

related to ionic repulsions between the membrane and the solute, thus leading to slightly lower rejections in ethanol.

In 1,4-dioxane, a different mechanism is probably at play. The solubility of RB in 1,4-dioxane is significantly lower than in ethanol, DMF, or water. In this regard, the solvent is expected to have a much higher preference for the polymer (PI) than for the solute, leading to high retentions observed experimentally for the studied systems. These tests suggest that the PI network confined in the γ-alumina layer could be slightly charged since RB retentions are the best in water and DMF, where the zwitterionic form is dominant. The charge could originate either from the presence of primary terminal amines, which is also suggested from the FTIR analysis, or the monomer ratio used during membrane preparation. As such, we propose that one can tune the final membrane properties by adjusting the in situ polymerization conditions, such as the monomer ratio.

To conclude, a comparison between different membranes from the literature with the A-5 membrane samples is shown in Figure 5.5. Evidently, A-5 is a potentially interesting membrane with permeabilities in different solvents between 1 and 1.6 L $m^{-2} h^{-1} bar^{-1}$ and retentions in the NF range (479 g mol^{-1}). However, since the water permeability of the pristine γ-alumina supported on α-alumina ($4 - 5$ L m^{-2} h^{-1} bar^{-1}) is relatively low, we expect that utilizing supports with a thinner intermediate layer, for example, of nanometre thickness, as well as an α-alumina support with a larger pore diameter and higher porosity can potentially improve the membrane performance even further.
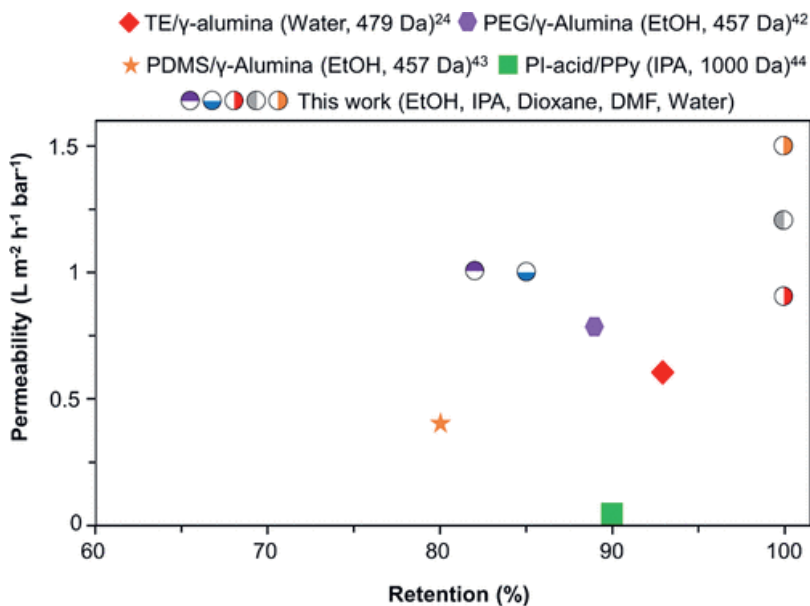
Figure 5.5: Comparison of the best-performing membrane from this work (A-5) with other membranes reported in the literature (solvents and M_w of dyes studied are given in brackets).[24,42–44] Membrane A-5 was tested in different solvents including water, IPA, EtOH, DMF, and dioxane with RB (479 Da) as solute to ensure a good comparison with the literature. The membranes used in this figure are similar in terms of the support or the membrane layer used.

5.4. Conclusion

In this work, PI networks were confined in mesoporous inorganic layers by top or inner pore surface-induced polyimidization. By pre-functionalizing the top surface of the support, the polymeric network was confined at the top and entrance of the pores. Inner pore surface functionalization led to a homogeneous polymer distribution throughout the functionalized ceramic layer. The two monomers employed, MA and PMDA, allowed the formation of a cross-linked and, thus, chemically resistant PI network inside the top layer of the ceramic support. By tuning the reaction time, we showed that the nanoconfinement of the polymer could also be effectively tuned. All these membranes were scrutinized through a series of characterization techniques, including SEM, FTIR, and pore diameter measurements, to demonstrate the influence of the applied methodology on their structure and final physicochemical properties. The as-prepared PI-nanoconfined membranes showed attractive separation performance with good retention of Rhodamine B (479 g mol^{-1}) in water and different organic solvents. At this moment, we do not foresee how to measure the resulting molecular weight of these nanoconfined PI networks, that we expect to be very small. This will be the object.

The principal asset of the work presented here relies on a demonstration of a method allowing control of the polymerization of a cross-linked polymer inside the confined space of the 5.5 nm pores of the γ-alumina layer for the preparation of hybrid NF membranes. This work is a forerunner for confining polymers in nanoporous substrates and regulating the location of the polymer growth. We assume that this method can be used to grow polymers with even higher chemical resistance, such as polybenzimidazoles, by using a similar preparation method as for polyimides. Furthermore, this method can be used as a tool in other fields to confine crosslinked polymers with low processability inside rigid supports to form, for example, low-density, high-strength, and thermally conductive nanocomposites for microelectronic insulation[45–47] or anticorrosion coatings.[48]

5.5. Supporting Information

1. Materials and methods used in this study
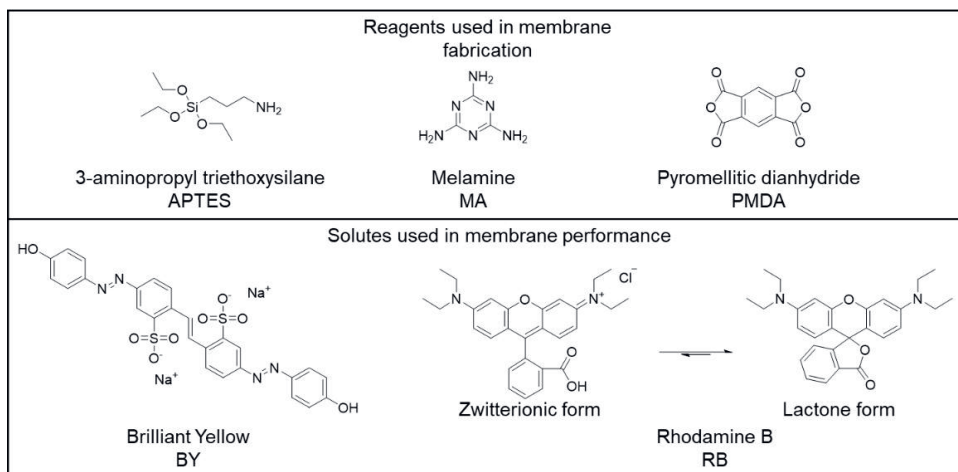
Figure S5.1: Chemicals used throughout this study. The chemical structures are given as well as their abbreviations as used in the article.
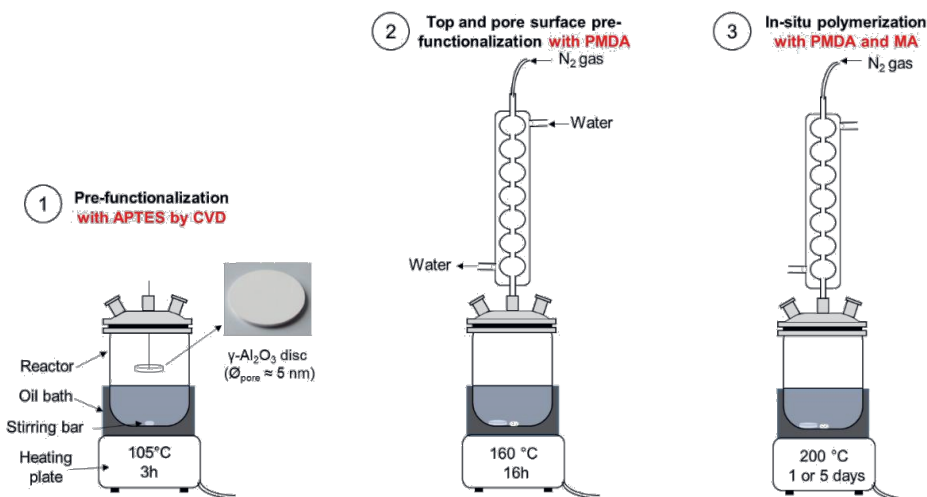
Figure S5.2: Schematic illustration of the equipment and procedure followed in the stepwise preparation of PI nanoconfined ceramic membranes.

2. FTIR spectra of the materials used in the preparation of the PI membranes given in the range of 4000 – 400 cm^{-1}
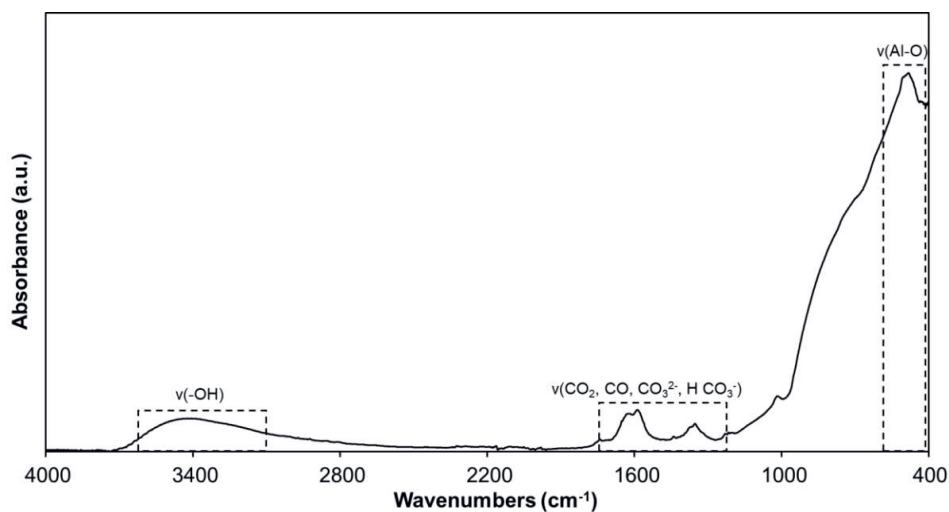
Figure S5.3: FTIR spectrum of pristine γ-alumina coated on α-alumina support.[50,51]
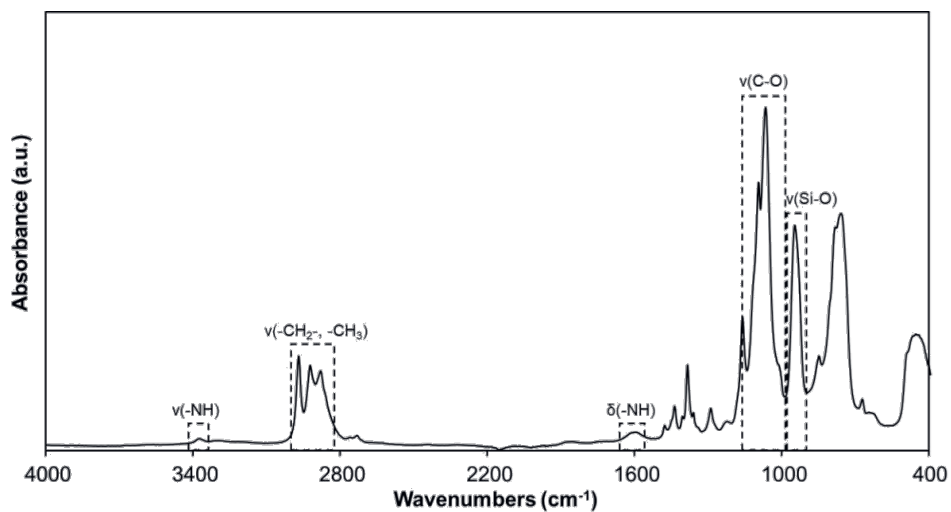
Figure S5.4: FTIR spectrum of pure APTES.[52,53]
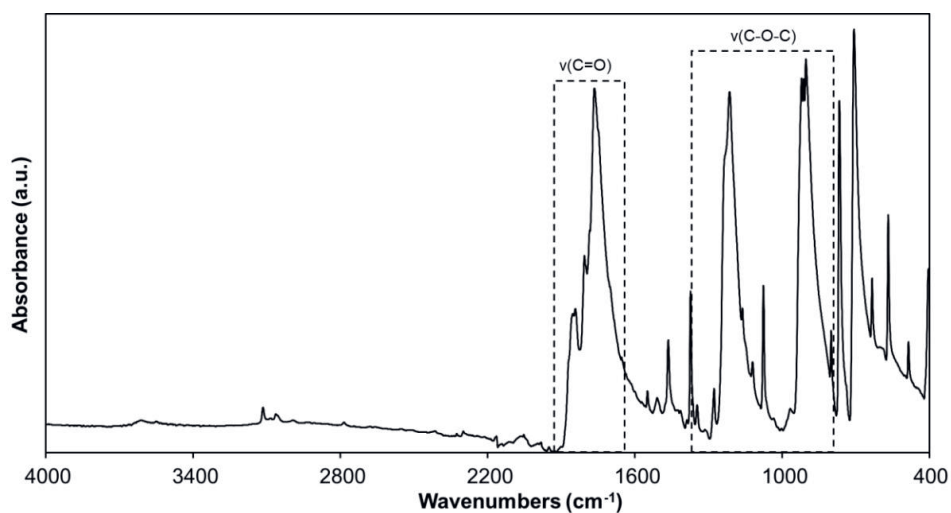
Figure S5.5: FTIR spectrum of PMDA.[54]
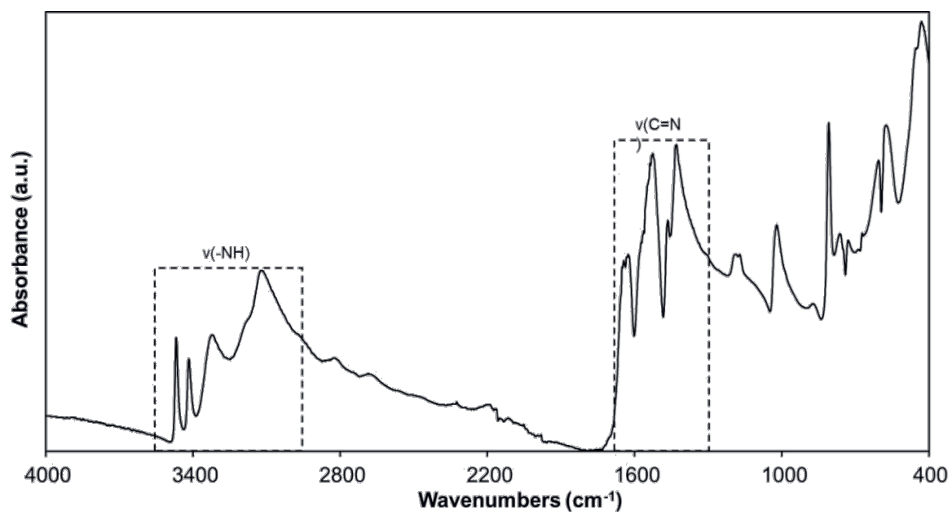
Figure S5.6: FTIR spectrum of MA.

3. FTIR spectra of the samples prepared given in the range of 4000 – 400 cm^{-2}
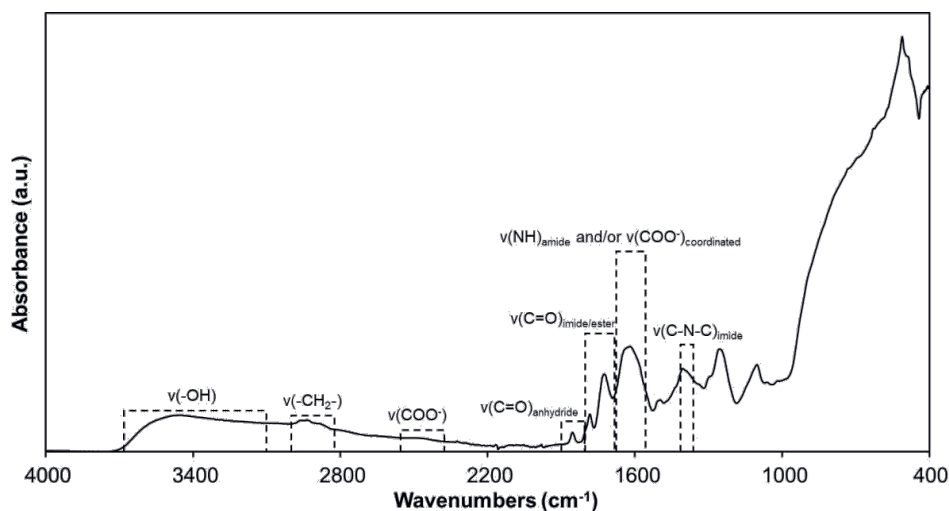
Figure S5.7: FTIR spectrum of sample A.
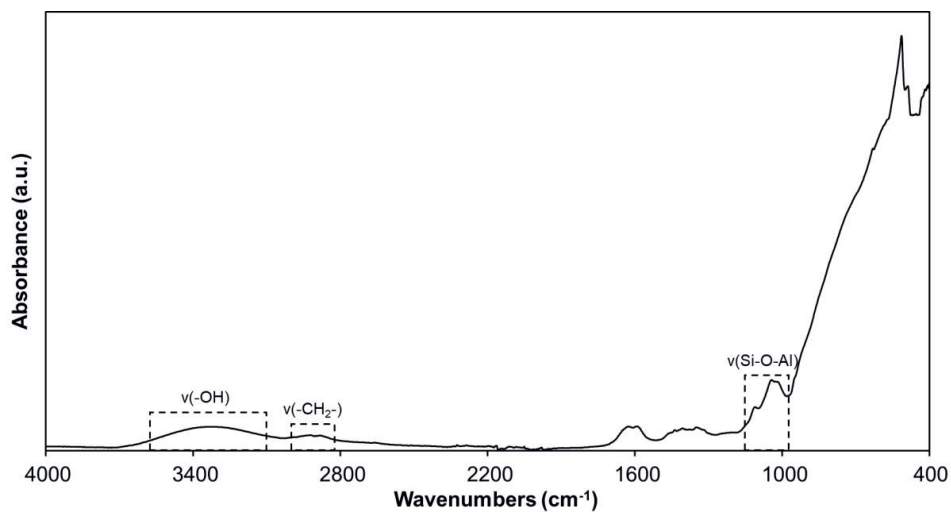
Figure S5.8: FTIR spectrum of sample B.
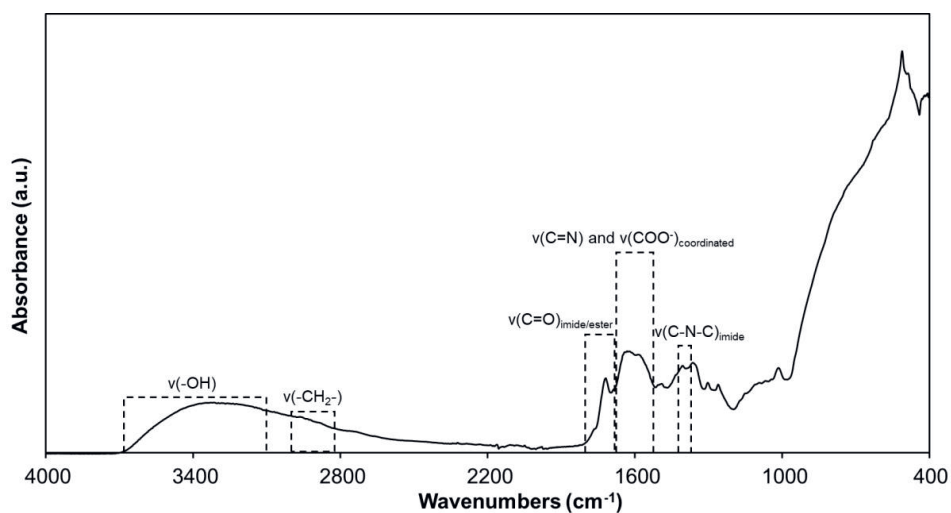
Figure S5.9: FTIR spectrum of sample A-1.
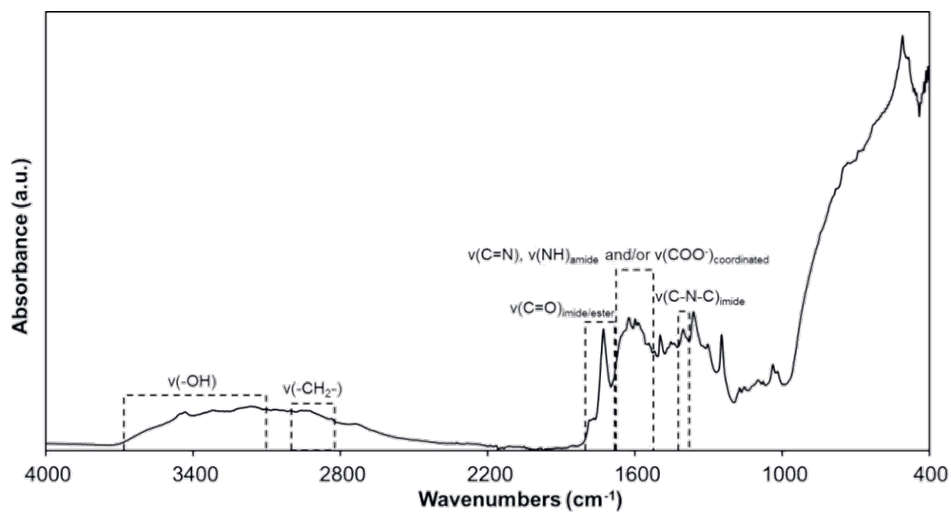
Figure S5.10: FTIR spectrum of sample B-1.
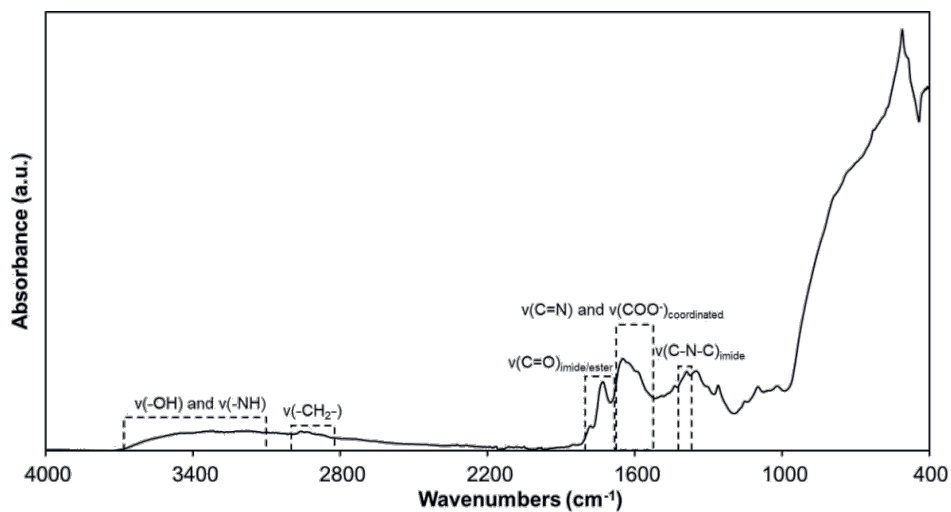
Figure S5.11: FTIR spectrum of sample A-5.
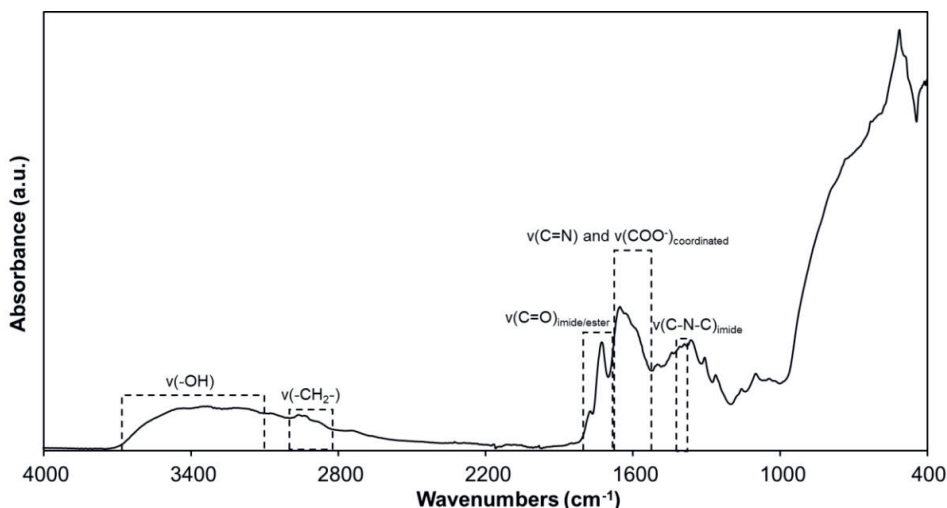
Figure S5.12: FTIR spectrum of sample B-5.

4. FTIR analysis of powder samples

The powders were isolated as precipitates from the membrane reaction mixture. The powders shown (I-1 and I-5) were collected after the preparation of samples A-1 and A-5. However, the powders collected from B-1/5 showed similar spectroscopic characteristics and were not included in this analysis. The FTIR spectra of both I-1 and I-5 are shown in Figures S5.13 and S5.14, respectively. The two sharp absorption bands at 1787 and 1727 cm^{-1} are characteristic of the carbonyl bond of the imide group.[55–57] Furthermore, the band at 1357 cm^{-1}, attributed to the C-N-C bond of the imide group, confirms the formation of the desired imide-linked network.[35,58,37] Additionally, the bands at 1654 and 1564 cm^{-1} indicate the presence of a triazine ring, a direct validation of MA in the samples. Between 3500 and 3000 cm^{-1}, several broad absorption bands appear, which can be attributed to amine terminating groups of the network. Unreacted amines are expected since amino functional groups were used in excess of the anhydride ones (dianhydride/triamine = 1.1) during membrane preparation. A weak absorption band at 1857 cm^{-1} indicates the presence of unreacted anhydride in the sample, which has either reacted partly or is physically adsorbed in the powder and, due to the low solubility of PMDA, is not washed off. Thus, FTIR analysis of the powders indicates the successful formation of an imide-linked network between MA and PMDA under the reaction conditions used in this work. In comparison with the four membranes, similar absorption bands are observed with the powders, but due to the considerable higher concentration of PI used and the absence of alumina during measurement, these powder FTIR-samples show a significantly higher resolution. Thus, similar chemical makeup between the powders and the PI network nanoconfined in the ceramic supports is expected.

184
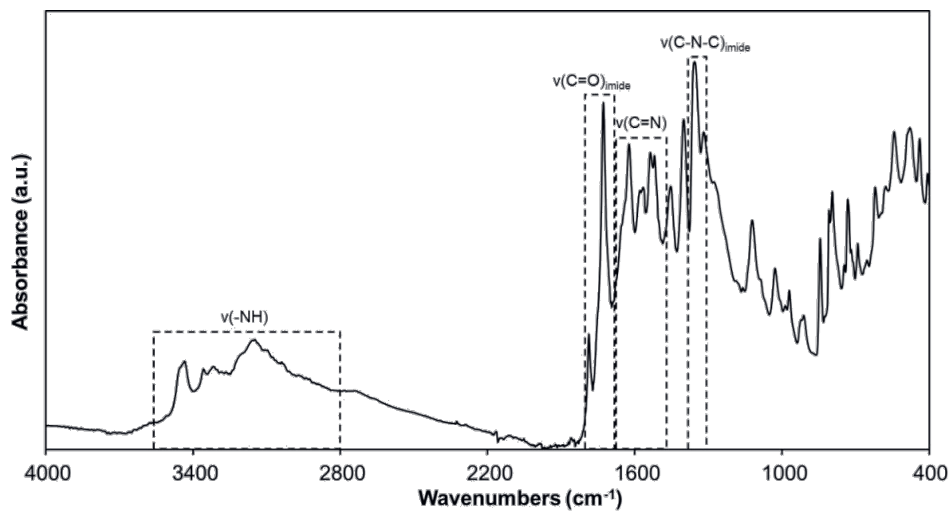
Figure S5.13: FTIR spectrum of sample I-1.
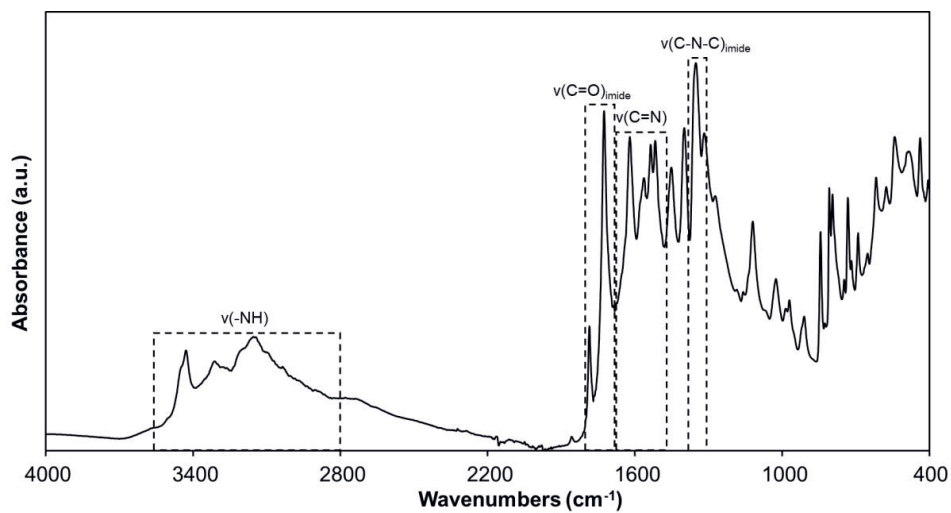
Figure S5.14: FTIR spectrum of sample I-5.

5. X-ray diffraction analysis

An attempt was made to analyse the crystallinity of the PI network confined in the ceramic support by means of XRD. However, due to the low concentration, as compared to the support, and potentially due to the confinement of the polymer in the ceramic, no reasonable data were collected from the analysis. In Figure S5.15, the XRD analysis of a PI nanoconfined sample is provided and correlated with the simulated XRD diffraction pattern of α-alumina. Evidently, the simulated and experimental results show that the PI network is not visible by means of XRD analysis.
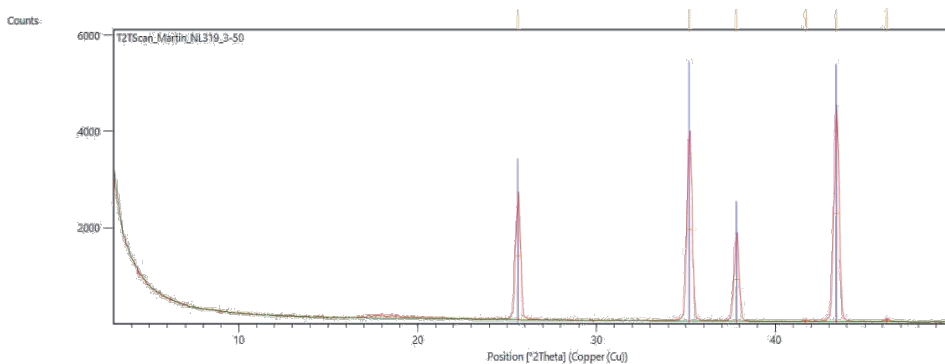
Figure S5.15: XRD analysis of PI nanoconfined sample (red) and correlation with molecular simulations (blue) of the α-alumina support.

6. Powder X-ray diffraction (XRD) analysis

The XRD patterns of the two PI samples are characteristic of a semicrystalline material. It can be denoted that when a reaction time of 5 days is used, the crystallinity of the material increases as evidenced from the decreasing amorphous background observed with sample I-5.
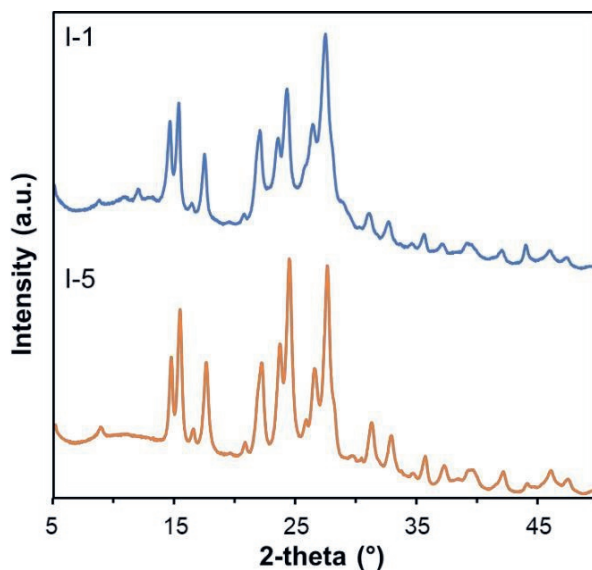
Figure S5.16: Powder XRD of the PI powders formed in the bulk solution during membrane fabrication for one day (I-1) and 5 days reaction (I-5).

Treatment of the PI powders at a temperature of 300 °C results in the appearance of the distinct diffraction peak at 44° 2θ as shown in Figure S5.17. This intensity of this peak is further enhanced by thermally treating the powders at 400 °C where all the other diffraction peaks of the PI matrix disappear. This can be attributed to degradation of the PI material.
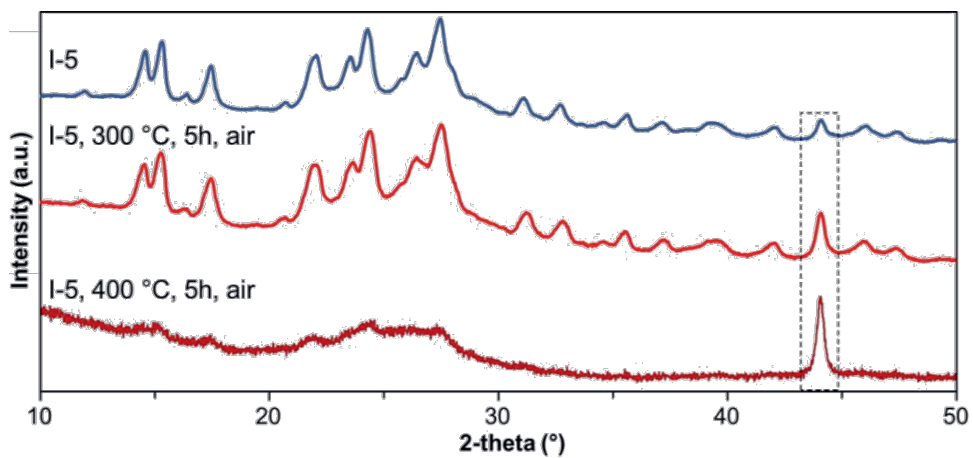
Figure S5.17: Powder XRD patterns of the I-5 powder after the synthesis (top), after treatment at 300 °C for 5h in air (middle) and after treatment at 400 °C for 5h in air (bottom).

7. Thermogravimetric analysis (TGA) of the PI powders

The thermal stability of the powder samples was analysed under a nitrogen atmosphere up to 1000 °C (5 °C/min). No weight loss is observed below 300 °C for both PI powders. The I-5 sample shows better thermal stability up to approximately 400 °C. These results are corroborated by the powder XRD analysis in section 6 of the Supporting Information, where the loss of crystallinity is observed at 400 °C.
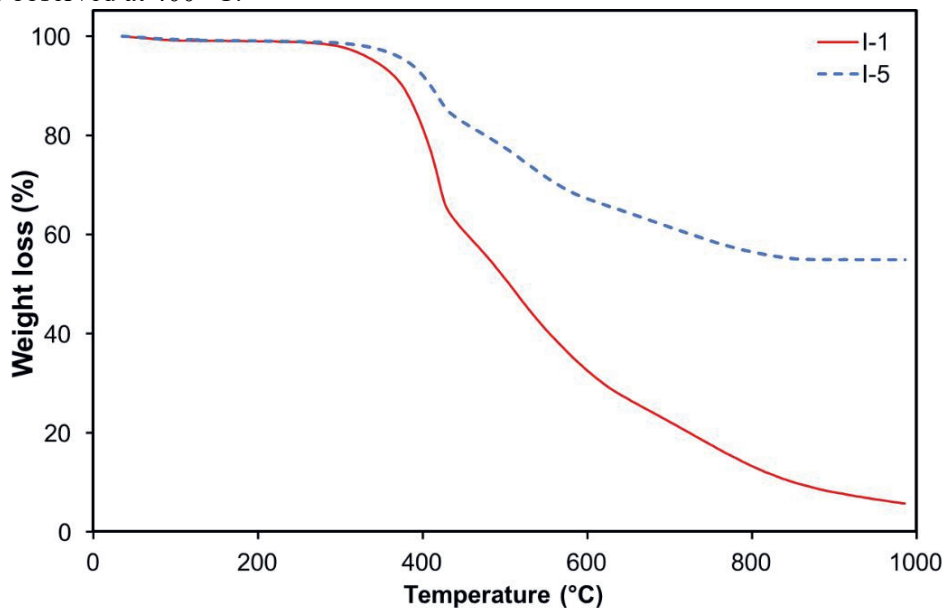
Figure S5.18: Weight loss of PI powders collected in the bulk solution during preparation of membrane samples.

8. Cyclohexane permporometry for pore size determination of the membrane samples

A stepwise pore size analysis after each reaction step and comparison with the pristine support was done by employing cyclohexane permporometry and the results are given in Figure S5.19. The γ-alumina pristine layer exhibits a relatively narrow pore size distribution with pore diameter of 5.5 nm. After reaction with APTES (sample A) the pore diameter has not been significantly affected and is seemingly similar to the one of the pristine γ -alumina layer. Further, functionalization with PMDA

leads to a significant pore size shrinkage as seen from the oxygen permeance over the partial pressure raw data (Figure 5.1b). Since there is not an obvious transition point observed at low cyclohexane partial pressures then pore size estimation cannot be done via this method. However, we can safely assume that the pore diameter is 1 nm or lower due to the limit of the measurement being associated with the molecular diameter of cyclohexane which is 0.5 nm.
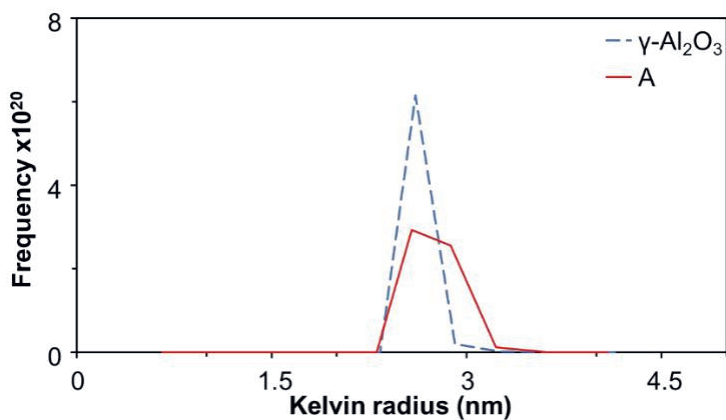
Figure S5.19: Pore radius distribution of the pristine γ-alumina layer and a γ-alumina layer after pre-functionalization with APTES by CVD (A). Values, calculated using the Kelvin equation.

9. Scanning electron microscopy (SEM)
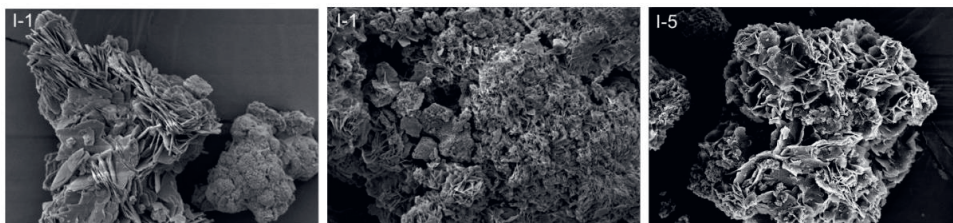
Figure S5.20: SEM Micrographs of the PI powders prepared for 1 (I-1) or 5 days (I-5).

10. High resolution scanning electron microscope (HR-SEM) analysis

At the top (Figure S5.21) the image of a pristine α-alumina supported γ-alumina layer. At the bottom (Figure S5.22) the top surface and cross-section micrographs of the pristine supported γ-alumina layer. On the cross-section micrograph the top layer is γ-alumina and the bottom layer is α-alumina.
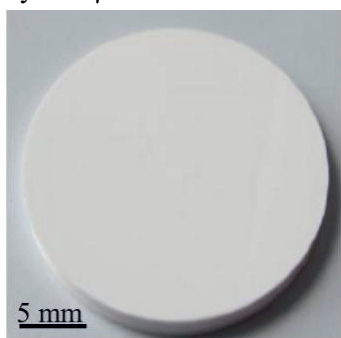
Figure S5.21: Photograph of the pristine support.
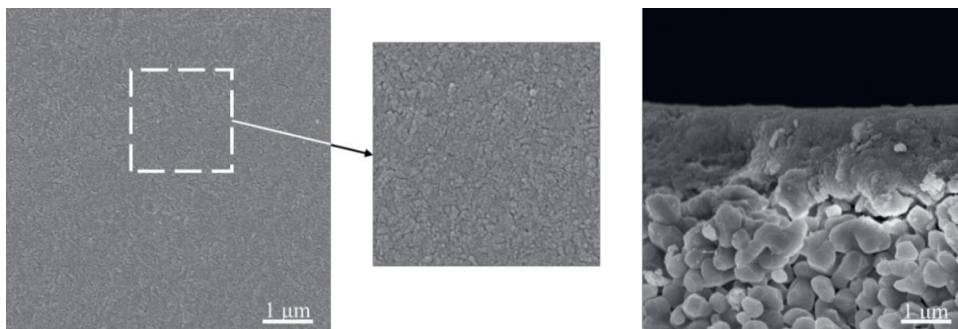
Figure S5.22: HR-SEM micrograph of the top surface (left and middle) and the cross-section of the pristine support.

11. Energy-dispersive X-ray spectroscopy (SEM-EDS)

The SEM-EDS analysis was done by acquiring a well focused image with secondary electron emission. Then, the backscattered electron (BEC) receiver was switched on and the image(s) (Figure S5.23A – S5.26A) was focused as best as possible at the magnification of 16k. Then, elemental analysis was done by a point analysis where three points across the cross-section of the membrane were taken in different depths (Table S5.1 – S5.3). Each point was measured for 300s in order to acquire an accurate measurement. For each set of points the three data points were averaged and used for the calculation of the carbon to aluminium ratio (C/Al) which were used in Figure 5.3. After the elemental analysis was completed the SEM image (Figure S5.23B – S5.26B) was recorded at the same spot as where the EDS analysis was performed, by only switching the secondary electron receiver on and focusing the image. A broken line, shown on SEM and BEC micrographs, separates the γ-alumina from the α-alumina layer. The γ-alumina layer, fully shown micrographs, has a thickness of 1.5 μm, whereas the α-alumina, partially shown, has a thickness of 2 mm.

A-1 sample analysis:
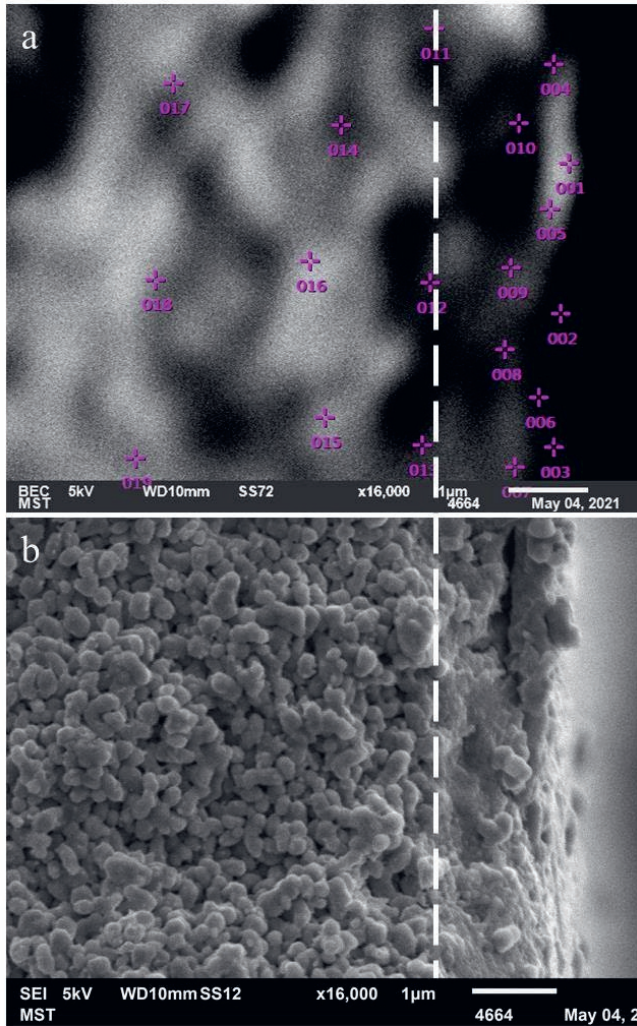
Figure S5.23: Cross-section micrographs of the same spot of a A-1 sample by using backscattered electrons analysis (a) and secondary electron analysis (b). For the elemental analysis as function of penetration depth, a point analysis was used, where three points were measured across the cross-section at different penetration depths. The white broken line denotes the limit between α-alumina (left) and γ-alumina (right).

Table S5.1: Raw data of the point analysis performed on a cross-section of A-1 sample. The points in the table correspond to the pink numbers on the micrograph in Figure S5.23a.

Point	Element (mass %)				C/Al ratio	Distance from top surface (μm)
	C	N	O	Al		
1	49	n.d.	24	27	1.8	
2	55	n.d.	12	33	1.6	0.1
3	46	n.d.	19	35	1.3	
4	24	n.d.	16	60	0.4	
5	74	n.d.	17	9	8.6	0.3
6	42	n.d.	19	39	1.1	
7	48	n.d.	23	29	1.6	
8	28	n.d.	19	53	0.5	0.7
9	53	n.d.	19	28	1.9	
10	50	n.d.	11	39	1.3	
11	20	n.d.	13	67	0.3	
12	28	n.d.	19	53	0.5	1.8
13	38	n.d.	26	35	1.1	
14	10	n.d.	34	55	0.2	
15	15	n.d.	37	48	0.3	3.2
16	21	n.d.	33	46	0.5	
17	10	n.d.	27	63	0.2	
18	15	n.d.	32	53	0.3	5.2
19	21	n.d.	35	43	0.5	

B-1 sample analysis:
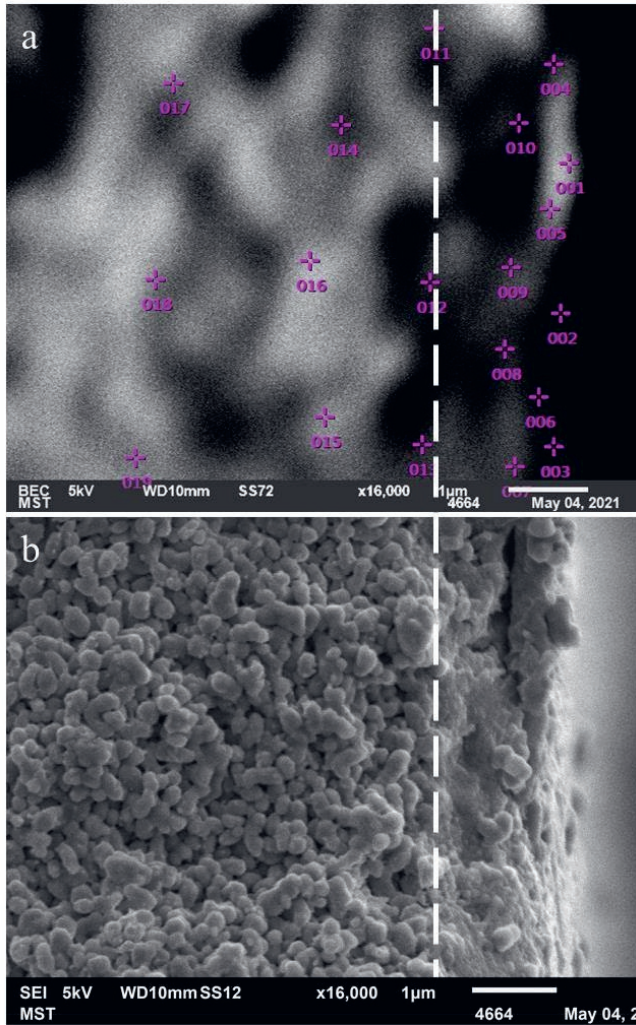
Figure S5.24: Cross-section micrographs of the same spot of a B-1 sample by using backscattered electrons analysis (a) and secondary electron analysis (b). For the elemental analysis as function of penetration depth, a point analysis was used, where three points were measured across the cross-section at different penetration depths. The white broken line denotes the limit between α-alumina (left) and γ-alumina (right).

Table S5.2: Raw data of the point analysis performed on a cross-section of B-1 sample. The points in the table correspond to the pink numbers on the micrograph in Figure S5.24a.

Point	Element (mass %)				C/Al ratio	Distance from top surface (µm)
	C	N	O	Al		
1	26	1	37	37	0.7	
2	20	1	37	43	0.5	0.3
3	22	1	38	39	0.6	
4	22	1	34	43	0.5	
5	25	1	33	41	0.6	0.6
6	21	1	36	42	0.5	
7	28	1	33	38	0.7	
8	23	0	34	43	0.5	0.9
9	26	1	31	42	0.6	
10	38	1	28	33	1.1	
11	46	nd	26	28	1.6	1.4
12	15	0	39	46	0.3	
13	10	nd	33	57	0.2	
14	11	0	40	50	0.2	3.2
15	6	nd	36	57	0.1	
16	6	0	32	61	0.1	
17	26	1	37	37	0.7	5.3
18	20	1	37	43	0.5	

A-5 sample analysis:
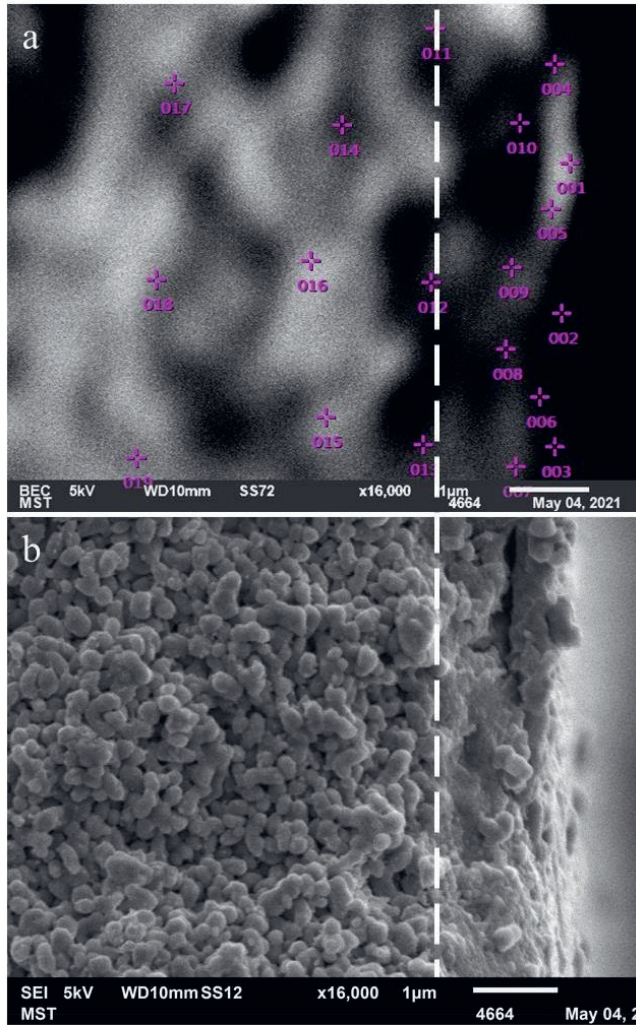
Figure S5.25: Cross-section micrographs of the same spot of a A-5 sample by using backscattered electrons analysis (a) and secondary electron analysis (b). For the elemental analysis as function of penetration depth, a point analysis was used, where three points were measured across the cross-section at different penetration depths. The white broken line denotes the limit between α-alumina (left) and γ-alumina (right).

Table S5.3: Raw data of the point analysis performed on a cross-section of A-5 sample. The points in the table correspond to the pink numbers on the micrograph in Figure S5.25a.

Point	Element (mass %)				C/Al ratio	Distance from top surface (µm)
	C	N	O	Al		
1	77	n.d.	19	5	15.9	
2	75	n.d.	17	8	9.3	0.1
3	68	n.d.	14	18	3.9	
4	75	n.d.	18	8	9.8	
5	69	n.d.	14	17	4.1	0.5
6	64	n.d.	12	24	2.7	
7	47	n.d.	7	46	1.0	
8	55	n.d.	9	36	1.5	0.8
9	66	n.d.	12	21	3.1	
10	15	n.d.	29	55	0.3	
11	18	n.d.	6	77	0.2	2.2
12	13	n.d.	6	81	0.2	
13	19	n.d.	35	46	0.4	
14	16	n.d.	28	56	0.3	4.1
15	12	n.d.	36	52	0.2	
16	12	n.d.	36	51	0.2	
17	21	n.d.	28	50	0.4	5.5
18	25	n.d.	27	48	0.5	

B-5 sample analysis:
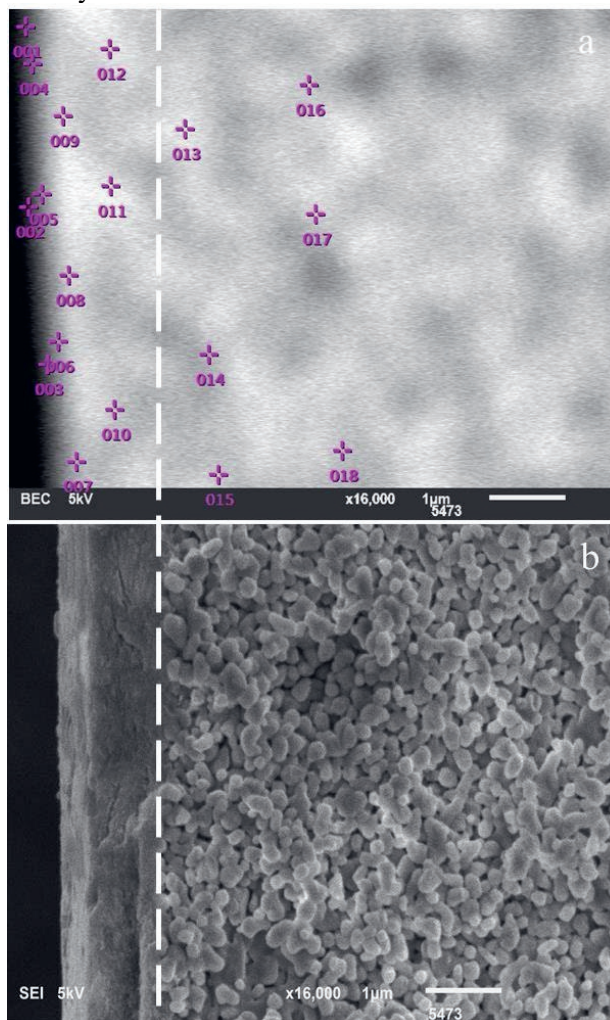
Figure S5.26: Cross-section micrographs of the same spot of a B-5 sample by using backscattered electrons analysis
and secondary electron analysis (b). For the elemental analysis as function of penetration depth, a point analysis was used, where three points were measured across the cross-section at different penetration depths. The white broken line denotes the limit between α-alumina (right) and γ-alumina (left).

Table S5.4: Raw data of the point analysis performed on a cross-section of A-5 sample. The points in the table correspond to the pink numbers on the micrograph in Figure S5.26a.

Point	Element (mass %)				C/Al ratio	Distance from top surface (μm)
	C	N	O	Al		
1	37	1	22	40	1	
2	46	1	20	33	2	0.1
3	39	1	23	36	3	
4	42	1	19	38	4	
5	46	1	20	34	5	0.3
6	46	1	20	34	6	
7	37	2	28	34	7	
8	35	1	25	39	8	0.6
9	32	1	27	40	9	
10	14	1	38	47	10	
11	13	1	38	49	11	1.2
12	15	1	33	51	12	
13	8	1	35	56	13	
14	7	1	36	56	14	2.3
15	7	1	41	51	15	
16	8	0	40	52	16	
17	10	1	37	52	17	3.9
18	6	1	40	54	18	

12. Long-term stability of A-5 membrane sample

Sample A-5 was tested in an aqueous solution of Rhodamine B for 5 days where the retention and water flux was monitored. The results show that the membrane's performance was stable after 5 days of testing.
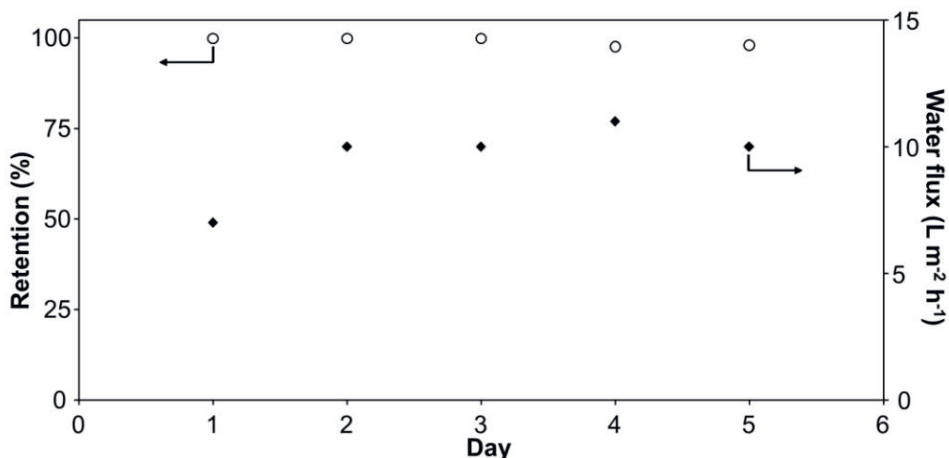
Figure S5.27: Stability of sample A-5 in an aqueous solution of RB under an applied pressure of 11 bars.

5.6. References

(1)   Sholl, D. S.; Lively, R. P. Seven Chemical Separations to Change the World. Nature 2016, 532, 435−437.

(2)   Marchetti, P.; Solomon, M. F. J.; Szekely, G.; Livingston, A. G. Molecular Separation with Organic Solvent Nanofiltration: A Critical Review. Chem. Rev. 2014, 114, 10735−10806.

(3)   Vandezande, P.; Gevers, L. E. M.; Vankelecom, I. F. J. Solvent Resistant Nanofiltration: Separating on a Molecular Level. Chem. Soc. Rev. 2008, 37, 365−405.

(4)   Merlet, R. B.; Pizzoccaro-Zilamy, M. A.; Nijmeijer, A.; Winnubst, L. Hybrid Ceramic Membranes for Organic Solvent Nanofiltration: State-of-the-Art and Challenges. J. Membr. Sci. 2020, 117839.

(5)   Volkov, A. V.; Parashchuk, V. V.; Stamatialis, D. F.; Khotimsky, V. S.; Volkov, V. V.; Wessling, M. High Permeable PTMSP/PAN Composite Membranes for Solvent Nanofiltration. J. Memb. Sci. 2009, 333, 88−93.

(6)   Darvishmanesh, S.; Van der Bruggen, B. Mass Transport through Nanostructured Membranes: Towards a Predictive Tool. Membranes 2016, 6, 49.

(7)   Baumgartner, B.; Puchberger, M.; Unterlass, M. M. Towards a General Understanding of Hydrothermal Polymerization of Polyimides. Polym. Chem. 2015, 6, 5773−5781.

(8)   Vanherck, K.; Koeckelberghs, G.; Vankelecom, I. F. J. Crosslinking Polyimides for Membrane Applications: A Review. Prog. Polym. Sci. 2013, 38, 874−896.

(9)   Product overview – PuraMem® Membranes for organic solvent nanofiltration (OSN) – Evonik Industries https://www.membraneseparation.com/en/organic-solvent-nanofiltration-with-puramemduramem/product-overview (accessed Jun 9, 2021).

(10)   Cai, D.; Su, J.; Huang, M.; Liu, Y.; Wang, J.; Dai, L. Synthesis, Characterization and Hydrolytic Stability of Poly (Amic Acid) Ammonium Salt. Polym. Degrad. Stab. 2011, 96, 2174−2180.

(11)   Morikawa, A.; Iyoku, Y.; Kakimoto, M.-A.; Imai, Y. Preparation of a New Class of Polyimide-Silica Hybrid Films by Sol-Gel Process. Polym. J. 1992, 24, 107.

(12)   Kuttiani Ali, J.; Maher Chabib, C.; Abi Jaoude, M.; Alhseinat, E.; Teotia, S.; Patole, S.; Hussain Anjum, D.; Qattan, I. Enhanced Removal of Aqueous Phenol with Polyimide Ultrafiltration Membranes Embedded with Deep Eutectic Solvent-Coated Nanosilica. Chem. Eng. J. 2021, 408, 128017.

(13)   Wei, C.; Qiang, R.; Lin, L.; Gao, Y.; Ma, S.; Zhang, X.; Huang, X. Combing Three-Dimensional Water Channels and Ultra-Thin Skin Layer Enable High Flux and Stability of Loose Polyimide/SiO2 Nanofiltration Membranes at Low Operating Pressure via One Step in-Situ Modification. J. Memb. Sci. 2021, 623, 118944.

(14)   Qiang, R.; Wei, C. J.; Lin, L.; Deng, X.; Zheng, T.; Wang, Q.; Gao, Y.; Zhang, Y. Bioinspired: A 3D Vertical Silicon Sponge-Inspired Construction of Organic-Inorganic Loose Mass Transfer Nanochannels for Enhancing Properties of Polyimide Nanofiltration Membranes. Sep. Purif. Technol. 2021, 259, 118038.

(15)   Mueller, N. C.; Van der Bruggen, B.; Keuter, V.; Luis, P.; Melin, T.; Pronk, W.; Reisewitz, R.; Rickerby, D.; Rios, G. M.; Wennekes, W.; Nowack, B.

Nanofiltration and Nanostructured Membranes Should They Be Considered Nanotechnology or Not? J. Hazard. Mater. 2012, 211-212, 275−280.

(16) Isaacson, S. G.; Lionti, K.; Volksen, W.; Magbitang, T. P.; Matsuda, Y.; Dauskardt, R. H.; Dubois, G. Fundamental Limits of Material Toughening in Molecularly Confined Polymers. Nat. Mater. 2016, 15, 294−298.

(17) Isaacson, S. G.; Fostvedt, J. I.; Koerner, H.; Baur, J. W.; Lionti, K.; Volksen, W.; Dubois, G.; Dauskardt, R. H. Synthesis of Polyimides in Molecular-Scale Confinement for Low-Density Hybrid Nanocomposites. Nano Lett. 2017, 17, 7040−7044.

(18) Liu, G.; Müller, A. J.; Wang, D. Confined Crystallization of Polymers within Nanopores. Acc. Chem. Res. 2021, 54, 3028−3038.

(19) Pizzoccaro-Zilamy, M.-A.; Huiskes, C.; Keim, E. G.; Sluijter, S. N.; van Veen, H.; Nijmeijer, A.; Winnubst, L.; Luiten-Olieman, M. W. J. New Generation of Mesoporous Silica Membranes Prepared by a Stöber-Solution Pore-Growth Approach. ACS Appl. Mater. Interfaces 2019, 11, 18528−18539.

(20) Home – inopor – the cutting edge of nano-filtrationhttps://www.inopor.com/en/ (accessed Nov 19, 2021).

(21) Pervaporation Membranes by Pervatechhttps://pervaporationmembranes.com/(accessed Nov 19, 2021).

(22) Abedini, S.; Parvin, N.; Ashtari, P.; Jazi, F. S. Microstructure, Strength and CO2 Separation Characteristics of α-Alumina Supported γ-Alumina Thin Film Membrane. Adv. Appl. Ceram. 2013, 112, 17− 22.

(23) Uhlhorn, R. J. R.; Veld, M. H. B. J. H. I.; Keizer, K.; Burggraaf, A. J. Synthesis of Ceramic Membranes. J. Mater. Sci. 1992, 27, 527− 537.

(24) Kyriakou, N.; Merlet, R. B.; Willott, J. D.; Nijmeijer, A.; Winnubst, L.; Pizzoccaro-Zilamy, M.-A. New Method toward a Robust Covalently Attached Cross-Linked Nanofiltration Membrane. ACS Appl. Mater. Interfaces 2020, 12, 47948−47956.

(25) Kyriakou, N.; Pizzoccaro-Zilamy, M.-A.; Nijmeijer, A.; LuitenOlieman, M.; Winnubst, L. Hydrolytic Stability of PEG-Grafted γAlumina Membranes: Alkoxysilane vs Phosphonic Acid Linking Groups. Microporous Mesoporous Mater. 2020, 307, 110516.

(26) Tanardi, C. R.; Pinheiro, A. F. M.; Nijmeijer, A.; Winnubst, L. PDMS Grafting of Mesoporous γ-Alumina Membranes for Nanofiltration of Organic Solvents. J. Memb. Sci. 2014, 469, 471−477.

(27) Merlet, R.; Winnubst, L.; Nijmeijer, A.; Amirilargani, M.; Sudhölter, E. J. R.; Smet, L. C. P. M. d.; Cob, S. S.; Vandezande, P.; Dorbec, M.; Sluijter, S.; Veen, H. v.; VanDelft, Y.; Wienk, I.; Cuperus, P.; Behera, S.; Hartanto, Y.; Vankelecom, I. F. J.; Wit, P. d. Comparing the Performance of Organic Solvent Nanofiltration Membranes in Non-Polar Solvents. Chemie Ing. Tech. 2021, 93, 1389−1395.

(28) Sun, C.; Zhou, F.; Shi, L.; Yu, B.; Gao, P.; Zhang, J.; Liu, W. Tribological Properties of Chemically Bonded Polyimide Films on Silicon with Polyglycidyl Methacrylate Brush as Adhesive Layer. Appl. Surf. Sci. 2006, 253, 1729−1735.

(29) Amirilargani, M.; Merlet, R. B.; Chu, L.; Nijmeijer, A.; Winnubst, L.; de Smet, L. C. P. M.; Sudhölter, E. J. R. Molecular Separation Using Poly (Styrene-Co-Maleic Anhydride) Grafted to γAlumina: Surface versus Pore Modification. J. Memb. Sci. 2019, 582, 298−306.

(30) Coates, J. Interpretation of Infrared Spectra, A Practical Approach. In Encyclopedia of Analytical Chemistry; John Wiley & Sons, Ltd: Chichester, UK, 2006. Doi: DOI: 10.1002/ 9780470027318.a5606.

(31) Merlet, R. B.; Amirilargani, M.; de Smet, L. C. P. M.; Sudhölter, E. J. R.; Nijmeijer, A.; Winnubst, L. Growing to Shrink: NanoTunable Polystyrene Brushes inside 5 Nm Mesopores. J. Memb. Sci. 2019, 572, 632−640.

(32) Tena, A.; Marcos-Fernández, A.; Lozano, A. E.; de la Campa, J. G.; de Abajo, J.; Palacio, L.; Prádanos, P.; Hernández, A. Thermally Treated Copoly(Ether-Imide)s Made from Bpda and Alifatic plus Aromatic Diamines. GAS Separation Properties with Different Aromatic Diamimes. J. Memb. Sci. 2012, 387-388, 54−65.

(33) Pinheiro, A. F. M.; Hoogendoorn, D.; Nijmeijer, A.; Winnubst, L. Development of a PDMS-Grafted Alumina Membrane and Its Evaluation as Solvent Resistant Nanofiltration Membrane. J. Memb. Sci. 2014, 463, 24−32.

(34) Mircescu, N. E.; Oltean, M.; Chis, V.; Leopold, N. FTIR, FTRaman, SERS and DFT Study on Melamine. Vib. Spectrosc. 2012, 62, 165−171.

(35) Li, Z.; Zhou, J.; Xu, R.; Liu, S.; Wang, Y.; Li, P.; Wu, W.; Wu, M. Synthesis of Three Dimensional Extended Conjugated Polyimide and Application as Sodium-Ion Battery Anode. Chem. Eng. J. 2016, 287, 516−522.

(36) Wang, Y.; Gao, Q.; You, Q.; Liao, G.; Xia, H.; Wang, D. Porous Polyimide Framework: A Novel Versatile Adsorbent for Highly Efficient Removals of Azo Dye and Antibiotic. React. Funct. Polym. 2016, 103, 9−16.

(37) Sadhasivam, B.; Muthusamy, S. Synthesis and Characterization of Optically Active Polyimides and Their Octa(Aminophenyl)- Silsesquioxane Nanocomposites. High Perform. Polym. 2016, 28, 547− 561.

(38) Kim, H.-J.; Nam, S.-M. High Loading of Nanostructured Ceramics in Polymer Composite Thick Films by Aerosol Deposition. Nanoscale Res. Lett. 2012, 7, 1.

(39) Baumgartner, B.; Bojdys, M. J.; Unterlass, M. M. Geomimetics for Green Polymer Synthesis: Highly Ordered Polyimides via Hydrothermal Techniques †. Polym. Chem. 2014, 5, 3771−3776.

(40) Duan, H.; Lyu, P.; Liu, J.; Zhao, Y.; Xu, Y. Semiconducting Crystalline Two-Dimensional Polyimide Nanosheets with Superior Sodium Storage Properties. ACS Nano 2019, 13, 2473−2480.

(41) Hinckley, D. A.; Seybold, P. G.; Borris, D. P. Solvatochromism and Thermochromism of Rhodamine Solutions. Spectrochim. Acta, Part A 1986, 42, 747−754.

(42) Tanardi, C. R.; Catana, R.; Barboiu, M.; Ayral, A.; Vankelecom, I. F. J.; Nijmeijer, A.; Winnubst, L. Polyethyleneglycol Grafting of Yalumina Membranes for Solvent Resistant Nanofiltration. Microporous Mesoporous Mater. 2016, 229, 106−116.

(43) Tanardi, C. R.; Nijmeijer, A.; Winnubst, L. Coupled-PDMS Grafted Mesoporous γ-Alumina Membranes for Solvent Nanofiltration. Sep. Purif. Technol. 2016, 169, 223−229.

(44) Li, X.; Vandezande, P.; Vankelecom, I. F. J. Polypyrrole Modified Solvent Resistant Nanofiltration Membranes. J. Memb. Sci. 2008, 320, 143−150.

(45) Zhou, Y.; Chen, Y.; Wang, H.; Wong, C. P. Creation of a Multilayer Aluminum Coating Structure Nanoparticle Polyimide Filler for Electronic Applications. Mater. Lett. 2014, 119, 64−67.

(46) Zhou, Y.; Bai, Y.; Yu, K.; Kang, Y.; Wang, H. Excellent Thermal Conductivity and Dielectric Properties of Polyimide Composites Filled with Silica Coated Self-Passivated Aluminum Fibers and Nanoparticles. Appl. Phys. Lett. 2013, 102, 252903.

(47) Li, X.; Dong, G.; Liu, Z.; Zhang, X. Polyimide Aerogel Fibers with Superior Flame Resistance, Strength, Hydrophobicity, and Flexibility Made via a Universal Sol−Gel Confined Transition Strategy. ACS Nano 2021, 15, 4759.

(48) Hicyilmaz, A. S.; Bedeloglu, A. C. Applications of Polyimide Coatings: A Review. SN Appl. Sci. 2021, 3, 363.

(49) Cuperus, F. P.; Bargeman, D.; Smolders, C. A. Permporometry: The Determination of the Size Distribution of Active Pores in UF Membranes. J. Memb. Sci. 1992, 71, 57−67.

(50) Liu, C.; Shih, K.; Gao, Y.; Li, F.; Wei, L. Dechlorinating Transformation of Propachlor through Nucleophilic Substitution by Dithionite on the Surface of Alumina. J. Soils Sediments 2012, 12 (5), 724–733. https://doi.org/10.1007/s11368-012-0506-0.

(51) Costa, T. M. H.; Gallas, M. R.; Benvenutti, E. V; Da Jornada, J. A. H. Study of Nanocrystalline γ-Al2O3 Produced by High-Pressure Compaction. J. Phys. Chem. B 1999, 103, 4278–4284. https://doi.org/10.1021/jp983791o

(52) Bistričić, L.; Volovšek, V.; Dananić, V. Conformational and Vibrational Analysis of Gamma-Aminopropyltriethoxysilane. J. Mol. Struct. 2007, 834–836, 355–363. https://doi.org/10.1016/j.molstruc.2006.10.036

(53) Zhang, Y.; Zhang, M.-S.; Zhang, Y.; Chen, X.-W.; Wang, J.-H. Green and Catalyst-Free Preparation of Triazinyl Polyimide for the Efficient Adsorption of Glycoproteins. RSC Adv. 2016, 6, 46002–46007. https://doi.org/10.1039/c6ra05411k.

(54) Yan, W.; Yuan, P.; Chen, M.; Wang, L.; Liu, D. Infrared Spectroscopic Evidence of a Direct Addition Reaction between Palygorskite and Pyromellitic Dianhydride. Appl. Surf. Sci. 2013, 265, 585–590. https://doi.org/10.1016/j.apsusc.2012.11.051.

(55) Wang, T.; Xue, R.; Chen, H.; Shi, P.; Lei, X.; Wei, Y.; Guo, H.; Yang, W. Preparation of Two New Polyimide Bond Linked Porous Covalent Organic Frameworks and Their Fluorescence Sensing Application for Sensitive and Selective Determination of Fe 3+. New J. Chem. 2017, 41 (23), 14272–14278. https://doi.org/10.1039/C7NJ02134H

(56) Fang, Q.; Zhuang, Z.; Gu, S.; Kaspar, R. B.; Zheng, J.; Wang, J.; Qiu, S.; Yan, Y. Designed Synthesis of Large-Pore Crystalline Polyimide Covalent Organic Frameworks. Nat. Commun. 2014, 5 (1), 4503. https://doi.org/10.1038/ncomms5503.

(57) Wang, Y.; Gao, Q.; You, Q.; Liao, G.; Xia, H.; Wang, D. Porous Polyimide Framework: A Novel Versatile Adsorbent for Highly Efficient Removals of Azo Dye and Antibiotic. React. Funct. Polym. 2016, 103, 9–16. https://doi.org/10.1016/J.REACTFUNCTPOLYM.2016.04.004.

(58) Taublaender, M. J.; Reiter, M.; Unterlass, M. M. Highly Crystalline, Nanostructured Polyimide Microparticles via Green and Tunable Solvothermal Polymerization. Macromolecules 2019, 52 (16), 6318–6329. https://doi.org/10.1021/acs.macromol.9b00985.

Chapter 6

A hybrid solid-state synthesis through pre-organization for the synthesis of polyimide materials

ABSTRACT

Inspired by the reported synthetic methods for polyimides, we have designed a new synthesis approach to synthesize a crosslinked, crystalline polyimide material made from the condensation reaction between pyromellitic dianhydride and melamine. This hybrid synthesis, which was done in the solid-state through pre-organization (SSP) of the monomers in solution, is a simple green method, as toxic solvents and specialized equipment (e.g., autoclave or ampules) become redundant. The products of the different synthetic methods available in literature and SSP were compared regarding purity and crystallinity using FTIR and XRD analysis. It was found that most synthetic methods lead to a pure polyimide product, with the exception of the conventional solid-state method, which always contained some impurities. The crystal structures of the final polyimides varied significantly between the different synthetic methods, but overall all polyimides showed a relatively good structural orientation. Our hybrid synthesis was able to form a pure and crystalline polyimide powder at 250 °C for a reaction time of 5 hours. As the reaction temperature is lower than the melting point of both monomers, the polyimidization reaction took place purely in the solid-state, which is not the case with the conventional solid-state reaction that occurs above the melting point of one of the reactants. The SSP method was successfully used to apply a polyimide coating on a porous support, demonstrating the potential utilization of the method in membrane preparation as well as coated layer on top of porous or dense surfaces.

6.1. Introduction

Crystalline polymers typically show better properties (e.g., thermal and chemical stability, electrical conductivity, and more) than their amorphous counterparts.[1] However, high molecular weight polymers, like polyimides (PIs) and, in particular, crosslinked polymers, are hard to process into a crystalline structure during post-synthesis treatment and are therefore isolated primarily as amorphous products.[1,2] Typically, crystalline crosslinked polymers have been formed under a controlled environment (e.g., limited water content, pressurized vessels)[3,4] through reticular chemistry (2D or 3D covalent organic frameworks or COFs), which implies the polycondensation reaction of the right combination of monomers under the optimal conditions (pressure, temperature, solvent mixture, catalyst, and water percent) to achieve a crystalline polymer.[5] However, in most cases, such polymers (imine and boron-based) consist of dynamic covalent bonds that, under certain conditions, are reversible.[3] This bond reversibility allows for the formation of highly crystalline polymers, but their stability remains a challenge, and furthermore cannot compete against irreversible polymers such as polyimides, triazine, benzimidazole, or benzoxazole.

Polyimides (PIs) with a high degree of crystallinity can be synthesized by the polycondensation reaction between (di)anhydrides and (di or tri)amines under solvothermal (ST) conditions (Figure 6.1a). However, their synthesis is usually done at high temperatures (> 200 °C), using toxic solvents, for example, n-methyl-2-pyrrolidone (NMP) or m-cresol, as well as long reaction times (3 – 7 days).[6] Solvothermal syntheses that use shorter reaction times (15h) have been possible by first pre-organizing the monomers in solution at room temperature to form a soluble supramolecular network. Then, the desired PI was formed successfully by thermally treating the solution at temperatures above 200 °C in a pressurized vessel.[7] However, such methods are usually performed under inert conditions since water or oxygen can significantly interfere in the reaction by reducing the monomer reactivity, the reaction yield, and the crystallinity of the final polymer. All these challenges render ST syntheses towards crystalline PIs costly and a significant environmental footprint (toxic wastes and excessive monomer losses due to low yields). Therefore, alternatives for the synthesis of crystalline polyimides are desirable.

An alternative to ST is the hydrothermal (HT) synthesis, which employs green solvents, such as water and ethanol, as the reactive media. It has also been used in the past to synthesize high molecular weight PIs.[1,4,7,8] HT syntheses are done in a stepwise manner, starting from the formation of a supramolecular network (through, for example, hydrogen or ionic bonding) of the(di)anhydride and (di or tri)amine monomers in solution (Figure 6.1b). This network typically precipitates spontaneously as a solid and then is reacted in solution (e.g., water, ethanol, glycerol)

in a pressurized vessel at temperatures above 160 °C. Thus far, HT syntheses have been used primarily for the preparation of linear crystalline PIs (poly(para-phenylene pyromellitimide))[9] and only a few isolated cases of crosslinked PIs (trisaminophenylbenzene and pyromellitic acid)[10] with a relatively good degree of crystallinity are reported. Furthermore, HT methods depend upon the pressure built up from the vapours of the low boiling point solvent formed during the reaction. Thus, they are highly dependent on pressurized containers, which can be an obstacle for upscaling the method and for functionalizing pressure-sensitive supports (e.g., elastomers) with PI layers.

On the other hand, solid-state (SS) methods involve a simple thermal treatment of a solid mixture prepared in a mortar and pestle and have been used extensively in literature in the synthesis of crystalline PIs for the preparation of adsorbents or battery components (Figure 6.1c).[11,12] The simplicity of the method, its green character, and the crystallinity and purity of the final PI products establishes the SS syntheses crucial for the fabrication of ordered PIs. SS synthetic routes are typically performed above the melting point of one of the components used in the reaction mixture (monomers, catalysts etc.).[11,13] In this way, the liquid monomers (typically melamine and pyromellitic dianhydride) act as the reaction medium. Due to the high melting point of the dianhydride monomers used, the reaction temperatures are typically above 250 °C. SS syntheses that employ a catalyst, or a mixture of additives, to reduce the reaction temperatures have achieved temperatures as low as 250 °C.[13] However, the use of catalysts or other additives increases the cost of the method, the washing step becomes more elaborate, and the conditions can be detrimental to the stability of the monomers (e.g., the triazine ring of melamine).[13] Furthermore, SS syntheses are directed mainly for forming free-standing PIs which significantly limits the method's applicability.

Even though SS syntheses seem to avoid using a pressure vessel and significantly simplify the preparation method, the temperatures are exceedingly higher than those used with HT or ST methods. So, perhaps a hybrid method that uses steps from both HT and SS syntheses can be combined to overcome the challenges of both methods. This could be achieved by mixing the two monomers (melamine and pyromellitic acid) in a green solvent to form a supramolecular network similar to the first step of the HT synthesis (Figure 6.1b). The supramolecular network (precursor) can then be subjected to simple thermal treatment, following the SS preparation protocol, and form the desirable polyimide network in the solid-state without phase transition. As monomers in the supramolecular network are close, they can potentially react at relatively low temperatures without phase transition (melting of one of the monomers) involved. This means that the structural organization of the supramolecular network can influence the final crystal structure of the PI product. Therefore, as the supramolecular network is held together by weak interactions (e.g.,

212

hydrogen bonding), its crystal structure can be "manipulated" in solution before forming the irreversible imide linkage. As the monomers are pre-organized in solution prior to the solid-state reaction, the method will be called solid-state through pre-organization or SSP, for short.
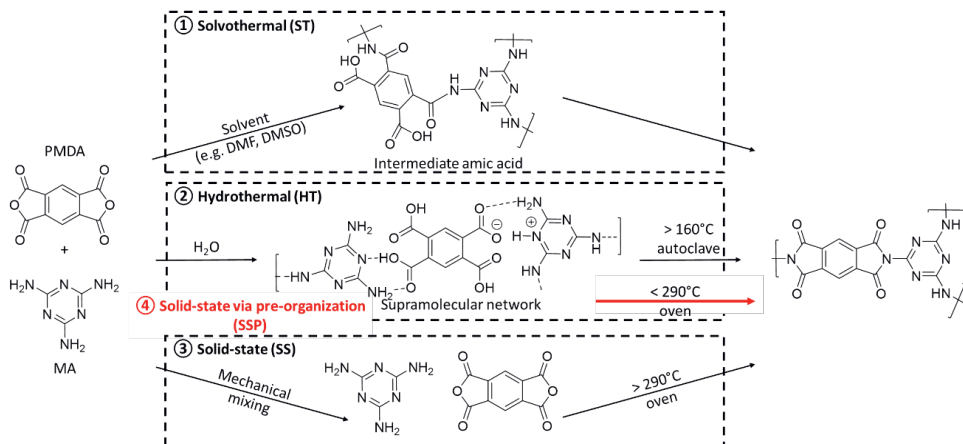
Figure 6.1: Reaction pathways that lead to a crosslinked PI material through the reaction of pyromellitic dianhydride (PMDA) and melamine (MA). (1) Solvothermal (ST) synthesis, which is typically done in a solvent at temperatures above 200 °C in a pressurized vessel (e.g., autoclave, ampule). (2) Hydrothermal (HT) synthesis follows the formation of a supramolecular network in water and thermal treatment in a green solvent. (3) Solid-state (SS) synthesis is done by mechanical mixing of the two monomers and thermal treatment in an oven under nitrogen. (4) Solid-state through pre-organization (SSP), a hybrid method combining the supramolecular network formation of HT, and then by a simple thermal treatment in an oven under nitrogen, the PI is formed.

To investigate whether a hybrid synthesis of HT and SS syntheses can be realized as mentioned above, we used the available knowledge in the literature on PI syntheses to develop a simple, cheap, and relatively green method for the fabrication of crystalline PIs. To do so, first, melamine (MA) and pyromellitic acid (PMA) were (pre-)organized in solution to form a supramolecular precursor. Then, the desired polyimide product was obtained by thermally treating the supramolecular precursor in the solid-state reaction. The polyimidization reaction was performed below and above the melting point of PMA to understand whether the pre-organization step can influence the temperature of imide formation. The PIs formed via this solid-state through the pre-organization method (SSP) were compared with crystalline PIs formed via other methods, such as solvothermal (ST) and SS with regards to product purity (analysed by FTIR), crystallinity (XRD), simplicity (utilization and upscaling) and environmental footprint. The SSP method was used to form both free-standing

PIs but also to coat an inorganic porous substrate to show the potential of the method compared to the more traditional SS methods.

6.2. Materials and methods

The solvents mesitylene (>99%, Acros Organics), n-methyl-2-pyrrolidone (NMP) (>99%, anhydrous, Merck), tetrahydrofuran (>99%, Merck), were used as received. Milli-Q was obtained through purifying water with Milli-Q™ Reference Water Purification System. HCl (37%, Merck), and formic acid (95%, Sigma Aldrich) were used as received. Melamine (MA) (98%, TCI Europe N.V.) and pyromellitic dianhydride (PMDA) (98%, TCI Europe N.V.) were used as received

6.2.1. Polyimide synthesis

Solid-state reaction (SS). The synthesis procedure used for the solid-state reaction was adapted from the procedure reported by Wang et al.[11] In a mortar, PMDA (2.18 g, 10 mmol, 1 eq.) and MA (1.26 g, 10 mmol, 1 eq.) were combined, and with a pestle the two monomers were stamped until a homogeneous mixture was formed. The white solid was then transferred to a crucible placed in a tubular oven under N_2 flow (10 mL min^{-1}). The oven was heated to 200, 270, 300 or 325 °C with a heating rate of 5 °C min^{-1} and left for 5 or 15 hours at the set temperature. The product was washed with 400 mL of hot water (70 – 80 °C), and the product was left to dry in a N_2 box at room temperature.

Solvothermal synthesis (ST). The solvothermal synthesis was reproduced by Fang et al.[6] In a pre-dried 10 mL ampule, PMDA (130.8 mg, 0.6 mmol, 1 eq.) and MA (50.5 mg, 0.4 mmol, 0.7 eq.) were added under N_2. Then, mesitylene (2 mL), NMP (2 mL), and isoquinoline (0.2 mL) were added to the ampule. Subsequently, the heterogeneous mixture was sonicated for 5 min and afterward flash-frozen using liquid nitrogen (-196 °C) while the ampule was kept under N_2. After the system was completely solidified, the ampule was evacuated (10^{-2} mbar), flame sealed, and subsequently placed inside a pre-heated oven at 200 °C and left for 5 days. Then, the ampule was cooled to room temperature, and the black solid obtained was washed first with anhydrous THF (20 mL). Then, the solid was placed in anhydrous THF (20 mL) for 8h under the static condition to remove any leftover impurities. Finally, the solid product was left to dry in an N_2 box at room temperature.

Solid-state through pre-organization (SSP). A supramolecular PMA-MA network was prepared either in water or NMP following the procedures described below:

Preparation of the supramolecular network in NMP: In an Erlenmeyer, under an inert atmosphere,-PMDA (1308 mg, 6 mmol, 1 eq.) was dissolved in anhydrous NMP (300 mL). In a different Erlenmeyer, MA (504 mg, 4 mmol, 0.7 eq.) was dispersed in anhydrous NMP (300 mL) by stirring rapidly. Water (215 µL, 12 mmol, 2 eq.)

214

was added to the PMDA solution to facilitate hydrolysis of the dianhydride towards the acid (PMA), and the mixture was stirred for more than 0.5h at room temperature. Thereafter, the MA dispersion was added to the PMA solution, and the mixture was stirred for 0.5 h or until the solid disappeared at room temperature. To the solution, water (150 mL) was added quickly, and a white precipitate was formed. After this step, the solid was filtered under vacuum, transferred to a crucible, and heated under N_2 at 250 or 325 °C (5 °C min^{-1}) for 15h. The product was washed with 400 mL of hot water (70 – 80 °C), after which it was left to dry in an N_2 box at room temperature. The samples prepared via the SSP method in NMP are denoted as SSP-N#, where # is the reaction temperature used (250 or 325 °C).

Preparation of the supramolecular network in water: PMDA (8.09 g, 37.3 mmol, 1 eq.) was added to water (100 mL) and heated to 80 °C for 1h. Separately, either a MA dispersion or solution was prepared. The MA dispersion was made by mixing 3.31 g of MA (25 mmol, 0.7 eq.) in 100 mL of water, followed by thorough stirring. The MA solution was prepared by dissolving 3.31 g of MA (25 mmol, 0.7 eq.) in 100 mL of water containing formic acid (2.75 mL), leading to the complete dissolution of MA. Next, the aqueous PMA solution was added to the MA dispersion or solution, and a white precipitated was formed immediately in both cases. The mixture was stirred overnight to allow for the complete precipitation of the supramolecular network. Then, the solid was filtered under a vacuum and transferred in a crucible. Hereafter, the solid was placed in an oven under N_2 and heated to 250 or 325 °C (5 °C min^{-1}) for 15h. The product was washed with 400 mL of hot water (70 – 80 °C), and was left to dry in an N_2 box at room temperature. The samples prepared via the SSP method in water are denoted as SSP-W# and in water/formic acid as SSP-F#, where # is the reaction temperature used (250 or 325 °C).

6.2.2. Preparation of a PI porous layer

For coating the alumina support with a PI network, the support was fitted in a vacuum-sealed in-house made setup. Then, 10 mL of an aqueous with a high (0.12 M) or low (0.04 M) concentration solution of MA containing an equal amount of formic acid (67 µL) was placed on top of the support, and the system was evacuated for 0.5h at 10^{-2} mbar. The excess solution was removed with pressurized air, and the impregnated support was immersed in a solution of PMA (0.065 M or 0.2M) in water (10 mL) and left for 15 min. Finally, the coated sample was treated at 250 °C for 15h under N_2.

6.2.3. Characterization

Fourier Transform Infrared spectroscopy (FTIR) measurements were done using a Perkin Elmer UATR Spectrum Two. Wavenumbers between 4000 and 400 cm^{-1} were scanned in reflectance mode at a resolution of 4 cm^{-1} for a minimum of 4 scans. Powder X-ray diffraction (XRD) analysis was performed on a Bruker D2 phaser at the wavelength of Cu Kα (λ = 1.5405 Å) (X-ray power: 40 kV, 40 mA) in Bragg-Brentano scanning mode between the angles 5 and 40° (2θ) were scanned with a step size of 0.02°. Scanning electron microscopy (SEM) was performed on JEOL JSM-6010LA SEM. The powders were placed on carbon tape and then sputtered with a layer of palladium/platinum (5 nm thickness) to avoid charging the sample. Cyclohexane permporometry was performed on in-house-built equipment. More details on the equipment and the experimental procedure used are described elsewhere.[14] The conformation of the supramolecular network was acquired by calculating the maximum number of conformer distributions between PMA and MA on a Wavefunction Spartan '14 at a semi-empirical level (PM6).

6.3. Result and Discussion

6.3.1. Synthesis and characterization of crystalline polyimides materials

As discussed in the introduction, crystalline polyimides (PI) are typically synthesized by either solvothermal or solid-state methods, with the former being considered a greener approach as no toxic solvents are involved. Therefore, we started our investigation on the formation of the model crystalline PIs selected in this study by exploring the solid-state reaction between melamine (MA) and pyromellitic dianhydride (PMDA). The solid-state synthesis was performed between 200 to 325 °C for 15h under inert conditions. Fourier-transform spectroscopy (FTIR) and X-ray diffraction analysis were used to identify the minimum temperature at which the formation of a pure and crystalline melamine-based PI material occurs.

FTIR results of the starting monomer mixture (MA and PMDA) and the solid-state reaction products prepared at 200, 270, 300, and 325 °C are provided in Figure 6.2a. The FTIR spectrum of the monomer mixture is composed of the characteristic vibration bands of the primary amine of MA appearing between 3600 and 3000 cm^{-1} and the absorption bands at 1845, 1804, and 1765 cm^{-1} ascribed to the C=O bond of PMDA. Similar absorption bands can be found in the FTIR spectrum of the individual monomers (Figure S6.1 and S6.4), which thus confirm the absence of reactions between the two monomers in the solid-state at room temperature. After thermal treatment of the precursor mixture at 200 °C (SS200), the bands associated with the primary amines slightly shift to the high wavenumber region (3700 – 3050 cm^{-1}). On the other hand, significant changes are observed in the region where the C=O bond absorbs. Additional bands at 1857, 1794, and 1773 cm^{-1} are denoted,

which can be attributed to unreacted anhydride. The band at 1733 cm^{-1} can originate from the presence of carboxylic acid as the product of the washing step or imide formation. Furthermore, the bands at 1673 and 1613 cm^{-1} indicate the formation of an amide bond in the sample. Overall, the SS200 spectrum suggests that the reaction between PMDA and MA starts at lower temperatures than the melting point of both monomers, respectively 293 and 345 °C. Still, primarily intermediate products (carboxylic acid and amide) are visible, and only a slight indication of imide bond formation is observed. At 270 °C (sample SS270), the bands at 3600-3000 cm^{-1} appear less intense compared to the SS200 sample, indicating changes in the chemical environment of MA. The intermediate products observed for SS200 (1857, 1794, 1773, and 1733 cm^{-1}) are also observed in the FTIR spectrum but with differences in relative intensity of the bands suggesting that some by-product reaction(s) are occurring between the two monomers. Still, the SS270 sample is primarily composed of intermediate products and starting materials rather than the desirable polyimide. Above 300 °C (samples SS300 and SS325), bands attributed to the primary amines seem to dissipate completely, and two new absorption bands appear at 1770 and 1719 cm^{-1} attributed to the C=O absorption of the imide group. Furthermore, the band present at 1351 cm^{-1} ascribed to the C-N-C bond confirms the formation of the imide bond in these samples. Nevertheless, the bands at 1797 and 1753 cm^{-1} attributed either to unreactive carboxylic acid or amic acid are present in the final products. The FTIR analysis shows that the solid-state reaction is initiated at temperatures below the melting temperature of the two monomers, forming intermediate products (amic acid) during the imidization reaction. However, the formation of the imide bond is only occurring above the melting point of PMDA (293 °C) and MA (345 °C), where the two monomers are in the liquid. One possible explanation for the presence of the unreactive carboxylic acid can be related to the monomer ratio typically used in the solid-state reaction (1:1, PMDA:MA) as amine groups are in excess compared to anhydride groups (3 amines per 2 anhydride groups). Therefore, a sample with a monomer ratio of 1.5:1 (PMDA:MA) was prepared. Unfortunately, increasing the PMDA content led to a product that still contains carboxylic acid, as shown by FTIR (Figure S6.6). As a result, the solid-state reaction shows a low conversion of anhydride to imide unrelated to temperature and monomer ratio.

XRD analysis was used to study the crystallinity of the different solid-state reaction products, and the results are given in Figure 6.2b and compared with the XRD diffractograms of the monomer mixture. Thermal treatment of the solid at 200 °C leads to a semicrystalline material with a large amorphous part. This can be the result of the ring opening of the anhydride group and the formation of the amide intermediate as detected by FTIR, leading to a distorted structure. At 270 °C, a new crystalline phase, called here A, is formed and characterized by a sharp and intense

diffraction peak at 26° (2θ) accompanied by a series of diffraction peaks of lower intensity at 13, 14.8, 17.6, 21.5, 22, 28.7 and 29.7° (2θ). The diffraction patterns of the samples prepared at 300 and 325 °C are relatively identical but with an increase amount of amorphous phase for the latter, which could be caused by intermediate by-products detected by FTIR. It is also important to note that the crystal structure obtained is very different from the results reported by Wang[11] and Chu[15] when using the solid-state synthesis approach with similar reaction conditions (monomer, chemical ratio, temperature, duration). The progressive transition from an amorphous to a crystalline structure suggests a transition below the melting point of both monomers. It is, therefore, possible that the PMDA and MA approach each other at 270 °C to reach a spatial orientation that resembles the orientation of the pure PI that is only formed at temperatures above 300 °C, as indicated by FTIR analysis. Thus, the intermolecular interactions that keep the two monomers separate at room temperature are broken below the melting point of the individual monomers as suggested by FTIR analysis, where a change in the C=O region (1900 – 1700 cm^{-1}) at 270 °C is observed. The XRD analysis and FTIR suggest that the two monomers react when they achieve the correct orientation in the crystal lattice. As a result, the organization of the two monomers in the solid-state can be energy intensive, increasing the energy needed for the PI reaction. Therefore, by reducing the energy needed for the orientation of the two monomers, one can potentially reduce the energy of the reaction and further reduce the reaction temperature for PI formation.
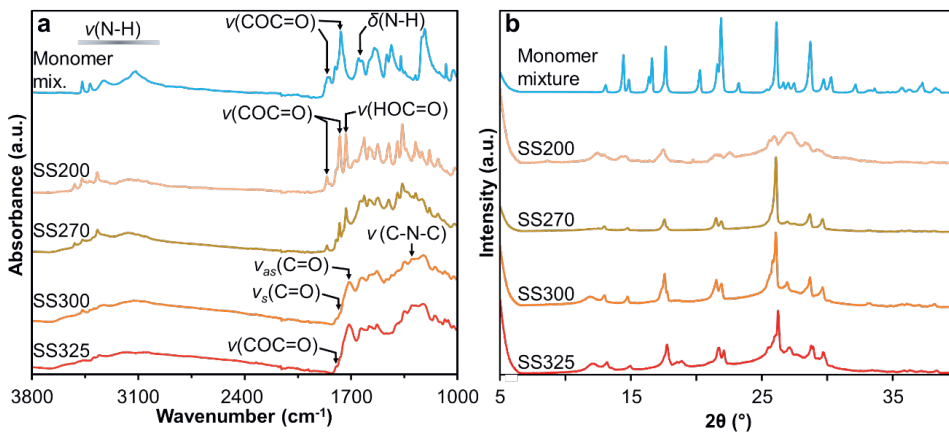
Figure 6.2: FTIR spectra (a) and XRD patterns (b) of the monomer mixture and reaction products after solid-state reaction at 200, 270, 300, and 325 °C.

A method to reduce the energy needed to achieve the desired structural orientation is by conducting the synthesis using solvothermal (ST) conditions. The ST approach uses a solvent mixture to solubilize the two monomers at relatively low temperatures (160 – 250 °C) and in a sealed vessel. Typically, a mixture of n-methyl-2-pyrrolidone

218

(NMP) and mesitylene is used, including a basic catalyst (e.g., isoquinoline) to enhance the reactivity between the monomers, PMDA and MA.[6]

The FTIR spectrum of the ST200 sample prepared at 200 °C is provided in Figure 6.3a and compared with solid-state samples prepared at 200 and 300 °C. The formation of polyimide material in the ST200 sample is confirmed by the presence of the characteristic vibration bands of the cyclic imide group between 1786 to 1727 cm^{-1} and at approximately 1350 cm^{-1}. No other C=O absorption bands are present in the FTIR spectrum, which was not the case at the same synthesis temperature with the SS method (Figure 6.2a, SS200). Compared with the SS300 sample (Figure 6.2a) where FTIR shows the PI formation, the presence of intermediate products is visible in the spectrum, showing that the solvothermal synthesis leads to PIs with higher purity.

The XRD diffractogram of the ST200 sample (Figure 6.3b) shows some degree of order with two broad diffraction peaks cantered at 13.5 – 18° (2θ) and 27.5° (2θ). This semicrystalline crystal phase, called here B, differs significantly from the crystal structure formed under solid-state conditions by the presence of broad diffraction peaks (Figure 6.2b). This means that in the liquid phase, the intermediate product formed between the two monomers before the imide formation differs significantly from the intermediate product formed in the solid-state. This can potentially alter the final crystal structure of the final PI material. Nevertheless, the PI product formed via the ST method still results in a relatively crystalline structure. Although, on the other hand, ST200 was formed after 5 days of reaction time, which is significantly more than the 15h used to form the solid-state samples SS300 and SS325, that procedure makes use of a toxic solvent that can limit its application.

With the aim of designing a synthesis approach that combined the advantages of the solid-state and solvothermal synthesis methods, the "solid-state through pre-organization"(SSP) route was designed to use a solvent in which a supramolecular network is formed, precipitated, and thermally treated in the solid-state to form a crystalline PI at either 250 or 325 °C. In this chapter, three different solvents were used to prepare the supramolecular networks: NMP, water, and a formic acid aqueous solution.
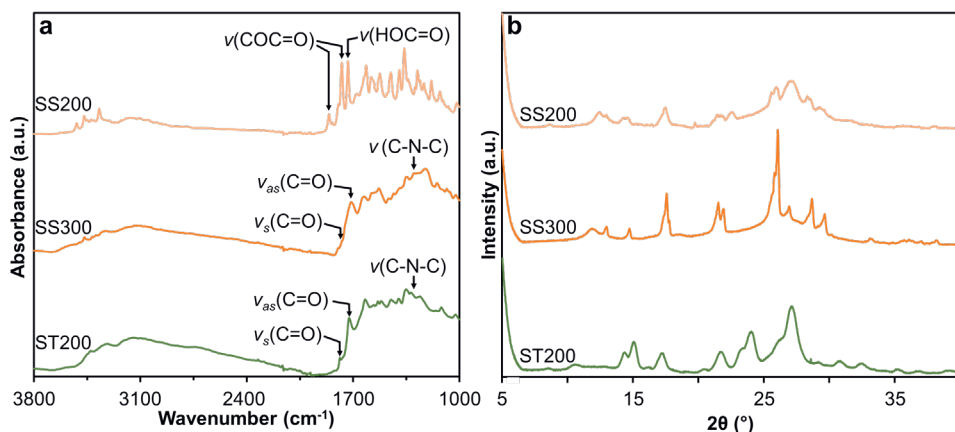
Figure 6.3: FTIR spectra (a) and XRD patterns (b) of samples prepared via the solid-state reaction at 200 (SS200) and 300 °C (SS300), and the sample ST200 prepared via the solvothermal synthesis.

The FTIR spectra of the supramolecular networks prepared in NMP, water and formic acid aqueous solution are given in Figure 6.4 (I) a, b and c. Overall, regardless of the solvent used, the spectrum of the supramolecular networks share similar absorption bands with vibration above 3000 cm^{-1}, denoting the presence of primary amines (N-H) involved in hydrogen-bonded interactions with possibly PMA molecules.[16] Between 3000 and 2000 cm^{-1}, the broad bands are attributed to the acidic proton attached to the aromatic nitrogen in the melamine ring (N-H$^+$).[16] The bands at 1637 and 1609 cm^{-1} are ascribed to the deformation of the primary (N-H) and tertiary amines (N-H$^+$).[16] Furthermore, the absorption bands at 1707 and 1670 cm^{-1} originate from the vibrations of the C=O bond of the carboxylic acid group.[16] Therefore, no chemical reaction is observed by FTIR between the two monomers in solution, but rather a supramolecular network is formed in all cases, which seems to be the product of transient bonding (hydrogen and ion bonds). Remarkably, the solvation of MA in both NMP and water/formic acid did not result in significant differences in the FTIR spectrum of the supramolecular network. This suggests that in water, MA can solubilize partially but quickly precipitates when it comes in contact with PMA as the supramolecular network seems to form instantaneously.

XRD analysis was used to study the crystallinity of the supramolecular networks produced via the SPP method, and the results are provided in Figure 6.5 I. Overall, the three supramolecular networks exhibited similar diffraction patterns, indicating a relatively structured network formed in solution. However, the network formed in NMP (Figure 6.5a, I) shows a higher degree of crystallinity, as the diffraction bands between 25 – 30° are less intense. Therefore, while the spectroscopic characteristics are similar between each supramolecular network, the structure obtained in NMP

differs slightly from the ones prepared in water or an aqueous solution of formic acid. This can be related to the aprotic polar character of NMP that allows for the dissolution of the kinetically controlled network, which can subsequently reorganize to the more desirable and crystalline thermodynamically controlled network. In comparison, water's polar protic nature instantaneously induces the network formation, resulting in the formation of the kinetically controlled product and, thus a more distorted structure.

After thermal treatment of the supramolecular networks at 250 and 325 °C, significant changes in the function of the temperature are observed via FTIR (Figure 6.4 II and III) and XRD (Figure 6.5 II and III) analysis. FTIR analysis shows a broad triplet band above 3000 cm^{-1}, indicating the presence of amine in samples. Still, the vibration bands at 1787, 1728, and 1358 cm^{-1} characteristic of the C=O and C-N-C bonds of the imide group are observed. Thus, confirming the formation of PI in all three samples prepared at 250 and 325 °C. Furthermore, thermal treatment of the solid supramolecular networks at 250 °C resulted in PI materials with high purity, as starting or intermediate groups are not observed. Thus, we observe with FTIR for the first time that the solid-state reaction of a supramolecular network consisting of PMA and MA takes place at temperatures below the melting point of PMA (250 °C) without using a catalyst or a eutectic mixture to lower the reaction temperature.[13]
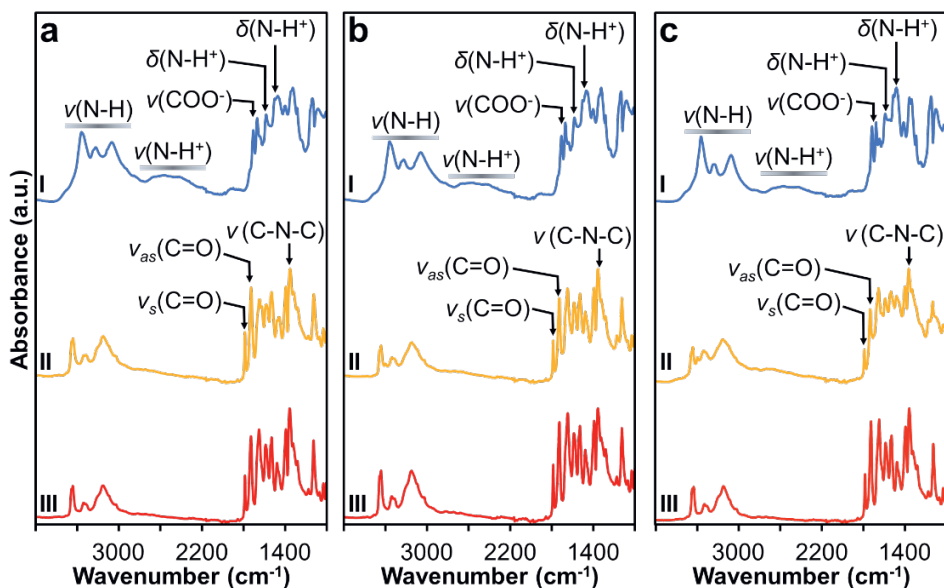
Figure 6.4: FTIR results of the supramolecular network precursors (I) before and after thermal treatment at 250 °C (II) and 325 °C (III) via the SSP method using NMP (a), water (b), or water/formic acid (c) as solvent.

The samples treated at 250 °C (Figure 6.5a II and b II) starting from the supramolecular networks formed in either NMP or water show significant but similar structural changes by XRD compared to their individual supramolecular precursors (Figure 6.5a I and b I). In comparison, the thermal treatment at 250 °C of the supramolecular network formed in the formic acid aqueous solution shows a very particular crystal structure (Figure 6.5c II). This could be attributed to the presence of formic acid molecules in the medium that could interfere with the coordination between the two monomers, whereas with NMP and water, there is no competition between the monomer/solvent molecules.

At 325 °C, all samples independent of the solvent used for the pre-reorganization step present identical crystal structures here named phase C. This crystalline phase is characterized by low-intensity diffraction peaks located at 7, 11.9, and 13°, a very intense diffraction peak at 14.5°, and a region with several reflexes between 21.9 and 28.8°. Compared to the samples treated at 250 °C, we assume that the crystal structure obtained at 325 °C presents an increased aromatic ring rotation as more energy is provided to the system, allowing the polymer to acquire a more thermodynamically stable configuration. For instance, this can be related to the free electron pair on the nitrogen atoms of the triazine rings that overlap with the free electron pair on the oxygen atom of the carbonyl group (part of the imide ring.
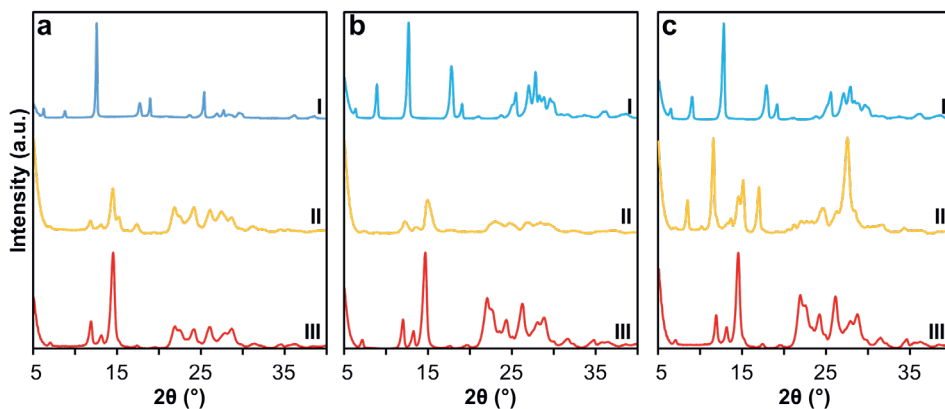
Figure 6.5: XRD patterns of the materials produced via the SSP method using either NMP (a), water (b) or formic acid aqueous solution (c) as solvent: the supramolecular networks (I) and samples treated at 250 (II) and 325 °C (III).

Remarkably, when the aqueous SSP method was performed with shorter reaction times of 5h a pure PI material was formed (Figure S6.8a II) and XRD (Figure S6.9a II). On the other hand, treatment of the supramolecular network, precipitated through the aqueous formic acid solution, at 250 °C for 5h resulted in a product that was partially imidized, as is evident from the presence of the C=O band of the amide group (Figure S6.8b). The partial imidization seems related to the formic acid in the supramolecular network. Due to the carboxylate group, formic acid can coordinate with MA and interrupt the reaction between PMA and MA. The presence of formic acid in the supramolecular network is not observed with FTIR as formic acid is the smallest of the carboxylic acids, and significant differences in the IR region are not expected with the supramolecular networks. An alternative explanation can be that the formic acid, similarly to PMA, reacts with MA to form an amide bond which hinders or slows down the formation of the imide bond. However, as thermal treatment of the supramolecular network after 15h at 250 °C results in a pure PI material, as shown by FTIR (Figure 6.4c, II), the amide formed between formic acid and MA is either not attained or is reversible at 250 °C.

Morphological analysis of the different powder samples produced in this work was done by scanning electron microscopy (SEM), and the results are given in Figure 6.6. The powders exhibit a large variation in morphology. Phase A obtained by SS reaction yielded relatively large and dense PI particles, ranging in size between 15 and 100 μm. The phase B (ST method) appeared to be made of lamellar particles assembled in a homogeneous flower-like structure with "petals" of 1 – 10 μm in length. The phase C obtained by the SSP method led to completely different macrostructures. The sample prepared in NMP shows micrometre-sized rod-like

223

structures. In water, smaller round particles clustered together into larger agglomerates are observed. However, with the aqueous solution of formic acid, nanocrystallites agglomerated on a dense structure are visible.
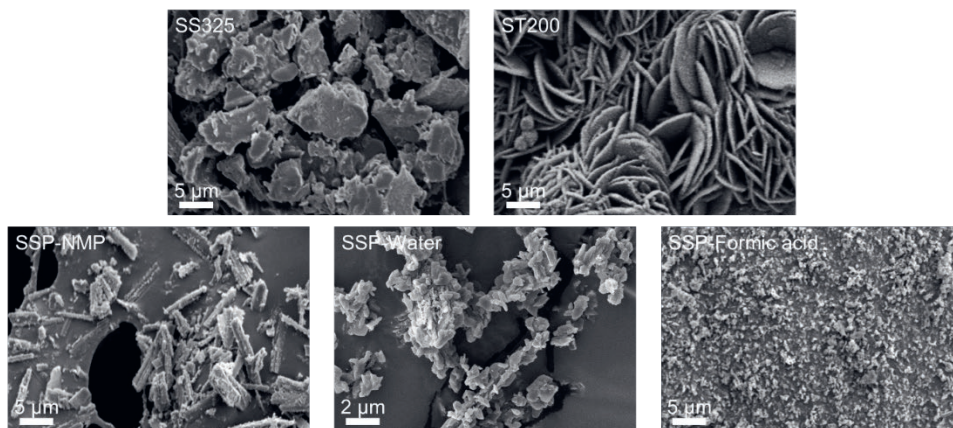
Figure 6.6: SEM micrographs of the different PIs crystal phases obtained by the different methodologies used in this work: phase A (SS325), phase B (ST200), and phase C (SSP-NMP, SSP-Water, and SSP-Formic acid).

6.3.2. Reflection on the possible formation mechanisms

FTIR showed that imide formation occurs throughout the different synthesis approaches used in this work, with the SS method leading to a slightly less pure product. XRD analysis indicated that each synthetic method used led to a different crystal structure named here A, B, and C. The mechanism for the imide formation, as shown in Figure 6.7, is overall similar and independent of the synthesis method used. First, the primary amine of MA attacks the anhydride (Figure 6.7, ①) or carboxylic acid (Figure 6.7, ②), forming an amic acid intermediate (Figure 6.7, ③ or ④) which depending on the orientation of the amide either undergoes rotation around the amide bond to approach the carboxylic acid or immediately undergoes the ring-closing reaction and forms the imide product (Figure 6.7, ⑤).[17] The main difference between the different reaction methods is the amic acid intermediate's lifetime; at higher temperatures, the ring-closing reaction occurs significantly faster, and the intermediate is consumed as fast as it forms.[17] As the mechanism is similar and independent of the synthesis, the differences observed in crystal structures between the phase A, B, and C must depend on the orientation of the monomers (beginning of the reaction), oligomers (middle of the reaction), and macromolecules (towards the end of the reaction) while they approach one another to react and form the irreversible imide ring. With this in mind, the presence of different molecules (solvent, catalysts, etc.) can significantly affect the final orientation of the polyimide and, thus of their crystal structure.

224

In the solid-state, the monomer mixture used shows no reaction at room temperature, and the pristine monomers' crystal structures are not affected by mixing (FTIR and XRD). In Figure 6.8b, PMDA molecules form clusters stabilized by dipole interactions.[18] MA is involved in strong intermolecular hydrogen bonds via the primary amines and aromatic nitrogen on the triazine ring (Figure 6.8b, green broken lines).[19] These intermolecular interactions keep the two monomers from mixing and only allow the solid-state reaction to commence at temperatures where the intermolecular interactions break or are near the melting point of PMDA. Above this critical temperature, the reaction towards the intermediate (Figure 6.7, ③ or ④) will occur quickly. Thus, the SS reaction will depend on the homogeneity of the monomer mixture, as MA molecules will react quickly with adjacent PMDA molecules. On the other hand, far apart molecules will need to melt and approach each other to react, which can be the reason for partial reactivity at temperatures above 270 °C and below the melting point of PMDA (293 °C).
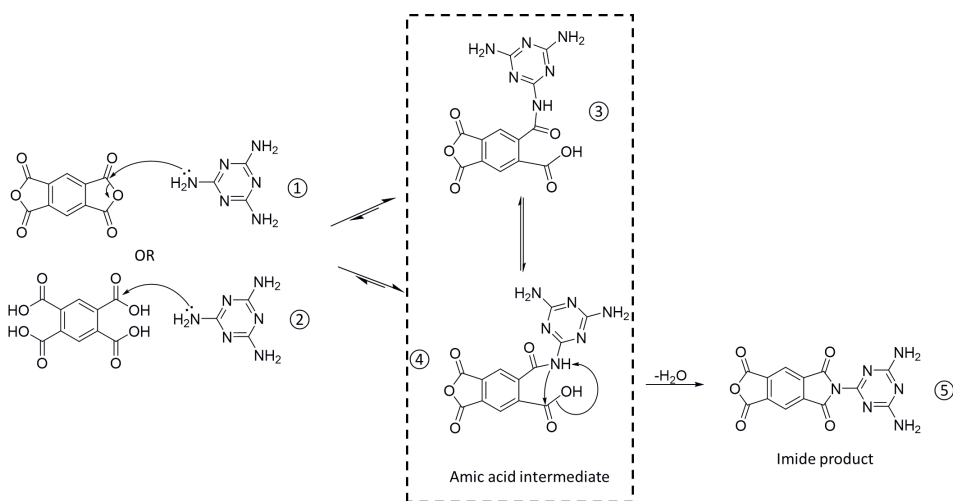
Figure 6.7: Mechanism of imide formation.[17]

In the ST synthesis, both monomers are in solution (> 100 °C) and are surrounded by the different solvent molecules. As the solvent molecules can affect the way PMDA and MA interact, the crystal phase B formed is different from the phase A (SS route). It is essential to mention that by comparing the crystallinity obtained under reflux conditions[20] and under ST conditions (Figure 6.3b, ST200), the utilization of a closed vessel does not show any significant effect on the crystallinity of the final PI. Furthermore, comparing the crystal structure obtained in only NMP under ST conditions,[21] the crystal structure of the PI formed still exhibits a similar crystal structure as with the ST200, which is formed in a solvent mixture consisting of NMP, mesitylene, and the basic catalyst isoquinoline. This means that only the

presence of NMP can affect the crystal structure, but mesitylene and isoquinoline do not significantly affect the orientation of the two monomers during the polyimidization reaction.

Similarly, the crystal structure of the supramolecular network formed from NMP or aqueous solutions is affected by the presence of the solvent molecules. Still, a significantly different crystal structure is obtained (phase C) via the SSP synthetic method than via the ST synthesis. This can be in relation to the precipitation of the supramolecular network and elimination of the solvent molecules from the network, which facilitates a different orientation of the monomers. As shown via computational modeling (Figure 6.8c), the two monomers interact strongly and are close to one another via hydrogen or ionic bonding. Their interaction allows the polyimidization reaction to occur at lower temperatures before PMA (281 °C) melts. In the aqueous solution of formic acid, the supramolecular network formed shows a similar crystal structure as the one formed in water. However, complete polyimidization occurred in water at 250 °C for 5h reaction time, whereas 15h was required when using a formic acid aqueous solution. Thus, we can safely assume that formic acid molecules remain in the network after precipitation and affect the reaction between PMA and MA.
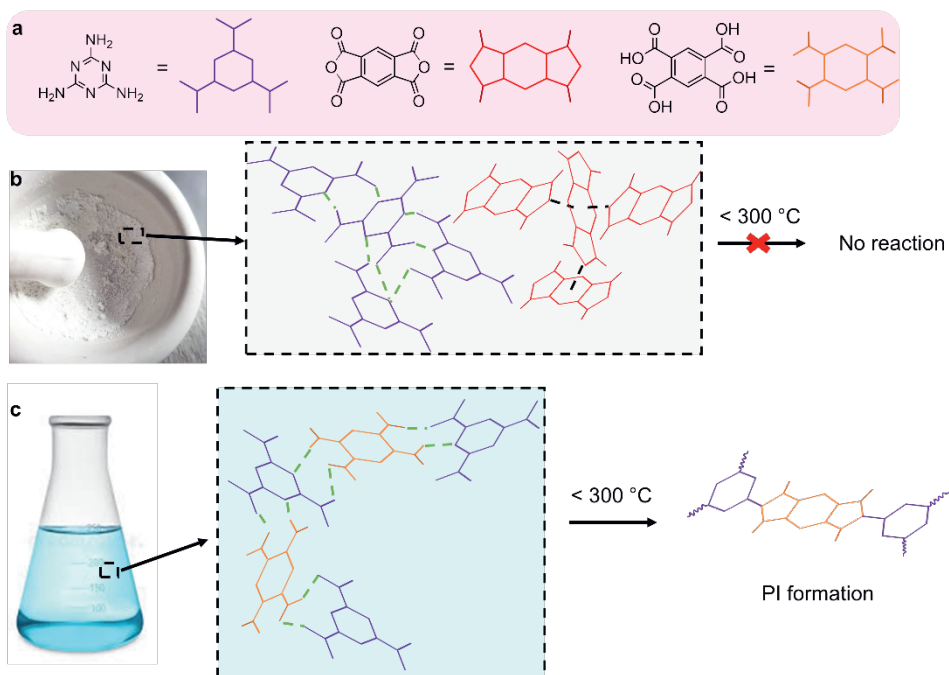
Figure 6.8: Schematic representation of the starting monomers (a), the solid precursor of the SS reaction (b) and the supramolecular precursor for the SSP reaction (c). The broken lines indicate either hydrogen or ionic bonding (green) and dipole interactions (black). The structural conformation for MA was adopted from [19] and for PMDA from [18]. The conformation for the supramolecular network was acquired on a Spartan '14.

6.3.3. Preparation of a first porous layer

The PI materials formed throughout this work exhibited good purities, and three different crystal structures were prepared. The SS and SSP methods can be regarded as green methods, whereas the ST methods use toxic solvents (such as NMP) and produce harmful waste. Compared to the SS method, the SSP method resulted in PIs with better purity and at lower reaction temperatures. The SSP method requires only simple equipment and can be performed in water and at ambient pressure. The simplicity and green character of the aqueous SSP methods means that it can be upscaled more easily than conventional methods. An additional advantage of the aqueous SSP method is that the solvation of the monomers can allow for the application of the PI network directly on top of a porous substrate. Therefore, as a proof-of-concept test, the supramolecular network was formed directly on top of a commercial flat-sheet mesoporous alumina support. Alumina flat-sheet supports are

regularly used as support to prepare nanofiltration membranes for lab-scale applications.[20,22] The alumina support was first impregnated under vacuum with a MA formic acid aqueous solution. Then, the impregnated support was transferred in a PMA aqueous solution, which resulted in precipitation of the supramolecular network. Finally, the samples were thermally treated for 15h. Two samples were prepared in this way, with two different monomer concentrations. The samples were analysed with FTIR and cyclohexane permporometry to investigate whether a PI is present on the support and any potential pore size change.

FTIR analysis provided in Figure S6.10 shows that a PI material was formed for both samples. However, at lower monomer concentrations, unreactive PMA remained on the surface of the support. On the other hand, with higher concentrations, a pure PI material formed. The pore size analysis (Figure S6.11) shows that for both samples, a pore shrinkage was observed, with the sample with a higher monomer concentration yielding a larger pore diameter shrinkage from 5.5 nm (pristine support) to 3 nm. These preliminary results suggest that the aqueous SSP method can potentially be used not only for forming a free-standing PI material but also for coating supports with a PI network. Still, further investigation is needed to assess the crystal structure and optimize the coating method to form potentially functional hybrid PI-coated inorganic materials for, e.g., membrane applications.

6.4. Conclusion

Melamine-based polyimide materials were prepared via solvothermal and solid-state synthesis methods and compared with a new, straightforward method that involves the solid-state reaction of a supramolecular network below the melting point of both monomers, the so-called SSP method (Solid-state through Pre-organization). Here, the starting monomers were dissolved (e.g., in water) to form a supramolecular network which precipitated rapidly from the solution. Subsequent thermal treatment of the solid led to the formation of a PI material. All the methods used in this work resulted in the formation of PI materials, as analysed by FTIR, and three crystal phases were determined by XRD analysis. By using a solvent in the ambient atmosphere, the SSP method overcame the energy barrier typically observed with solid-state methods, leading to the reaction of the two monomers below their melting points. Such methods allow for greener (aqueous SSP) and cheaper (reaction duration of 5h) synthesis routes for forming high-performance polymers. Furthermore, the SSP method can be expanded to accommodate other monomers that are thermally sensitive and, therefore, cannot be used in traditional solid-state syntheses. Besides, using a solvent to form the supramolecular precursor means that the method can be potentially applied for the synthesis of free-standing polymers and coating substrates for applications such as coating electronics, batteries, and more.[23] Additionally, the

SSP method was used to coat a porous inorganic substrate to demonstrate the applicability of the method.

6.5. Supporting Information

1. Spectroscopic characterization of starting and synthesized materials
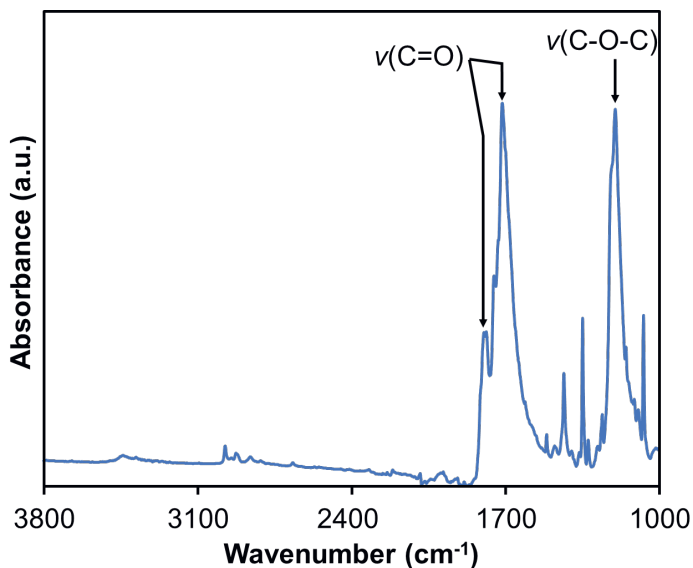
Figure S6.1: FTIR spectrum of the pristine PMDA.
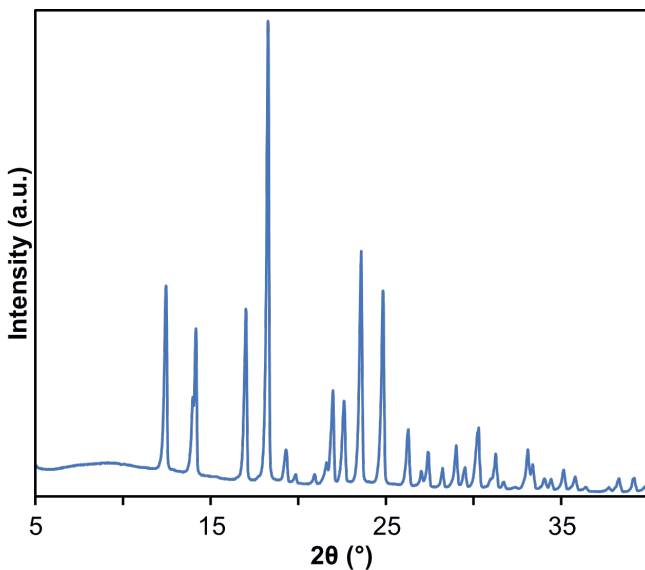
Figure S6.2: XRD diffractogram of the pristine PMDA.
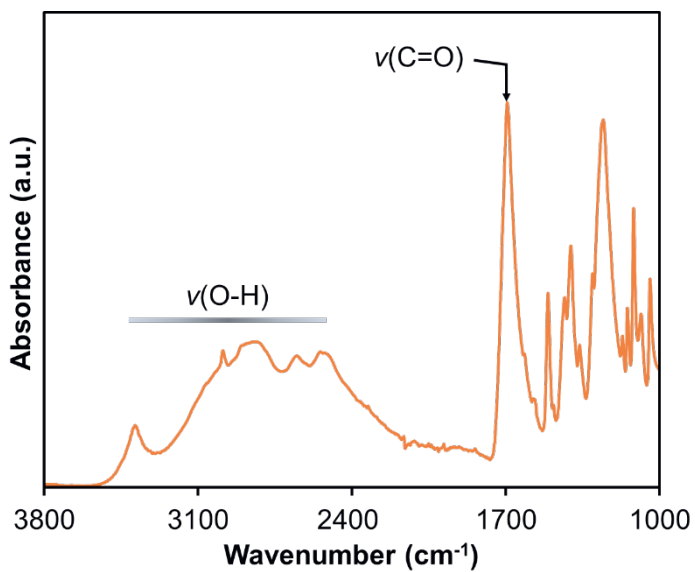
Figure S6.3: FTIR spectrum of the pristine PMA.
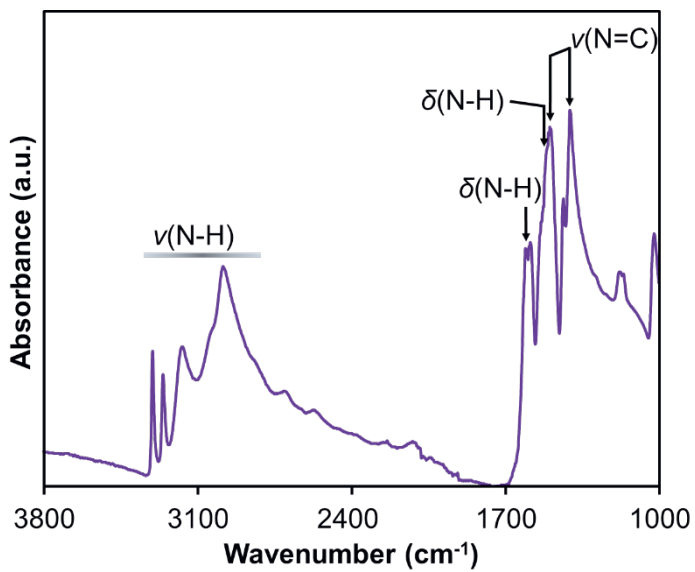
Figure S6.4: FTIR spectrum of the pristine MA.
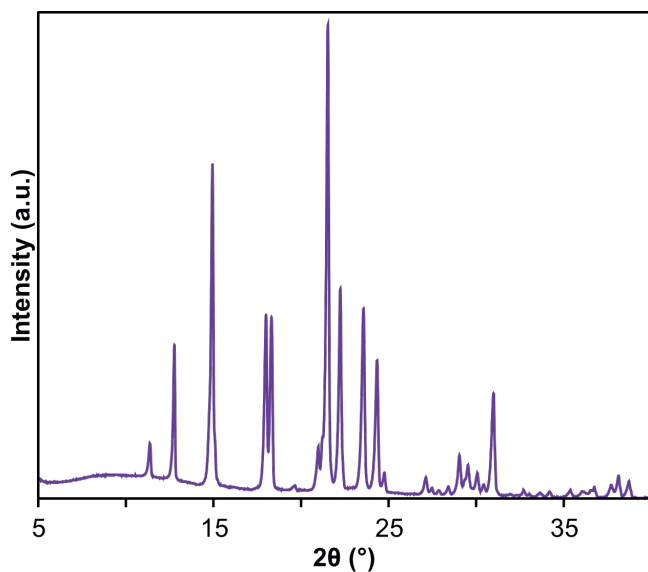
Figure S6.5: XRD diffractogram of the pristine MA.
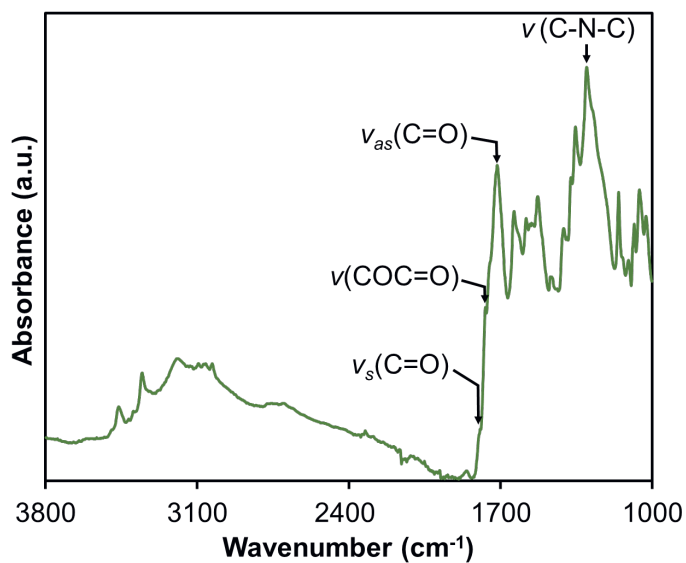
Figure S6.6: FTIR spectrum of the solid state product prepared with an 1:1 monomer ratio (PMDA:MA) and at 325 °C for 5h under N_2.
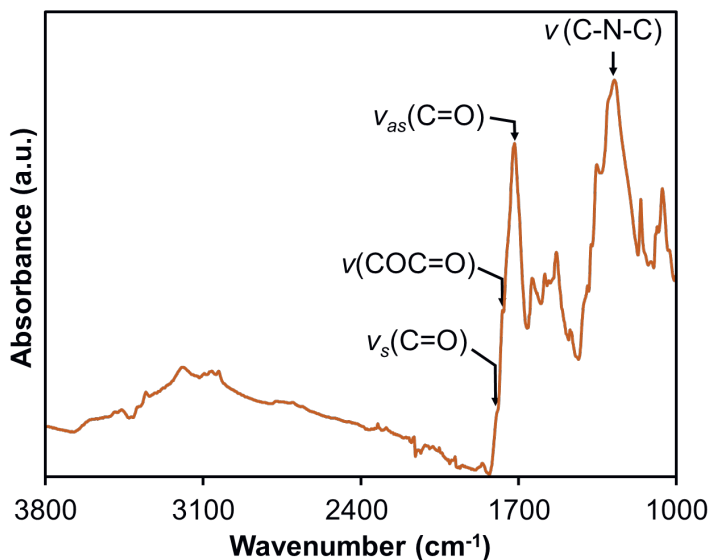
Figure S6.7: FTIR spectrum of the solid-state product prepared with a 1.5:1 monomer ratio (PMDA:MA) and at 325 °C for 15h under N_2.
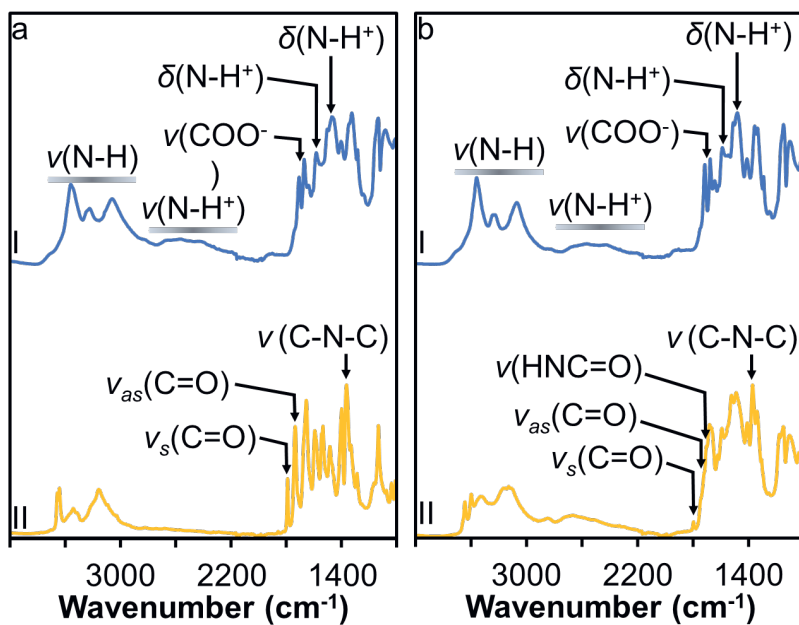
Figure S6.8: FTIR spectra of the supramolecular precursors (I) formed in water (a) and water/formic acid (b) and the thermally treated material at 250 °C for 5h under N_2 (II).

2. X-ray diffraction analysis of precursors and synthesized materials
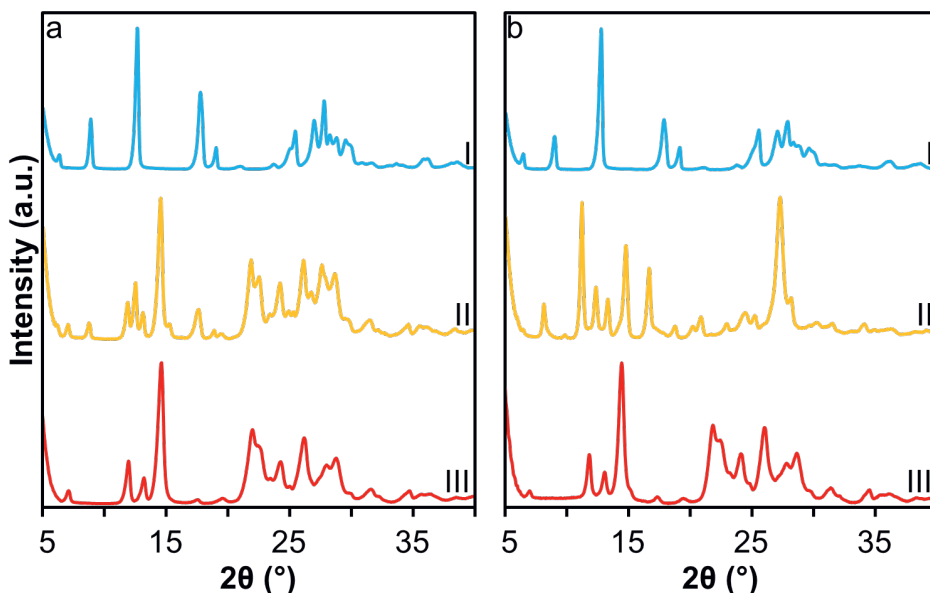
Figure S6.9: XRD diffractograms of the supramolecular networks (I) formed in water (a) or water/formic acid (b) and subsequently thermally treated at 250 °C for 5 h (II) or 15 h (III).

3. Analysis of the porous polyimide layer coated on an alumina substrate
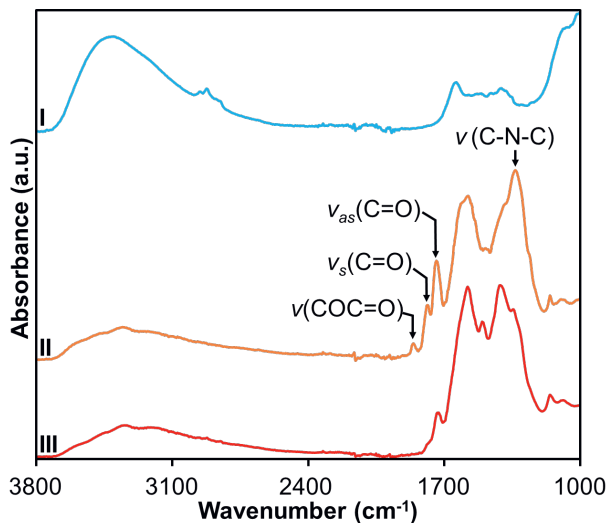
Figure S6.10: FTIR spectra of the pristine porous alumina support (I), PI coated with low monomer concentration (II) and PI coated with high concentration (III).

Cyclohexane permporometry is used for measuring the pore size distribution of mesoporous materials. This is done by filling the active pores (open) with cyclohexane through capillary condensation (saturated environment). Then the cyclohexane partial pressure is reduced, and oxygen can pass through the pores as they slowly open. The oxygen permeance is measured at the bottom side of the substrate. At cyclohexane relative pressures above 0.5, the pristine support (Figure S6.11, I) has all pores plugged and shows a significant drop in oxygen permeance. As the relative decreases from 0.5 to 0.4, the oxygen permeance increases significantly (steep transition). This means that the pores have opened due to cyclohexane desorption. As the pores open together, the transition from plugged pores to open (t-layer remains) is steep. Further lowering of the cyclohexane relative pressure leads to further pore opening (desorption), however insignificant as only the t-layer is gradually reduced. To calculate the pore radius, the Kelvin equation is used, shown below:

$$lnP_r = -\frac{n\gamma_s v cos\theta}{r_K RT} \qquad (1)$$

where P_r is the relative cyclohexane vapor pressure, n is a prosses parameter (for adsorption 1 and for desorption 2), γ_s is the gas-solid interfacial tension (J m^{-2}), v is the molar volume of cyclohexane (m^3 mol^{-1}), θ is the contact angle ($°$), and r_K is the Kelvin radius (m), R is the gas constant (J mol^{-1} K^{-1}) and T the temperature (K). According to the Kelvin equation (1), the pore opens gradually as a function of the relative cyclohexane pressure. Larger pores open first, followed by smaller pores, and at relative pressures near 0, all the pores are opened. Below relative pressures of 0.5, the larger pores will open. Most pores will open together as the pristine support has a relatively narrow pore size distribution. Smaller pores will open below 0.4 relative cyclohexane pressure. Coating the support with a PI material via the SSP method moves the transition point to lower partial pressures, as shown in Figure S6.11a (II and III). This means that the coating of the substrate led to pore shrinkage.
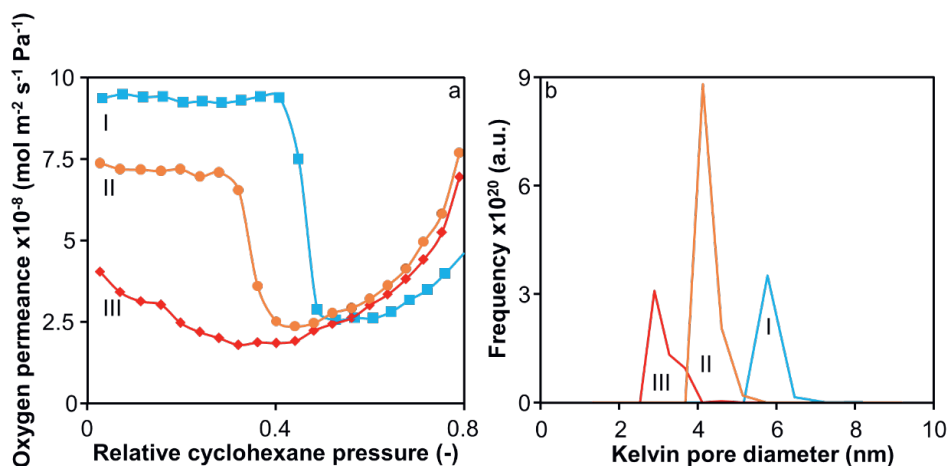
Figure S6.11: Cyclohexane permporometry analysis. (a) Oxygen permeance over the relative cyclohexane pressure of the pristine alumina support (I), PI coated with low monomer concentration (II), and PI coated with high concentration (III). (b) The calculated Kelvin pore diameters of the pristine alumina support (I), PI coated with low monomer concentration (II), and PI coated with high concentration (III).

6.6. References

(1)   Baumgartner, B.; Bojdys, M. J.; Unterlass, M. M. Geomimetics for Green Polymer Synthesis: Highly Ordered Polyimides via Hydrothermal Techniques. *Polym. Chem.* **2014**, *5*, 3727–3938. https://doi.org/10.1039/c4py00263f.

(2)   Vanherck, K.; Koeckelberghs, G.; Vankelecom, I. F. J. Crosslinking Polyimides for Membrane Applications: A Review. *Prog. Polym. Sci.* **2013**, *38* (6), 874–896. https://doi.org/10.1016/j.progpolymsci.2012.11.001.

(3)   Ding, S. Y.; Wang, W. Covalent Organic Frameworks (COFs): From Design to Applications. *Chemical Society Reviews*. January 21, 2013, pp 548–568. https://doi.org/10.1039/c2cs35072f.

(4)   Taublaender, M. J.; Glöcklhofer, F.; Marchetti-Deschmann, M.; Unterlass, M. M. Green and Rapid Hydrothermal Crystallization and Synthesis of Fully Conjugated Aromatic Compounds. *Angew. Chemie Int. Ed.* **2018**, *57* (38), 12270–12274. https://doi.org/10.1002/anie.201801277.

(5)   Yaghi, O. M.; O'Keeffe, M.; Ockwig, N. W.; Chae, H. K.; Eddaoudi, M.; Kim, J. Reticular Synthesis and the Design of New Materials. *Nat. 2003 4236941* **2003**, *423* (6941), 705–714. https://doi.org/10.1038/nature01650.

(6)   Fang, Q.; Zhuang, Z.; Gu, S.; Kaspar, R. B.; Zheng, J.; Wang, J.; Qiu, S.; Yan, Y. Designed Synthesis of Large-Pore Crystalline Polyimide Covalent Organic Frameworks. *Nat.   Commun.*   **2014**,   *5*   (1),   4503.

https://doi.org/10.1038/ncomms5503.

(7)   Duan, H.; Lyu, P.; Liu, J.; Zhao, Y.; Xu, Y. Semiconducting Crystalline Two-Dimensional Polyimide Nanosheets with Superior Sodium Storage Properties. *ACS Nano* **2019**, *13*, 2473–2480. https://doi.org/10.1021/acsnano.8b09416.

(8)   Baumgartner, B.; Puchberger, M.; Unterlass, M. M. Towards a General Understanding of Hydrothermal Polymerization of Polyimides. *Polym. Chem.* **2015**, *6* (31), 5773–5781. https://doi.org/10.1039/c5py00231a.

(9)   Taublaender, M. J.; Reiter, M.; Unterlass, M. M. Highly Crystalline, Nanostructured Polyimide Microparticles via Green and Tunable Solvothermal Polymerization. *Macromolecules* **2019**, *52* (16), 6318–6329. https://doi.org/10.1021/acs.macromol.9b00985.

(10)   Lahnsteiner, M.; Caldera, M.; Moura, H. M.; Cerrón-Infantes, D. A.; Roeser, J.; Konegger, T.; Thomas, A.; Menche, J.; Unterlass, M. M. Hydrothermal Polymerization of Porous Aromatic Polyimide Networks and Machine Learning-Assisted Computational Morphology Evolution Interpretation. *J. Mater. Chem. A* **2021**, *9*, 19754–19769. https://doi.org/10.1039/d1ta01253c.

(11)   Wang, T.; Xue, R.; Chen, H.; Shi, P.; Lei, X.; Wei, Y.; Guo, H.; Yang, W. Preparation of Two New Polyimide Bond Linked Porous Covalent Organic Frameworks and Their Fluorescence Sensing Application for Sensitive and Selective Determination of Fe [3+]. *New J. Chem.* **2017**, *41* (23), 14272–14278. https://doi.org/10.1039/C7NJ02134H.

(12)   Li, Z.; Zhou, J.; Xu, R.; Liu, S.; Wang, Y.; Li, P.; Wu, W.; Wu, M. Synthesis of Three Dimensional Extended Conjugated Polyimide and Application as Sodium-Ion Battery Anode. *Chem. Eng. J.* **2016**, *287*, 516–522. https://doi.org/10.1016/j.cej.2015.11.063.

(13)   Maschita, J.; Banerjee, T.; Savasci, G.; Haase, F.; Ochsenfeld, C.; Lotsch, B. V. Ionothermal Synthesis of Imide-Linked Covalent Organic Frameworks. *Angew. Chemie* **2020**, *132* (36), 15880–15888. https://doi.org/10.1002/ange.202007372.

(14)   Cuperus, F. P.; Bargeman, D.; Smolders, C. A. Permporometry. The Determination of the Size Distribution of Active Pores in UF Membranes. *J. Membr. Sczence* **1992**, *71* (1–2), 57–67. https://doi.org/10.1016/0376-7388(92)85006-5.

(15)   Chu, S.; Wang, Y.; Guo, Y.; Zhou, P.; Yu, H.; Luo, L.; Kong, F.; Zou, Z. Facile Green Synthesis of Crystalline Polyimide Photocatalyst for Hydrogen Generation from Water †. *J. Mater. Chem.* **2012**, *22*, 15519. https://doi.org/10.1039/c2jm32595k.

(16)   Pretsch, E.; Bühlmann, P.; Affolter, C. *Structure Determination of Organic*

Compounds; 2000. https://doi.org/10.1007/978-3-662-04201-4.

(17) Ghosh, M. K.; Mittal, K. L. *Polyimides : Fundamentals and Applications*; Marcel Dekker, 1996.

(18) Pore, T.; Ernst, M.; Confalonieri, G. Premelting Anomalies in Pyromellitic Dianhydride: Negative Thermal Expansion, Accelerated Radiation Damage, and Polymorphic Phase Transition. *J. Phys. Chem. C* **2022**. https://doi.org/10.1021/acs.jpcc.2c00220.

(19) Yuan, X.; Luo, K.; Zhang, K.; He, J.; Zhao, Y.; Yu, D. Combinatorial Vibration-Mode Assignment for the FTIR Spectrum of Crystalline Melamine: A Strategic Approach toward Theoretical IR Vibrational Calculations of Triazine-Based Compounds. *J . Phys. Chem A* **2016**, *120*, 7427–7433. https://doi.org/10.1021/acs.jpca.6b06015.

(20) Kyriakou, N.; Winnubst, L.; Drobek, M.; De Beer, S.; Nijmeijer, A.; Pizzoccaro-Zilamy, M.-A. Controlled Nanoconfinement of Polyimide Networks in Mesoporous γ-Alumina Membranes for the Molecular Separation of Organic Dyes. *ACS Appl. Nano Mater* **2021**, *4*, 14035–14046. https://doi.org/10.1021/acsanm.1c03322.

(21) Duan, H.; Lyu, P.; Liu, J.; Zhao, Y.; Xu, Y. Semiconducting Crystalline Two-Dimensional Polyimide Nanosheets with Superior Sodium Storage Properties. *ACS Nano* **2019**, *13*, 2473–2480. https://doi.org/10.1021/acsnano.8b09416.

(22) Kyriakou, N.; Merlet, R. B.; Willott, J. D.; Nijmeijer, A.; Winnubst, L.; Pizzoccaro-Zilamy, M.-A. New Method toward a Robust Covalently Attached Cross-Linked Nanofiltration Membrane. *ACS Appl. Mater. Interfaces* **2020**, *12* (42), 47948–47956. https://doi.org/10.1021/acsami.0c13339.

(23) Sezer Hicyilmaz, A.; Ayse, ·; Bedeloglu, C. Applications of Polyimide Coatings: A Review. **2021**, *3*, 363. https://doi.org/10.1007/s42452-021-04362-5.

Chapter 7

Reflections and perspectives

7.1. Introduction

The work described in this thesis focuses on the preparation and application of organically-functionalized inorganic membranes for molecular separations of aqueous mixtures. In general, ceramic membranes are set strict requirements as they are primarily targeted for applications under extreme conditions such as separations at high temperatures or with reactive chemicals.[1] In the context of the molecular separations of an aqueous mixture, the membrane material selected must exhibit a high chemical resilience against the various mixtures for which they are used, but they still need to show good affinity towards those mixtures in order to perform well (meaning high solvent flux and solute retention). To achieve this, stable organically-functionalized inorganic membranes comprising irreversible chemical bonds are crucial throughout the whole membrane system, including the covalent bond between the inorganic and organic parts. Reversible chemical (C=N, C(O)OC, B-O-B etc.) and physical (dipole-dipole, hydrogen bonding etc.) bonds are sensitive to their environment and can break under even mild conditions, leading to membrane degradation. Therefore, this work was focused on chemically attaching small linear or cross-linked polymers on top or inside mesoporous γ-alumina layer coated on α-alumina supports.

Grafting of small polymers has been proven in the past[2–6] to yield chemically stable membranes in the presence of organic solvents (such as toluene, ethanol, hexane etc.). However, little has been done on the stability of grafted inorganic membranes in aqueous solutions or mixtures of water and solvent. Thus, further research was needed to understand and identify stable grafting methods for aqueous applications. Furthermore, the polymer should show a hydrophilic character and a hydrolytically stable bonding with the inorganic support to ensure a stable organic phase in water. In that sense, this work was focused on three main topics:

1. Study of the hydrolytic stability of covalent bond between the linking group and inorganic support

2. Controlled formation of the selective organic layer
    - 2.1. Polyethylene glycol (PEG) grafted membranes
    - 2.2. Polythioether (TE) grafted membranes
    - 2.3. Polyimide (PI) grafted membranes
3. Understanding the transport behaviour through the hybrid membranes developed in this work.

This chapter reflects on the above research lines, providing information on important findings, remaining challenges, and future opportunities generated through this work. The samples discussed in the following sections with their respective description and the respective chapters where they are discussed in detail are given in Table 7.1.

240

Table 7.1: Summary of samples described in this work with their respective sample codes, descriptions, and reference chapters.

Membrane	Description	Chapter #
γ-Al$_2$O$_3$	Pristine inorganic support	All
PEGPA	Pristine PEG(10)-phosphonic acid	2 & 3
MPEGPA	Pristine methoxy-PEG(10)-phosphonic acid	2 & 3
MePEG11Si	Methoxy-PEG(11)-silane grafted membrane	2
MePEG10PA	Methoxy-PEG(10)-phosphonic acid grafted membrane	2
PEG10PA	PEG(10)-phosphonic acid grafted membrane	2
GM150/200	Methoxy-PEG(10)-phosphonic acid grafted membrane at 150 or 200 °C	3
GP150/200	PEG(10)-phosphonic acid grafted membrane at 150 or 200 °C	3
Al-SiM/TE	Thioether-based network grafted membrane	4
A-1	Polyimide grafted membrane 1d reaction time, route A	5
A-5	Polyimide grafted membrane 5d reaction time, route A	5
B-1	Polyimide grafted membrane 1d reaction time, route B	5
B-5	Polyimide grafted membrane 5d reaction time, route B	5
A-5T	Polyimide grafted membrane 5d reaction, thermally post-treated	7.4

7.2. Hydrolytically stable covalent bond between the linking group and inorganic support

The first challenge was to obtain a chemical bond between the inorganic surface and organic moiety, which is stable under the desired membrane application, meaning, in our case, stable in an aqueous environment. In this work, inorganic supports were chemically functionalized with two different linking groups: organosilanes and organophosphonic acids. Organosilanes are most typically used in literature to link the organic and inorganic phases and were applied in the work described in Chapters 2, 4, and 5 of this thesis. Organosilanes are highly versatile as they can be grafted in both liquid (Chapter 2) and vapor phases (Chapters 4 and 5). There is a large availability of commercial organosilanes, which renders them highly important in the surface functionalization of inorganic materials. In this thesis, three types of organosilanes have been used to create different membranes. In Chapter 2, PEG-functionalized silanes were grafted on γ-alumina layers by a reflux grafting-to method. In contrast, in Chapters 4 and 5, smaller organosilanes (3-mercaptopropyl

trimethoxysilane or MPTMS and 3-aminopropyl triethoxysilane or APTES, respectively) were grafted via the vapor phase method on the outer surface of inorganic supports and were used as initiators for the polymerization reaction. This demonstrates the versatile character of organosilanes and their wide range of applications. However, organosilanes have the disadvantage of low hydrolytic stability, particularly when grafted on γ-alumina supports, as shown in Chapter 2 where the PEG-silane grafted membranes showed significant degradation in water, even after 24 h of testing. The results indicate that these PEG silanes can only be utilized for water-free applications, such as organic solvent nanofiltration (OSN). In Chapters 4 and 5, the organosilane grafted membranes were used as linkers where a polymeric network, either polythioether (TE) or polyimide (PI), was grown. These final TE or PI grafted hybrid organic-inorganic membranes were tested in an aqueous solution successfully without any performance change after testing for 48-96 h. It is expected that, due to the relatively bulky polymeric chain, the PEG-silane grafted membranes is a relatively sparsely grafted (low grafting density) (Figure 7.1a). On the other hand, vapor phase grafting of APTES has been shown to yield dense monolayers[7] (high grafting density) that are known to exhibit better hydrolytic stability (Figure 7.1b).[8] Still, to confirm that the grafting density can influence the hydrolytic stability of the graft, further investigation should be done on comparable systems. Additionally, the effect of the polymer properties (hydrophilic, hydrophobic, basic, acidic etc.) and the crosslinking degree should be further investigated on the hydrolytic stability of the organic layer. This can be done by permeating water through the different membranes for prolonged periods, as described in Chapter 2.
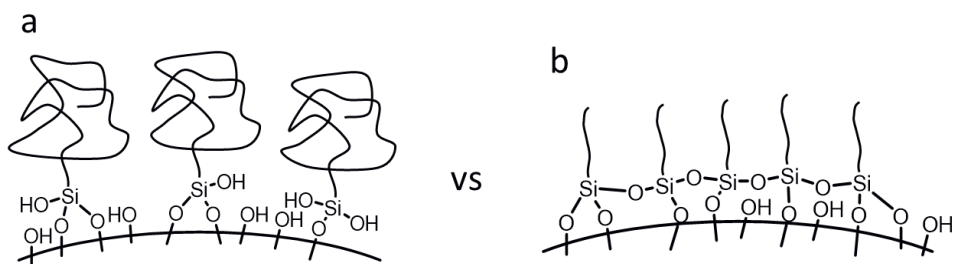
Figure 7.1: Schematic representation of grafting organosilane with a bulky (e.g., PEG) organic chain (a) and with a compact (small) molecule (e.g., MPTMS and APTES) (b). The organic chain's size (bulky character) can influence the grafting density on the inorganic surface as a steric hindrance from the organic tail hinders the reaction between adjacent aluminols and free organosilanes. Sparsely grafted surfaces (a) have easier access to water at the grafted site (Al-O-Si), which can lead to hydrolytic cleavage of covalent bonds. On the other hand, compact organic chains

lead to denser monolayers (b) and can have better "protection" against hydrolytic cleavage.

PEG-phosphonic acid grafted supports (Chapter 2) were clearly more stable in an aqueous environment than the PEG-silane grafted membranes, as they exhibited high hydrolytic stability up to 216h. A significant additional advantage of organophosphonic acids to organosilanes is that the grafting can be performed in water (Chapter 2), a green solvent, or in the solid-state with minimal amounts of solvents used (Chapter 3). In both cases, grafting led to hydrolytic stable hybrid membranes that performed well in aqueous media. Interestingly, both methods for organophosphonic acid grafting used simple laboratory tools (such as flasks and ovens) and were performed under mild conditions (100 – 200 °C, no anhydrous solvents etc.). This work also showed that organophosphonic acid grafting was affected by the functional groups on the organic chain. Particularly, polar groups, such as hydroxyl, resulted in lower grafting densities than apolar (alkyl) organic groups. Another issue of phosphonic acids is their acidic character, which can protonate the organic group that bears proton acceptors (e.g. amines) and form zwitterionic ions mostly soluble in water. An example is 3-aminopropyl phosphonic acid which, due to its zwitterionic character, can influence the grafting density on the inorganic surface.[9] In general, phosphonic acids are incredibly valuable as they form stable covalent bonds with γ-alumina and titania, do not promote homocondensation reactions, and can easily be prepared through the reaction between organophosphites and halogenated organic molecules. The latter allows for broadening the use of organic-phosphonic acids to a variety of specialty materials that are not commercially available.

In conclusion, the most suitable linking group depends strongly on the targeted application (anhydrous or aqueous environment), the materials used (polymers or small molecules), and the way of grafting (vapor or solution phase). In addition, the compatibility between the linking group and the type of inorganic support should be considered.[10]

7.3. Controlled formation of the selective organic layer

The application targeted in this work was the separation and purification of aqueous mixtures. Thus, the polymers chosen to functionalize the inorganic support must exhibit affinity toward the water. As such, polyethylene glycol (PEG), cross-linked thioether (TE), and cross-linked polyimide (PI) were used to functionalize mesoporous γ-alumina layer coated on α-alumina supports. All three polymers bear polar aprotic groups (Figure 7.2), which can act as hydrogen bond acceptors, as shown by water contact angle analysis on the grafted membrane surface (Figure 7.3). Overall, the water contact angles of the polymer grafted membranes were between

30 and 80°, indicating that the membrane surfaces remain relatively hydrophilic (water contact angles < 90°) after organic functionalization.
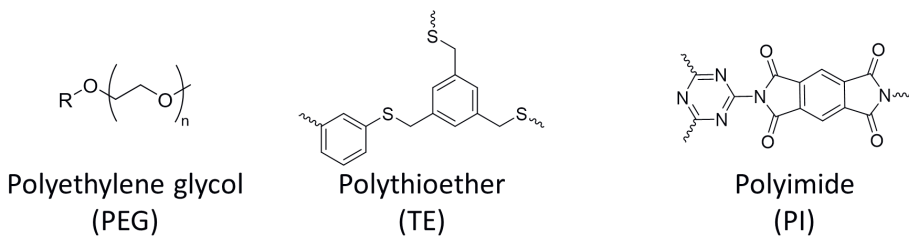
Figure 7.2: The three polymers used to functionalize the γ-alumina layer towards formation of hydrophilic hybrid organic-inorganic nanofiltration membranes.
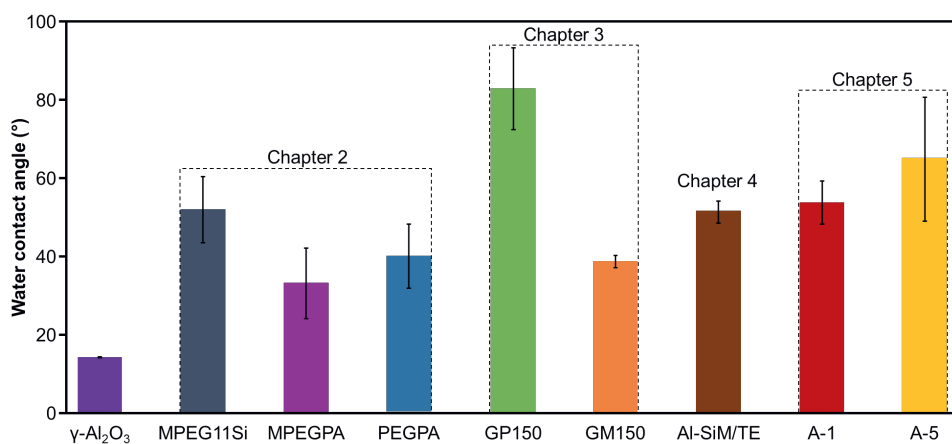
Figure 7.3: Water contact angle of selected membranes prepared in this work and compared with the pristine support (γ-Al₂O₃).

The methods used to graft the inorganic surface are categorized as grafting-to and grafting-from. As the polymer was grafted in one step, the PEG grafted membranes are categorized to the grafting-to method. On the other hand, the TE and PI grafted membranes are attributed to the grafting-from approach, as the polymer was grown in-situ from a grafted initiator on the inorganic surface. More information on the two methods can be found in the introduction (Chapter 1).

7.3.1. Polyethylene glycol (PEG) grafted membranes

In both Chapters 2 and 3, PEG-grafted membranes were prepared. The aim of the project was to functionalize the pore surface of the γ-alumina layer and shrink the pore diameter from 5.5 nm (pristine support) to 2 nm (limit of the cyclohexane

permporometry method used) or less. Two synthesis methods were applied: in Chapter 2 the fabrication was done in water under reflux conditions, whereas in Chapter 3 the grafting took place in the solid state. Both methods are simple, straightforward, and relative green techniques as small amounts of chemicals or green solvents are used.

The grafting reaction between PEG phosphonic acid and γ-alumina follows a condensation mechanism, where water is released as the by-product (Figures 7.4a and b). Two reaction pathways are at play during grafting of the organophosphonic acid with the inorganic surface; firstly, by nucleophilic attack from the aluminols on the inorganic surface (Figure 7.4a), and secondly, by coordination on a Lewis acid site (O-Al-O) and subsequent nucleophilic attack from adjacent hydroxyl groups (Figure 7.4b).[8] As γ-alumina layers are rich in both aluminols (Al-OH) and Lewis acid sites, they can react via both reaction pathways with PEG phosphonic acids. In water, γ-alumina is hydrated, and the Lewis acid sites can be blocked by adsorbed water molecules (Figure 7.4c, top), which means that coordination of the phosphoryl group with Lewis acid is not favoured. Additionally, as the inorganic surface is saturated with water, the equilibrium of the grafting reaction shifts towards the starting materials, leading to low reaction yields and densities. In the solid state (> 150 °C), the Lewis acid sites are free, allowing for the phosphoryl to coordinate, and the water by-product is quickly removed in the form of vapor (Figure 7.4d). As a result, the reaction yields and the grafting densities in the solid state are expected to be higher compared to solution-phase grafting in water. Comparing TGA results from the decomposition of MPEGPA (no intermolecular side reactions in the solid state), grafted γ-alumina flakes prepared in water (6% weight loss) or in the solid state (8% weight loss) show a 33% more weight loss with samples prepared in the solid state at 150 °C. Furthermore, the solid-state grafting at even higher temperatures (200 °C; 10% weight loss) resulted in higher weight losses of 67% compared to the solution phase grafting, indicating that in the solid-state, the grafting reaction is indeed favoured.
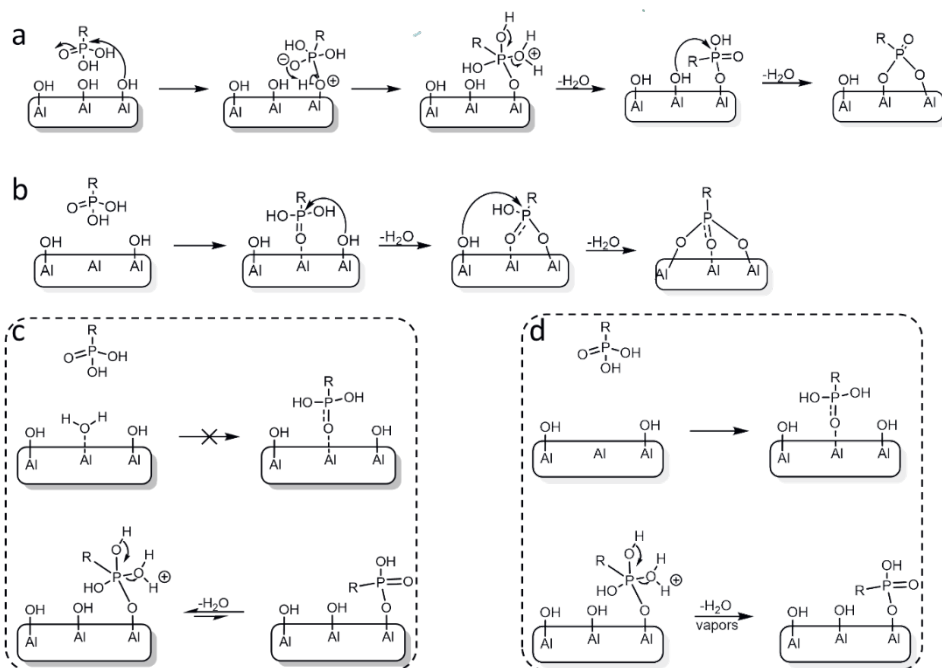
Figure 7.4: Schematic representation of condensation mechanisms between organophosphonic acids an alumina: (a) between an aluminol (Al-OH) and an organophosphonic acid (b) via coordination of the phosphoryl group (P=O) on a Lewis acid site (O-**Al**-O) and subsequent nucleophilic attack from an adjacent aluminol. (c) The proposed reaction mechanism occurs in water (Chapter 2). (d) The proposed reaction mechanism occurs in the solid state (Chapter 3).

Different polymers can be grafted in place of PEGs to control the polarity of the orgnanophosphonic acid grafted membranes. For example, in Chapter 3, the n-octadecyl phosphonic acid (ODPA) was grafted successfully in the solid state. However, due to the apolar nature of the ODPA, the hybrid grafted material can show more hydrophobic properties. In the same way, by grafting ODPA on inorganic membranes, hydrophobic membranes for organic solvent nanofiltration (OSN) can be made. Alternatively, the organically modified membranes' hydrophilicity (or polarity) can be increased further (lower contact angles) by employing polymers that exhibit stronger hydrogen bond donors or more polar groups, such as polyvinyl alcohol, polyacrylic acids or ionic polymers. As a result, more polar surfaces with lower water contact angles and hence potentially higher water fluxes can be obtained. However, using protic polar functional groups in these molecules can significantly affect the grafting reaction and potentially lead to undesired side products, as observed with PEGPA in Chapter 3. Stepwise formation of a highly polar polymeric layer can be done by protecting and thus deactivating the functional group (e.g.,

246

ester) and subsequently deprotecting after grafting (e.g., ester to carboxylic acid) to avoid undesirable side products during grafting.

Other important parameters that can influence the performance of the final hybrid organic-inorganic membrane are the pore diameter and tortuosity of the inorganic layer to be grafted. Using brush-like polymers, like the PEG-grafted membranes, higher grafting densities on the pore surface can result in smaller pore diameters. In Chapter 2, PEG phosphonic acid grafted membranes showed a small decrease in the pore diameter with pore shrinkages between 1.1 (PEGPA) and 1.5 nm (MPEGPA). On the other hand, in Chapter 3, impregnation combined with a solid-state reaction resulted in a larger decrease in pore diameter with a pore shrinkage of 2.1 nm for membranes prepared at 150 °C (GP/GM150) and 4 nm or more for membranes prepared at 200 °C (GP/GM200). As in both cases (described in respectively Chapters 2 and 3), PEG-grafted membranes were functionalized with PEG-phosphonic acids with a similar number of repeating units (n = 10). The observed pore diameter differences indicate an influence of the preparation method on the grafting densities. Higher grafting densities through the solid-state reaction result in more extended PEG chains and smaller pore diameters. Figure 7.5 shows three possible cases of an inorganic pore grafted with PEG. The first case (Figure 7.5a) shows an inorganic pore that exhibits low grafting density, allowing the polymeric chain to adopt a mushroom-like conformation, thus, leading to a low pore size shrinkage. The first case describes the membranes fabricated in Chapter 2. The second case (Figure 7.5b) shows an inorganic pore with grafting density leading to more extended polymeric chains and thus larger pore shrinkages. Finally, the third case (Figure 7.5c, top view) shows an inorganic pore with significantly higher grafting densities, which force the polymeric chains to extend towards the unreacted wall of the pore, hindering further grafting of PEG oligomers. As a result, the pore shrinks significantly, but the grafting remains inhomogeneous (Figure 7.5c, top and cross view). The PEG grafted membranes described in Chapter 3 can be categorized in the second and third cases (Figure 7.5b and c). The membrane performance section of this evaluation chapter will provide a more detailed discussion.
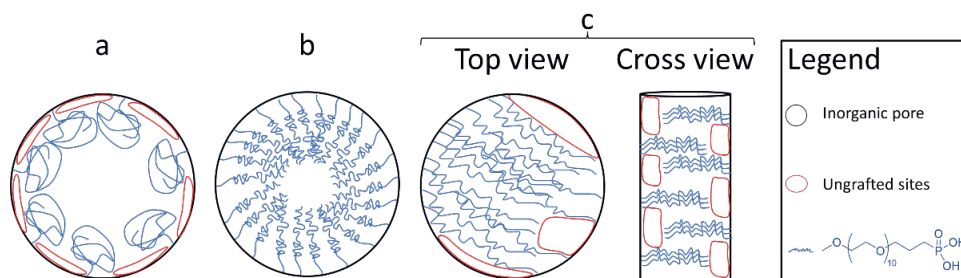
Figure 7.5: Schematic representation of the three possible cases of an inorganic pore grafted with PEG. At low grafting densities, the grafted species (blue colour) adopts a mushroom-like conformation, resulting in low pore diameter shrinkage (a). At high grafting densities, the PEG chains (blue colour) stretch out and significantly shrink the pore diameter (b). At extremely high grafting densities, the PEG chains overstretch and block potential grafting sites on the inorganic pore leading to seemingly low pore diameters but inhomogeneous grafting (c, top view). The cross view is also provided to show how the high grafting densities can influence the homogeneity of the grafted pore (c, cross view).

In conclusion, grafting with organophosphonic acids was possible in both water and in the solid state, with the latter leading to higher grafting densities. The goals of the two projects were achieved, but many questions remain open and will be discussed in section 7.4. Both methods are simple to perform and can be easily upscaled for industrial applications. A preliminary understanding of the structural characteristics of the PEG grafted membranes was done in Chapter 3. However, a deeper understanding of the grafting density and morphology of the pores after grafting needs to be done through more elaborate membrane performance tests. These will be discussed in section 7.4.

7.3.2. Polythioether (TE) grafted membranes

In Chapter 4 a novel preparation of a TE grafted membrane is described. The aim of the project was to prepare an ultrathin, chemically stable organic layer on top of porous inorganic supports. For the formation of the TE grafted membranes, the inorganic support was functionalized with 3-mercaptopropyl trimethoxysilane (MPTMS) under vapor phase conditions (CVD). The MPTMS was used as the initiator molecule from which the polymeric network was grown (grafting-from). In order to functionalize only the top surface of the inorganic support, a pore blocking agent (glycerol) was used. As a viscous high boiling point liquid, glycerol can infiltrate the mesoporous γ-alumina layer and remain there during the grafting reaction. Subsequently, two "click" reactions were used; firstly in solution between the grafted inorganic support and 1,3,5-tris(bromomethyl)benzene (3Br) under basic conditions and in the vapour phase with 1,3-benzenedithiol (2SH) at 80 °C for 4h.

Since the two monomers (3Br and 2SH) were in two different phases (liquid and gaseous), the reaction can occur at the interface between the gas and liquid phase.

During this research on TE grafted membranes, it was observed that the washing step after initiator grafting (CVD) played a significant role in the formation of a defect-free layer, as washing the initiator-grafted sample with anisole to remove unreacted MPTMS, did not wash out glycerol from the porous inorganic support. By blocking the inorganic pores with glycerol, diffusion of monomers inside the inorganic pores was hindered, resulting in the "click" reaction occurring on top of the support. On the other hand, when the initiator-grafted support (after CVD) was washed with water, a defected layer formed, showing that the washing step can be crucial in the reproducibility of the method as the presence of water in the solution can affect the subsequent fabrication steps.

Due to the high yield of "click" reactions, the organic layer was formed by using significantly lower amounts of starting materials (0.05 – 0.2 wt.%) than traditional interfacial polymerizations (1 – 3 wt.%). In addition, "click" reactions, as they are undisturbed by water, can be executed in the ambient atmosphere without the need to control the environment (e.g., glove box). Finally, "click" reactions generate minimal and harmless by-products and, therefore can be viewed as sustainable alternatives to traditional interfacial polymerizations. Furthermore, other "click" chemistry tools, such as the liquid/liquid[11] or vapor phase[12] azide-alkyne cycloaddition, can also be used as they form chemically robust covalent groups that can be used for aqueous nanofiltration applications.

The TE grafted membrane exhibited a water contact angle of ~50°, which indicates a hydrophilic surface. However, due to the apolar backbone of the TE network, it is assumed that the hydrophilicity of the layer can be increased more by using monomers that bear polar functional groups on the aromatic polymeric backbone, like hydroxyl or amine groups. As mentioned before, "click" reactions are orthogonal reactions, which means they can react in the presence of other reactive groups towards the desirable product. Hence, implementing "click" reactions in the membrane fabrication can facilitate the formation of membranes with a wider range of properties (charged, superhydrophilic, superhydrophobic etc.) in just a single step.

For the structural properties (tortuosity, pore size, and shape) of the TE layer, little can be said, as both monomers used (2SH and 3Br) have a high degree of rotational freedom. Consequently, the thio-bromo "click" reaction leads to forming a large series of conformers (Figure 7.6), which in turn lead to an amorphous structure. So, a microporous organic layer is indicated (Chapter 4, permporometry) with a random shape. The tortuosity of the layer is expected to be relatively high as the number of conformers formed from the reaction between 2SH and 3Br, is also large (21 total

conformers). Therefore, rigid monomers can be used to control the pore size and, potentially, the tortuosity of the polymeric layer. However, the nature of the thio-bromo "click" reaction bears little to no stereo control, and thus the formation of well-ordered (crystalline) materials can be challenging. Other "click" reactions, such as the copper catalysed alkyne–azide cycloaddition (CuCAAC), can use rigid monomers that result in chemically stable and potentially crystalline networks.[13]
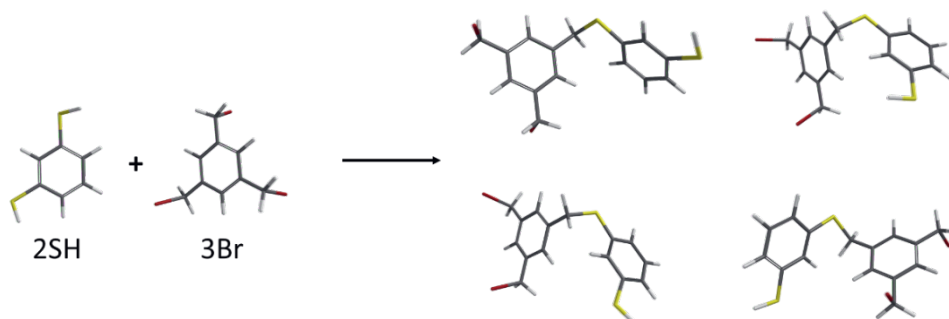
Figure 7.6: Potential conformers produced from the thio-bromo "click" reaction between 2SH and 3Br. The conformers were calculated with Spartan '14 Wavefunction.

In conclusion, the fabrication method described in Chapter 4 shows an alternative more sustainable way of producing ultrathin organic layers compared to conventional liquid/liquid interfacial polymerizations. The aim of the project was mostly achieved. However, the performance of the membrane can still be improved (see section 7.4). The preliminary results show that the thio-bromo "click" reaction can effectively be used to fabricate hybrid inorganic membranes. Furthermore, the method can be expanded to other monomers (e.g. 1,4-benzenedithiol) that can potentially form more open structures or functionalized monomers (2,5-diamino-1,4-benzenedithiol) that can lead to more hydrophilic polymers. In addition, other "click" reactions can be incorporated in membrane fabrication, leading to more crystalline networks (controlled pore shape and tortuosity).

7.3.3. Polyimide (PI) grafted membranes

In Chapter 5, PI grafted membranes were prepared via an in situ polymerization method. The aim of the project was to fabricate a crystalline two-dimensional (2D) PI layer at the top of the support. A 2D crystalline layer would provide high control over the pore size and tortuosity of the membrane layer. The PI grafted membranes were formed through the reaction of melamine (MA) and pyromellitic dianhydride (PMDA). Theoretically, the two monomers exhibit a low degree of rotational

250

freedom, which can facilitate the formation of a crystalline and 2D polymeric layer. To grow the polymer from the inorganic support (grafting-from), 3-aminopropyl triethoxysilane (APTES) was grafted at the top surface of the inorganic support. In a similar way, as described in Chapter 4, glycerol was used as a pore blocking agent to limit the grafting of the initiator (APTES) at the top surface. For the formation of the PI network, two routes were used. The first route consisted of the in situ polymerization, initiated from the top surface (from APTES), of PMDA with MA at 200 °C for 1 or 5 days. This resulted in hybrid organic-inorganic membranes with the polymeric network anchored on the support surface and at the pore entrance. In the second route, an additional step was used to functionalize the initiator molecules with PMDA, as was done before in the literature.[14] However, PMDA reacted with the whole inorganic surface, resulting in the PI network growing from the support's top and inner pore surface. The second route resulted in a homogeneous distribution of the polymer over the inorganic matrix, meaning in the inorganic pore and on the surface. Compared to the first, the second route allowed for less control over the thickness of the polymeric layer with more reaction steps involved. Thus the first route is more suitable for membrane fabrication. With both routes it was found that the PI network formed was a semicrystalline 3D network. Also, it was observed that the washing step after the initiator grafting affected the reproducibility of the membrane formation. Still, further investigation is needed to understand the implication of remaining glycerol in the inorganic layer during polymer growth.

The advantage of the method described in Chapter 5, is the formation of a cross-linked chemically inert polymer in a single step without additional fabrication steps involved, as is normally done with linear PI membranes.[15] However, such methods have many disadvantages, such as the toxicity of solvents (NMP, mesitylene, and isoquinoline) or the long reaction times.

Literature reported that the combination of PMDA and MA could result in various crystal structures, including a 2D conformation.[16–18] Therefore, to further investigate whether a 2D polymeric network could be obtained with PMDA and MA, several methods reported in the literature were explored and described in Chapter 6. Here the work is focused on the formation of crystalline PI networks through the condensation of PMDA and MA under different experimental conditions. Typically, 2D crystalline PIs are formed solvothermally at temperatures above 200 °C and for reaction times up to 5 days, but this could not be reproduced. However, it was possible to form crystalline PIs via a greener solid-state method at a temperature of 250 °C, so below the melting point of PMDA (283 °C), by first forming a supramolecular network between the two monomers. This latter method was also applied on top of inorganic supports to show that it can potentially be used for membrane fabrication. Even though the PI hybrid membranes (physically attached) were not tested, FTIR and permporometry results still show that a PI material is

present on the surface of the supports that shrunk the pore size near NF range (Chapter 6). These preliminary results can be used further to prepare PI hybrid membranes in a simple green method.

As was observed in both Chapters 5 and 6, the combination of PMDA and MA mainly results in semicrystalline (containing both highly ordered and amorphous phases) materials. However, other triamine monomers combined with PMDA have been reported in the literature to yield 2D crystalline materials.[19,20] Such monomers (2,4,6-tris(4-aminophenyl)-benzene   or   2,4,6-tris(4-aminophenyl)-amine)   are significantly larger than MA and lead to pore diameters (> 3 nm), so outside the NF range. On the other hand, other types of crystalline polymers, such as polyimines, which are typically reversible under aqueous conditions, can grow from a grafted inorganic support (e.g., γ-alumina). Polyimines can subsequently be transformed into significantly more stable polymers through simple synthetic procedures, such as oxidation,[21] without the loss of crystallinity. In this way, the pore size and tortuosity of the organic layer can be effectively controlled by simply choosing the right combination of monomers, as shown in Figure 7.7.
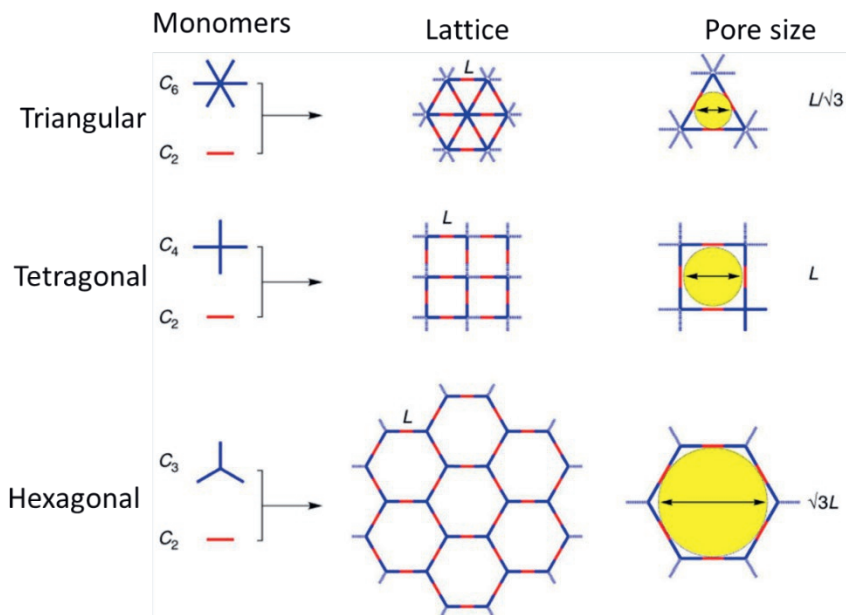
Figure 7.7: Schematic representation of different possible monomer conformations, their lattice formed, and their pore size estimation. This is based on monomers that have a low degree of rotational freedom, and their reaction will lead to the thermodynamic 2D product. The figure was adopted from [22].

In conclusion, the fabrication method reported in Chapter 5 leads to a crosslinked 3D network without any additional steps required. The formation of a 2D layer under the reflux conditions (Chapter 5) was not observed. Furthermore, the use of toxic solvents and the long reaction times reduce the importance of the method. Nevertheless, from Chapter 5 we have learned that the polyimidization reaction is initiated from the grafted initiator, and controlling the location of this initiator can lead to control of the location of the polymerization reaction. Still, further investigation is needed to understand the importance of glycerol during the in situ polymerization reaction.

Additionally, an alternative method was described in Chapter 6 to synthesize crystalline PI materials in water without the use of pressurized equipment (autoclave). This method was attempted on inorganic membranes and the preliminary results show PI formation at the top surface of the support and pore shrinkage. Further investigation can show whether the method described in Chapter 6 can yield chemically stable membranes.

7.4. Understanding the transport behaviour through our hybrid membranes

Understanding and predicting the transport behaviour of a membrane is one of the biggest challenges of membrane science. In this work, different types of nanofiltration membranes were developed, starting from an ultrafiltration γ-alumina layer with 5.5 nm in pore diameter coated on an α-alumina support with 80 nm in pore diameter. The α-alumina supports were purchased from a commercial source and used as received, however, the γ-alumina layer was prepared in-house. In Chapters 2, 3, and 4, two γ-alumina coatings were used, resulting in a total of 3 μm thickness. In Chapter 5, a single γ-alumina coating was used, which resulted in a thickness of 1.5 μm. In Chapter 2, the pristine support exhibited a water permeability between 8 and 9 L m^{-2} h^{-1} bar^{-1}. However, in Chapters 3 and 4, the pristine support's water permeability was reduced to 3 – 6 L m^{-2} h^{-1} bar^{-1}. In Chapter 5, the pristine support exhibited a water permeability of 4.5 L m^{-2} h^{-1} bar^{-1}, even though a single γ-alumina layer was used. In Chapter 5, the pristine support exhibited a water permeability of 4.5 L m^{-2} h^{-1} bar^{-1}, even though a single γ-alumina layer was used. In order to find an explanation for this difference in water permeability, the permeability of the different α-alumina batches used during this research was investigated. It was found that a newer batch of supports, as used in chapters 3. 4, and 5, exhibited 30% lower water permeability than the first batch used or the research described in Chapter 2. As the thickness and pore diameter of the bare α-alumina support was identical for batches, the porosity and/or tortuosity might have been different, explaining the difference in permeability. Finally, inorganic supports with better specifications (larger pore diameter, higher porosity, thinner layers, etc.) can exhibit lower flow resistance to solvent and improve the overall performance of

the final organic-inorganic membrane. However, as the scope of this work was focused on studying the effect of organic functionalization of the inorganic support on transport and separation behaviour, the well-defined mesoporous γ-alumina layers coated on α-alumina supports were used throughout this work.

All hybrid organic-inorganic membranes prepared in this work were analysed with cyclohexane permporometry and further tested on retention in aqueous solutions of Brilliant Yellow (BY, 629 Da) and Rhodamine B (RB, 479 Da). The results of these tests are summarized in Table 7.2. Overall, the organically functionalized membranes showed a large variation in membrane performance.

Table 7.2: Pore diameter, water permeability, BY, and RB retention of membranes described in this work.

Membrane	Kelvin diameter (nm)*	Water perm. ($L\ m^{-2}\ h^{-1}\ bar^{-1}$)	BY (629 Da) retention (%)	RB (479 Da) retention (%)	Chapter #
γ-Al_2O_3	5.5	3-4	75	14	-
PEG10PA	4	1	98	78	2
MePEG10PA	4.4	1	n.d.	n.d.	2
GP150	3.4	0.5	94	15	3
GP170	3.2	0.25	92	53	3
GP200	< 2	n.d.	n.d.	n.d.	3
GM150	3.6	0.5	99	84	3
GM200	< 2	0.03	98	75	3
Al-SiM/TE	< 2	0.6	100	93	4
A-1	< 2	1.6	100	76	5
A-5	< 2	1.5	100	99	5
B-1	< 2	1.6	100	74	5
B-5	< 2	0.5	100	99	5

* The Kelvin diameter was determined by cyclohexane permporometry. Membranes, denoted with Kelvin diameter < 2, have a pore diameter below the experimental limit of the equipment (2 nm).

The PEG-grafted membranes showed the smallest pore shrinkage, as analysed by cyclohexane permporometry, but still, their water permeability significantly decreased compared to the pristine alumina support. However, it should be pointed out that the pore size analysis was performed with an apolar solvent (cyclohexane), and as the polymer brushes are relatively hydrophilic, due to the etheric unit, it is expected that the polymer will collapse on the inorganic pore wall when in contact with cyclohexane, resulting in a relatively large pore. On the other hand, when in contact with water (used for retention tests), the PEG brushes extend away from the inorganic pore wall, resulting in relatively low permeability.

Overall, solution phase grafting (Chapter 2) resulted in lower grafting densities than solid-state grafting (Chapter 3). This difference in grafting density can significantly affect the permporometry analysis, where the lower grafting density samples will favour a more collapsed pore structure than the higher grafting density samples. Besides, the brushes during the solid-state grafting (Chapter 3) can crosslink and thus lead to a more rigid structure in the pores that can be less influenced by solvent effects. On the other hand, low grafting densities mean more inorganic surfaces, allowing for higher dye adsorption capacity. The RB adsorption was measured for both PEG10PA and GP150 under similar filtration conditions (pressure, duration, temperature, and stirring) and above recoveries of 40%. For PEG10PA, adsorption of 10% was calculated, whereas, for GP150, a maximum of 1% RB adsorption was determined. This difference in dye adsorption is an additional proof that the grafting density in the pores is significantly lower for PEG10PA than GP150. In conclusion, to compare the two systems in regard to pore size and separation, the permporometry analysis needs to be performed with various solvents, including the solvent used for the filtration test. Secondly, the maximum dye adsorption capacity of the grafted membranes before the retention test must be identified. Only then the two types of membranes can be compared impartially.

To further understand the grafting density's influence on the membrane's performance and correlate it with the pore size measurements, the PEG-grafted membranes should be tested under different trans-membrane pressures (TMP) and with solutes of varying size and charge. By studying the membrane performance of PDMS-grafted γ-Al$_2$O$_3$ membranes, Merlet et al.[23] observed that the rejection of a solute increases with TMP via a nonlinear relation regardless of sol vent used. Constant rejection is achieved for all solvents at different TMP, which depends on the swelling effect of the solvent on the polymer brushes. With this information at hand and by employing the Spiegler-Kedem (SKK) model, one can estimate a convection pore diameter formed in the solution during the retention tests (Figure 7.8a).[23] However, brush-type layers typically do not form a dense structure, and the space between the grafted polymers is expected to take part in rejection, especially at lower TMP[23]. This space can be regarded as a diffusive pore (Figure 7.8b). The influence of this diffusive pore on rejection also depends on the grafting density. The different PEG-grafted membranes can be studied further in detail in the way described above to understand the pore morphology (space between the brushes, grafting density, pore homogeneity, etc.).
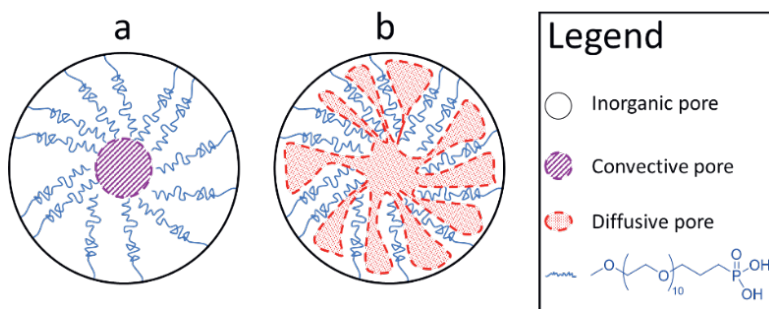
Figure 7.8: Schematic representation of PEG-phosphonic acid grafted inorganic pores in a "good" solvent, with brushes exhibiting maximum swelling. At high pressures, the solute transport through the membrane is predominately based on convective flow; therefore, the pore is called convective pore (a). However, a diffusive pore is formed at lower pressures due to the intermolecular space between the brushes (b). This way, solutes that are bigger than the convective pore can permeate through the grafted layer and lower the separation performance of the membrane.

Comparing the PI-grafted membranes shows that the A-5 membrane showed both the best water permeability (1.6 L m^{-2} h^{-1} bar^{-1}) and retention (100% BY and 99% RB). Still, the B-5 and Al-SiM/TE membranes showed promising results as they both exhibited relatively acceptable permeabilities (0.5 and 0.6 L m^{-2} h^{-1} bar^{-1}) and retentions (RB > 90%). The PEG-grafted membranes, on the other hand, showed, overall, lower RB retentions. This difference can be related to the nature of the layers formed as both the PI- and TE-grafted membranes exhibit crosslinked aromatic organic layers, whereas the PEG-grafted membranes form brush-like layers. The permeability performance of the TE- and PI-grafted membranes could potentially be enhanced by using larger monomers, particularly with the TE layers. Examples include 1,3-benzenedimethanethiol or 4,4′-thiobisbenzenethiol for more flexible TE layers. For alternative PI networks, monomers that can be used are, for example, 1,3,5-tris(aminomethyl)benzene, tris(4-aminophenyl)-amine, or perylene-3,4,9,10-tetracarboxylic dianhydride. Such layers can have more flexibility and hence swell more during filtration, leading to better solvent permeabilities while retaining lower retentions. However, this needs further research.

7.4.1. Performance in solvent/water mixtures

Even though the hybrid organic-inorganic membranes described in this work were stable in water, their stability and performance in solvent mixtures have not yet been established. Studies in literature with commercial polymeric membranes reported the detrimental effects of solvent/water mixtures on the performance and stability of these membranes, which were not observed in pure solvents (see also Chapter 1).[24,25]

Therefore, some of the membranes described in this work that performed well in aqueous RB solutions were tested with a mixture of RB in DMF/water (20:80 v/v%). Membranes that showed a relatively stable performance int his mixture were then tested in a mixture of RB in IPA/water (20:80 v/v%). Otherwise, membranes that failed one of the criteria were tested immediately in water to investigation whether any changes in membranes had occurred. Finally, all the membranes after the RB in IPA/water test were subjected to a retention test with an aqueous RB solution to assess any changes that might have occurred during the filtration tests in the solvent/water mixtures. The results of the retention tests are given in Figure 9.
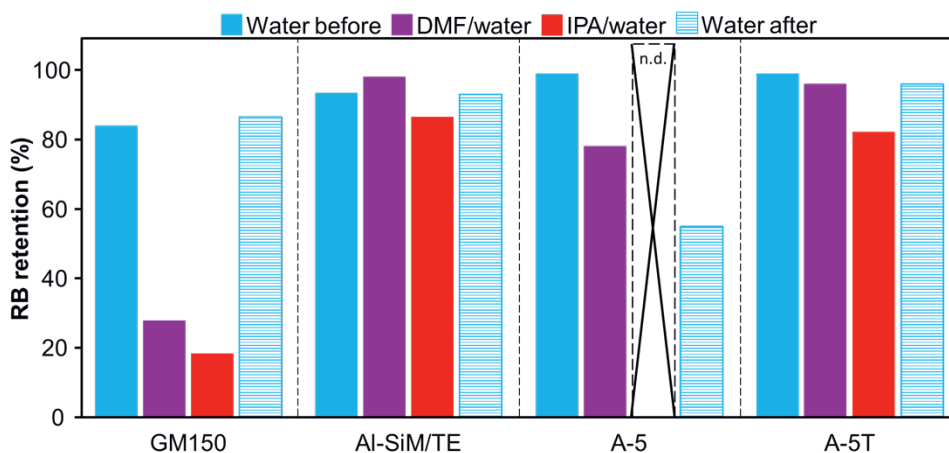
Figure 7.9: Rhodamine B (RB) retention of hybrid organic-inorganic membranes in pure water before the mixtures (blue filled), DMF/water (purple), IPA/water (red), and in water after (blue lines) testing in mixtures. The retention in water was repeated after testing the membranes in solvent mixtures to understand the effects of the mixtures on the stability of the membranes. The A-5 was not stable in DMF/water and therefore was not tested further in IPA/water (n.d. denotes that the value was not determined). As some membranes were permeating slowly, the tests in each solvent and solvent mixture were performed for up to two days to reach a recovery of 35-50%.

From the PEG-grafted membranes, GM150 was selected, as it showed reasonable performance with RB in water (Figure 7.9, blue filled). However, in both DMF/water and IPA/water, the RB retention dropped significantly below 30%, with a small drop in permeability ($0.2 - 0.3$ L m^{-2} h^{-1} bar^{-1}). Interestingly, after the filtration tests in the solvent mixtures, GM150 showed an RB retention in pure water (Figure 7.9, "water after") of 87%, while also the water permeability (0.4 L m^{-2} bar^{-1}) was not affected by the solvent/water. It can therefore be assumed that the PEG brush-like layer was not chemically altered. Besides, RB can also be influenced by the presence of the organic solvents as they can destabilize the charged conformation of the solute

(zwitterionic) and promote the neutral form (lactone), as was also discussed in Chapter 5. However, the currently available data cannot clearly explain which solute transport mechanism is dominant for GM150 samples in the solvent/water mixtures. More information can be gained from swelling studies of the PEG polymers in the solvent mixtures and by comparing those with PEG swelling in water. In this way, the effect of the solvent mixtures on the polymer brushes can be identified. Furthermore, additional retention studies with neutral solutes can facilitate in understanding the effect of the charge in the separation performance of the GM150 membranes in the solvent mixtures.

In contrast, TE-grafted membranes (Al-SiM/TE) showed a relatively stable RB retention throughout the various solvent mixtures, with retentions above 85% overall. Al-SiM/TE showed the worst performance in IPA/water, with the RB retention dropping to 87 %, which can be due to the IPA favouring the lactone conformation of RB and hence any charge effects during the separation tests are reduced, and therefore the performance is slightly lower. It can be assumed that no degradation has occurred in the polymeric network as the performance of the TE-grafted membranes shows only a slight variation in the solvent mixtures and remained the same in pure water afterward (Figure 7.9, "water after"). Additionally, due to the crosslinked polymeric layer, the Al-SiM/TE sample showed only little to no effect on the solvent mixtures. The permeability of Al-SiM/TE was in all cases in the order of 0.5 – 0.7 L m^{-2} h^{-1} bar^{-1}. Compared to reported results in the literature,[24,25,] the presence of solvent in water did not show any detrimental effects, such as an increase in permeability due to delamination,[25] on the polymeric layer. This can be related to the covalent attachment of the layer with the inorganic support or due to a lower degree of swelling of the polymeric layer in the presence of the two solvent mixtures used here. Swelling studies on TE-grafted membranes can give some more information on membrane performance.

For the PI-grafted membranes, the best performing sample, A-5, was tested only in DMF/water showing a strong drop in RB retention of 78%, compared to the RB retention in pure water (99%; 1 L m^{-2} h^{-1} bar^{-1}). Additionally, a significant increase in permeability was observed (2 L m^{-2} h^{-1} bar^{-1}), indicating that some sort of degradation occurred during the test in the DMF/water mixture. A subsequent test in an aqueous RB solution showed a 55% retention, indicating that the A-5 sample significantly degrades in a DMF/water solution, which was not observed in either pure water or DMF (Chapter 5). As both GM150 and Al-SiM/TE did not show any signs of degradation, we expect that the inorganic support is not affected by the solvent/water mixtures; instead, the PI network is degrading or removed from the inorganic matrix. This indicates that the preparation method did not yield a highly crosslinked network and/or covalently attached PI particles with the inorganic

surface. So, it is expected that the A-5 sample consists of PI particles that are deposited on the inorganic surface and are only partially grafted.

To study whether a simple thermal treatment could increase the stability of the A-5 sample, an A-5 sample t to has undergone a thermal treatment at 250 °C for 5h under N_2 (A-5T). Surprisingly this A-5T sample showed more stability in the solvent/water mixtures overall. However, the sample's permeability was significantly reduced (0.07 – 0.1 L m^{-2} h^{-1} bar^{-1}) as well. These results indicate that the thermal treatment facilitated a more stable PI network on top of the support. As the RB retention remains fairly similar throughout the different solvent/water mixtures, the crosslinking degree between the deposited PI particles is expected to be enhanced via the (extra) thermal treatment. As the membrane's permeability was significantly reduced, further optimization is needed to achieve either a thinner PI layer, by for example, reducing the reaction time or a more open structure, which can be achieved by using other monomers, as discussed before in this chapter.

Overall, the different membranes, excluding A-5, showed good stability against the aggressive solvent mixtures. Once again, the performance of the brush-type layers (GM150) were more dependent on the solvent (mixture) used, as was also discussed in Chapter 1. On the other hand, crosslinked layers, such as Al-SiM/TE, exhibit more stable performance in polar solvents and mixtures.

7.5. Conclusion

In this final chapter, many questions that arose from the preparation and testing of these hybrid organic-inorganic membranes are discussed. Overall, four different membrane types are described, which differ in regards to either the polymer functionalized on the inorganic support or the method of preparation (grafting-to vs. grafting-from). The polymers used were polyethylene glycol (PEG; Chapters 2 and 4), polythioether (TE; Chapter 4), and polyimide (PI; Chapter 5). The PEG-grafted membranes, as described in Chapters 2 and 3, were prepared via a grafting-to approach in solution and the solid-state, respectively. On the other hand, both TE and PI were prepared via a grafting-from method. The methods described in Chapters 2, 3, and 4 can be considered sustainable (or green) due to the solvents (Chapter 2) or the small amount of materials used (Chapters 3 and 4) in the membrane preparation. These membranes have the potential for aqueous nanofiltration applications (Table 7.1), and the preliminary results shown here (Figure 7.9) indicate that the Al-SiM/TE, PEG-phosphonic acid grafted, and PI-grafted membranes, after thermal treatment, can be applied in industrial solvent mixtures. However, the membrane fabrications still need optimization as the solvent permeabilities are low (> 1 L m^{-2} h^{-1} bar^{-1}). Potential research pathways to improve the performance of these membranes are mentioned throughout this chapter. Finally, a precise comparison between brush-like and crosslinked layers is not possible. However, the results shown in Figure 7.9

suggest a stronger dependency between membrane performance and the medium used (solvent) with brush-like layers compared to crosslinked layers.

7.6. References

(1)   Merlet, R.; Winnubst, L.; Nijmeijer, A.; Amirilargani, M.; Sudhölter, E. J. R.; Smet, L. C. P. M. de; Cob, S. S.; Vandezande, P.; Dorbec, M.; Sluijter, S.; Veen, H. van; VanDelft, Y.; Wienk, I.; Cuperus, P.; Behera, S.; Hartanto, Y.; Vankelecom, I. F. J.; Wit, P. de. Comparing the Performance of Organic Solvent Nanofiltration Membranes in Non-Polar Solvents. *Chemie Ing. Tech.* **2021**, *93* (9). https://doi.org/10.1002/CITE.202100032.

(2)   Merlet, R. B. Growing to Shrink: Grafting Alumina Mesopores for Molecular Separations, Ph.D. thesis, University of Twente, Enschede, The Netherlands, 2019. https://doi.org/10.3990/1.9789036548953.

(3)   Tanardi, C. R. Organically-Modified Ceramic Membranes for Solvent Nanofiltration: Fabrication and Transport Studies, Ph.D. thesis, University of Twente, 2015. https://doi.org/10.3990/1.9789462331358.

(4)   Pinheiro, A. F. M. Development and Characterization of Polymer-Grafted Ceramic Membranes for Solvent Nanofiltration, Ph.D. thesis, University of Twente, Enschede, The Netherlands, 2013. https://doi.org/10.3990/1.9789036535229.

(5)   Mustafa, G. Development of an Efficient Antifouling Grafting to Enhance the Applicability of Ceramic Nanofiltration Membranes in Water Treatmen, Ph.D. thesis, Universiteit Antwerpen, Antwerpen, Belgium, 2016.

(6)   Rezaei Hosseinabadi, S.; Wyns, K.; Meynen, V.; Carleer, R.; Adriaensens, P.; Buekenhoudt, A.; Van der Bruggen, B. Organic Solvent Nanofiltration with Grignard Functionalised Ceramic Nanofiltration Membranes. *J. Memb. Sci.* **2014**, *454*, 496–504. https://doi.org/10.1016/J.MEMSCI.2013.12.032.

(7)   Pinheiro, A. F. M.; Nijmeijer, A.; Sripathi, V. G. P.; Winnubst, L. Chemical Modification/Grafting of Mesoporous Alumina with Polydimethylsiloxane (PDMS). *Eur. J. Chem.* **2015**, *6* (3), 287–295.

(8)   Pujari, S. P.; Scheres, L.; Marcelis, A. T. M.; Zuilhof, H. Covalent Surface Modification of Oxide Surfaces. *Angew. Chemie - Int. Ed.* **2014**, *53* (25), 6322–6356. https://doi.org/10.1002/anie.201306709.

(9)   Gys, N.; Siemons, L.; Pawlak, B.; Wyns, K.; Baert, K.; Hauffman, T.; Adriaensens, P.; Blockhuys, F.; Michielsen, B.; Mullens, S.; Meynen, V. Experimental and Computational Insights into the Aminopropylphosphonic Acid Modification of Mesoporous TiO_2 Powder: The Role of the Amine Functionality on the Surface Interaction and Coordination. *Appl. Surf. Sci.* **2021**, *566*, 150625. https://doi.org/10.1016/J.APSUSC.2021.150625.

(10) Merlet, R. B.; Pizzoccaro-Zilamy, M. A.; Nijmeijer, A.; Winnubst, L. Hybrid Ceramic Membranes for Organic Solvent Nanofiltration: State-of-the-Art and Challenges. *J. Memb. Sci.* **2020**, *599*, 117839. https://doi.org/10.1016/j.memsci.2020.117839.

(11) Rapakousiou, A.; Sakamoto, R.; Shiotsuki, R.; Matsuoka, R.; Nakajima, U.; Pal, T.; Shimada, R.; Hossain, A.; Masunaga, H.; Horike, S.; Kitagawa, Y.; Sasaki, S.; Kato, K.; Ozawa, T.; Astruc, D.; Nishihara, H. Liquid/LiquidI Nterfacial Synthesis of AC Lick Nanosheet. *Chem. Eur.J* **2017**, *23*, 8443–8449. https://doi.org/10.1002/chem.201700201.

(12) Bu, J.; Pilo, A. L.; McLuckey, S. A. Gas Phase Click Chemistry via Ion/Ion Reactions. *Int. J. Mass Spectrom.* **2015**, *390*, 118–123. https://doi.org/10.1016/j.ijms.2015.05.010.

(13) Rapakousiou, A.; Sakamoto, R.; Shiotsuki, R.; Matsuoka, R.; Nakajima, U.; Pal, T.; Shimada, R.; Hossain, A.; Masunaga, H.; Horike, S.; Kitagawa, Y.; Sasaki, S.; Kato, K.; Ozawa, T.; Astruc, D.; Nishihara, H. Liquid/Liquid Interfacial Synthesis of a Click Nanosheet. *Chem. - A Eur. J.* **2017**, *23* (35), 8443–8449. https://doi.org/10.1002/chem.201700201.

(14) Fan, H.; Gu, J.; Meng, H.; Knebel, A.; Caro, J. High-Flux Membranes Based on the Covalent Organic Framework COF-LZU1 for Selective Dye Separation by Nanofiltration. *Angew. Chemie Int. Ed.* **2018**, *57* (15), 4083–4087. https://doi.org/10.1002/anie.201712816.

(15) Vanherck, K.; Koeckelberghs, G.; Vankelecom, I. F. J. Crosslinking Polyimides for Membrane Applications: A Review. *Prog. Polym. Sci.* **2013**, *38* (6), 874–896. https://doi.org/10.1016/j.progpolymsci.2012.11.001.

(16) Kuehl, V. A.; Wenzel, M. J.; Parkinson, B. A.; Sousa Oliveira, L. de; Hoberg, J. O. Pitfalls in the Synthesis of Polyimide-Linked Two-Dimensional Covalent Organic Frameworks. *J. Mater. Chem. A* **2021**, *9* (27), 15301–15309. https://doi.org/10.1039/D1TA01954F.

(17) Wang, T.; Xue, R.; Chen, H.; Shi, P.; Lei, X.; Wei, Y.; Guo, H.; Yang, W. Preparation of Two New Polyimide Bond Linked Porous Covalent Organic Frameworks and Their Fluorescence Sensing Application for Sensitive and Selective Determination of Fe $^{3+}$. *New J. Chem.* **2017**, *41* (23), 14272–14278. https://doi.org/10.1039/C7NJ02134H.

(18) Duan, H.; Lyu, P.; Liu, J.; Zhao, Y.; Xu, Y. Semiconducting Crystalline Two-Dimensional Polyimide Nanosheets with Superior Sodium Storage Properties. *ACS Nano* **2019**, *13*, 2473–2480. https://doi.org/10.1021/acsnano.8b09416.

(19) Maschita, J.; Banerjee, T.; Savasci, G.; Haase, F.; Ochsenfeld, C.; Lotsch, B. V. Ionothermal Synthesis of Imide-Linked Covalent Organic Frameworks.

*Angew.   Chemie   **2020**,   *132*   (36),   15880–15888. https://doi.org/10.1002/ange.202007372.

(20) Fang, Q.; Zhuang, Z.; Gu, S.; Kaspar, R. B.; Zheng, J.; Wang, J.; Qiu, S.; Yan, Y. Designed Synthesis of Large-Pore Crystalline Polyimide Covalent Organic Frameworks.   *Nat.   Commun.*   **2014**,   *5*   (1),   4503. https://doi.org/10.1038/ncomms5503.

(21) Wei, P.-F.; Qi, M.-Z.; Wang, Z.-P.; Ding, S.-Y.; Yu, W.; Liu, Q.; Wang, L.-K.; Wang, H.-Z.; An, W.-K.; Wang, W. Benzoxazole-Linked Ultrastable Covalent Organic Frameworks for Photocatalysis. *J. Am. Chem. Soc.* **2018**, *140* (13), 4623–4631. https://doi.org/10.1021/jacs.8b00571.

(22) Dalapati, S.; Addicoat, M.; Jin, S.; Sakurai, T.; Gao, J.; Xu, H.; Irle, S.; Seki, S.; Jiang, D. Rational Design of Crystalline Supermicroporous Covalent Organic Frameworks with Triangular Topologies. *Nat. Commun.* **2015**, *6* (1), 7786. https://doi.org/10.1038/ncomms8786.

(23) Merlet, R. B.; Tanardi, C. R.; Vankelecom, I. F. J.; Nijmeijer, A.; Winnubst, L. Interpreting Rejection in SRNF across Grafted Ceramic Membranes through the Spiegler-Kedem Model. *J. Memb. Sci.* **2017**, *525*, 359–367. https://doi.org/10.1016/J.MEMSCI.2016.12.013.

(24) Van Der Bruggen, B.; Braeken, L.; Vandecasteele, C. Flux Decline in Nanofiltration Due to Adsorption of Organic Compounds. *Sep. Purif. Technol.* **2002**, *29* (1), 23–31. https://doi.org/10.1016/S1383-5866(01)00199-X.

(25) Tempelman, K.; Casanova, S.; Benes, N. E. The Effect of Hydrocarbon Pollution on Polysulfone-Based Membranes in Aqueous Separations. *Sep. Purif.   Technol.   **2019**,   *224*,   348–355.* https://doi.org/10.1016/j.seppur.2019.05.013.

List of Publications

Nikos Kyriakou, Marie-Alix Pizzoccaro-Zilamy, Arian Nijmeijer, Mieke Luiten-Olieman, Louis Winnubst, *Hydrolytic stability of PEG-grafted γ-alumina membranes: Alkoxysilane vs Phosphonic acid linking groups*, Microporous and Mesoporous Materials 307 (2020) 110516. DOI: 10.1016/j.micromeso.2020.110516

Nikos Kyriakou, Renaud B. Merlet, Joshua D. Willott, Arian Nijmeijer, Louis Winnubst, and Marie-Alix Pizzoccaro-Zilamy, *New Method toward a Robust Covalently Attached Cross-Linked Nanofiltration Membrane* ACS Appl. Mater. Interfaces 2020, 12, 47948−47956. DOI: 10.1021/acsami.0c13339

Nikos Kyriakou, Louis Winnubst, Martin Drobek, Sissi de Beer, Arian Nijmeijer, and Marie-Alix Pizzoccaro-Zilamy, Controlled Nanoconfinement of Polyimide Networks in Mesoporous γ-Alumina Membranes for the Molecular Separation of Organic Dyes, ACS Appl. Nano Mater. 2021, 4, 14035−14046. DOI: 10.1021/acsanm.1c03322

Acknowledgements

Dear reader,

For your name to be mentioned here, means that I appreciated your contribution. Unfortunately, if you are not, I would care less about you. Just kidding! You can be certain that your contribution is highly important to me, as these books cost a lot. Kind of you, if you would share the copy with the person next to you, of course, after you have found your name in here.

Of course, I'd like to start with Louis, my guide through the last 5 long years. Dank u! I greatly appreciate all our scientific and social discussions through which I have developed more personally and professionally. You have always demanded more from me and this stimulated me to want the same for myself. I am grateful for the trust you showed in me all these years and for the efforts and time you have invested in me to learn and develop to the person I am today. To my co-supervisor Arian, I am grateful for your feedback, eye for detail and both the scientific and non-scientific discussions. A big thanks to both of you for the opportunities and the support you gave me during this time.

Marie, I am extremely grateful that you have become my co-supervisor during the second year of my Ph.D. From that moment on you have helped me overcome many troubles that I faced in both my personal and professional life. Your scientific drive and commitment to get the best out of our work pushed me always above my limits and led to the professional I am today. I am grateful for the trust you showed me into supervising Chin Yin, Nicolas, Anneloes and Elmar with you. To all four of you Chin Yin, Nicolas, Anneloes and Elmar thank you for the fun times we had together and for the patience you showed especially during COVID which I think was the most challenging time for all of us.

Frank, you have played a pivotal role into completing this work but also into making my time at IM more interesting and fun. You were always able to provide the best solution quickly and accurately. But I would mostly cherish the coffee breaks we shared and the futsal games we played together. Thank you also for the help you gave me during my shoulder injury, which was one of my toughest times during my Ph.D.

I also want to thank all the other MST staff that have in any way supported me during this time: Cindy, Harman (or Harmen, or whatever), Bob, Iske, Herman, Ineke, Mieke, Lidy, Annet,. Special thanks to Martin Drobek and Sissi de Beer for their crucial input contribution to our work. Additionally, thanks to Mark Smithers and Bianca Ruel for SEM/EDS and NMR expertise.

To my paranymphs Renaud and Farzaneh thank you for the times inside and outside the lab, your contribution these last years was crucial. Renaud, the first two years for a starting Ph.D. student are always the most challenging but I was lucky to have you as a colleague. These two years you taught me a lot about membranes and polymers. Your contribution goes beyond my Ph.D. work and into my personal life as I see you now as more of a friend than a colleague. Farzaneh, even though we were not able to collaborate directly in our Ph.D. work still you were actively involved in my work and I highly appreciate that as you helped me a lot whenever I was stuck. Thank you for all the discussions during coffee breaks that made this journey more enjoyable. A big thanks to both of you for being my paranymphs.

To the futsal team(s), it was always a pleasure and a lot of fun to play with you. To the Friday afternoon borrelers, that was one of the most cherished times of my Ph.D. A big thanks to all of you for your snarky (Antoine) remarks, jokes and the always fun stories (Harm(e)an, of course). I am grateful that I was able to share a beer, probably more, with all of you. To Josh and Alberto, we had fun times together at UT and outside. The BBQs and the parties we joined were always more fun with you two.

To the rest of the IM and MST cluster not yet mentioned a big thank you for the jokes and scientific and otherwise (weird) discussion during coffee breaks. Thank you Dennis, Jurjen, Burak, Wouter, Mariël, Rian, Kristianne, Moritz, Jeff, Patrick, Jason, Anne, Zainab, Shu, Pim, Dona, Arputha, Rob, Wiebe, Tymen, Nieck, Jouri and Matthijs and all others not listed.

Στην οικογένειά μου, ένα μεγάλο ευχαριστώ για την υποστήριξη και την αμέριστη πίστη που μου έδειξαν σε όλη τη διάρκεια των σπουδών μου. Στους γονείς μου, σας ευχαριστώ που πάντα πιστεύετε σε μένα και με ωθούσατε να βγάλω το καλύτερο από τον εαυτό μου. Εκτιμώ πολύ όλα όσα δώσατε για να με στηρίξετε κατά τη διάρκεια των σπουδών μου στην Ελλάδα και την Ολλανδία. Χωρίς εσάς, αυτή η δουλειά δεν θα ήταν δυνατή. Στην αδερφή μου, Χρύσω, ήσουν πάντα δίπλα μου, ακόμα και από μακριά. Ο χρόνος που περάσαμε μαζί στη Θεσσαλονίκη ήταν μοναδικός και είμαι ευγνώμων που μπόρεσα να το έχω αυτό. Στον κουνιάδο μου, Βαλάντη, θα ήθελα να σε ευχαριστήσω που με συμπεριλάβες, με την Χρύσω, στον γάμο σας και που ήσουν και είσαι εκεί για την αδερφή μου. Οι οικογενειακές συγκεντρώσεις, οι διακοπές και οι έξοδοι είναι πιο διασκεδαστικό να έχω εσένα και την αδερφή μου μαζί. To Rachel, thanks for being with me through tis journey. It was tough on both of us but we always managed to find our ways. Thanks for always believing in me even when I didn't. Of course I shouldn't forget my two dogs, Jimmy and Phoebe, who have helped immensely in making my life harder, but more interesting and fun, the last 2.5 years of my Ph.D. Βαλεντίνο, ήσουν πάντα εκεί για μένα και εκτιμώ ιδιαίτερα την υποστήριξή σου στην προσωπική και επαγγελματική

μου ζωή. Τάσο, παρόλο που είχες πολλά στη ζωή σου, πάντα έδειχνες την παρουσία σου στη ζωή μου και σε ευχαριστώ για αυτό. Μετά από τόσα χρόνια φιλίας με ωραίες αναμνήσεις αλλά και κακουχίες, εσύ και ο Βαλεντίνος είστε περισσότερο οικογένεια παρά φίλοι.

To all my friends, Giorgos, Charilaous, Polis, Theodoros, Thanasis, Josse, Jordy, Andrej, Rafaël, Daniel, Nabil, Djuun, Klaas, Paul and Renato. You all made this period more fun and easier to go through with your jokes and your spirit (stupidity). It was and is always a pleasure to hang out with you. Can't wait till our next (gay) week(end) away.

About the author

Nikos Kyriakou was born in Limassol (Cyprus) in 1987. After finishing army in 2006 he moved to Thessaloniki (Greece) where he obtained his BSc in Chemistry. Then, he moved to Amsterdam (the Netherlands) where he did his MSc studies in Chemistry. The next 1.5 years he worked for Shell as a research assistant. There he realized that to increase the growth prospects in industry as a chemist a Ph.D. can be important. So after searching for a while he found an interesting position in the Inorganic Membranes group at the University of Twente. There he worked under the supervision of Louis Winnubst, Marie-Alix Pizzoccaro-Zilamy and Arian Nijmeijer in the project titled "Solvent Tolerant Nanofiltration and Reverse Osmosis membranes (STNF) for the purification of industrial aqueous streams" funded by the Institute for Sustainable Process Technology (ISPT). On the 14th of October, Nikos Kyriakou defended his Ph.D. thesis in Enschede (the Netherlands).